ONLINE ISSN 2189-8871

TECHNICAL REPORTS OF THE METEOROLOGICAL RESEARCH INSTITUTE No. 76

Contribution of JMA to the WMO Technical Task Team on Meteorological Analyses for Fukushima Daiichi Nuclear Power Plant Accident and Relevant Atmospheric Transport Modeling at MRI

BY

K. Saito, T. Shimbori, R. Draxler, T. Hara, E. Toyoda, Y. Honda, K. Nagata, T. Fujita, M. Sakamoto, T. Kato, M. Kajino, T.T. Sekiyama, T.Y. Tanaka, T. Maki, H. Terada, M. Chino, T. Iwasaki, M.C. Hort, S.J. Leadbetter, G. Wotawa, D. Arnold, C. Maurer, A. Malo, R. Servranckx and P. Chen

気象研究所技術報告
第 76 号

WMO福島第一原発事故に関する気象解析技術タスクチーム活動と気象研究所の大気拡散モデリング

斉藤和雄・新堀敏基・R. Draxler
原旅人・豊田英司・本田有機・永田和彦・藤田司・坂本雅巳
加藤輝之・梶野瑞王・関山剛・田中泰宙・眞木貴史
寺田宏明・茅野政道・岩崎俊樹
M.C. Hort, S.J. Leadbetter, G. Wotawa, D. Arnold, C. Maurer, A. Malo, R. Servranckx, P. Chen

気 象 研 究 所
METEOROLOGICAL RESEARCH INSTITUTE, JAPAN

OCTOBER 2015

The *Technical Reports of the Meteorological Research Institute* has been issued at irregular intervals by the Meteorological Research Institute (MRI) since 1978 as a medium for the publication of technical report including methods, data and results of research, or comprehensive report compiled from published papers. The works described in the *Technical Reports of the MRI* have been performed as part of the research programs of MRI.

気象研究所技術報告　第76号　平成27年10月
TECHNICAL REPORTS OF THE METEOROLOGICAL
RESEARCH INSTITUTE No.76, October 2015
doi:10.11483/mritechrepo.76

Contribution of JMA to the WMO Technical Task Team on Meteorological Analyses for Fukushima Daiichi Nuclear Power Plant Accident and Relevant Atmospheric Transport Modeling at MRI

by

Kazuo Saito and Toshiki Shimbori
Meteorological Research Institute, Japan Meteorological Agency

Roland Draxler
Air Resource Laboratory, National Oceanic and Atmospheric Administration, USA

Tabito Hara, Eizi Toyoda, Yuki Honda, Kazuhiko Nagata, Tsukasa Fujita and Masami Sakamoto
Japan Meteorological Agency

Teruyuki Kato, Mizuo Kajino, Tsuyoshi T. Sekiyama, Taichu Y. Tanaka and Takashi Maki
Meteorological Research Institute, Japan Meteorological Agency

Hiroaki Terada and Masamichi Chino
Japan Atomic Energy Agency

Toshiki Iwasaki
Tohoku University

Matthew C. Hort and Susan J. Leadbetter
Met Office, United Kingdom

Gerhard Wotawa, Delia Arnold and Christian Maurer
Central Institute for Meteorology and Geodynamics, Austria

Alain Malo and Rene Servranckx
Canadian Meteorological Centre

Peter Chen
World Meteorological Organization

Contents

序

2011 年 3 月 11 日の東北地方太平洋沖地震は、マグニチュード Mw9.0 という日本観測史上最大の超巨大地震であった。この地震動と津波は未曾有とも言える甚大な被害を東日本の各地にもたらした。東京電力福島第一原子力発電所では、国際原子力事象評価尺度（INES）でレベル 7 に分類される深刻な事故が発生し、大量の放射性物質が大気と海洋に放出された。気象庁は、環境緊急対応（Environmental Emergency Response: EER）地区特別気象センター（Regional Specialized Meteorological Center: RSMC）として、国際原子力機関（IAEA）の要請に応じて、事故直後から大気中に放出された放射性物質の拡散予測情報を作成し、5 月 23 日まで提供した。この業務は世界気象機関(WMO)の「全球データ処理・予報システムに関するマニュアル」に基づくもので、気象庁予報部数値予報課が中心となって行われる。全球大気移流拡散数値モデルを用いて行うため、約 100km 四方の格子を一単位とする分解能となっており、放射性物質の放出条件も単純なものが仮定されているため、日本国内での放射性物質の拡散・沈着を予測・推定するためのものではない。

上記の気象庁の正式業務としての環境緊急対応とは別に、2011 年 8 月に WMO から気象庁長官宛に福島第一原子力発電所事故に関する気象データと解析に関する協力要請があった。この要請は、原子放射線の影響に関する国連科学委員会（United Nations Scientific Committee on the Effects of Atomic Radiation=UNSCEAR）が作成する福島第一原発事故に関する評価報告書に関して UNSCEAR が WMO に対し行った気象解析に関する協力要請に基づくものであった。気象庁では、総務部企画課国際室、予報部（業務課、数値予報課）と気象研究所で対応を協議し、WMO が設置するタスクチームに気象研究所からメンバーを出すとともに、予報部数値予報課が中心となって事故期間中の気象庁メソ解析や解析雨量のデータを WMO の国際気象通報式で用いられている標準書式である二進形式格子点資料気象通報式（第 2 版）（GRIB2）に変換し、関連ツールの整備を行った。気象庁が行った WMO タスクチームに関わる活動とその背景は、気象研究所と気象庁数値予報課のスタッフが主な著者となって気象庁業務に関する刊行物である「測候時報」に 2014 年 6 月にまとまられている。タスクチーム活動に関連して行われた気象庁領域拡散モデルの改良の一部は、気象庁のオキシダント予測業務及び降灰予報業務の改善にも貢献した。

本技術報告は、タスクチーム活動に係る気象庁の貢献について技術的な部分を中心により詳細に英文で記述するとともに、タスクチームメンバーや WMO 事務局、日本原子力研究開発機構からも共著執筆を頂いて、放出源推定や放射性物質の移流拡散沈着モデル計算について記述している。また関連する気象研究所と気象庁での大気輸送拡散沈着モデリングとして、前述の EER モデルや日本学術会議による大気輸送拡散沈着モデルの相互比較などについても記述している。本報告がタスクチーム活動に関する技術的な資料として出版されることに関して、関係者の労を多とし協力頂いた多くの方々に改めて感謝したい。

2015 年 6 月

研究調整官
竹内　義明

WMO福島第一原発事故に関する気象解析技術タスクチーム活動と気象研究所の大気拡散モデリング

斉藤和雄[*1]、新堀敏基[*2]、Roland Draxler[*3]
原旅人[*4]、豊田英司[*5]、本田有機[*4]、永田和彦[*6]、藤田司[*6]、坂本雅巳[*4]
加藤輝之[*1]、梶野瑞王[*7]、関山剛[*7]、田中泰宙[*7]、眞木貴史[*7]
寺田宏明[*8]、茅野政道[*8]、岩崎俊樹[*9]
Matthew C. Hort[*10], Suzan J. Leadbetter[*10],
Gerhard Wotawa[*11], Delia Arnold[*11], Christian Maurer[*11]
Alain Malo[*12], Rene Servranckx[*12], Peter Chen[*13]

2011 年 3 月 11 日に発生した東北地方太平洋沖地震とそれに伴って発生した津波は、東日本大震災と呼ばれる大きな災害を各地にもたらした。東京電力福島第一原子力発電所（福島第一原発）は、地震とこれに伴う津波によって被災し、極めて重大で広範囲に影響を及ぼす原子力事故が発生した。原子放射線の影響に関する国連科学委員会（United Nations Scientific Committee on the Effects of Atomic Radiation=UNSCEAR）は、2011 年 5 月に行われた第 58 回総会において、東日本大震災による福島第一原発事故に関する放射線被曝のレベルと影響に関する評価報告書を作成することを決定し、世界気象機関（WMO）に対し放射性物質の移流拡散沈着を評価するための気象解析に関する協力を求めた。これに対応するため、WMO では 5 か国（米国、英国、カナダ、オーストリア、日本）からのメンバーによる「福島第一原発事故に関する気象解析についての技術タスクチーム」（Technical Task Team on Meteorological Analyses for Fukushima Daiichi Nuclear Power Plant Accident、以下「タスクチーム」）を設置することを決め、気象庁に対してタスクチームへの専門家の推薦を含めた協力についての要請を行った。タスクチームの主目的は、気象解析の利用がどのように移流拡散沈着計算を改善できるかを調べることであった。

気象庁は、事故当事国の気象センターとしてタスクチーム活動に中心的に協力し、4 次元変分法データ同化に基づく現業メソ解析と解析雨量データを WMO の標準書式である GRIB2 に変換してタスクチームへ提供した。タスクチームでは、3 回の会合と 4 回の電話会議を行い、気象解析場の評価のための大気輸送拡散沈着モデル実験を行い、UNSCEAR に気象解析場として気象庁メソ解析と解析雨量を提供するとともに、タスクチームとしての最終報告書を 2013 年 2 月に作成した。気象庁は、大気汚染気象センターのオキシダント予測や地震火山部から発表される降灰予報業務に用いられている領域移流拡散モデルをタスクチーム活動で使用するために改良し、放射性物質の半減期・沈着性ガスの湿性沈着や軽量粒子の重力落下

*1 気象研究所予報研究部
*2 気象研究所火山研究部
*3 米国海洋大気庁大気資源研究所
*4 気象庁予報部数値予報課
*5 気象庁予報部業務課
*6 気象庁予報部アジア太平洋気象防災センター
*7 気象研究所環境・応用気象研究部
*8 日本原子力研究開発機構
*9 東北大学大学院理学研究科
*10 英国気象局
*11 オーストリア地球気象力学中央研究所
*12 カナダ気象局
*13 世界気象機関

の取り扱いなどを新たに追加した。この改良モデルを用いてタスクチームで定めた実験手順に従って、格子間隔 5km で単位放出に対する放射性物質の濃度と沈着の計算を行った。

UNSCEAR の福島第一原発事故に関する評価報告書は 2014 年 4 月に刊行され、上記に述べたタスクチーム活動については、2014 年 6 月に発刊された気象庁測候時報の第 81 巻に和文でまとめられている。この技術報告では、タスクチーム活動に係る気象庁の貢献について GRIB2 フォーマットのファイルやその変換ツールの詳細も含めて詳しく英文で記述するとともに、測候時報で簡単に触れた気象研究所での大気輸送拡散沈着モデル実験などについて記述した。

本報告の構成は以下のとおりである。B 章ではタスチームについての概論と会合について記述した。C 章では、タスクチームへの気象庁の貢献について述べ、現業メソ解析と解析雨量についての説明とそれらのデータを取り扱うために開発された関連ツールについて記述した。D 章では、タスクチームが行った大気輸送拡散沈着モデル実験について述べた。E 章には、気象庁の領域移流拡散モデルとその改良について記述し、放出源高度や計算粒子数、湿性沈着に関する係数や乾性沈着の高度に関する感度実験の結果を載せた。F 章では、他のタスクチームメンバー国の大気輸送拡散沈着モデルについて紹介し、それらの計算結果をセシウム-137 についての大気濃度と沈着についての測定結果に対するモデル検証とともに示した。G 章には、関連する気象研究所と気象庁での大気輸送拡散沈着モデリングについて紹介し、日本学術会議による大気輸送拡散沈着モデルの相互比較への参加や放出源の逆推定についても言及した。東北大学理学研究科の岩崎俊樹教授による大気輸送拡散沈着モデル計算の必要性に関する特別寄稿も含めている。参考文献は H 章にまとめている。I 章に WMO からの厚意により、タスクチーム会合報告の写しを付録として付した。

タスクチーム活動と本報告の作成に関連して、多くの方々の協力を頂いた。気象庁予報部数値予報課には竹内義明課長（当時）の理解のもと多くの協力を頂いた。片山桂一予報官からはモデル計算に関する情報を、佐藤芳昭数値予報モデル開発推進官には原稿についての丁寧なコメントを頂いた。また総務部企画課の長谷川直之課長（当時）、吉田隆技術開発調整官（当時）と郷田治稔技術開発調整官、国際室の木村達哉室長、予報部業務課の石田純一調査官（当時）にも様々な助力・手配の労を頂いた。気象研究所では、三上正男研究総務官（当時）、中村誠臣研究調整官（当時）や企画室から様々な助力・助言を頂いた。露木義気候研究部長（当時）には、原稿全体を閲読頂き丁寧なコメントを頂いた。予報部数値予報課の根本昇技官（当時）はメソ解析と解析雨量データの提供用 GRIB2 への変換の実施に関して C-3 節と C-6 節に、米国海洋大気庁 (NOAA) の Glen Rolph 博士は D-4 節の NOAA のタスクチームウェブサイトに、予報研究部の国井勝研究官は G-4 節の気象研究所のモデル計算に、それぞれ大きな貢献をしている。タスクチーム第 1 回会合での日本からの報告に際して、東京大学大気海洋研究所の中島映至教授、鶴田治雄特任研究員、京都大学防災研究所の竹見哲也准教授、名古屋大水循環研究センターの加藤雅也研究員、坪木和久教授、産業技術総合研究所の近藤裕昭博士、海洋研究開発機構の滝川雅之博士の各位からは、気象学会秋季大会スペシャルセッションでの発表資料の提供を頂いた。また主著者の講演発表に関わる出張において、文部科学省 HPCI 戦略プログラム「超高精度メソスケール気象予測の実証」の補助を受けた。これらに深く感謝するものである。

A. Preface[1]

The 2011 off the Pacific coast of Tohoku Earthquake (Great East Japan Earthquake) and tsunami occurred on 11 March 2011 and caused severe damage in Japan. The United Nations Scientific Committee on the Effects of Atomic Radiation (UNSCEAR) was asked to produce a scientific report for the General Assembly on the levels and effects of radiation exposure caused by the accident at the Fukushima Daiichi Nuclear Power Plant, and UNSCEAR requested the World Meteorological Organization (WMO) to develop a set of meteorological analyses for assessing the atmospheric transport, dispersion, and deposition of radioactive materials. In response to UNSCEAR's request, the WMO's Commission for Basic Systems convened a technical task team of experts from five countries (Austria, Canada, Japan, United Kingdom, and the United States) in November 2011. The primary aim of this team was to examine how the use of meteorological analyses could improve atmospheric transport, dispersion, and deposition model (ATDM) calculations.

As the Regional Specialized Meteorological Center of the country in which the accident occurred, the Japan Meteorological Agency (JMA) collaborated with the WMO Task Team by providing its mesoscale analysis based on operational four-dimensional variational data assimilation and radar/rain gauge-analyzed precipitation (RAP) data in the standard WMO format (GRIB2). To evaluate the quality of the meteorological analyses, the WMO Task Team conducted test simulations with their regional ATDMs and different meteorological analyses. JMA developed a regional ATDM for radionuclides by modifying its operational regional atmospheric transport model, which had been previously used for photochemical oxidant predictions and volcanic ashfall forecasts. The modified model (hereafter referred to as JMA-RATM) newly implemented dry deposition, wet scavenging, and gravitational settling of radionuclide aerosol particles. The preliminary and revised calculations of JMA-RATM were conducted with a horizontal concentration and deposition grid resolution of 5 km and a unit source emission rate, in accordance with the Task Team's protocols.

This technical report describes JMA's contribution to the WMO Task Team and summarizes the Task Team activities and relevant ATDM modeling carried out at the Meteorological Research Institute (MRI) of JMA.

The authors of this technical report thank many people for their help in making both our participation in Task Team activities and this technical report possible. In particular, we are grateful to Yoshiaki Takeuchi (then Director), Keiichi Katayama, Jun-ichi Ishida, and Yoshiaki Sato of the Numerical Prediction Division of JMA, and Naoyuki Hasegawa, Takashi Yoshida, Harutoshi Goda, and Tatsuya Kimura of the Planning Division of JMA, for their help with both the Task Team activities and the preparation of this technical report. We also thank Masao

[1] K. Saito

Mikami, Tadashi Tsuyuki, Masaomi Nakamura, and staff of the Office of Planning of MRI for their help during the production of this technical report. A report on the Task Team activities in Japanese has been published in Sokko-jiho (Saito et al., 2014), the bulletin of JMA's business reports. Noboru Nemoto of the Numerical Prediction Division of JMA, Glenn Rolph of the U.S. National Oceanic and Atmospheric Administration, and Masaru Kunii of MRI contributed Sections C-3 and C-6, D-4, and G-4, respectively. A part of this study was supported by the Ministry of Education, Culture, Sports, Science and Technology through its High-Performance Computing Infrastructure Strategic Program for Innovative Research (SPIRE) Field 3, "Ultra-high Precision Meso-Scale Weather Prediction."

The report is organized as follows. Section B presents an overview of the WMO Task Team and the Task Team meetings. Section C reports on JMA's contributions to the WMO Task Team. The operational mesoscale analysis and RAP data, including a data conversion tool prepared by JMA to facilitate their use by the scientific community, are described. In Section D, the ATDM experiments conducted by the Task Team members are presented. Section E describes the JMA-RATM and the modifications implemented to support the Task Team activities. Experiments conducted to test the sensitivity of the JMA-RATM calculations to some of the ATDM parameters (release height, number of computational particles, wet scavenging coefficient and application height, and dry deposition application height) are also described. Section F introduces the ATDMs of each of the Task Team member countries, and the results of those ATDM calculations are presented and verified against ^{137}Cs deposition measurements and the air concentration time series. In Section G, relevant ATDM modeling conducted at MRI and JMA is introduced, including an ATDM intercomparison performed by the Science Council of Japan and an emission source estimation made by using an inverse model. A special contribution from Prof. Toshiki Iwasaki of Tohoku University illustrates the necessity to utilize ATDM modeling in the nuclear power plant accident. Section H is the list of references. Section I, the appendix, contains copies of the WMO Task Team meeting reports, courtesy of the WMO.

B. Overview

B-1. Overview of the WMO Task Team[1]

The World Meteorological Organization (WMO) organized a small Task Team (TT) to respond to a request from the United Nations Scientific Committee on the Effects of Atomic Radiation (UNSCEAR) to assist them with the meteorological aspects of a dose assessment from the radiological releases from the Fukushima Daiichi nuclear power plant accident.

The TT consisted of participants from the Canadian Meteorological Centre (CMC), the U.S. National Oceanic and Atmospheric Administration (NOAA), the Met Office UK (UKMET), the Japan Meteorological Agency (JMA), and the Austrian Zentralanstalt für Meteorologie und Geodynamik (ZAMG) (Table B-1-1). A representative from the European Commission Joint Research Centre's ENSEMBLE project (Ispra, Italy) was later invited to participate in the data analysis phase of the effort.

The TT's primary mission was to examine how the use of enhanced meteorological analyses and the introduction of additional meteorological observational data, could improve atmospheric transport, dispersion and deposition calculations. Although the direct evaluation of meteorological analyses is possible by comparing weather observations with the analyses, the TT members agreed that the best way to evaluate the suitability of the various meteorological analyses for the assessment was to actually use the meteorological data in Atmospheric Transport Dispersion and Deposition Models (ATDM) and compare the model predictions against radiological monitoring data, total accumulated deposition as well as time-varying air concentrations at a few locations.

Naturally the evaluation of the ATDM calculations relies not only upon the meteorological data, but also upon the time varying source term used in the calculation, a preliminary version of which was provided to the TT by the UNSCEAR source reconstruction group.

The methodology for evaluating the meteorological analyses by computing the dispersion and deposition and comparing these calculations with measurement data was designed during the first meeting (WMO, 2011; see I-1) of the TT and then updated during the TT's second meeting (WMO, 2012a; see I-2). The general approach was that each of the TT participants would run their own ATDM using the meteorological data analysis fields already available to them and, if possible, the higher spatial and temporal resolution fields provided by JMA (see C-3). The ATDM calculations were standardized as much as possible in terms of input and output parameters but each ATDM would retain its unique treatment of the meteorological input data, dispersion, and deposition computations, thereby providing a range of possible solutions due to variations in model parameterizations as well as the driving meteorological analysis data (see D-1).

At the conclusion of the TT's efforts, 20 simulations using different ATDM-meteorology combinations were available and 18 of these were used in the final analysis. The meteorological analyses, the individual ATDM air concentration and deposition calculations, and various ensemble

[1] R. Draxler, M. Hort, A. Malo, K. Saito, R. Servranckx, and G. Wotawa

mean calculations were made available to UNSCEAR community as described in the third and final meeting report (WMO, 2012b; see I-3) which also has been published (Draxler et al., 2013).

Because all of the TT ATDM calculations were done using a constant unit-source emission rate during the respective time window (3 hours), varying the source term between the time windows did not require re-running any of the ATDM calculations. The preliminary source term used in the WMO evaluation was not the same as the final source term adopted by UNSCEAR (2013; 2014), and after the completion of the TT efforts under the guidance of WMO, the TT continued its work independently to re-compute all of the statistics and graphics (Draxler et al., 2015) using the source term of Terada et al. (2012) (see D-2). In addition, other WMO ATDM modeling centers were invited to add their computations to the NOAA web page summarizing the TT calculations (see D-4).

Table B-1-1. List of the WMO Task Team members.

Name	Country	Affiliation	Remarks
Roland Draxler	United States of America	National Oceanic and Atmospheric Administration (NOAA)	Air Resources Laboratory (ARL) Chairman of the Task Team
Matthew Hort	United Kingdom	Met Office (UKMET)	Research Scientific Manger RSMC Exeter EER
Gerhard Wotawa	Austria	Zentralanstalt für Meteorologie und Geodynamik (ZAMG)	Data, Methods and Modelling Division EER ATDM
Kazuo Saito	Japan	Japan Meteorological Agency (JMA)	Meteorological Research Institute (MRI)
René Servranckx*	Canada	Canadian Meteorological Center (CMC)	Chairman of CBS EER Group
Peter Chen	--	World Meteorological Organization (WMO)	Chief, Data Processing and Forecasting Systems (DPFS) Division Secretary of the Task Team

* Absent at the 1st meeting. Alain Malo (CMC) participated in the 2nd meeting.

B-2. Task Team meetings[1]

B-2-1. The first task team meeting

The Task Team's first meeting was conducted at WMO Headquarters in Geneva from November 30th to December 2nd, 2011.

The following eight items were confirmed as the terms of reference (ToR) for the Task Team:

a) Determine the relevant meteorological observational data sets and related information required to support the meteorological analyses and identify their archive location and availability;

(b) Determine which of the existing meteorological analyses are of sufficient spatial and temporal detail so that can be used to estimate the atmospheric transport, dispersion, and surface deposition of radionuclides that were released from the nuclear accident and identify their archive location and availability;

(c) Identify gaps in the existing meteorological analyses that if addressed would make them more suitable for estimating atmospheric transport, dispersion, and deposition and in coordination with the WMO Secretariat, identify which members will provide updated analyses;

(d) Based upon the observational data and analyses, prepare a report on the temporal and spatial variations in atmospheric conditions during the nuclear accident;

(e) Evaluate the suitability and quality of the observational data and meteorological analyses for computing atmospheric transport, dispersion, and surface deposition by comparing the computational results with radiological measurements;

(f) Estimate the uncertainty in the atmospheric transport, dispersion and deposition (ATM) computations by comparing the results from several different ATMs and using different meteorological analyses;

(g) Liaise and assist where possible with the UN Scientific Committee on the Effects of Atomic Radiation (UNSCEAR), in their study on the levels and effects of exposure due to the Fukushima Daiichi nuclear accident.

(h) Propose possible enhancements to the WMO EER system, including additional products and/or additional modes of operation with the relevant international organizations.

Although the period of interest was from 11 March through 20 April, 2011, the Task Team focused their study from 11 – 31 March 2011 because the largest emissions occurred during this early period. The Task Team regarded the JMA 4D-VAR mesoscale analysis meteorological data as the most suitable for local and regional scale simulations.

---

[1] K. Saito, P. Chen and R. Draxler

In the first meeting, JMA presented its observation network, available meteorological fields during the accident period, its numerical weather prediction (NWP) system and mesoscale 4D-VAR, the JMA regional ATM, and other relevant studies in Japan (Section B-3-1).

As one of the main decisions of meeting, JMA decided to prepare its meso-ground surface analysis and meso-analysis data in the original model coordinate system by the end of June 2012 and to be distributed in the GRIB2 format to the other Task Team members.

It was decided that the domain of the regional atmospheric transport dispersion and deposition model (ATDM) experiment should target an area of 30 degrees east-west and 20 degrees north-south (Fig. B-2-1), with horizontal resolution of 0.05 degree (about 5 km). The first meeting report has been uploaded on the WMO website (WMO, 2011; Appendix I-1).

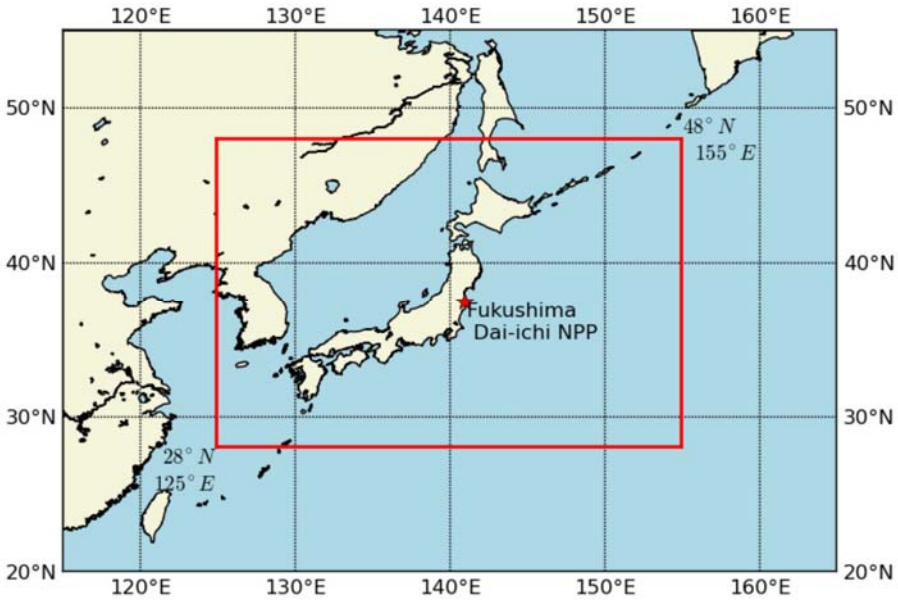

Fig. B-2-1. Domain of regional ATDM experiment of the Task Team. After Draxler et al. (2013a).

B-2-2. The first telephone meeting

A telephone meeting of the Task Team members was held on February 13, 2012. Because some ATDM simulations were already carried out in Group B of UNSCEAR using global analysis data of ECMWF (originally 0.125 degrees), the Task Team decided not to perform global ATDM simulations, but to focus on regional ATDM experiments. It was decided that the period of the experiment would cover 11-31 March 2011 and each simulation would be for a 3 hour emission period followed for up to 72 hours for each radionuclide release. Table B-2-1 shows the basic specifications of ATDM experiment. For further detail of the experiments, see Section D-1.

Table B-2-1. Specifications of the regional ATDM experiment of the Task Team.

		Remarks
Horizontal resolution	0.05 degree (about 5 km)	
Domain	125E-155E, 28N-48N	Fig. B-2-1
Initial time	2011 March 11-31, 3-hourly	Totally 168 times
Forecast time	72 hours	
Emission rate	Unit release (1 Bq/hr)	Linear sum based on estimated release rate is computed
Release height	From ground to 100 m	
Computation	Concentration average from the ground to 100 m AGL and surface deposition for Noble gases (Ngas), Depositional gases (Dgas), Light particles (Lpar)	half - life period is considered for Iodine-131 (^{131}I)

B-2-3. The second Task Team meeting

The Task Team's second meeting was held in the United Kingdom Met Office London Branch on May 1-3, 2012. In addition to the six members of the Task Team, Dr. Florian Gering (Federal Office for Radiation Protection of Germany), Dr. Oliver Isnard (Radiation Protection Nuclear Safety Institute of France), and Mr. Peter Bedwell (UK Health Protection Agency) participated, as experts from the UNSCEAR working groups.

Preliminary runs of the regional ATDMs targeting on March 11 to 31 were presented by the four centers (ATDM NOAA-HYSPLIT, UKMET-NAME, the CMC-MLDP0, and JMA-RATM; see Appendix I-2). From JMA, rainfall analysis data (Section C-4) and mesoscale analysis data (Section C-2) for the whole period were distributed to the meeting attendees. In addition, JMA offered to provide a software tool to convert these files to a latitude-longitude grid, while retaining the vertical hybrid terrain-following grid and also with an option to convert these data to pressure-level surfaces by the end of June 2012 (see Section C-6).

The TT members reviewed and made one modification to its ToR (in paragraph (f)), which is found in Annex III of the meeting report (see Appendix I-2).

B-2-4. The 2nd-4th telephone meetings

On June 7, 2012, the second telephone meeting was held. The regional ATDM simulation results of each team member and assessment methods based on the sampling data were discussed. JMA commented that a file conversion tool proposed in the second meeting would be prepared by the end of June.

On July 23, the third telephone meeting was held. The chairman of the Task Team (Draxler) reported on the meeting of the Expert Group B of UNSCEAR that took place in the previous week. The Task Team confirmed the necessity to finish all ATDM calculations of the Task Team by the end of September.

On October 4, the fourth telephone meeting was held. In addition to the successful NOAA, CMC and UKMET ATDM calculations using the JMA Meso analysis, ZAMG reported that they would use the JMA rainfall analysis in the calculation of wet deposition.

Discussions were held about the Fukushima special Symposium carried out in the 93rd annual meeting of the American Meteorological Society and ATDM intercomparison by Science Council of Japan (SCJ) to target the Fukushima nuclear accident (see Section G-1).

B-2-5. The third task team meeting

The Task Team third meeting was carried out on 3-5 December 2012 at the Austrian Meteorology and Geodynamic Central Research Institute (ZAMG).

Almost all the proposed ATDM calculations were completed, and verification results were shown. As an additional topic, the ensemble analyses of the Task Team's ATDM experiments were prepared and presented by Dr. Stefano Galmarini (EC Joint Research Center). The final report of the third meeting of the Task team (WMO, 2012b) has been uploaded on WMO website (http://www.wmo.int/pages/prog/www/CBS-Reports/documents/FINAL-REPORT-Vienna-Dec2012.pdf, with a detailed description of verification results presented in Annex III. Based on Annex III, a final report of the Task Team activity has been published as the WMO technical publication No. 1120 (Draxler et al., 2013). A summary of the scientific findings obtained in the Task Team activities has been published in a special issue of the Journal of the Environmental Radioactivity (Draxler et al., 2015).

B-3. Overview of JMA's contribution to the WMO Task Team[1]

B-3-1. JMA's presentation at the first Task Team meeting

In the first Task Team meeting (Section B-2-1), JMA presented the following information on its observation, analysis, and prediction systems and summary of the meteorology during the accident period as potential contributions to the Task Team activity:

1) Observation network of JMA (Section C-1-1) and the example of the JMA precipitation analysis rainfall (Section C-4)
2) Characteristic features of the meteorological field in the accident period (Surface weather charts, surface wind field observed by the JMA's AWS network (AMeDAS) with 24-hour accumulated rainfall based on precipitation analysis, and 950hPa wind field from JMA Meso-scale (MESO) analysis (Section C-9)
3) Specifications of the numerical weather prediction products and operational analysis systems of JMA (global and mesoscale forecast-analysis systems) (Section C-7), MESO 4DVAR analysis (Section C-8) and hourly MESO atmospheric analysis, and the list of the data assimilated in the operational analysis systems (Section C-1-2)
4) Introduction of JMA's ATDMs (global ATM for EER; Section G-2) and regional ATM (Section E).
5) Relevant studies at MRI and JMA (Section B-2 and Section G)

As for 5), based on the special session at the autumn meeting of the Meteorological Society of Japan (Kondo et al., 2012), the following nine topics were introduced:

・Global transport model using MASINGAR (Tanaka)
・Regional passive tracer model using WRF (Kajino)
・MRI regional chemical transport model using NHM-Chem (Kajino; Section G-3)
・Emission flux estimation by inverse model (Maki; Section G-5)
・Regional Deposition of Radioactive cesium (Cs) and iodine (I) by the Accident of the Fukushima Daiichi NPP (Tsuruta et al., Univ Tokyo)
・High-Resolution modeling and analyses of wind and diffusion fields over Fukushima (Takemi and Ishikawa, Kyoto Univ.)
・Transport and deposition analysis by AIST-MM (Kondo et al., AIST)
・Deposition estimation using WRF/Chem (Takigawa et al., JAMSTEC)
・Transport and diffusion simulation using CReSS (Kato et al., Nagoya Univ.)

B-3-2. MESO Analysis of JMA

To assist in the regional ATDM calculations, JMA provided their MESO analysis fields to the WMO Task Team and UNSCEAR for the period of 11 to 31 March 2011, at three-hourly intervals and at a 5-km horizontal resolution. The MESO analyses are produced by the operational JMA regional

[1] K. Saito, T. Fujita, T. Kato, T. Hara, K. Nagata, Y. Honda and E. Toyoda

non-hydrostatic 4D-VAR system, which assimilates a variety of local meteorological observations, including 16 radio sondes and 31 wind profilers, Doppler radial winds from 16 JMA C-band radars and 9 Doppler radars for airport weather, total precipitable water vapor derived from about 1,200 GPS stations of the Geospatial Information Authority of Japan and satellite data (Section C-1).

One of the unique features of JMA MESO analysis is that the JMA Radar/Rain Gauge-Analyzed Precipitation (RAP) data, based on the JMA radar network and rain gauge observations (see B-3-3 and C-4), is also assimilated in the 4D-VAR. These data are assimilated in hourly time slots in the 3-hour data assimilation windows by the inner loop (simplified nonlinear/adjoint) model with a horizontal resolution of 15 km, and all analysis fields including liquid and solid precipitation are produced by a 3-hour forecast of the non-linear outer-loop model (JMA nonhydrostatic model (JMA-NHM); Saito et al., 2006; 2007; 2012) of the incremental 4D-VAR with a horizontal resolution of 5 km. The JMA-MESO analysis covers Japan and its surrounding area by 719 (x-direction) x 575 (y-direction) grid points on a Lambert Conformal projection (see Fig. 1 of Draxler et al. (2015)) up to about 21 km above ground level (AGL). It has 50 vertical levels, including 11 levels below 1 km AGL. Although the original horizontal and vertical grid configurations of the JMA Mesoscale model and 4D-VAR analysis (JNoVA; C-8) are Arakawa-C and Lorentz types, respectively, for handling simplicity all data on the staggered points (horizontal and vertical wind speeds) are interpolated to the scalar points (position of pressures and potential temperatures) in the data provided to the Task Team.

Figure B-3-1 shows averaged surface precipitation (mm per hour) by JMA-MESO for 15 March 1200-1500 UTC for rain (left), snow (center) and total precipitation (right). The time evolution of 950 hPa winds and mean sea level pressure by JMA-MESO for 15 March 2011 is shown in Fig. C-9-7. One-hour average surface precipitation by JMA precipitation analysis for 15 March 1200-1500 UTC is shown in Fig. B-3-2.

For more scientific details of JMA nonhydrostatic 4D-VAR, see Section C-8.

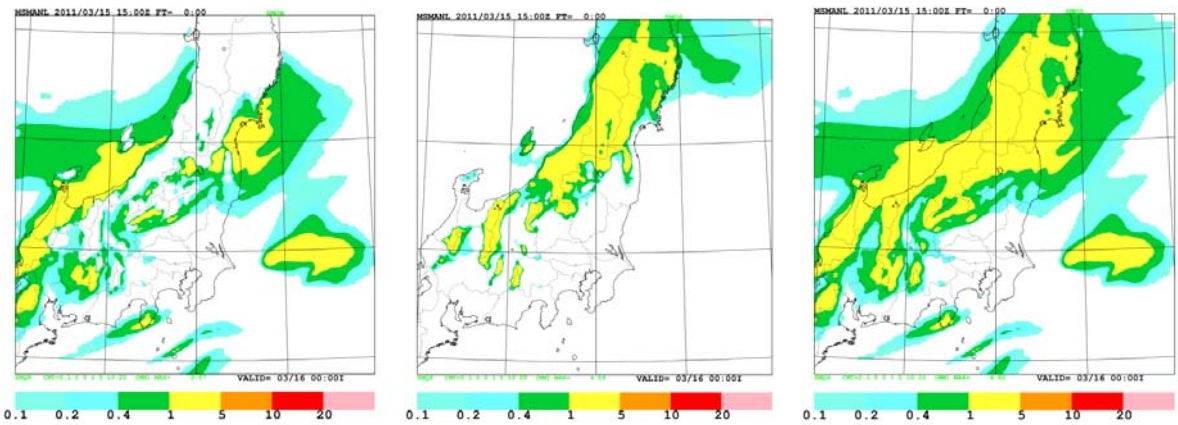

Fig. B-3-1. Averaged surface precipitation (mm per hour) by JMA-MESO for 15 March 1200-1500 UTC. Rain (left), snow (center) and total precipitation (right). After Saito et al. (2015).

B-3-3. Radar/Rain Gauge-Analyzed Precipitation (RAP)

JMA provided the RAP dataset at 30-minute intervals, with a horizontal resolution of 45 seconds (about 1.11 km at 37°N) in longitude and 30 seconds (about 0.93 km) in latitude covering a region from 118-150°E and from 20-48°N (2560 by 3360 grid points). RAP is produced from calibrating radar reflectivity data with one-hour accumulated rain gauge precipitation data. In addition to the JMA network of 20 C-band radars and 1,300 surface observations (Section C-1-1), echo data from additional 26 C-band radars operated by the Ministry of Land, Infrastructure, Transport and Tourism and precipitation data from additional 8,700 rain gauges in Japan are collected in the real-time operation. A more detailed description of the RAP processing is found in section C-4.

JMA-RAP intensities at one-hour intervals for 15 March 1200-1500 UTC are shown in Fig. B-3-2. This illustrates a good agreement between RAP and the JMA-MESO total precipitation (Fig. B-3-1). A circle-shaped very small intense precipitation area is seen around the radar site at Sendai (38.3N, 140.9E) for 1200-1300 UTC (left), which is due to a bright-band observed by the Sendai radar.

For more details of the JMA precipitation analysis, see Section C-4. A documentation of GRIB-2 format of RAP data is given in Section C-5.

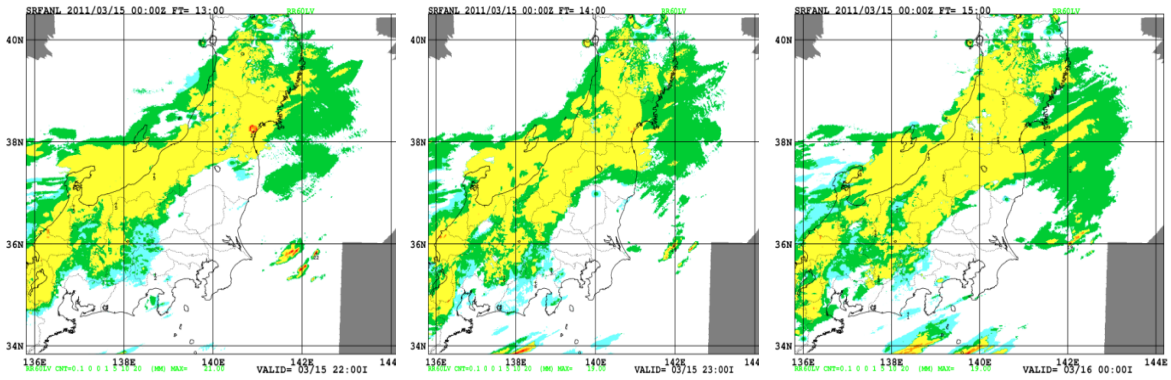

Fig. B-3-2. Rainfall intensity (mm) by JMA-RAP for 15 March. 1200-1300 UTC (left), 1300-1400 UTC (center) and 1400-1500 UTC (right). Colour shade corresponds to Fig. B-3-1. After Saito et al. (2015).

B-3-4. File converter kit and WMO FTP site

JMA provided the MESO and RAP data in GRIB2 format to members of the Task Team and UNSCEAR group B. The MESO data is produced on a Lambert conformal projection in the horizontal coordinate and a terrain-following hybrid vertical coordinate. Furthermore, while the GRIB2 format is officially regulated by WMO as a common format to exchange meteorological data, for some users it is not an easy task to decode and process GRIB2. Considering the situation, JMA also prepared a software tool to read and process the MESO and RAP data. This file converter tool is prepared as a UNIX software kit (C-6) and provides the following three functions;

i) conversion of the GRIB2 format data to the FORTRAN sequential binary format data (GrADS),

ii) re-projection of the data from the Lambert conformal projection to a regular latitude-longitude projection,

iii) conversion of the data from terrain-following hybrid vertical coordinates to an isobaric coordinate at user-specified pressure surfaces.

Figure B-3-3 illustrates the conceptual diagram of the file conversion kit. Both the JMA-MESO and RAP data, detailed instructions, and the above mentioned file converter kit were made available to the UNSCEAR community through a password protected FTP site hosted by WMO. The data were once uploaded on the WMO web server to the scientific community for research purposes, and are still available on the understanding that JMA is acknowledged as the data source.

For more details of the converter kit, see Section C-7.

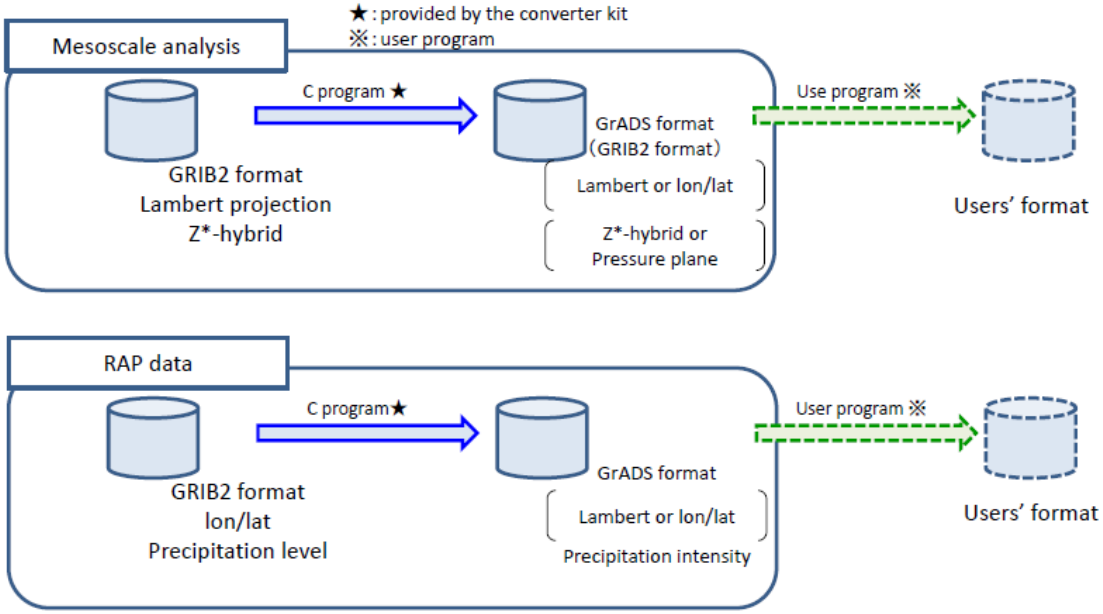

Fig. B-3-3. Conceptual diagram of the file conversion kit provided by JMA. Reproduced from Saito et al. (2015). For more detail, see C-7.

B-4. Offer of Data[1]

The WMO Task Team at its first meeting in Geneva, Switzerland, 30 November - 2 December 2011 (B-2-1 and I-1), determined that all of the observational data collected by JMA are potentially useful in evaluating the meteorological analyses and any subsequent dispersion and deposition calculations using the analysis data, and also, possibly serviceable for use by other groups involved in the UNSCEAR assessment.

Among the observational data, correct precipitation is presumed to be the most critical element in the deposition calculations. In this aspect, JMA agreed to provide its Radar/Rain Gauge analyzed precipitation fields (C-4). Also, the meteorological NWP analysis data created by JMA, namely, the 4D-Var mesoscale analysis (C-2) into which very dense observational data are operationally assimilated, was determined as the most suitable for local and regional scale atmospheric transport, dispersion and deposition modeling (ATDM), while other mesoscale analyses provided by other meteorological centers could possibly be used in the assessment of uncertainty limits to the critical meteorological fields and their inclusion into any future data archive is encouraged. Thus JMA agreed to provide these dataset along with analyzed precipitation data after reprocessing them from their internal archive format to GRIB2 (C-3 and C-5). The mesoscale analysis data was first encoded in the native Lambert Conformal horizontal coordinates on the original model levels (C-7）.

At the meeting the possibility of improvement of the 4D-Var analysis fields by reanalysis with more observational data was discussed, but finally it was agreed that there is not much room for improvement in the 4D-VAR analysis fields. These data were supposed to be provided to Task Team participants for evaluation purposes and subsequently to UNSCEAR after consultation with their data working group.

At the second Task Team meeting, held in London, United Kingdom, 1 - 3 May 2012 (B-2-3 and I-2), it turned out that the JMA high resolution precipitation analyses (derived from radar and rain gauge data) was not yet applied in the computations by members other than NOAA and JMA due to a technical reason related to its coordinates, and JMA suggested offering data conversion software to promote its usage (C-6).

After preliminary provision of the dataset in May 2012, JMA finally provided its Radar/Rain Gauge analyzed precipitation fields and the 4D-Var mesoscale analysis fields, both in GRIB2 format for the period of 11 – 31 March 2011, along with data conversion software in July 2012. The data set was successfully used by most of the members in their ATDM computations.

The JMA data mentioned above were made available to the UNSCEAR community through a WMO-hosted password protected web site with instructions and a file converter kit for different coordinate systems. The data are available to the scientific community for research purposes with acknowledgement (WMO, 2013).

[1] T. Fujita and Y. Honda

C. JMA data and meteorological analyses

C-1. Observation data of JMA[1]

This subsection describes the observation network for Meso-scale NWP system at JMA based on the documents presented at the first Task Team meeting held at Geneva in 2011 (Section B-2-1).

C-1-1. Upper air observations

Figure C-1-1 shows the upper air observation network of JMA as of March 2011. It consists of 31 wind profilers so-called WINDAS (wind profiler data acquisition system) and 16 radiosonde stations. These data are collected at the control center in the headquarters of JMA through the Automated Data Editing and Switching System (ADESS) in real time, and assimilated by the Mesoscale analysis (see C-2).

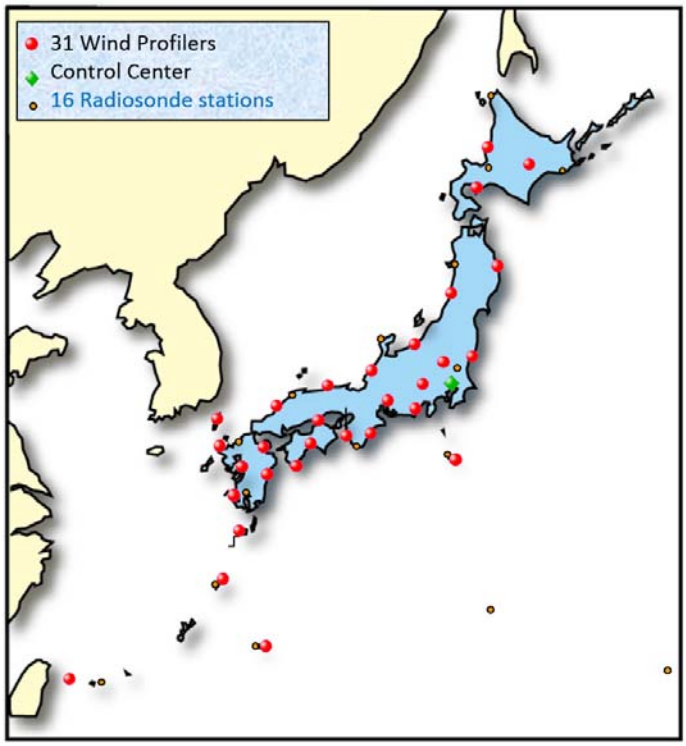

Fig. C-1-1. Upper air observation network of JMA. Large red circles indicate wind profilers, and small orange circles show raidosonde stations. After Saito et al. (2015).

C-1-2. Surface observations

Figure C-1-2 shows the surface observation network of JMA as of March 2011. JMA has totally 1,579 surface observation stations which consist of 156 manned and special automated weather stations (AWSs), and an AWS network so-called AMeDAS (Automated Meteorological Data Acquisition System). In AMeDAS, there are four types of AWSs. They

[1] K. Saito and K. Nagata

are 686 AWSs for precipitation, temperature, wind, and sunshine duration, 79 AWSs for precipitation, temperature and wind, 356 AWSs for precipitation, and 302 AWSs for snow depth. The right figure of Fig. C-1-2 is the enlarged view over East Japan, where averaged horizontal distance of AMeDAS is about 17 km for precipitation. These precipitation data are used for precipitation analysis (section C-4) and the analysis data are assimilated in Meso-scale 4D-VAR Analysis (section C-8).

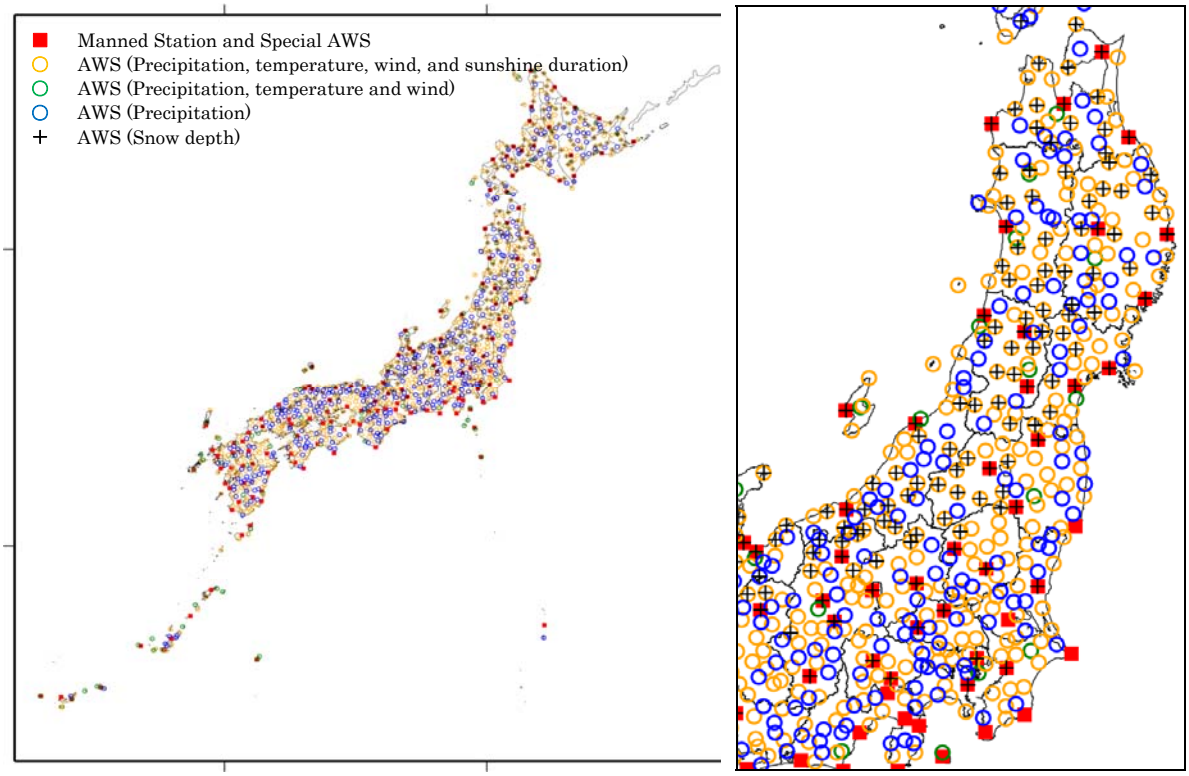

Fig. C-1-2. Left) Surface observations of JMA. Solid squares indicate manned and special AWS station. Red (green, blue) circles indicate AWS. Right) Enlarged view over East Japan.

C-1-3. Radar network

Figure C-1-3 shows the radar network of JMA. As of March 2011, JMA has 20 C-band operational meteorological radars, and 16 of them are Doppler radars[2]. Radar reflectivity data are calibrated and composited by the surface rain gauge data as the precipitation Nowcasting (Fig. C-1-4). Precipitation Nowcasting provides precipitation intensity forecasts of swiftly growing convections with a spatial resolution of 1 km up to an hour ahead to assist disaster prevention activities. Radial winds observed by these Doppler radars and Doppler Radars for Airport Weather are assimilated in Mesoscale 4D-VAR (section C-8).

[2] JMA's all 20 C-band operational radars have been Doppler radar since March 2013.

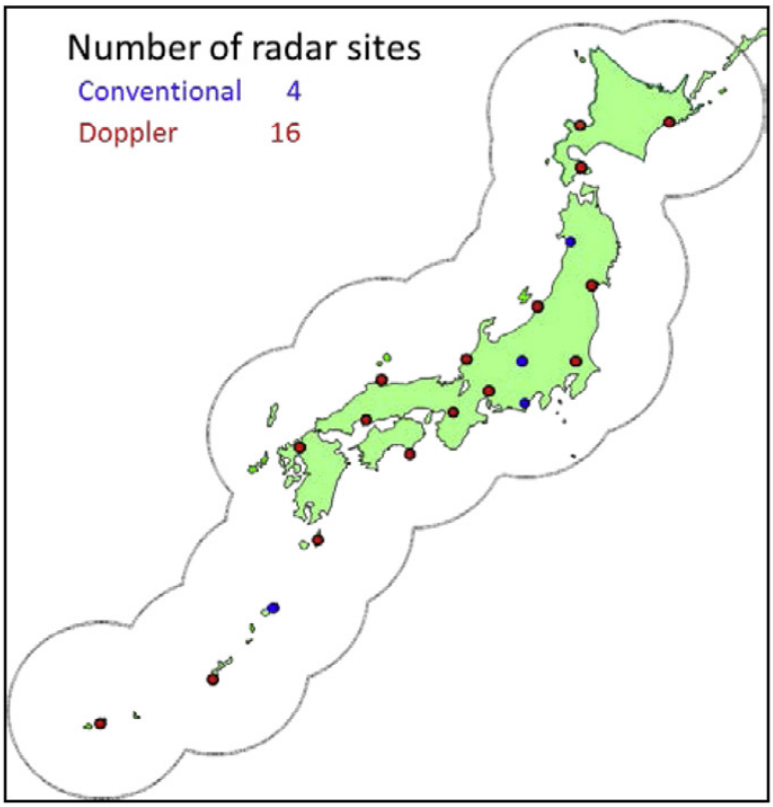

Fig. C-1-3. Weather radar network of JMA as of March 2011. Red circles indicate the Doppler radars and blue circles indicate the conventional radars. Doppler Radars for Airport Weather are not indicated.

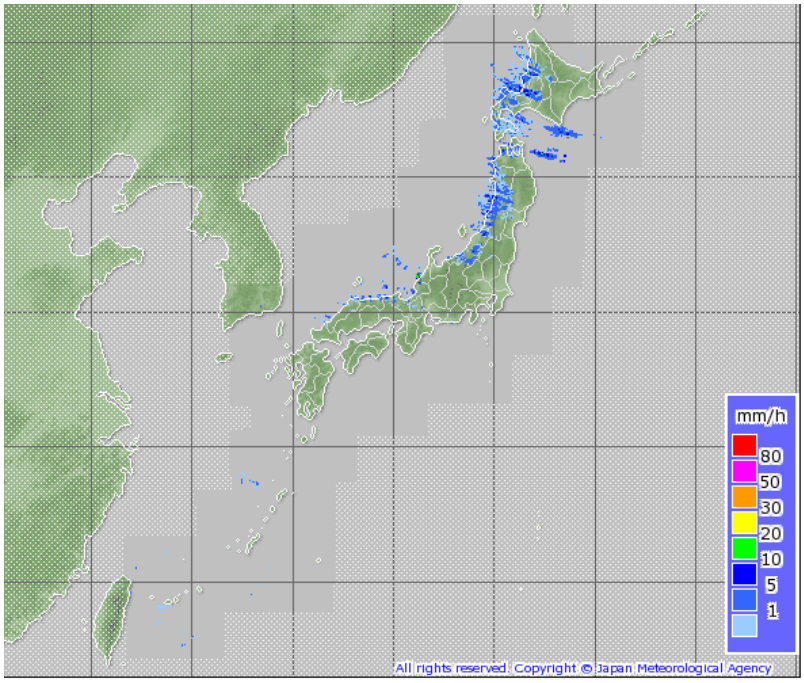

Fig. C-1-4. Example of radar composite precipitation Nowcasting of JMA. .

C-1-4. GPS network

Figure C-1-5 shows GPS ground receiver network by the Geospatial Information Authority of Japan, so-called GEONET. GEONET was originally deployed to obtain geospatial information in Japan, while total precipitable water vapor (TPW) information is analyzed by JMA in real time (Shoji, 2009). There are about 1,200 GPS stations in GEONET, and GPS-derived TPW data have been assimilated in Meso-scale Analysis since October 2009 (section C-8).

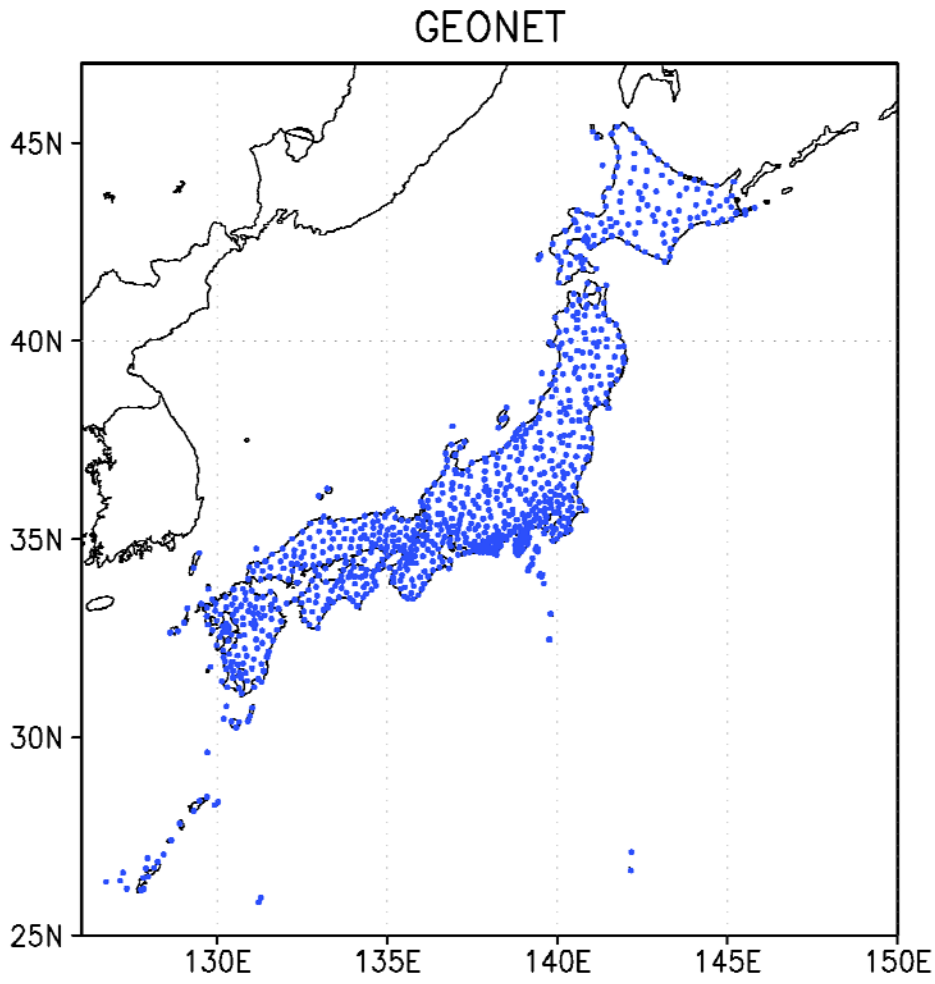

Fig. C-1-5. GPS network by Geospatial Information Authority of Japan.

C-2. NWP system at JMA[1]

This subsection describes operational NWP systems at JMA based on the documents presented at the first Task Team meeting held at Geneva in 2011 (Section B-2-1).

C-2-1. JMA deterministic NWP systems

Table C-2-1 shows deterministic NWP systems of JMA as of March 2011[2]. Two NWP systems are operated in JMA to support its official forecasting. The main objective of the Meso-scale NWP system is to support JMA's short range forecast for disaster prevention. The forecast model operated in the Meso-scale NWP system is the JMA nonhydrostatic model with a horizontal resolution of 5 km (MSM: Meso-Scale Model; Saito et al., 2007; JMA, 2013). Lateral boundary condition is given by the forecast of the JMA global spectral model (GSM). Initial condition of MSM is prepared by Meso-scale Analysis, which employs the JMA nonhydrostatic 4D-VAR system (Section C-8).

Table C-2-2 lists observations used in JMA NWP systems as of March 2011. Here. G means that the data are used in the Global Analysis, M in the Meso-scale Analysis (MESO), L in the Local Analysis, and Q in the hourly analysis. The observations described in C-1 are included in the table (shown in red letters).

Table. C-2-1. Deterministic NWP systems of JMA as of March 2011.

		Global NWP System	Meso-scale NWP System
	Objectives	Short and Medium range forecast	Short range forecast for disaster mitigation
	Forecast Domain	The whole globe	Japan and its surroundings (3600km x 2880km)
NWP Model	NWP Model	Global Spectral Model (GSM)	Meso-Scale Model (MSM)
	Horizontal Resolution	T_L959 (0.1875deg., ~20km)	5km
	Vertical Levels	60 Levels, up to 0.1 hPa	50 Levels, up to about 22km
	Forecast Hours (Initial Times)	084 hours (00, 06, 18UTC) 216 hours (12UTC)	15hours(00,06,12,18UTC) 33hours (03,09,15,21UTC)
Data Assimilation System	Data Assimilation System	Global Analysis (GSM 4D-Var)	Meso-scale Analysis (JNoVA 4D-Var)
	Horizontal Resolution	TL319 (0.5625deg., ~60km)	15km
	Vertical Levels	60 Levels, up to 0.1 hPa	40 Levels, up to around 22km
	Data Cut-Off	+02h20m [Early Analysis]	+50min
		+05h25m (06/18UTC) +11h25m (00/12UTC) [Cycle Analysis]	
	Assimilation Window	-3h~+3h	-3h~0

[1] K. Saito and Y. Honda

[2] JMA has been operating local forecast model (LFM) with a horizontal resolution of 2 km since 2013. Specifications of global and Meso-scale NWP systems have also been enhanced in the following years (JMA, 2013).

Table. C-2-2. Observations used in JMA NWP systems as of March 2011.

	Kind	P	T	UV	RH	IPW	RR	Doppeler Velocity	Radiance	Refractivity
Direct Observations	Land Surface Observations	GM	L	L						
	Automated Weather Stations		LQ	LQ						
	Sea Surface Observations	GM	GM							
	Aircraft Observations		GMLQ	GMLQ						
	Upper Air Sounding	GM	GM	GM	GM					
	Upper Air Wind Profiles	GM		GM						
Remote Sensing	Wind Profiler			GMLQ						
	Doppler Radar							MLQ		
	Radar/Raingauge-Analyzed Precipitation						M			
	Radar Reflectivity				M					
	Ground-Based GPS					ML				
Bogus	Typhoon Bogus	GM		GM						
GEO Satellite	Atmospheric Motion Vector			GMQ						
	Clear Sky Radiance								GM	
LEO Satellite	Polar Atmospheric Motion Vector			G						
	Microwave Sounder								GM	
	Microwave Imager						M		GM	
	Scatterometer			G						
	GPS Radio Occultation									G

C-2-2. History of operational Meso-scale NWP system at JMA

The first operational Meso-scale NWP system at JMA started in March 2001 using a spectral hydrostatic model. The horizontal resolution was 10 km, the number of vertical levels was 40, and the forecast was conducted every six hours. The forecast model was replaced by the JMA nonhydrostatic model in 2004 (Saito, 2006) and the model resolution, vertical model levels, and operation time interval were enhanced to 5 km, 50 levels, and 3 hour in 2006, respectively. Fig. C-2-1 shows the model domain of MSM as of March 2011, which covers Japan and its surrounding areas with grid numbers of 721x577 (3,600 km x 2,890 km)[3]. The main purpose of the Meso-scale NWP system is to support short-term weather forecast for disaster prevention, while its forecasts are used for very short range precipitation forecast and forecast for aviation (Terminal Area Forecast, TAF).

[3] The model domain of MSM has been enlarged to 4,320 km x 3,300 km since March 2014 (JMA, 2014).

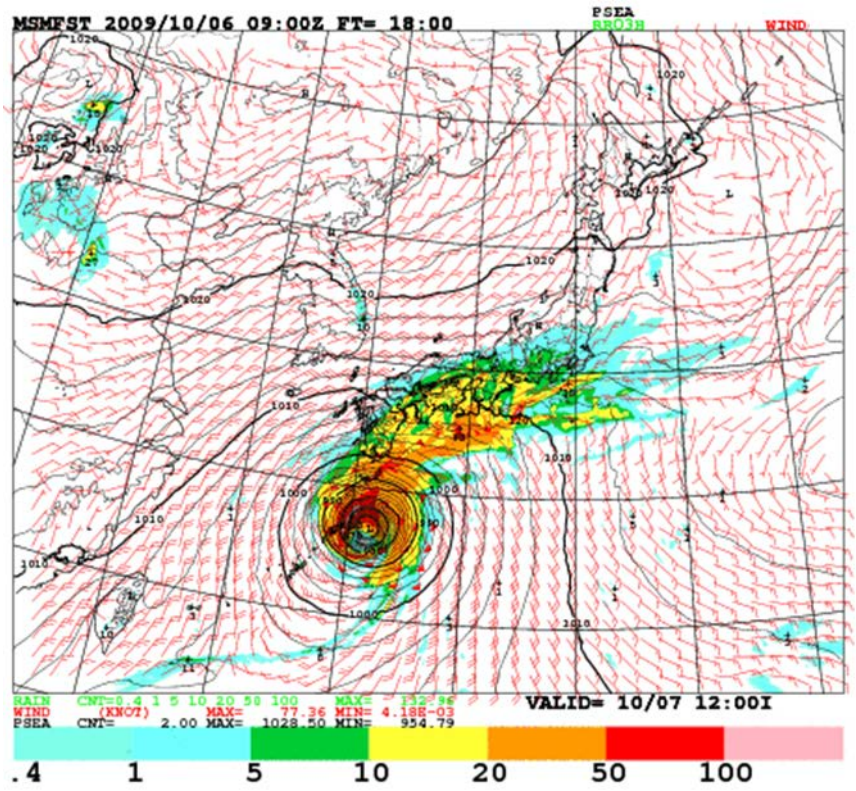

Fig. C-2-1. Domain of MSM (as of 2011) and an example of its forecast.

Several modifications have been done to Meso-scale NWP system since its start of 2001. Table C-2-3 lists the main modifications added to the operational Meso-scale NWP system at JMA from 2001 to 2011. It includes the modifications of the data assimilation system and the use of observation data, such as the implementation of JMA nonhydrostatic 4DVAR in 2009 (Section C-9),introduction of the global positioning system (GPS)-derived total precipitable water vapor (TPWV) data in 2009 (Ishikawa, 2010), and introduction of 1D-Var retrieved water vapor data from radar reflectivity in 2011 (Ikuta and Honda, 2011).

These modifications have contributed to the remarkable improvement of the QPF performance of MSM (Fig. C-2-2).

Table. C-2-3. Modifications for operational Meso-scale NWP system at JMA up to 2011. After Saito (2012).

Year. Month	Modification
2001. 3	Start of Meso-scale NWP system (10kmL40+OI)
2001. 6	Wind profiler data
2002. 3	Meso 4D-Var
2003. 10	SSM/I microwave radiometer data
2004. 7	QuikSCAT Seawinds data
2004. 9	Nonhydrostatic model
2005. 3	Doppler radar radial winds data
2006. 3	Enhancement of model resolution (5kmL50)
2007. 5	Upgrade of physical processes
2009. 4	Nonhydrostatic 4D-Var
2009. 10	GPS total precipitable water vapor (TPWV) data
2011. 6	Water vapor data retrieved from radar reflectivity

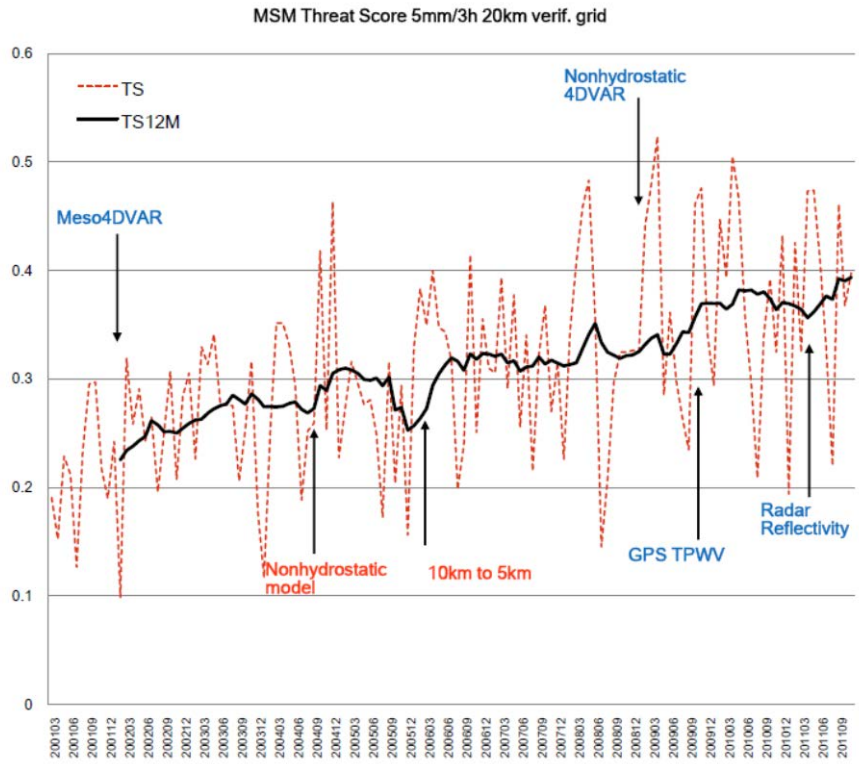

Fig. C-2-2. Domain Threat score of MSM for three-hour precipitation averaged for FT = 3 h to 15 h with a threshold value of 5 mm/3 hour from March 2001 to November 2011. The red broken line denotes the monthly value, while the black solid line indicates the 12-month running mean. After Saito (2012).

C-3. Data configurations of JMA mesoscale analysis[1]

For the task team, the 4D-VAR mesoscale analysis (MA) data in the GRIB2 format, bit-oriented data exchange format standardized by the World Meteorological Organization (WMO) Commission for Basic Systems (CBS) were provided in May 2012. Data configurations of provided data are described as follows:

Horizontal grid numbers: 719 in an x-direction and 575 in a y-direction,

Horizontal resolution: 5 km,

Vertical layers: 48 with the terrain following hybrid vertical coordinate,

Model top height: 21.801km,

Map projection: Lambert conformal conic projection with standard latitudes of 30°N and 60°N, and standard longitude of 140°E, and grid point of (488, 408) corresponds to 30°N and 140°E.

Here grid point of (1, 1) is located at the northwestern edge. Three kinds of files in the GRIB2 format were provided, found in detail in Table C-3-1; the first is model plain data including atmospheric elements such as winds, temperature and hydrometeors, the second is surface land data, and the last is sea surface temperature data.

For the scientific basis of JMA 4D-VAR mesoscale analysis, see C-8.

[1] T. Kato, T. Hara and N. Nemoto

Table C-3-1. Mesoscale analysis (MA) data in the GRIB2 format provided by JMA.

Model plain data of JMA mesoscale analysis

File name: jma_ma_met_hybrid-coordinate_yyyyMMddhhmm.grib2bin

Element		Unit	Layer	Grib code
U	x-wind speed on Lambert projection	m/s	1,2,--,48	0,2,2
V	y-wind speed on Lambert projection	m/s	1,2,--,48	0,2,3
W	z-wind speed	m/s	1,2,--,48	0,2,9
Z	height *	m	surface 1,2,--,48	0,3,5
PT	potential temperature	K	1,2,--,48	0,0,2
QV	water vapor mixing ratio (specific humidity)	kg/kg	1,2,--,48	0,1,2
QC	cloud water mixing ratio	kg/kg	1,2,--,48	0,1,22
QR	rain water mixing ratio	kg/kg	1,2,--,48	0,1,24
QCI	cloud ice mixing ratio	kg/kg	1,2,--,48	0,1,23
QS	snow mixing ratio	kg/kg	1,2,--,48	0,1,25
QG	graupel mixing ratio	kg/kg	1,2,--,48	0,1,32
P	pressure	Pa	surface 1,2,--,48	0,3,0
PSEA	sea level pressure	Pa	surface	0,3,1
RAIN	previous 3-hour accumulated precipitation amount	kg/m^2	surface	0,1,8

*) Terrain height of model is stored as surface in Z.

Surface land data of JMA mesoscale analysis

File name: jma_ma_land-surface_yyyyMMddhhmm.grib2bin

Element		Unit	Grib code
TUGD	soil temperature (4 layers) *	K	2,0,2
KIND	surface kind (1-4) **		2,192,0

*) depth of layers from the surface: 0.02m, 0.115m, 0.39m, 0.89m

**) 1: no snow on land, 2: no ice over the sea, 3: snow on land, 4: ice over the sea

Surface ocean data of JMA mesoscale analysis

File name: jma_ma_ocean_sst_yyyyMMddhhmm.grib2bin

Element		Unit	Grib code
SST	sea surface temperature	K	10,3,0

C-4. Quantitative Precipitation Estimation (QPE) and Quantitative Precipitation Forecasting by JMA[1]

Radar/Rain gauge-Analyzed Precipitation (referred to here as “R/A”) is a QPE product of JMA (see Fig. C-4-1). It shows one-hour cumulative rainfall with a spatial resolution of 1 km, and is issued every 30 minutes.

JMA collects data from about 10,000 rain gauges operated by JMA (see Fig. C-1-2), the Ministry of Land, Infrastructure, Transport and Tourism (MLIT) and local governments every ten minutes or every hour (rain gauges are located in every 7-km grid square on average) and data from 46 C-band radars operated by JMA (see Fig. C-1-3) and MLIT with a spatial resolution of 1 km every five minutes. Each radar covers an area of 500 km × 500 km. All of these data are used for producing the R/A.

The R/A data are produced with the following steps. First, echo intensity data obtained every five minutes are accumulated. If echoes move too fast, one-hour accumulated echo intensities sometimes show an unnatural striped pattern. To avoid such unnatural patterns, accumulation is conducted taking account of echo movements.

Second, to produce accurate R/A, calibration of one-hour accumulated radar data is performed to fit the distribution of one-hour accumulated rain gauge data. Calibration is conducted in two steps. First, each piece of radar data is calibrated to fit averaged rain gauge data within the relevant observation range. Then, detailed calibration of radar data over land is conducted to fit rain gauge data on local scales.

After the above calibration, R/A is produced using the calibrated accumulation of echo intensities by transforming the coordination from zenithal projection into latitude-longitude grids with equidistant cylindrical projection. Nagata (2011) which explains how to produce R/A in detail is carried in the following pages. Further, JMA has issued “High-resolution Precipitation Nowcasts” since August 2014.

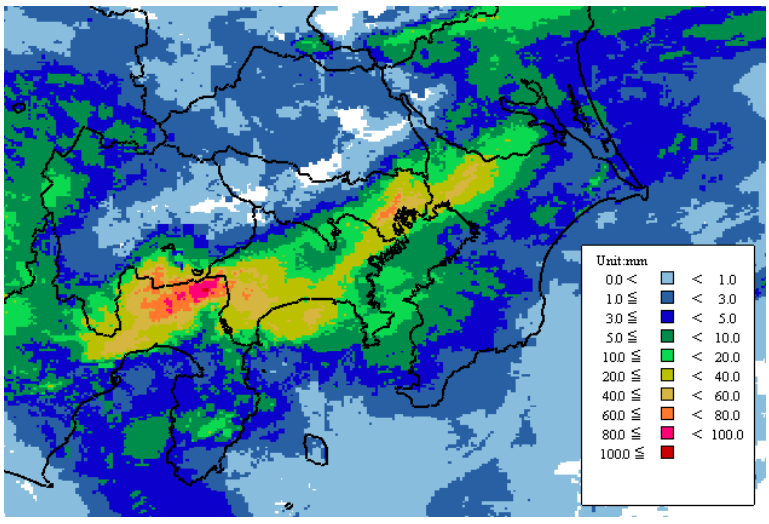

Fig. C-4-1. Sample of R/A product (06 UTC, 8 Sep. 2010).

[1] K. Nagata

Quantitative Precipitation Estimation and Quantitative Precipitation Forecasting by the Japan Meteorological Agency

Kazuhiko NAGATA
Forecast Division, Forecast Department
Japan Meteorological Agency

1. Introduction

Typhoons sometimes hit countries in East Asia and Southeast Asia, and may bring various hazards including sediment-related disasters, flooding and inundation. To prevent and mitigate damage from such disasters, analysis and forecasting of precipitation amounts is very important. Analysis relating to the distribution of rainfall amounts is called Quantitative Precipitation Estimation (QPE), and that relating to forecasting is called Quantitative Precipitation Forecasting (QPF). The Japan Meteorological Agency (JMA) developed QPE and QPF products as well as QPE/QPF-induced products using radar data, rain gauge data and numerical weather prediction (NWP) output. Figure 1 shows the relationships that link these various data and products, including QPE and QPF.

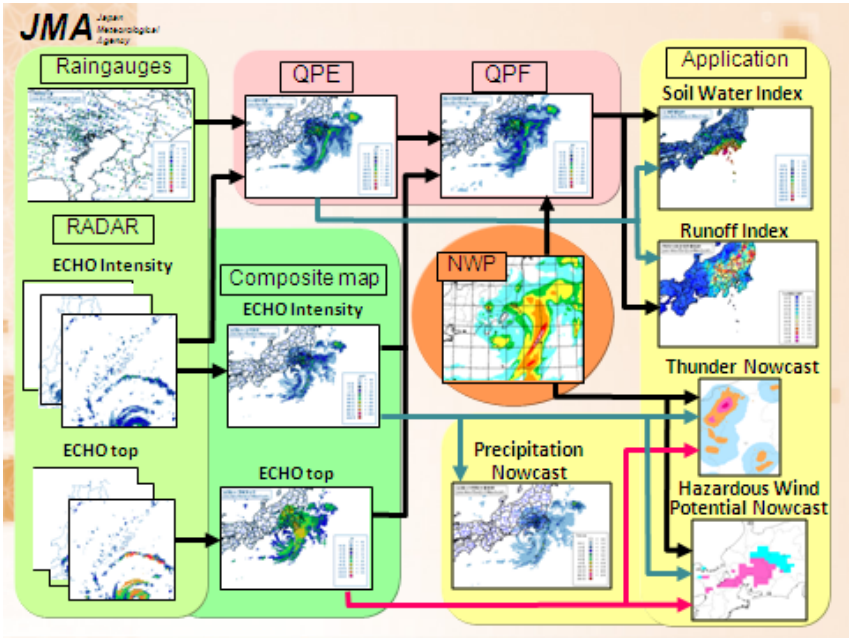

Fig. 1 Various precipitation products derived from rain gauge and radar data

2. Radar/Rain gauge-Analyzed Precipitation

Radar/Rain gauge-Analyzed Precipitation (referred to here as “R/A”) is a QPE product of JMA. It shows one-hour cumulative rainfall with a spatial resolution of 1 km, and is issued every 30 minutes. Figure 2 shows a sample.

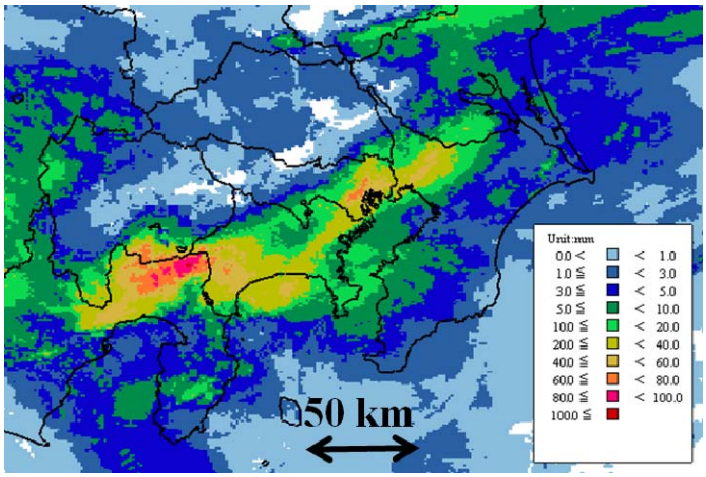

Fig. 2 Sample of R/A product (06 UTC, 8 Sep. 2010)

2.1 Observation data used to produce R/A

Both rain gauge and radar data are used to produce R/A. Although rain gauges measure precipitation amounts with satisfactory accuracy, they can observe only at a single point. Conversely, radars can observe large areas at the same time with a higher spatial resolution than the rain gauge network, but may produce readings different from those obtained with a ground-based rain gauge as they measure amounts of rain overhead. Their accuracy is also not as reliable as that of rain gauges because they are remote sensing instruments. For monitoring and prediction of sediment-related disasters, flooding and inundation, the rain gauge network is too rough and radar observation lacks sufficient accuracy. For this reason, JMA produces R/A by calibrating one-hour accumulated radar echo data with one-hour accumulated rain gauge precipitation data. It collects data from 10,000 rain gauges operated by JMA, the Ministry of Land, Infrastructure, Transport and Tourism (MLIT) and local governments every ten minutes or every hour (rain gauges are located in every 7-km grid square on average) and data from 46 C-band radars operated by JMA and MLIT with a spatial resolution of 1 km every five minutes. Each radar covers an area of 500 km × 500 km.

2.2 R/A algorithms

The procedure for producing R/A involves the following three steps:

1. Accumulation of radar intensity data
2. Calibration of radar data
3. Composition of calibrated radar data

This section briefly describes each process.

2.2.1 Accumulation of radar intensity data

First, echo intensity data obtained every five minutes are accumulated. If echoes move too fast, one-hour accumulated echo intensities sometimes show an unnatural striped pattern (see the image on the left of Fig. 3). To avoid such unnatural patterns, accumulation must be conducted taking account of echo movements (see the image on the right of Fig. 3). In this process, the observed echoes are divided into pieces and traced every five minutes. Then, by summing up the echo intensities passing a grid, the one-hour accumulated echo intensity of the grid is estimated. Quality checking of echo intensities is also conducted at this stage.

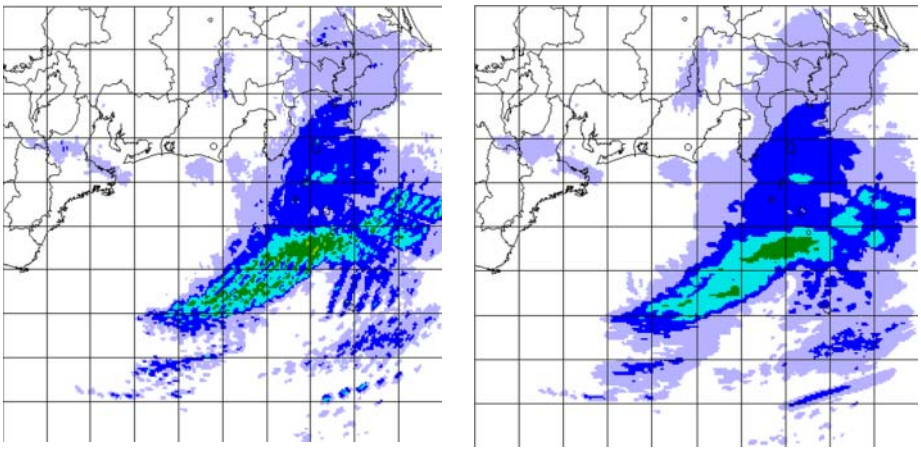

Fig. 3 Accumulation of radar intensity data
Left: one-hour accumulated echoes; right: as per the figure on the left, but with consideration of echo movements

2.2.2 Calibration of radar data

To produce accurate QPE, calibration of one-hour accumulated radar data is performed to fit the distribution of one-hour accumulated rain gauge data. Calibration is conducted in two steps. First, each piece of radar data is calibrated to fit averaged rain gauge data within the relevant observation range. Then, detailed calibration of radar data over land is conducted to fit rain gauge data on local scales.

2.2.2.1 Calibration over the whole radar observation range

Values of one-hour precipitation estimated from the accumulation of radar echo intensities in a certain grid are generally different from observation values from a rain gauge in the grid. As rain gauge measurement is more reliable, the accumulation of radar echo intensities is calibrated with rain gauge observations within the radar observation range to meet the following two conditions:

(1) The average of the calibrated accumulation for radar echo intensities over a certain domain should be equal to that of all other radars observing the same domain.
(2) The average of the calibrated accumulation for radar echo intensities over a certain grid should be equal to the average of the rain gauge observations.

Figure 4 shows a sample of this calibration. The figure on the left shows one-hour precipitation estimated

from the accumulation of radar echo intensities; the central figure shows one-hour precipitation after calibration to meet the two conditions outlined above; and the figure on the right shows the one-hour precipitation observed by rain gauges. The original accumulation of radar echo intensities (left) in a certain grid is less than the rain gauge observation in the same grid (right). Due to calibration, the central figure shows more precipitation than that on the left. The figure on the right is closer to the central figure than the left figure.

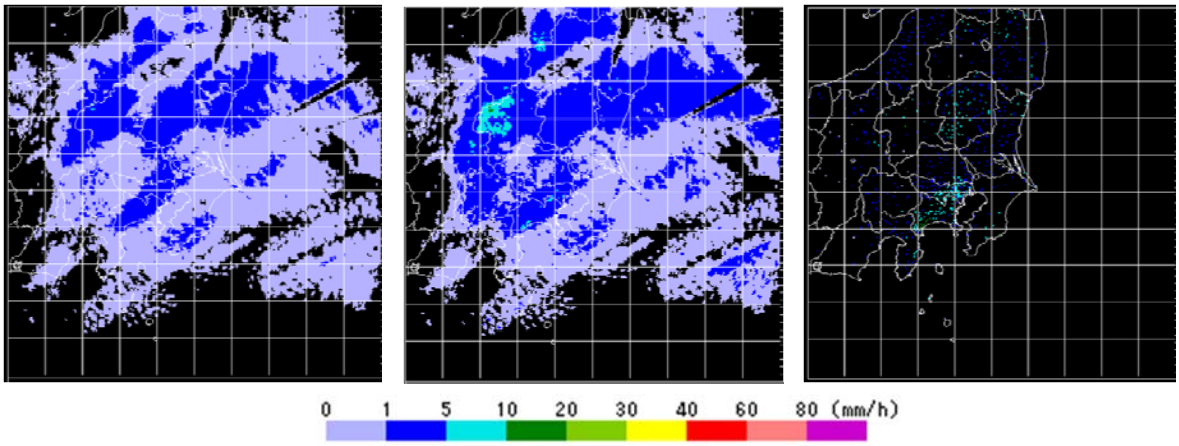

Fig. 4 Left: sample of one-hour precipitation estimated by accumulating echo intensities; center: after calibration; right: from raingauge observations

2.2.2.2 Calibration over land

The calibrated echo intensities explained above are further calibrated to enable expression of more detailed patterns of precipitation on local scales (Makihara, 2000). For example, the calibrated accumulation of echo intensities for a certain grid *g* derived using the method described in 2.2.2.1 is calibrated again using data from rain gauges within about 40 km of that grid. A calibration factor for grid *g* is calculated with weighted interpolation of the calibration factors of the surrounding grids that contain rain gauges within 40 km of the grid. Here, the calibration factor for the grid is defined as the ratio of rain gauge observation values to the calibrated accumulation of radar echo intensities in the grid using the method outlined in 2.2.2.1. The following factors are taken into account to calculate the weight of interpolation:

(1) Distances between grid *g* and rain gauges
(2) Differences between echo intensity for grid *g* and those for grids containing rain gauges
(3) Beam attenuation rate for precipitation
(4) Uniformity of rain gauge distribution

Multiplying the calibrated echo intensities by the calibration factor as determined above gives the estimated precipitation for grid *g*.

Figure 5 shows a sample of this calibration. The figure on the left shows calibrated accumulation of radar

echo intensities calculated using the method outlined in 2.2.2.2, and that on the right shows one-hour rain gauge data (in the same way as the image on the right of Fig. 4). The figure on the left matches the rain gauge data better than the central image in Fig. 4.

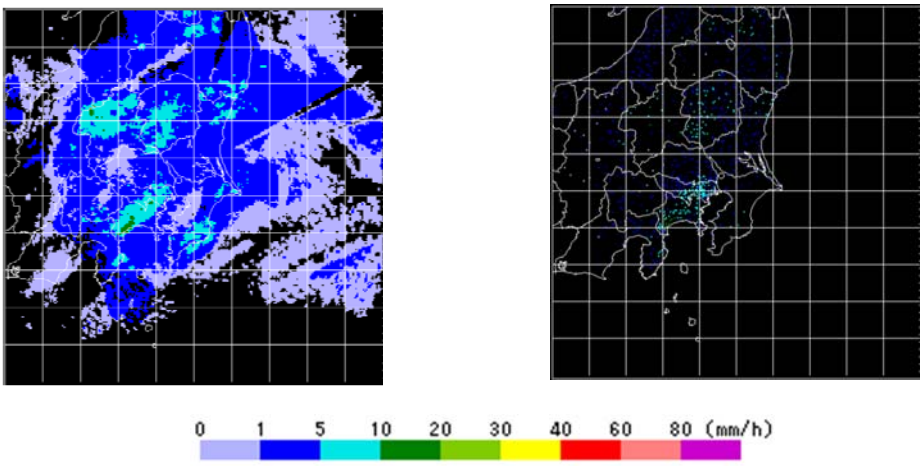

Fig. 5 Left: sample of one-hour precipitation after calibration over land; right: the corresponding raingauge observations (as per the image on the right of Fig. 4)

2.2.3 Composition of calibrated radar data

After the above calibration, a composite precipitation map is produced using the calibrated accumulation of echo intensities calculated using the method outlined in 2.2.2.2 from 46 radars located around the country by transforming the coordination from zenithal projection into latitude-longitude grids with equidistant cylindrical projection. If two or more radars observe the same grid, the greater value is selected. Figure 6 shows calibrated echo intensities covering each region and a composite precipitation map of the country.

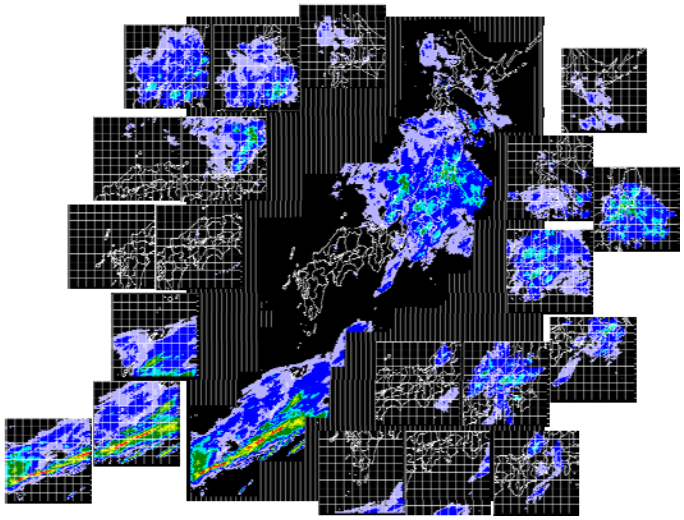

Fig. 6 Radar data covering each region and a composite precipitation map

2.3 Accuracy of R/A

To assess the accuracy of R/A, experimental R/A data for verification excluding rain gauge data at about 200 observing points were prepared, and were compared with the excluded rain gauge data. Rain gauge observation values were compared with R/A values for nine grids (a central grid and the eight grids surrounding it) considering location errors equivalent to the dimensions of one grid (i.e., 1 km) stemming from wind-related advection of raindrops before their arrival at ground level, and/or errors resulting from coordinate transform.

Figure 7 shows a scatter plot comparing hourly R/A values and corresponding rain gauge measurements taken over a period of four months during the warm season (from August to November of 2009). Only the best R/A values out of the nine grids are plotted. The figure shows close agreement between R/A values and rain gauge measurements.

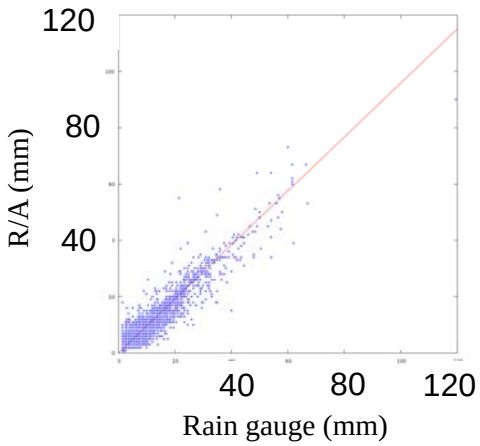

Fig. 7 Scatter plot of R/A and rain gauge data with a regression line (red) (R/A = 0.96 × Raingauge)

3. Very-short-range Forecasting of Precipitation

Very-short-range Forecasting of Precipitation (referred to here as “VSRF”) is a QPF product of JMA. It provides hourly precipitation forecasting up to six hours ahead with a spatial resolution of 1 km. VSRF is calculated by merging the forecast precipitation with values from JMA’s mesoscale model (MSM) and the extrapolated composite echo intensity. Figure 8 shows a sample of VSRF. An outline of the procedures for producing VSRF is given below.

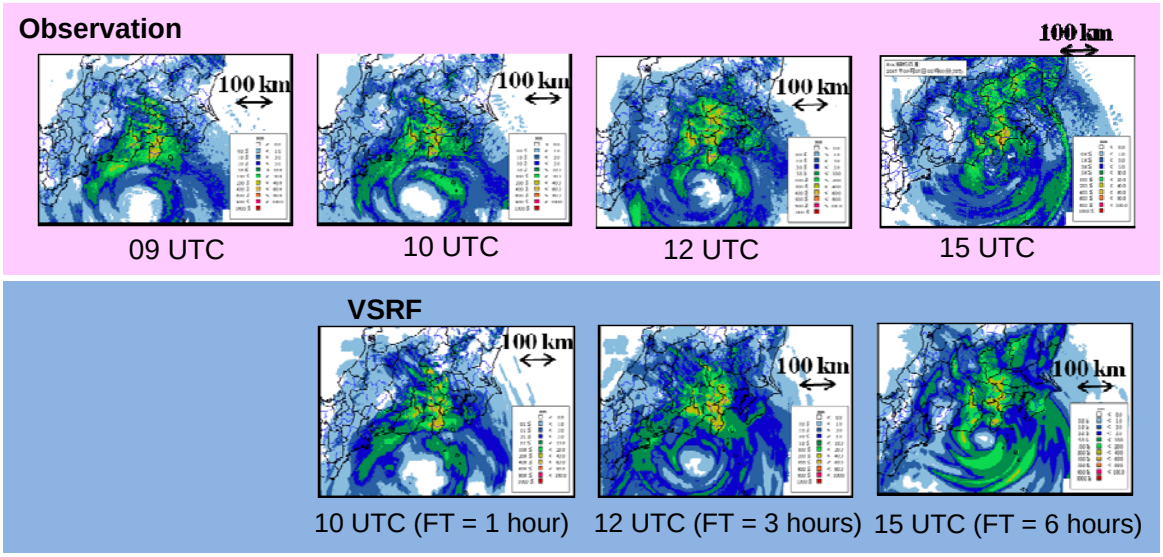

Fig. 8 Sample of VSRF (initial time: 09 UTC, 6 Sep. 2007)

3.1 VSRF algorithms

Generally, extrapolation is the best method of precipitation forecasting for a time frame within a few hours from the present. However, a numerical model gives better performance gradually over time. JMA therefore conducts VSRF by both using extrapolation and merging model output. The procedure for producing VSRF consists of two parts:

1. The extrapolation method
2. The merging method

3.1.1 Extrapolation method

3.1.1.1 Movement vectors

First, the area over Japan is divided into 50-km grid squares. Then, the movement vectors of precipitation systems are estimated for every 50-km grid using a pattern matching method, which indicates the systems' direction and speed of movement. In order to avoid any adverse influence from orographic effects on this estimation[1], time subtractions of R/A are used. Thirty candidates for movement vectors in the grid with the highest matching scores are obtained accordingly using the differences among R/A (t = 0 h), R/A (t = -1 h), R/A (t = -2) and R/A (t = -3 h). Then, the most suitable candidate vector is selected in consideration of time-space smoothness. Movement vectors gradually approach the speed of 700-hPa winds of the MSM as the forecast time increases. Figure 9 shows a sample of a movement vector (left) and the one-hour accumulated precipitation forecast with this movement vector (right).

[1] Orographic effects in a grid cause precipitation systems to look static or appear to move more slowly than they actually do.

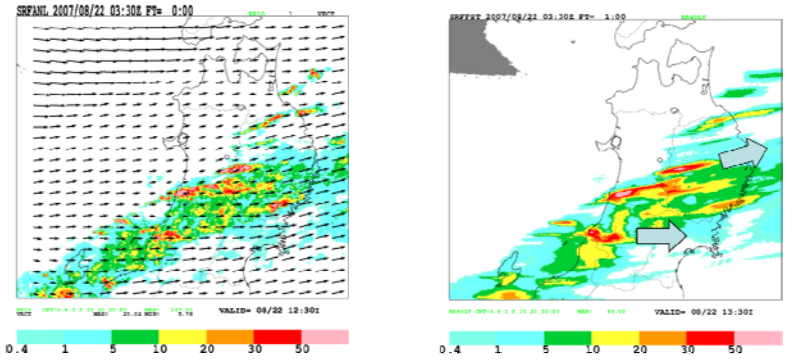

Fig. 9 Sample of movement vectors and forecast one-hour accumulated precipitation
Left: initial echo intensity (shading) and movement vectors (arrows); right: forecast one-hour accumulated precipitation. The block arrows show precipitation system direction of movement.

3.1.1.2 Orographic effects

Precipitation caused by orographic enhancement is sometimes seen to be stationary over the windward side of mountains. The algorithm follows the concept of the seeder-feeder model (Browning & Hill, 1981). Rainfall passing through a feeder cloud generated by orographic effects becomes enhanced due to water droplets in the feeder cloud.

Precipitable water, which is estimated using data for temperature, relative humidity and wind from the surface to 850 hPa in the MSM, is used to judge whether feeder clouds are generated. If so, precipitation is enhanced depending on the amount of rainfall from the seeder cloud. Figure 10 shows orographic enhancement of precipitation.

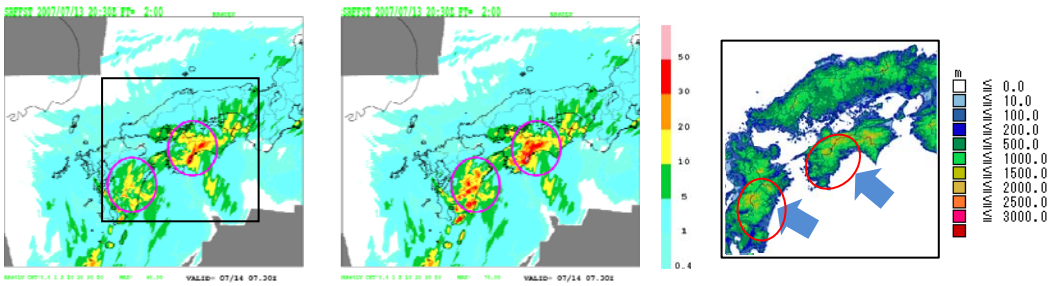

Fig. 10 Orographic enhancement (inside the circles of the figures to the left and center)
Left: forecast one-hour accumulated precipitation without orographic effects; center: as per the image on the left, but with orographic effects; right: altitude map showing the square area from the figure on the left. The block arrows show precipitation system direction of movement.

The dissipation of echo on the lee side of mountains is also considered. This occurs when the echo top is low, the angle between the directions of mid- and low-level winds is small, and no echoes are present in the dissipation area. Echo dissipation is clearer when echo intensity is stronger and the travel time from the mountaintop to the dissipation area is longer. Echo dissipation is estimated statistically from 700-hPa winds, 900-hPa winds and the relative humidity of the MSM. Figure 11 shows a case of echo dissipation.

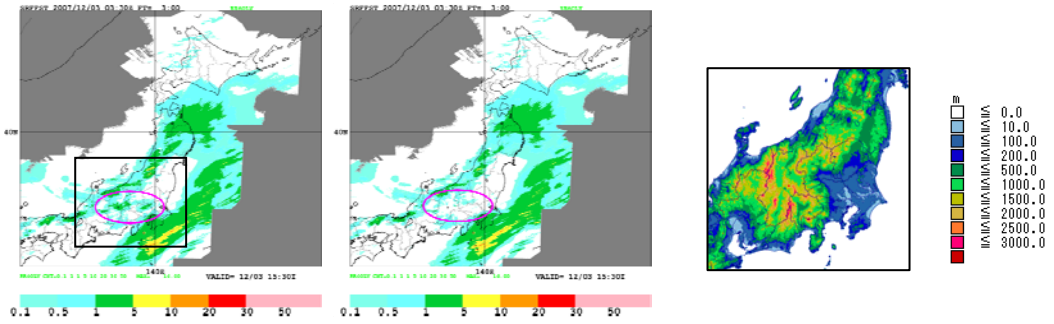

Fig. 11 Echo dissipation (inside the circles of the figures to the left and center)
Left: forecast one-hour accumulated precipitation without orographic effects; center: with orographic effects; right: topographic map with altitude showing the square areas from the figures to the left and center.

3.1.1.3 Accumulation of forecast intensity

The initial field used for VSRF is a composite echo intensity field obtained in the process of making R/A. The echo intensity field is shifted along the movement vector with a time step of two or five minutes. One-hour precipitation at a particular point is calculated as the sum of the echo intensities passing that point. In the process, enhancement and dissipation of precipitation due to orographic effects are considered.

3.1.2 Merging of extrapolation method and MSM

The performance of the conventional extrapolation method is satisfactory up to three to four hours from the initial time. For forecast times of more than six hours, the results of the MSM are considered superior to those of the extrapolation method. It is expected that four- to six-hour forecasts can be improved by merging the results of the extrapolation method and those of the MSM with a different blending ratio over time. The blending ratio is estimated from the accuracy levels of the extrapolation method and the MSM over the past few hours (Araki, 2000). VSRF is the output of this merging process, for which a sample is shown in Figure 12. The precipitation in the red circle for VSRF is from an extrapolation method forecast, and that in the blue circle is from the MSM. R/A more closely corresponds to VSRF than to extrapolation method forecasting and the MSM due to the merging of the extrapolation method forecast and the MSM.

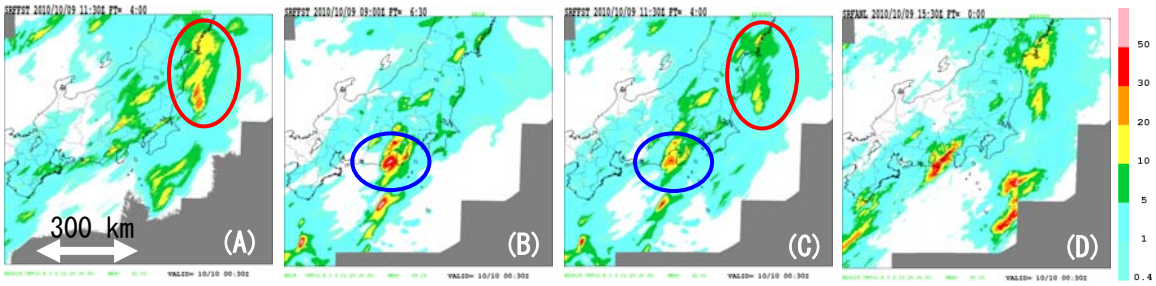

Fig. 12 Merging process

Forecasting with (A) the extrapolation method, (B) the MSM and (C) VSRF for 1530 UTC on 9 Oct., 2010, and (D) R/A for the same time. The initial time of (A) and (C) is 1130 UTC (FT = 4), and that of (B) is 0900 UTC (FT = 6.5). Precipitation in the red circle for VSRF originates from the extrapolation method, and that in the blue circle originates from the MSM. The amount of precipitation depends on the blending ratio.

3.2 Accuracy of VSRF

Critical Success Index (CSI) values for VSRF, the extrapolation method (EXT), the MSM and the persistent forecast (PST) for averaged hourly precipitation from June to August 2010 are shown in Fig. 13. Here, the region over Japan was divided into 20-km grid squares. The threshold of rainfall is 1 mm/hour. The figure shows that VSRF exhibits superior performance over the whole forecast time.

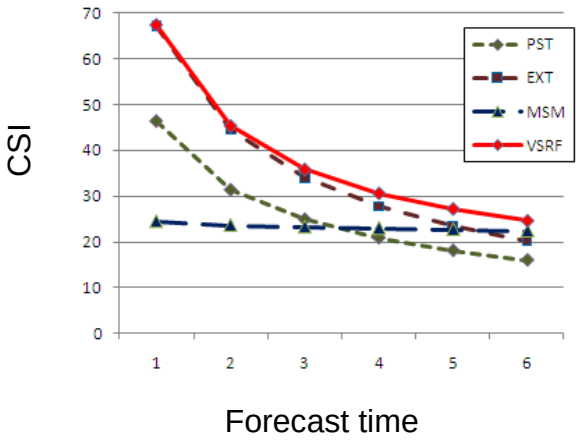

		Event observed	
		Yes	No
Event forecast	Yes	A	B
	No	C	D

$$CSI = A / (A + B + C) \times 100$$

Fig. 13 CSI of VSRF, the extrapolation method (EXT), the MSM and the persistent forecast (PST) verified from June to August 2010

4. Applications of QPE/QPF

Precipitation figures alone do not provide enough information for forecasters to monitor and forecast sediment-related disasters because such events are closely linked to the amount of moisture in the soil. JMA uses the Soil Water Index to monitor and forecast sediment-related disasters.

Precipitation figures alone also provide insufficient information for forecasters to monitor and forecast flood disasters because such events are closely linked to the amount of water outflow to rivers as well as the time lag of water as it moves along river channels. JMA uses the Runoff Index to monitor and forecast flood disasters.

4.1 Soil Water Index

The Soil Water Index (referred to here as the "SWI") is calculated up to six hours ahead with a spatial resolution of 5 km showing the risk of sediment-related disasters (debris flow, slope failure, etc.) caused by heavy rain. Figure 14 shows a sample of the SWI.

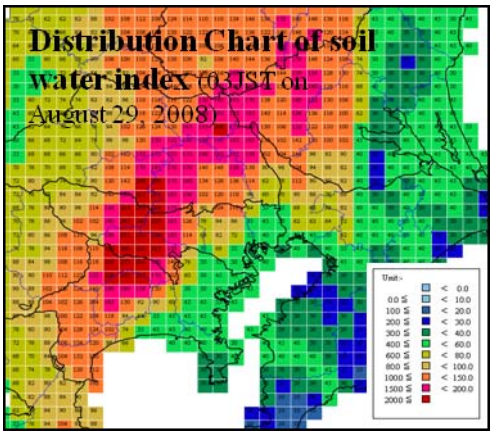

Fig. 14 Soil Water Index distribution chart

The risk of sediment-related disasters caused by heavy rain becomes higher when the amount of moisture in soil increases. Such disasters may sometimes be caused by rainfall from several days before.

The amount of moisture in the soil is indexed using the tank model method to indicate how much rainwater is contained in soil based on rainfall analysis (see Fig. 15). R/A and VSRF are used as input for the tank model.

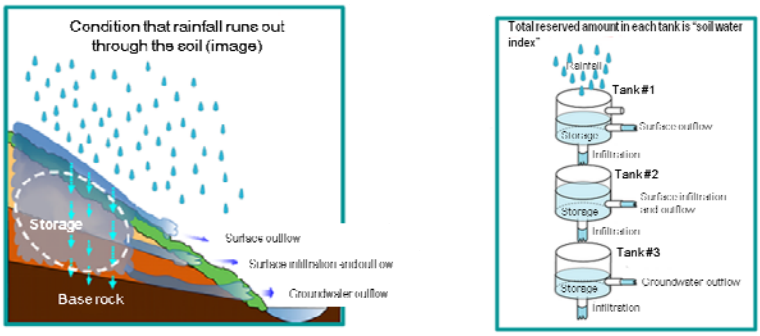

Fig. 15 Outline of tank model
Left: Condition in which rainfall runs out through soil; right: The total reserved amount in each tank is used to form the Soil Water Index.

Sediment-related disasters frequently occur in areas with high SWI values. Figure 16 shows a time-sequence representation of the SWI in a grid where a sediment-related disaster actually occurred. Its timing approximately coincided with the peak SWI value.

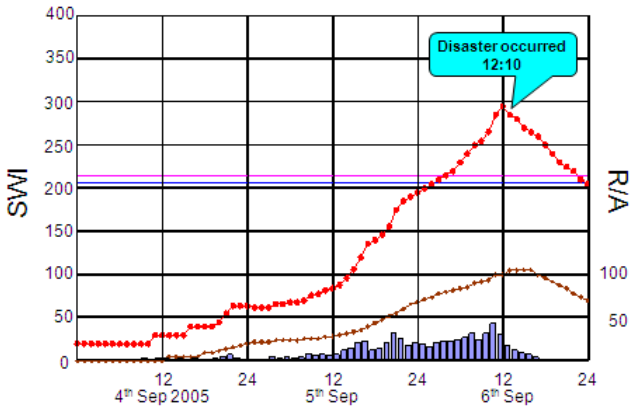

Fig. 16 Time-sequence representation of SWI and rainfall amounts in a grid where a sediment-related disaster occurred. The red line shows the SWI, the brown line shows 24-hour cumulative rainfall, and the bars show 1-hour cumulative rainfall.

Since May 2010, the SWI has been used by forecasters at JMA's meteorological observatories when issuing heavy rain warnings/advisories to call attention to the risk of sediment disasters.

4.2 Runoff Index

The Runoff Index (referred to here as the “RI”) is calculated up to six hours ahead with a spatial resolution of 5 km showing the risk of flooding for individual rivers in the country. The amount of rainfall is not directly linked to the risk of flooding for the following two reasons:

1. There is a time difference between the occurrence of rainfall and increased water levels in rivers.
2. It takes time for water to run down river channels.

Accordingly, when monitoring and forecasting flood risk, the above two effects should also be carefully considered in addition to accurate QPE/QPF (see Fig. 17).

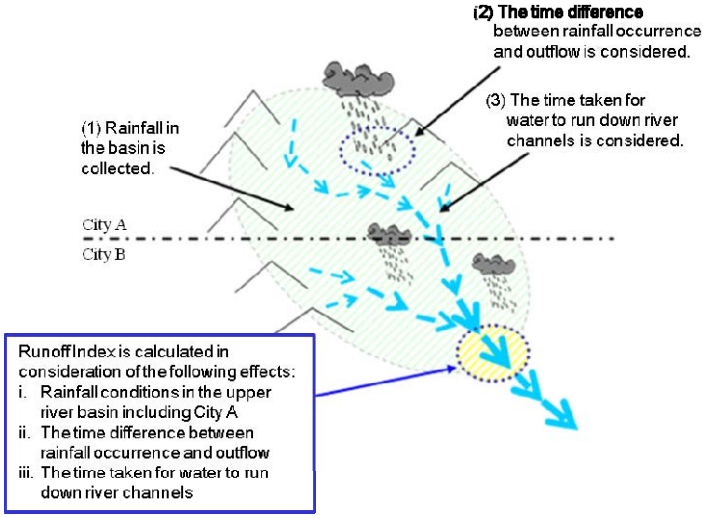

Fig. 17 Three effects to be considered in evaluating flood risk

In the RI, the tank model is used to estimate outflow, and includes the processes of water flowing down the slopes of the basin (covering an area of about 5 km × 5 km) to the river, and then down the river channel. The RI is calculated targeting rivers with a length of 15 km or more. R/A and VSRF are used as inputs for the tank model. Figure 18 shows a sample of the RI.

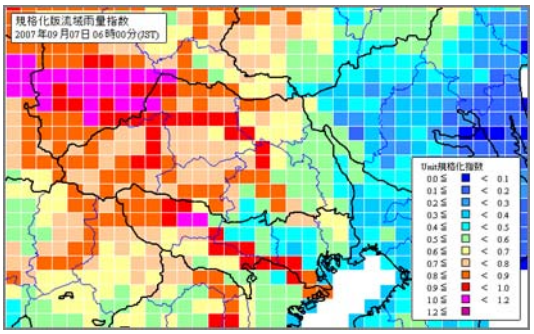

Fig. 18 Sample of the RI shown in 5-km grids

Floods frequently occur in areas with high RI values. Figure 19 shows a time series representation of the RI and water levels in a grid where actual flooding occurred. The time series corresponds closely to the water level of the river.

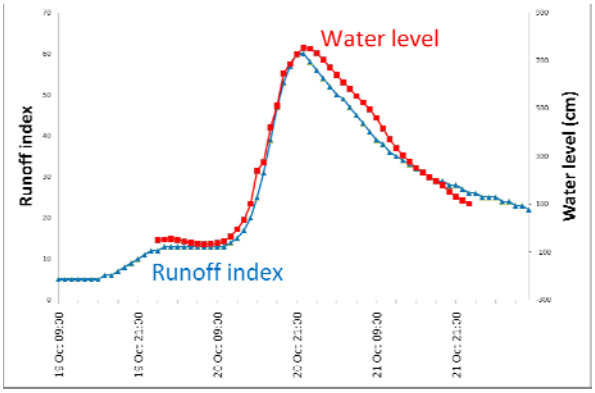

Fig. 19 Time series of the RI and water levels for a grid in which flooding occurred. The red line shows the water level, and the blue line shows the RI.

Since May 2010, the RI has been used by forecasters at JMA's meteorological observatories when issuing flood warnings/advisories to call attention to the risk of flooding.

References

Araki, K., 2000: Six-hour forecasts of precipitation. Reports of the Numerical Prediction Division, **47**, 36 – 41 (in Japanese).

Browning, K. A., F. F. Hill, 1981: Orographic Rain. Weather, **35**, 326 – 329.

Makihara, Y., 2000: Algorithms for precipitation nowcasting focused on detailed analysis using radar and raingauge data, Study on the Objective Forecasting Techniques, Technical Reports of the Meteorological Research Institute, **39**, 63 – 111.

C-5. GRIB2 templates for JMA Radar/Rain gauge-Analyzed Precipitation data[1]

FM 92 GRIB (Gridded Binary) is a standard data format for storing grid data, defined by WMO (World Meteorological Organization). It is a container format made from eight kinds of sections to hold various types of data structure, by selecting templates for grid definition (section 3), product definition (section 4), and data representation (section 5). Each template is identified by 16 bit numbers and is called like DRT (Data Representation Template) 5.200 for example.

The JMA Radar/Rain gauge-Analyzed Precipitation data is stored in GRIB format using two uncommon templates: PDT (Product Definition Template) 4.50008 (R/A product metadata) and DRT 5.200 (run-length encoding). PDT 4.50008 is JMA's local extension, not to be described in the WMO Manual on Codes[2]. DRT 5.200 is an agreed international standard, but the Manual does not contain a description of the compression algorithm for historical reason. Documentation for those templates has been provided in Japanese language only (JMA, 2006).

An English version of the documentation was prepared for the task team activity, and is included in this section for future reference.

[1] E. Toyoda
[2] https://www.wmo.int/pages/prog/www/WMOCodes.html

GRIB2 templates for JMA Radar/Rain gauge-Analyzed Precipitation data: PDT 4.50008 and DRT 5.200

June 27, 2012 (rev5)
TOYODA Eizi
Japan Meteorological Agency

Introduction

Radar/Rain gauge-Analyzed Precipitation (hereafter called R/A) data of Japan Meteorological Agency (JMA) is grid data of precipitation. It is given in standard WMO Code FM92 GRIB Edition 2, but it includes templates not described in WMO Manual on Codes. This document supplements WMO Manual to decode that dataset.

PDT 4.50008

Product definition template (PDT) 4.50008 is locally modified version of PDT 4.8 defined by JMA. This template is identical to standard PDT 4.8 (average, accumulation and/or extreme values or other statistically-processed values at a horizontal level or in a horizontal layer in a continuous or non-continuous time interval) until octet 58, and the rest is additional fields for quality-control purpose.

Octet	Type	Contents	Actual Value
10	Code table 4.1	Parameter category	1 (Humidity)
11	Code table 4.2	Parameter number	200 [Note 1]
12	Code table 4.3	Type of generating process	0 (analysis)
13	Local code	Background generating process identifier	150 (very short range forecast)
14	Local code	Analysis or forecast generating process identifier	255 (missing)
15-16	Integer	Hours after reference time of data cutoff	0
17	Integer	Minutes after reference time of data cutoff	0

18	Code table 4.4	Indicator of unit of time range	0 (minutes)
19-22	Integer	Forecast time in units defined by octet 18	variable
23	Code table 4.5	Type of first fixed surface	1 (surface)
24	Integer	Scale factor of first fixed surface	255 (missing)
25-28	Integer	Scaled value of first fixed surface	$2^{32} - 1$ (missing)
29	Code table 4.5	Type of second fixed surface	255 (missing)
30	Integer	Scale factor of second fixed suraface	255 (missing)
31-34	Integer	Scaled value of second fixed surface	$2^{32} - 1$ (missing)
35-36	Integer	Year — end of overall time interval	variable
37	Integer	Month — end of overall time interval	variable
38	Integer	Day — end of overall time interval	variable
39	Integer	Hour — end of overall time interval	variable
40	Integer	Minute — end of overall time interval	variable
41	Integer	Second — end of overall time interval	variable
42	Integer	Number of time range specifications used in statistical process	1
43-46	Integer	Total number of data values missing in statistical process	0
47	Code table 4.10	Statistical process	1 (Accumulation)
48	Code table 4.11	Type of time increment between successive fields used in statistical process	2 (Same reference time, forecast time incremented)
49	Code table 4.4	Unit of time for time range over which statistical processing is done	0 (minutes)
50-53	Integer	Length of the time range over which statistical processing is done	60
54	Code table 4.4	Unit of time for time increment between the successive fields used	0
55-58	Integer	Time increment between successive	0 (continuous)

		fields	
59-66	Two-bit fields	Radar status block 1 [Note 2]	
67-74	Two-bit fields	Radar status block 2 [Note 2]	
75-82	Flag table	Rain gauge availability [Note 2]	

Notes:

[1] parameter number 200 is used for one-hour precipitation (water equivalent) [mm] with RLE packing scheme (DRT 5.200). Theoretically it should be 52 (Total precipitation rate [kg.m-2.s-1]), since GRIB regulation 92.6.2 discourages use of parameter names not orthogonal to other parts of PDT/DRT. Unfortunately the parameter has tradition much longer than the regulation, thus it cannot be changed for compatibility reasons.
[2] octets 59-82 describe availability and operation status of data sources. Officially the template only describes this blocks as “defined by data producing centre”. Details are given below for informational purpose, but Japan’s National Focal Point for Codes and Data Representation Matters to WMO (not me) may not be aware of recent changes and hence cannot be responsible to different practices.

Radar status block 1 (informational)

Block 1 describes operation status of data sources, mostly radar sites operated by JMA. Place names in capital letters are registered to WMO Publication No.9 Volume A, and number (starting from 47) is station index.

Bits	Type	Description
1-2	R	47415 SAPPORO/KENASHIYAMA
3-4	R	47419 KUSHIRO/KOMBUMORI
5-6	R	47432 HAKODATE/YOKOTSUDAKE
7-8	R	47590 SENDAI
9-10	R	47582 AKITA
11-12	R	47572 NIIGATA/YAHIKOYAMA
13-14	R	47695 TOKYO/KASHIWA
15-16	R	47611 NAGANO/KURUMAYAMA
17-18	R	47659 SHIZUOKA/MAKINOHARA

19-20	R	47705 FUKUI/TOJIMBO
21-22	R	47636 NAGOYA
23-24	R	47773 OSAKA/TAKAYASUYAMA
25-26	R	47791 MATSUE/MISAKAYAMA
27-28	R	47792 HIROSHIMA/HAIGAMINE
29-30	R	47899 MUROTOMISAKI
31-32	R	47806 FUKUOKA/SEFURISAN
33-34	R	47869 TANEGASHIMA/NAKATANE
35-36	R	47909 NAZE/FUNCHATOGE
37-38	R	47937 NAHA/ITOKAZU
39-40	R	47920 ISHIGAKIJIMA/OMOTODAKE
41-42	R	47909 NAZE/FUNCHATOGE, in special operation
43-44	R	47937 NAHA/ITOKAZU, in special operation
45-46	B	Gauges in AMeDAS network used
47-48	B	Other raders used
49-50	B	Other rain gauges used
51-60		reserved
61-62	M	Modelling data
63	bit	OOM is used in forecast
64	bit	MSM is used in forecast

Notes:
(1) This table is taken from documentation dated November 2006. Later changes may exist.
(2) Bits are counted as in BUFR. Bit 64 is the most significant bit of the first octet of the block. Bit 1 is the least significant bit of the last octet of the block.

Each two-bit pair represents operation status of data source (radar or gauge).

Upper bit	Lower bit	Type R	Type M	Type B

(#2)	(#1)			
0	0	No data (bulletin missing)	Not used	Unused
0	1	Observation done, echo presents	Latest run used	Used
1	0	Observation done, echo absent	Second-latest run used	reserved
1	1	No operation	reserved	reserved

Radar status block 2 (informational)

Block 2 covers radar sites *not* operated by JMA. Each two-bit pair is operation status encoded in the same way as in block 1.

Bits	Description
1-2	Pinneshiri [Pinne Yama*]
3-4	Otobe Dake*
5-6	Muri Yama
7-8	Hako Dake*
9-10	Monomi Yama*
11-12	Shirataka Yama*
13-14	Nishi Dake
15-16	Hōdatsu Zan*
17-18	Yakushi Dake*
19-20	Hijiri Kōgen
21-22	Akagi San*
23-24	Mitsutōge Yama
25-26	Ōgusu Yama
27-28	Takasuzu Yama*
29-30	Gozaisho Yama*

31-32	Jatōge
33-34	Miyama
35-36	Jōgamoriyama
37-38	Rakansan [Osorakan Zan*]
39-40	Ōwasan
41-42	Myōjin San*
43-44	Takashiro Yama
45-46	Shakadake [Shakagadake*]
47-48	Kunimi Yama*
49-50	Happongi Yama (Gotō Shi)
51-52	Yae Dake*
53-64	reserved

Notes:
(1) This table is translated from documentation dated November 2006. Later changes may exist.
(2) Name of radar sites may have different spelling, as they are not registered to WMO. Names marked with asterisk (*) are found in “Gazetteer of Japan” (2007, http://www.gsi.go.jp/ENGLISH/pape_e300284.html).

Flag table for rain gauge availability

Availability of each data source (mostly rain gauges in a prefecture) is indicated by a bit each.

Bit	Data source
1	gauges in AMeDAS network
2	gauges operated by Water and Disaster Management Bureau, MLIT (Ministry of Land, Infrastructure, Transport and Tourism)
3	gauges operated by Road Bureau, MLIT
4-17	reserved
18	gauges in Hokkaido (hereafter proper name is prefecture of Japan)
19	gauges in Aomori

20	gauges in Akita
21	gauges in Iwate
22	gauges in Miyagi
23	gauges in Yamagata
24	gauges in Fukushima
25	gauges in Ibaraki
26	gauges in Tochigi
27	gauges in Gunma
28	gauges in Saitama
29	gauges in Tokyo
30	gauges in Chiba
31	gauges in Kanagawa
32	gauges in Nagano
33	gauges in Yamanashi
34	gauges in Shizuoka
35	gauges in Aichi
36	gauges in Gifu
37	gauges in Mie
38	gauges in Niigata
39	gauges in Toyama
40	gauges in Ishikawa
41	gauges in Fukui
42	gauges in Shiga
43	gauges in Kyoto
44	gauges in Osaka
45	gauges in Hyogo

46	gauges in Nara
47	gauges in Wakayama
48	gauges in Okayama
49	gauges in Hiroshima
50	gauges in Shimane
51	gauges in Tottori
52	gauges in Tokushima
53	gauges in Kagawa
54	gauges in Ehime
55	gauges in Kochi
56	gauges in Yamaguchi
57	gauges in Fukuoka
58	gauges in Oita
59	gauges in Nagasaki
60	gauges in Saga
61	gauges in Kumamoto
62	gauges in Miyazaki
63	gauges in Kagoshima
64	gauges in Okinawa

Note: translated from documentation dated November 2006. Later changes may exist.

DRT 5.200: Run-length packing

Data representation template (DRT) 5.200 is an international standard registered in WMO Manual on Codes. The structure of data section (section 7) is, unfortunately, not described enough to implement software.

Data Representation Section (Sec5) Structure

Taken from WMO Manual, with modification of words for ease of understanding.

Octet	Type	Contents
12	Integer	Number of bits used for each packed value in the run length packing with level values (only 8 has been used at the time of writing)
13-14	Integer	*MV* - Maximum value within the levels that is actually used in this GRIB message
15-16	Integer	*MVL* - Maximum value of level (predefined)
17	Integer	Decimal scale factor of representative value of each level
18 ... 19+2*(*MVL*-1)	Integer[*MVL*]	List of scaled representative values of each level from 1 to *MVL*

Data Section (Sec7) Structure

Octet	Type	Contents
1-4	Integer	Length of the section
5	Integer	Number of the section (7)
rest	(described below)	Packed grid data

Run length encoding (RLE) is a technique that compresses data into a series of pair of repeated element and repetition count. There are lots of specific encodings of the name in the information technology industry. Microsoft DIB (bitmap) format is famous one, but is differnt from JMA's.

Firstly, in lexical (small-scale) viewpoint, packed grid data is considered as a sequence of **bytes**. The size of byte is given at octet 12 of data representation section. It may not be eight, but as far as I know, all implementations uses 8 bits per byte (hence it's same as octet).

Switching to syntax (large-scale) viewpoint, **Packed grid data** is a sequence of sets, each of which represents a consecutive grid points with the same value. A **set** consists of a **data byte** (value equals to or less than *MV*) and an optional repetition count sequence (hereafter called **RCS**) that is a sequence of **digits**, each of which is bytes with value more than *MV*. The structure in BNF is as follows:

packed_grid_data := *(set)
set := data_byte rcs
data_byte := <any byte whose value is *MV* or less>
rcs := *(digit)
digit := <any byte whose value is more than *MV*>.

RCS describes number of consecutive grid points in the set. The number is decremented by one, and then expressed in positional notation with base $B = 255 - MV$ (note: each digit may take value one of B possibilities between $MV + 1$ and 255) and digits are sorted in little-endian order. Thus the number of consecutive grid points R is given as follows:

$$R = 1 + \sum_{i=1}^{N} B^{(i-1)}[a_i - (MV + 1)],$$

where N is the number of bytes in repetition count sequence and a_i is i-th byte in the sequence. When RCS is missing in a set, that means $R = 1$.

Value of the “data byte” is different from that of original data described by the parameter. The byte value is called **level**, which is an index to the list of “representative value” at the end of data representation section. Each value in the table is scaled by the decimal scale factor (octet 17 of DRS). The original data Y is given by a similar formula to regulation 92.9.4:

$$Y \cdot 10^{D} = X = table[L],$$

where D is the decimal scale factor, X scaled value, L level, and *table*[*L*] is L-th (1-starting) entry in the table. The idea of level is something like Beaufort’s scale giving approximate value of wind speed. “Maximum value of level” *MVL* in Section 5 is the number of these levels, which is fixed number 98 for current R/A. Note that *MV* is often less than *MVL* (*MV* cannot be more than *MVL*).

Note that the “level zero” is defined to mean missing value, hence the list of levels in DRS does not include an entry for zero. As far as I know, JMA never used the standard bit-map (GRIB2 Section 6) with run length packed data. Bit-map octets cannot be shorter than one-eighth of grid point counts, but this run length packing can be as short as a single set if almost entire field is zero.

A compact algorithm can decode this data structure, as shown in Appendix.

Appendix: decoding algorithm

Following code in C is only for clarification of algorithm. There is no warranty.
It assumes that a byte in RLE has eight bits, and also C type "`char`" has exactly eight bits.
Bit-map processing is to be done after `decode()` function, although JMA doesn't use bit-map with run-length packing.

```
#include <stdlib.h>
#include <math.h>

	unsigned
get_uint2(unsigned char *p)
{
	return (p[0] << 8) | p[1];
}

	unsigned long
get_uint4(unsigned char *p)
{
	return (p[0] << 24) | (p[1] << 16) | (p[2] << 8) | p[3];
}

	int
decode(const unsigned char *drs, /* SECTION 5 */
	const unsigned char *ds, /* SECTION 7 */
	double *buf, /* RESULT */
	unsigned long buflen)
{
	unsigned long i, ib, npixel, iend, nrepeat, mv, ir;
	double scale_factor, decimal_factor, xlated;
	scale_factor = (drs[16] & 0x80) ? -(drs[16] & 0x7F) : drs[16];
	decimal_factor = pow(10.0, scale_factor);
	if (drs[11] != 8) { return -1; } /* BYTE SIZE IS NOT 8 */
	npixel = get_uint4(drs + 5);
	if (buflen < npixel) { return -1; }  /* OVERRUN */
	iend = get_uint4(ds) - 1;
	mv = get_uint2(drs + 12);
	ib = npixel - 1;
	nrepeat = 0;
	for (i = iend; i >= 5; i++) {
		if (ds[i] > mv) {
			nrepeat *= (255 - mv);
			nrepeat += (ds[i] - mv - 1);
		} else {
			if (ib < ++nrepeat) { return -1; }  /* OVERRUN */
			if (ds[i] == 0) {
				xlated = -1.0;  /* MISSING VALUE */
			} else {
				xlated = get_uint2(drs + 17 + 2 * (ds[i] - 1))
				* decimal_factor;
			}
			for (ir = 0; ir < nrepeat; ir++) {
				buf[--ib] = xlated;
			}
			nrepeat = 0;
		}
	}
	if (ib > 0) { return -1; } /* UNDERRUN */
	return 0;
}
```

C-6. Radar / Rain gauge-Analyzed Precipitation Dataset by JMA[1]

For the task team, the Radar / Rain gauge-Analyzed Precipitation dataset was provided by JMA in GRIB2 format. It gives the most reliable and finest precipitation analysis fields and is to be used with the atmospheric transfer models for computing rain wash. Details of the data set including data configuration and format are described in a pdf document file (the following pages) and shared along with the dataset as the contribution of JMA among the Task Team members.

[1] T. Fujita and N. Nemoto

Radar / Rain gauge-Analyzed Precipitation Dataset by JMA

This document describes basic information needed to handle the Radar / Rain gauge-Analyzed Precipitation Dataset (RA) by the Japan Meteorological Agency (JMA), which is provided to the WMO Technical Task Team on Meteorological Analyses for Fukushima Daiichi Nuclear Power Plant Accident. Since the concept and overview of the data are mostly given in Nagata (2011)[1], the data description given below is rather limited: the file format, data area, and so on.

1. File names of the Radar / Rain gauge-Analyzed Precipitation dataset

The generic file names of the RA dataset are specified as follows:

```
Z__C_RJTD_yyyyMMddhhmmss_SRF_GPV_Ggis1km_Prr60lv_ANAL_grib2.bin
```

where two consecutive underscores are given between the first Z and C, while a single underscore is used in other places. The specific character string '`yyyyMMddhhmmss`' should properly stand for the year in four digits, month, day, hour, minute, and second in two digits in Coordinated Universal Time (UTC) at observation, while the observation time shows the end of accumulation period. For example, the one hour accumulated analyzed rainfall amount data from 1000 UTC to 1100 UTC on March 12, 2011 is stored in:

```
Z__C_RJTD_20110312110000_SRF_GPV_Ggis1km_Prr60lv_ANAL_grib2.bin
```

Note that the minutes are `00` or `30` since the data is given every thirty minutes, and the seconds are always assumed to be `00`.

2. Grid alignment and the number of grids

The horizontal resolution of the data is 45 seconds in longitude and 30 seconds in latitude. The entire area streches from 118 degree to 150 degree in East, and from 20 degree to 48 degree in North (Fig. 1), in a way that each tiny region of 45 seconds by 30 seconds is arranged within the entire region without any overlap nor gap, which means tiny regions of total 2560 by 3360 are defined in the area.

[1] <http://www.jma.go.jp/jma/jma-eng/jma-center/rsmc-hp-pub-eg/techrev/text13-2.pdf>

3. File format

The data is encoded and formatted in the form of FM92 GRIB Edition 2 (WMO, 2011) [2] with specific extensions for this usage. The sizes of the data files vary from 100 kB to 500 kB or more depending on the meteorological condition at the observation time. Users should refer to the Appendix for more detail in addition to WMO (2011).

Discrete level values of precipitation intensity are compressed in a run length encoding, and set into the sixth octet and after in the seventh section. Note that the maximum value of the data in one file, which naturally differs file by file, is referred to as the standard value for the run length compression of the data in the file (MV, octets 13-14 in the fifth section), and that once the RA dataset is processed by the program mentioned in the next section, the compressed data is re-encoded in the simple compression and the run length rule is not applied anymore.

4. Data Handling Program

A data conversion program `conv_jma_grib2` is prepared by JMA for the users' convenience. The program is originally designed to convert the JMA Meso-analysis data, but also usable to convert the RA dataset. Users should refer to the User's Manual (JMA, 2012) on the `conv_jma_grib2` program for the details.

APPENDIX GRIB2 Format for the Radar / Rain gauge-Analyzed precipitation

The GRIB2 files for the Radar / Rain gauge-Analyzed precipitation (R/A) employ a template of local use 4.50008 in section 4. It is almost identical to the template 4.8 with n = 1 (octet 42), but the following records are additionally placed:

(1-58 same as the template 4.8 with n = 1)

59-66 Flags on radar operations PART1

67-74 Flags on radar operations PART2

75-82 Flags on rain gauge operations

[2] <ftp://ftp.wmo.int/Documents/MediaPublic/Publications/CodesManual_WMO_no_306/WMO306_Vol_I.2_2011_en.pdf>

The flags above indicate which radar or rain gauge sites are in operation to analyze the precipitation intensity, however, the details are not shown here because the information is longish and considered unimportant for the task teams' work. Toyoda (2012) provides full details on the extensions defined by JMA.

Discrete level values of precipitation intensity (lv), parameter category 0 (moisture) and number 200 (local use) specified in section 4, are stored in section 7 with the run length packing, as section 5 describes that the template 5.200 is used. The level values should be interpreted to precipitation intensity with a table stored in section 5 (List of MVL scaled representative values of each level from lv=1 to MVL). lv= 0 means no observation (missing).

REFERENCES

JMA, 2012: conv_jma_grib2 − a tool to convert GRIB2 provided for UNSCEAR by JMA — Users' Manual by the Japan Meteorological Agency, 7 p.

Nagata, K., 2011: Quantitative Precipitation Estimation and Quantitative Precipitation Forecasting by the Japan Meteorological Agency. , RSMC Tokyo - Typhoon Center Technical Review No.13, 37-50.

Toyoda, E., 2012: GRIB2 templates for JMA Radar/Rain gauge-Analyzed Precipitation data: PDT 4.50008 and DRT 5.200, a document submitted to WMO Inter-Programme Expert Team on Data Representations and Codes. http://goo.gl/Y6JMh

WMO, 2011: Manual on Codes – International Codes, Part B -Binary Codes. WMO Publication No.306 Volume I.2, Geneva, Switzerland.

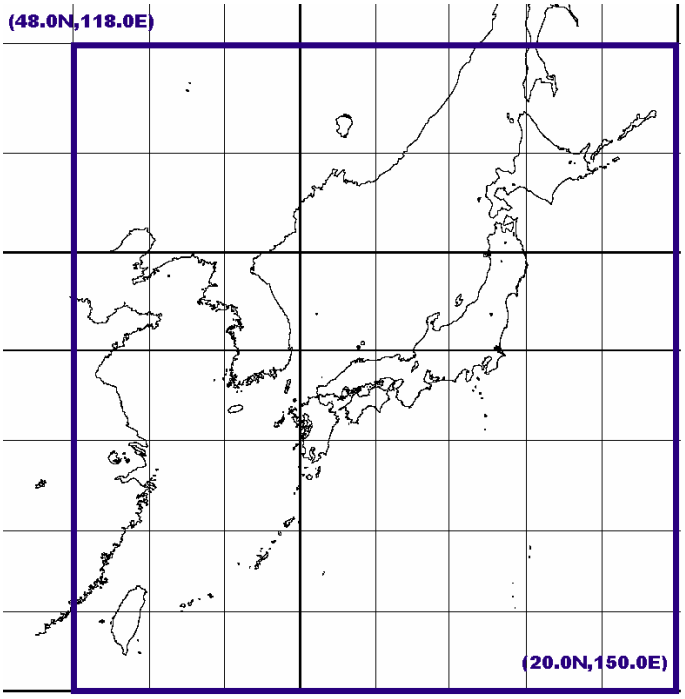

Fig. 1　Area of the RA dataset.

C-7. File converter tool[1]

Following an agreement reached by the task team, JMA offered the Radar/Rain Gauge analyzed precipitation (R/A) fields (see C-4) and the 4D-VAR mesoscale analysis (MA) fields (see C-3 and C-8) in the GRIB2 format, bit-oriented data exchange format standardized by the World Meteorological Organization (WMO) Commission for Basic Systems (CBS). However, a horizontal coordinate such as the Lambert conformal conic projection, the terrain following hybrid vertical coordinate, and the run length encoding (RLE) used in the provided datasets might not be familiar to some members of the task team. Moreover, decoding data described in the GRIB2 often requires special technics and knowledge.

In order to help members' work, JMA also provided a converter tool (called "conv_jma_grib2") to process the offered data. Its functions are schematically displayed in Fig.C-7-1. The "User Manual" of the tool distributed to the task team members is shown from the following page, which describes details of its functions, usages (compiling and running) and some examples in use. The tool was written fully in C programing language from scratch, and scripts to generate compiling environment depending on various users' system was attached, which helped the tool available on many systems. Only one small bug was fixed just after it was released to the members, but no further defects have been reported.

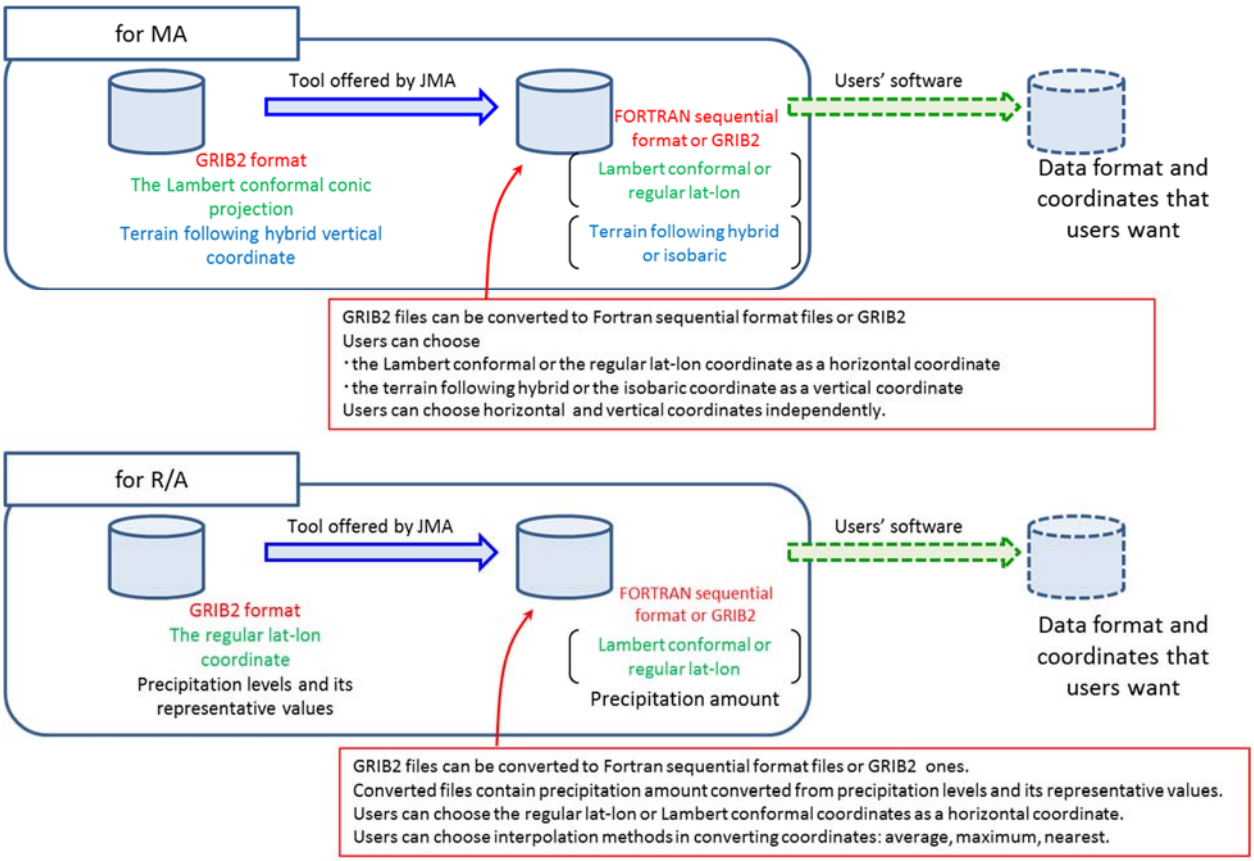

Fig. C-7-1. A schematic figure showing functions of the converter tool provided by JMA.

[1] T. Hara

conv_jma_grib2

— a tool to convert GRIB2 provided for UNSCEAR by JMA —
Users' Manual

by the Japan Meteorological Agency

1 Introduction: what does the tool do?

The Japan Meteorological Agency (JMA) has provided the operational mesoscale analysis (MA) in the GRIB2 format to members of the task team. MA employs the Lambert conformal conic projection as a horizontal coordinate, but it has been revealed that the projection might not be familiar to some people. In addition, a terrain following hybrid coordinate adopted by MA could be another factor to hamper members' work.

Furthermore, while the GRIB2 format is regulated by the WMO and established as a common format to exchange meteorological data, it might not an easy task to decode and process them.

Considering the situation, JMA has decided to provide a tool to convert horizontal and vertical coordinates as well as the data format. The tool provides functions

- to convert the GRIB2 format to the FORTRAN sequential format which is much more familiar and can be visualized by the GrADS, a popular tool in the meteorological society.
- to re-project data in the GRIB2 to other projection.
- to convert the terrain following hybrid vertical coordinate to the isobaric coordinate with arbitrary pressure planes.

The tool is applicable for the following GRIB2 files provided to the UNSCEAR task team.

- `jma_ma_met_hybrid-coordinate_201103DDHH00.grib2.bin`
  (MA for the atmosphere)
- `jma_ma_land-surface_201103DDHH00.grib2.bin`
  (MA for the land surface)
- `jma_ma_ocean_sst_201103DDHH00.grib2.bin`
  (MA for the sea surface temperature)
- `Z__C_RJTD_201103DDHHMN00_SRF_GPV_Ggis1km_Prr60lv_ANAL_grib2.bin`
  (Radar/Raingauge analyzed precipitation)

2 Setup

The source codes described in C can be complied as the following.

```
$ tar xvzf conv_jma_grib2-1.00.tar.gz
$ cd conv_jma_grib2-1.00
$ ./configure
$ make
```

After the compilation finishes successfully, the executable file `conv_jma_grib2` is generated in the current directory. You can copy the executable to another directory you like.

The `configure` script automatically determines endian of your computer and the executable built is compatible to your computer.

Note that `makedepend` (a tool to generate dependencies automatically) is used in the compilation. Even if `makedepend` is not installed in your computer, the codes are compiled successfully using the prescribed dependencies in `src/.depend.default` as long as no modifications are added into the codes. If you are going to add some modifications but `makedepend` is not installed, you might need to update the dependencies by hand, which `makedepend` automatically does. `config.log` generated after running `configure` tells you whether `makedepend` is installed in your computer and used in compiling them.

3 Basic Usage

As the first practice, just type as follows with a GRIB2 file provided by JMA.

```
$ conv_jma_grib2 grib2_file
```

You obtain a converted file in the FORTRAN sequential format with a GrADS ctl file. The converted file is put with a file name combined the original GRIB2 file name (including a directory path) and "`.dat`" and "`.ctl`", that is, if your GRIB2 file is named as `/home/john/sample.grib2`, file names of the converted ones are `/home/john/sample.grib2.ctl` and `/home/john/sample.grib2.dat`. If `-o output_file` is added to the option line, the output file name can be altered to `output_file`.

You can see what elements are stored by looking at the ctl file. This operation just converts file formats and no coordinate transformations are done. By opening the ctl file with GrADS, you can draw elements stored in the file. In the case of converting GRIB2 files of the Radar/Raingauge-Analyzed Precipitation (R/A), converted files contain precipitation intensity (parameter category:1, number:8), while discritized levels of precipitation intensity (parameter category:1, number:200) is stored in the original GRIB2 files. It is also the case when you convert the original GRIB2 to the GRIB2 again with `-g` option.

Note that converted FORTRAN sequential files are described in the big endian even if the byte order of your computer is the little endian. While the GrADS can recognize the endian because the endian is specified in a "OPTION" line in the ctl file, take care of that when you try to read the file by your own programs (FORTRAN compilers usually have a "big endian" mode, with which `read`/`write` statement in FORTRAN read/write sequential files in the big endian even on little-endian machines).

Furthermore, the first point of the GRIB2 is at the northwest edge (j increases from north to south), however, converted files in the FORTRAN sequential format have the first point at the southwest edge (j increases from south to north). That is why no "`yrev`" option is placed in the OPTION line in ctl files.

By default, ctl files for GrADS assume a linear grid even if the Lambert projection is employed. The generated ctl file should be like the following:

```
#pdef 719 575 LCCR 30.000 140.000 487.977067 168.019156 30.000 60.000 140.000 5000.000 5000.000
#xdef 963 linear 107.000000 0.051922
#ydef 668 linear 19.000000 0.044966
xdef 719 linear 1.000000 1.000000
ydef 575 linear 1.000000 1.000000
```

Although the GrADS ignores lines starting with `#`, parameters related to the Lambert projection is written down in a `pdef` statement. In this case, the numbers of grids specified by `xdef` and `ydef` is real grid numbers. You can draw this file with GrADS but map drawn is not correct.

If `-c` option is specified, the parameters in the ctl files will be

```
pdef 719 575 LCCR 30.000 140.000 487.977067 168.019156 30.000 60.000 140.000 5000.000 5000.000
xdef 963 linear 107.000000 0.051922
ydef 668 linear 19.000000 0.044966
#xdef 719 linear 1.000000 1.000000
#ydef 575 linear 1.000000 1.000000
```

This time, the GrADS interprets the `pdef` statement, and draw figures interpolating the Lambert projected grids to linear Latitude/Longitude coordinate. Real grid numbers are appeared in the `pdef` statement, but numbers specified by `xdef` and `ydef` are not related to the real grid numbers (they are adjusted so that the entire domain can be drawn).

4 Coordinate transform

This tool has a function to transform horizontal and vertical coordinates.

All options explained in the Section 3 are also available when options for a horizontal and/or vertical coordinate transform are specified.

Of course, the vertical transform is valid only for the atmospheric analysis (not for land, sst, and R/A analysis).

4.1 Horizontal transform

If you are going to change a horizontal coordinate of the provided GRIB2 data, you should create a configuration file describing parameters of the destination projection. The configuration file is put as an option in the command line with `-h` like

```
$ conv_jma_grib2 -h config_h.txt grib2_file
```

4.1.1 Converting to the Latitude/Longitude coordinate

When converting data in the GRIB2 to those on the Latitude/Longitude coordinate, an example of the configuration file content, saved as `config_sample/config_h_ll.txt`, should be like the following:

```
proj = LL
nx = 201
ny = 201
dx = 0.05
dy = 0.05
xlat = 40.0
xlon = 130.0
xi = 1.0
xj = 1.0
```

- `proj` must be `LL` (Latitude/Longitude)
- `nx`, `ny`: the numbers of grids of x- and y-direction.
- `dx`, `dy`: grid spacing of x- and y- direction. (unit: degree)
- `xlat`, `xlon`, `xi`, `xj`: (`xi`, `xj`) on the coordinate corresponds to the point identified by `xlat` and `xlon`. In the coordinate the configuration file assumes, a point of (1, 1) is located at the northwest edge and `xj` increases from north to south (the coordinate value of the first point is 1, not 0).

  When a coordinate you want to convert to is the Latitude/Longitude, it is easy and understandable to set the latitude and longitude of the first point (i.e. the most northwestern point) to `xlat` and `xlon`, and `xi` = `xj` = 1.0.

4.1.2 Converting to the Lambert Coordinate

When you are going to convert the JMA GRIB2 data (ex. Radar/Raingauge Analyzed Precipitation) to those on the Lambert coordinate, a configuration file on parameters for the target coordinate is required. An example of what should be described in the configuration, saved as `config_sample/config_h_lm.txt`, is as follows.

```
proj = LMN
nx = 719
ny = 575
dx = 5000.0
dy = 5000.0
xlat = 30.0
xlon = 140.0
xi = 488.0
xj = 408.0
slat1 = 30.0
slat2 = 60.0
slon = 140.0
```

The format of the configuration file is similar to that for converting to the Latitude/Longitude coordinate, mentioned in the previous subsection. This time, `proj` must be `LMN` (Lambert North). In addition to parameters used also for the Latitude/Longitude coordinate, two standard latitude and a standard longitude must be set to `slat1`, `slat2` and `slon` in degree. Along the standard latitudes and longitude, no expansion or shrink occurs in the projection from the Earth sphere to the plane. It is strongly recommended that when you would like to use the Lambert projection, `slat1` = 30, `slat2` = 60 and `slon` = 140. In the case of the Lambert projection, `dx` and `dy` mean grid spacings at the standard latitude and longitude at the points identified by `slat1`, `slat2` and `slon`. (Parameters in the example shown above is used in the JMA meso analysis).

Wind components u and v in the GRIB2 depict x- and y- direction winds on the Lambert projection, respectively (not zonal and meridional winds). When the Lambert coordinate is converted to the Latitude/Longitude one, u and v are rotated so that the rotated winds u' and v' can be interpreted as zonal and meridional winds. The details of the rotation are described in Appendix A.

Note that conversion of the original MA GRIB2 described in the Lambert projection to another Lambert projection with different parameters (ex. smaller region) is also possible.

The original domain is expected to cover the entire domain of the converted one. If the tool finds a point on the target coordinate locating out of the original domain, it abnormally halts with an error message by default. However, adding `-d` to the command line option allows you to include points

which are not covered by the original coordinate. MISSING (`undef` in GrADS) are stored into these points.

For almost elements in the GRIB2, the tool calculated values on the target coordinate by the linear interpolation of values on four adjacent points on the original coordinate. There are two exceptions.

1. In converting `KIND` (surface kind such as land, sea, land covered by snow, sea covered by ice) stored in the land surface analysis, the tool uses a value on the nearest point selected from the four adjacent points (because a fractional "`KIND`" obtained by the linear interpolation as the other elements is meaningless.)

2. In converting Radar/Raingauge Analyzed precipitation originally on the Latitude/Longitude coordinate to other coordinate, three options for the interpolation are available. The following characters should be placed in the command line after `-r`.

   - `m`: averaged values over grids on the original projection which are covered by the grid on the target projection are adopted.
   - `x`: maximum values over grids on the original projection which are covered by the grid on the target projection are adopted.
   - `n`: values on the nearest grids on the original projection is adopted.

4.2 Vertical transform

When you are going to transform the original terrain following hybrid coordinate of MA to the isobaric coordinate, the configuration file describing a list of pressures of the isobaric planes is required like the following, saved as `config_sample/config_v.txt`.

```
pout = 1000.0, 950.0, 925.0, 850.0, 700.0, 500.0, 300.0, 250.0, 200.0, 100.0
```

Each value in the list is separated by a comma, and the unit of pressure is hPa. No line breaks should be inserted. Pressures in the list should be in descending order. Arbitrary pressure (but note that the top of MA is located around 40hPa) can be specified as long as the number of pressures in the list is less than 100.

With the configuration file describing a list of pressures, you can run the tool like

```
$ conv_jma_grib2 -v config_v.txt grib2_file
```

If surface pressure of one point on one isobaric plane is less than that of the isobaric plane, it means that the point is located underground. Because extrapolated (physically meaningless) values are stored to underground points by default, you should determine validness of each point by comparing surface pressure and that of a isobaric plane. If `-u` is added in the command line, values on underground points are set to MISSING (`undef`) instead of the extrapolated values.

When converting to the isobaric coordinate, temperature is stored instead of potential temperature in the original GRIB2.

Note that you would like to transform horizontal and vertical coordinate simultaneously, both `-h config_h` and `-h config_v` should be placed in the command line. If the both are requested, the vertical coordinate is transformed before the horizontal one.

5 Other Command line options

-l

If `-l` is specified in the command line, a file containing values of latitudes and longitudes of all points in the domain is generated in the GrADS format with a ctl file.

-p

If `-p` is specified in the command line, records in the GRIB2 are printed. After printing them, the tool exits. No files are generated besides the printed information.

6 Quick reference

```
conv_jma_grib2 grib2_file [-h config_h_file] [-v config_v_file] [-o output_file]
               [-g] [-p] [-d] [-r m|x|n] [-l] [-c] [-u]
      -g: output in GRIB2 format
      -p: only print records in grib2_file
      -d: allow out of domain in coordinate conversion
      -c: use pdef in GrADS ctl files
      -u: set MISSING to values located underground
      -r: RA interpolation option
          m: mean
          x: max
          n: nearest
      -l: output lat and lon in GrADS format
```

The identical explanation can be obtained by just executing the tool without any arguments.

One or more options can be specfied in general.

7 Examples

1. Just convert the GRIB2 file format to the GrADS one.

```
$ conv_jma_grib2 /home/john/jma_ma_met_XXXX.grib2.bin
```

   The tool generates `jma_ma_met_XXXX.grib2.bin.dat` and `jma_ma_met_XXXX.grib2.bin.ctl` in a directory `/home/john`.

2. Just convert the GRIB2 file format to the GrADS one, but a file name of outputs is specified.

```
$ conv_jma_grib2 /home/john/jma_ma_met_XXXX.grib2.bin -o after
```

   Files named `after.dat` and `after.ctl` in the current directory.

3. The original GRIB2 files for R/A depict precipitation intensity with discrete integer level values. The following operation produces a GRIB2 file again, but the discrete level values are interpreted to real-number values using the conversion table in the original GRIB2 files. The generated GRIB2 files do not employ any local-use templates, while the original ones use some of them.

```
$ conv_jma_grib2 /home/john/Z__C_RJTD_XXXX_Prr60lv_ANAL_grib2.bin -g
```

   A GRIB2 file containing real-number precipitation intensity is created with a name `/home/john/Z__C_RJTD_XXXX_Prr60lv_ANAL_grib2.bin.grib2.bin`.

4. Convert a horizontal coordinate following a configuration file

```
$ conv_jma_grib2 /home/john/jma_ma_met_XXXX.grib2.bin -h config_h.txt
```

   where `config_h.txt` should be prepared in advance.

   The tool generates `jma_ma_met_XXXX.grib2.bin.dat` and `jma_ma_met_XXXX.grib2.bin.ctl` in a directory `/home/john`.

```
$ conv_jma_grib2 /home/john/jma_ma_met_XXXX.grib2.bin -h config_h.txt -d
```

   By adding `-d` in the command line, points which the original data do not contain is fulfilled by `undef` instead that the tool abnormally aborts.

```
$ conv_jma_grib2 /home/john/jma_ma_met_XXXX.grib2.bin -h config_h.txt -g
```

   this operation generates a GRIB2 file `jma_ma_met_XXXX.grib2.bin.grib2.bin` instead of the file in the GrADS format.

```
$ conv_jma_grib2 Z__C_RJTD_XXXX_Prr60lv_ANAL_grib2.bin -h config_h.txt -r n
```

   Transform a coordinate of R/A following a configuration file `config_h.txt`. In interpolating, values on the nearest grids on the original projection is adopted.

5. Convert a vertical coordinate following a configuration file

```
$ conv_jma_grib2 /home/john/jma_ma_met_XXXX.grib2.bin -v config_v.txt
```

A rule to name files are the same as former examples.

```
$ conv_jma_grib2 /home/john/jma_ma_met_XXXX.grib2.bin -v config_v.txt -u
```

Values located underground in the generated file is set to `undef`.

6. Convert horizontal and vertical coordinate simultaneously

```
$ conv_jma_grib2 jma_ma_met_XXXX.grib2.bin -h config_h.txt -v config_v.txt
```

A Lambert conformal conic projection

Coordinates x and y on the projected rectangular plane are given by:

$$(x - x_0)D_X = \rho(\phi)\sin[\alpha(\lambda - \overline{\lambda})] - \rho(\phi_0)\sin[\alpha(\lambda_0 - \overline{\lambda})],$$
$$(y - y_0)D_Y = \rho(\phi)\cos[\alpha(\lambda - \overline{\lambda})] - \rho(\phi_0)\cos[\alpha(\lambda_0 - \overline{\lambda})]$$

where

$$\rho(\phi) = \frac{R\cos\phi_1 U(\phi)^\alpha}{\alpha U(\phi_1)^\alpha}, \quad (R = 6371000 \text{ m: Radius of the Earth})$$
$$\alpha = \frac{\ln(\cos\phi_1) - \ln(\cos\phi_2)}{\ln U(\phi_1) - \ln U(\phi_2)}$$
$$U(\phi) = \tan\left(45^\circ - \frac{\phi}{2}\right),$$
D_X, D_Y : `dx`, `dy`,
ϕ_1, ϕ_2 : `slat1`, `slat2`,
$\overline{\lambda}$: `slon`,
ϕ_0, λ_0 : `xlat`, `xlon`,
x_0, y_0 : `xi`, `xj`.

The symbols used above (`dx`, `dy`, `slat1`, `slat2`, `slon`, `xlat`, `xlon`, `xi` and `xj`) are explained in Section 4.1.2.

When you would like to convert x- and y- direction winds on the Lambert projection to zonal and meridional winds, you should rotate the wind vectors by the following angle θ ($\theta > 0$: clockwise rotation)

$$\theta = \alpha(\lambda - \overline{\lambda}),$$

where λ is the longitude of the point. Under the usual and recommended condition (`slat1` $= 30^\circ$, `slat1` $= 60^\circ$ and `slon` $= 140^\circ$), $\alpha \simeq 0.715$.

C-8. JMA Meso-scale 4D-VAR analysis[1]

JMA operates a data assimilation system for Meso-scale Analysis to initialize MSM (Section C-2-1). As of March 2011, the Meso-scale Analysis adopted a 4D-VAR data assimilation system, which employs JMA-NHM as a time integration operator, named the "JMA Nonhydrostatic model"-based Variational Analysis Data Assimilation (JNoVA; Honda et al. 2005, Honda and Sawada, 2008, 2009).

The analysis of 4D-VAR is obtained by minimizing a cost function in an iterative process. JNoVA adopts the incremental approach (Courtier et al. 1994) to reduce the computational cost for operational use. In the incremental approach, a low-resolution model is used in the iterative process called the "inner loop" to obtain an analysis increment while a high-resolution model is used to obtain an analysis. The minimization process is carried out as follows (ordinal numbers correspond to those in Fig. C-8-1):

1. Initialized with the previous Meso-scale Analysis, run the high-resolution (5km) forecast model within the data assimilation window (0 to 3-hours) to obtain the first guess.
2. Perform quality-control of observations (see Section 2.3 for details) and calculate deviations of the observations from the first guess.
3. Execute the JNoVA to assimilate the quality-controlled observations on a low-resolution (15km) space. This step is iterated to minimize the cost function until pre-defined criteria is satisfied. At the end, analysis increments at the beginning of the data assimilation window are obtained.
4. Add the analysis increments (on the low-resolution space) to the (high-resolution) first guess at the beginning of the data assimilation window through an interpolation process, and make an initial condition for the next step.
5. With the initial condition made in the previous step, run the high-resolution (5km) forecast model within the data assimilation window to obtain an analysis at the end of the data assimilation window.

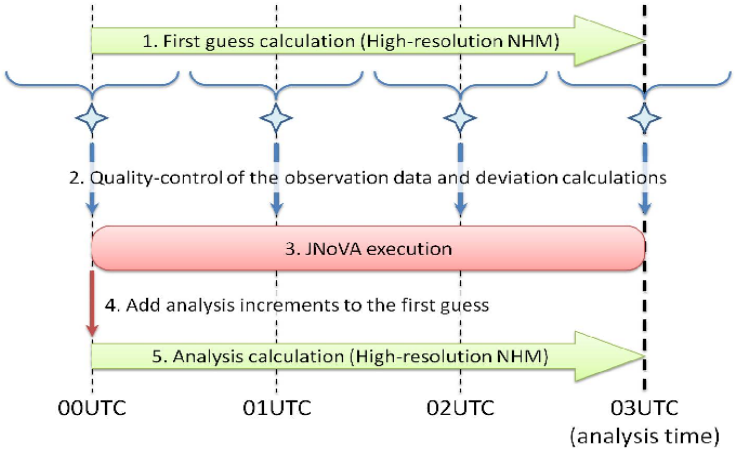

Fig. C-8-1. Schematic procedure of the Meso-scale Analysis (an example of 03UTC analysis).

[1] Y. Honda

Table C-8-1. Specification of MSM, NLM and ADM used in JNoVA.

	MSM	NLM	ADM
Resolution	5km, 50layers	15km, 40layers	15km, 40layers
Horizontal advection	Flux form fourth-order with advection correction	Flux form fourth-order with advection correction	Flux form fourth-order
Solver of pressure equation	HE-VI	HE-VI	HE-VI
Targeted moisture diffusion	Considered	Considered	Not considered
Moist physics	3-ice bulk microphysics	Large scale condensation	Large scale condensation
Convection	Modified Kain-Fritsch	Modified Kain-Fritsch	None
Turbulence	Mellor-Yamada -Nakanishi-Niino level 3	Deardorff	Deardorff
Surface flux	Beljaards and Holtslag	Louis (land) and Kondo (sea)	Louis (land) and Kondo (sea)
Ground temperature	Four-layer thermal diffusion	Four-layer thermal diffusion	Four-layer thermal diffusion
Radiation	Considered	Considered	Not considered

In JNoVA, a simplified nonlinear version of the JMA-NHM (NLM) is used in the inner loop to provide trajectories at every iteration instead of the tangent linear model (TLM) of the NLM due to discontinuity and nonlinearlity of the JMA-NHM. In addition, the adjoint model (ADM) of the NLM is used to provide gradient information of the cost function. The specification of these inner models, NLM and ADM, as well as MSM is briefly listed in Table C-8-1.

JNoVA is capable of assimilating variety of observational data from conventional data to satellite data. The observation used in Meso-scale Analysis as of March 2011 is listed in Table C-2-2. One of the unique characteristics of Meso-scale Analysis is the direct assimilation of precipitation, which is crucial for reproducing the realistic precipitation in the analysis.

In April 2009, JNoVA was introduced in Meso-scale Analysis by replacing a previous 4D-Var system. Before its introduction, twin experiments were conducted under almost the same conditions as the operational system in summer (2006/7/16 – 8/31) and in winter (2007/12/23 – 2008/1/23) to compare the performance of JNoVA with that of a previous 4D-Var based on a limited-area hydrostatic spectral model. The quantitative precipitation forecast (QPF) of JNoVA is better than that of the previous 4D-Var for all thresholds according to the equitable threat score (ETS) of three-hourly accumulated precipitation forecasts (Fig. C-8-2). Upper-air verification reveals that the analysis of JNoVA is better than that of the previous 4D-Var, although the impact on the forecast is quite limited (not shown). From surface verification, it is found that the root mean square errors (RMSEs) of the surface temperature in summer and the surface wind in winter are reduced, and that the scores of other

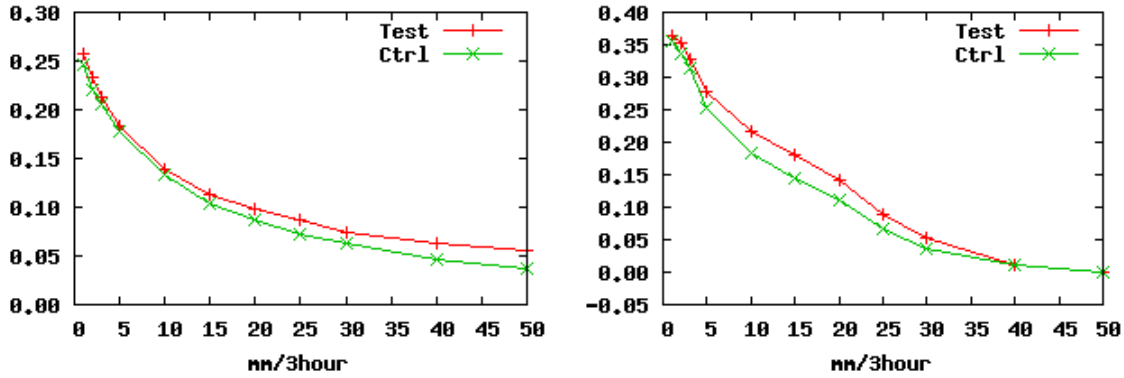

Fig. C-8-2. Equitable threat scores of three-hourly accumulated precipitation forecasts in summer (right) and winter (left). The red and green lines show the results of JNoVA (Test) and the previous 4D-Var (CTRL), respectively. The horizontal axis is the threshold value of the rainfall amount.

surface variables are neutral (not shown). In the case of Typhoon Wukong (T0610), its typhoon track forecast as well as precipitation forecast was improved by JNoVA (Fig. C-8-3). More figures are found in Honda and Sawada (2009).

Further detailed information on Meso-scale Analysis and JNoVA can be found in Section 2.6 of JMA (2013).

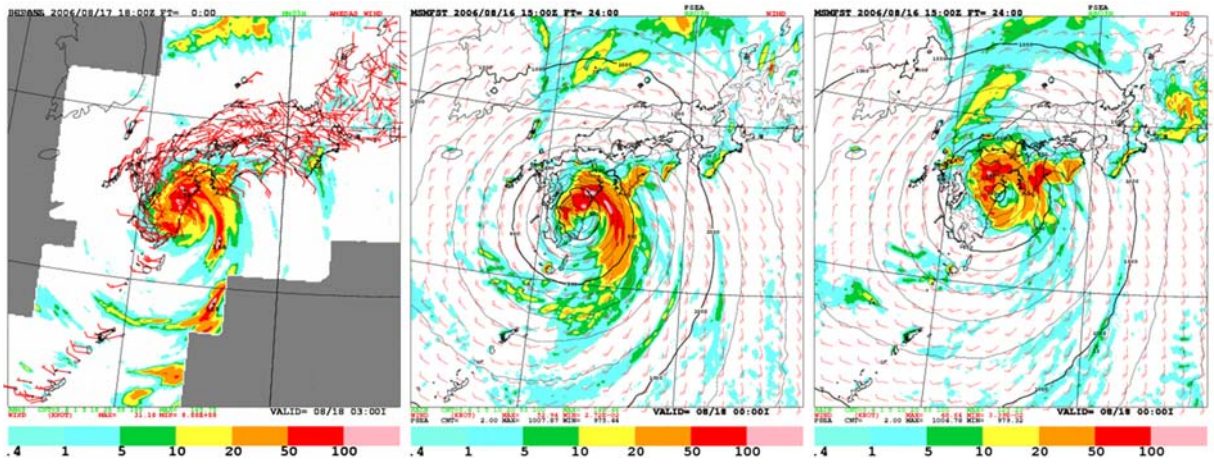

Fig. C-8-3. Three-hourly accumulated precipitation of 24-hour forecasts from 17 Aug. 2006 at an initial time of 15 UTC. From the left, RA, the forecast of JNoVA and that of the previous 4D-Var are shown

C-9. Meteorological Field[1]

Before the hydrogen explosions of Fukushima Daiichi nuclear power plant, two weak low pressure troughs accompanying a low pressure system passed over the Japanese Islands between 9 and 11 March 2011, bringing light rain over wide areas of eastern Japan (not shown). On 12 March, a high pressure system covered the main island of Japan, and moved to the Pacific Ocean about 1000 km east of the island on 13 March; however it continued to cover eastern Japan. The wind direction was from the south below a height of 1 km and from the west above the height in the afternoon of 12 March, the time of the hydrogen explosion of No.1 reactor (Fig. C-9-1a). During the daytime of 14 March, the time of the hydrogen explosion of No.3 reactor, south-southwesterly (westerly) winds dominated below (above) a height of 1 km (Fig. C-9-1b).

Between 12 and 15 March, a weak low pressure system (hereafter Low A) formed north of Taiwan and moved eastward off the southern coast of the main island of Japan (Fig. C-9-2). After 15 March the system moved toward the northeast while developing rapidly. Light rain was observed over eastern Japan from the afternoon of 15 March to the morning of 17 March, while less rain was observed there until the morning of 15 March (Fig. C-9-4). In particular, rain was observed in the Fukushima prefecture during the night from 1700 JST 15 to 0400 JST 16 March (e.g., Fig. C-9-5), a time corresponding with significant emissions. Weak precipitation intensity was observed over most areas of the Fukushima prefecture, and the precipitation systems had low vertical structures (Fig. C-9-6).

North-northeasterly low-level winds dominated during the morning of 15 March. In particular, the wind speed exceeded 10 m s^{-1} over south areas of the Ibaraki prefecture at the time of the container burst of No. 2 reactor. In the afternoon, the wind direction rotated clockwise and gradually changed to south over the Fukushima prefecture (Fig. C-9-7). This wind change was caused by another low pressure system (Low B) that formed over the Kanto Plain, east of Low A (Fig. C-9-3). Chino et al. (2011) estimated that the maximum I-131 emissions occurred between 0900-1500 JST (0000-0600 UTC), 15 March. During that period the winds had the eastward component (cold color) below a height of 1 km and westerly winds (warm color) dominated above the height (Fig. C-9-1c). The low-level easterly component was brought from the circulation of Low A located over the ocean southeast of Ibaraki prefecture (Fig. C-9-2). After 1500JST southeast winds appeared associated with Low B around a height of 1 km and lasted until 0200JST next day (Figs. C-9-1c and 1d).

Between 18 and 19 March, a high pressure system covers widely the Japanese Islands (middle-row panels in Fig. C-9-2), and winds were generally from the west. Then, a low pressure system passed over the main island of Japan from 20 and 22 March (bottom panels in Fig. C-9-2), bringing moderate rain over the Kanto area (bottom panels in Fig. C-9-4).

[1] T. Kato

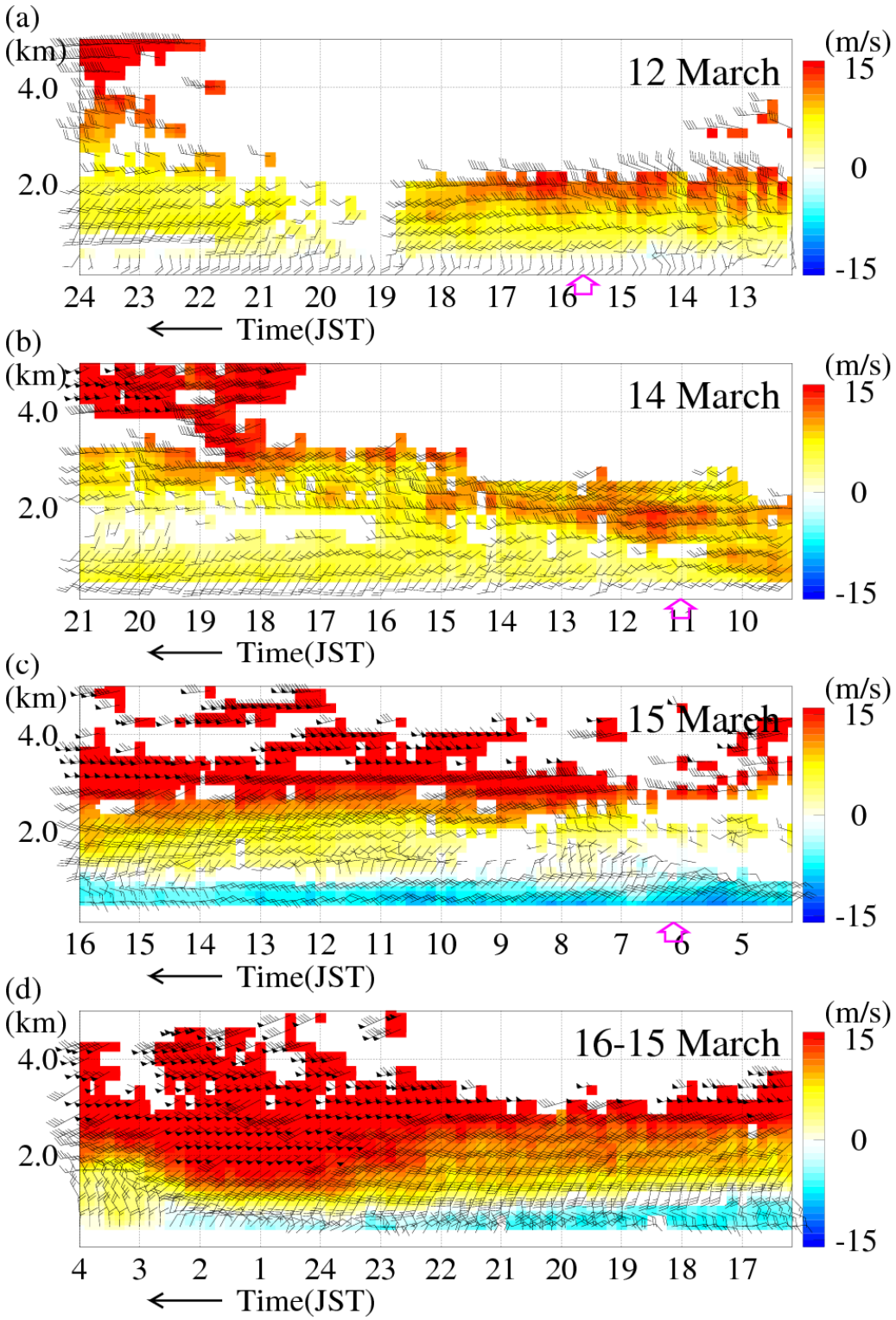

Fig. C-9-1. Time series of horizontal winds (arrows) and zonal wind speed (color shade) below a height of 5 km observed by a JMA wind profiler at Mito (See its location in Fig.C-9-7). (a) From 1210 JST to 2400 JST, March 12. (b) From 0910 JST to 2100 JST, March 14. (c) From 0410 JST to 1600 JST, March 15. (d) From 1610 JST, March 15 to 0400 JST, March 16. Pink arrows show the times of hydrogen explosion of No. 1 reactor for (a) and No.3 reactor for (b) and that of container burst of No.2 reactor for (c). Full and half barbs denote 5 m s^{-1} and 2.5 m s^{-1}, respectively, and pennants denote 25 m s^{-1}.

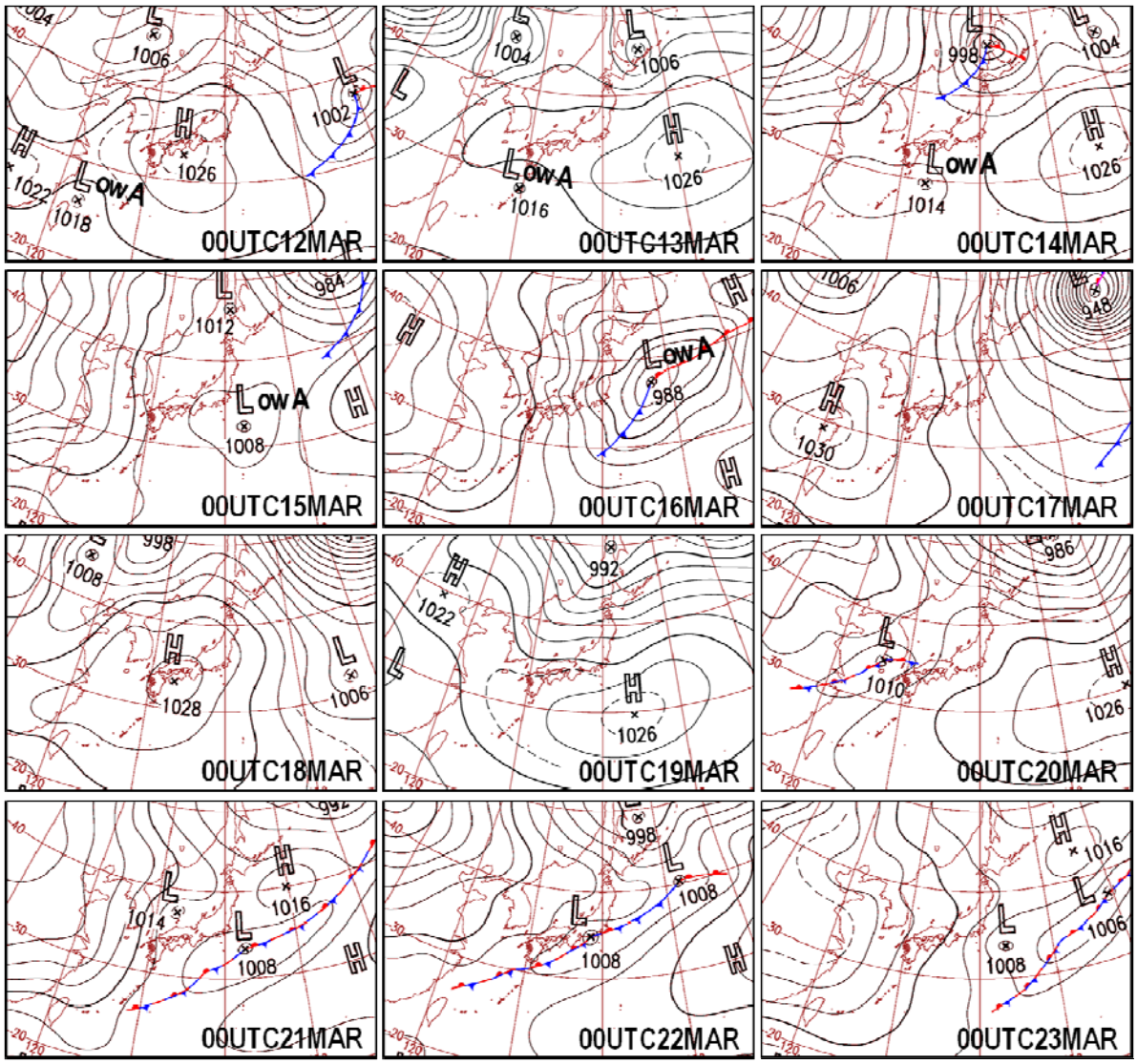

Fig. C-9-2. Surface weather charts at 00UTC (09 JST) from 12 to 23 March, 2011.

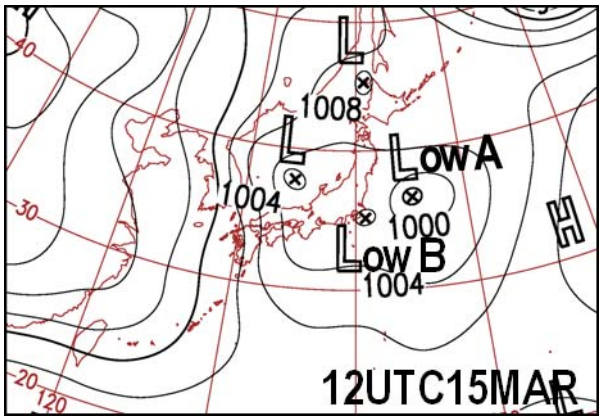

Fig. C-9-3. Surface weather charts at 12UTC (21 JST) 15 March 2011.

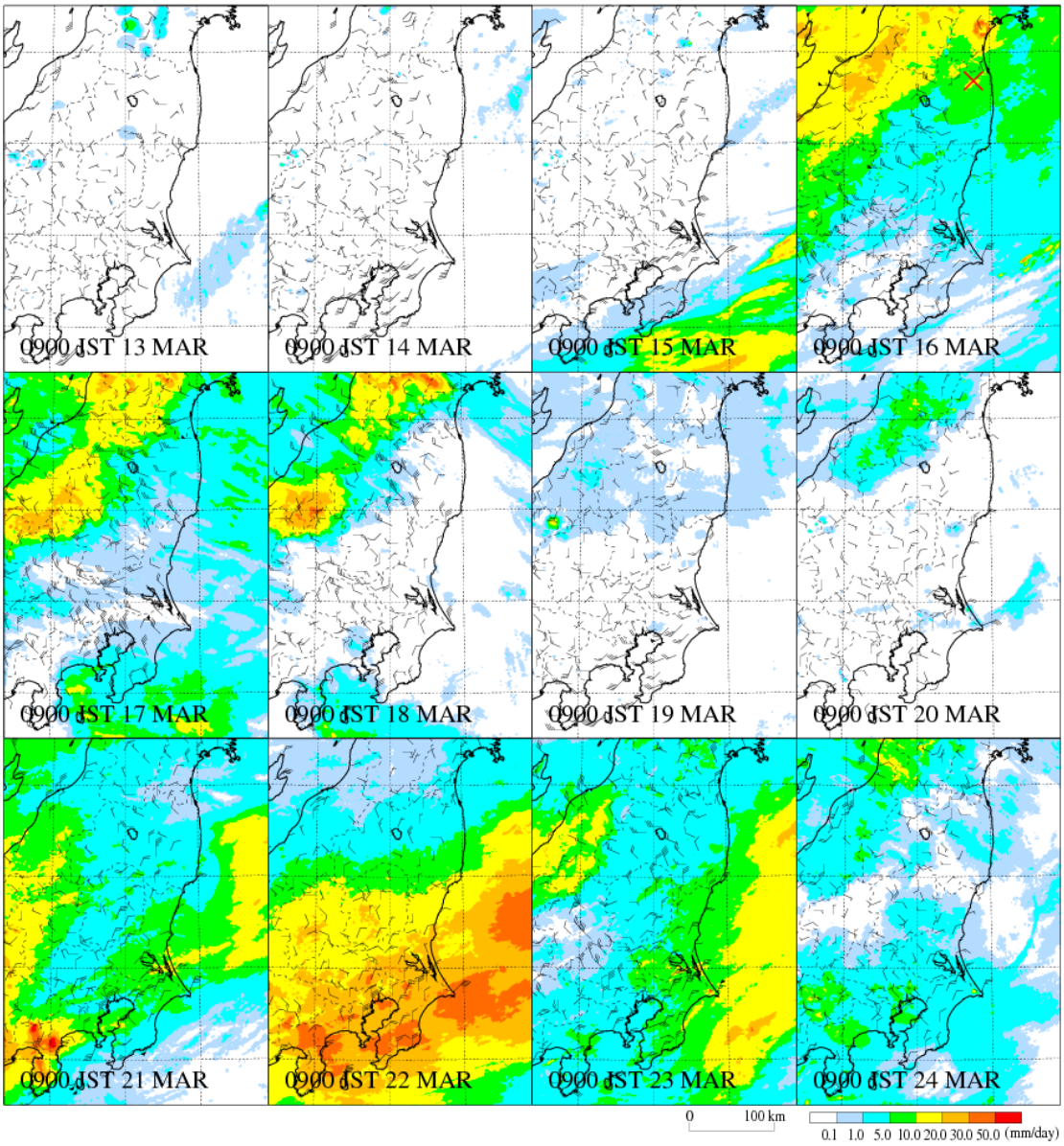

Fig. C-9-4. Horizontal distributions of 24-hour accumulated precipitation amounts and observed surface winds at 0000 UTC (0900 JST) between 13 and 24, March 2011. Red cross on the left-top panel shows the location of Iidate.

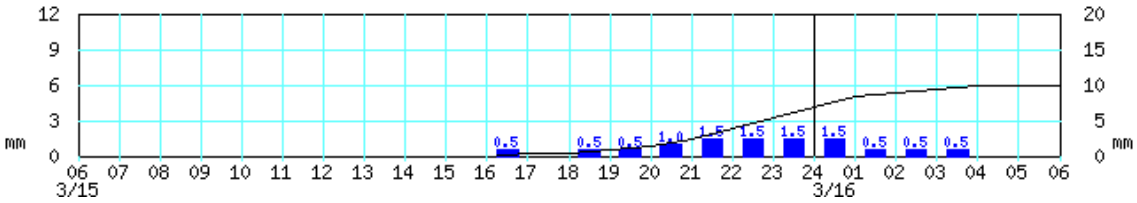

Fig. C-9-5. Time series of hourly accumulated precipitation amounts (bar) and total amount (line) at Iidate (See its location in the left-top panel of Fig.C-9-4) between 0600 JST 15 and 0600 JST 16, March 2011.

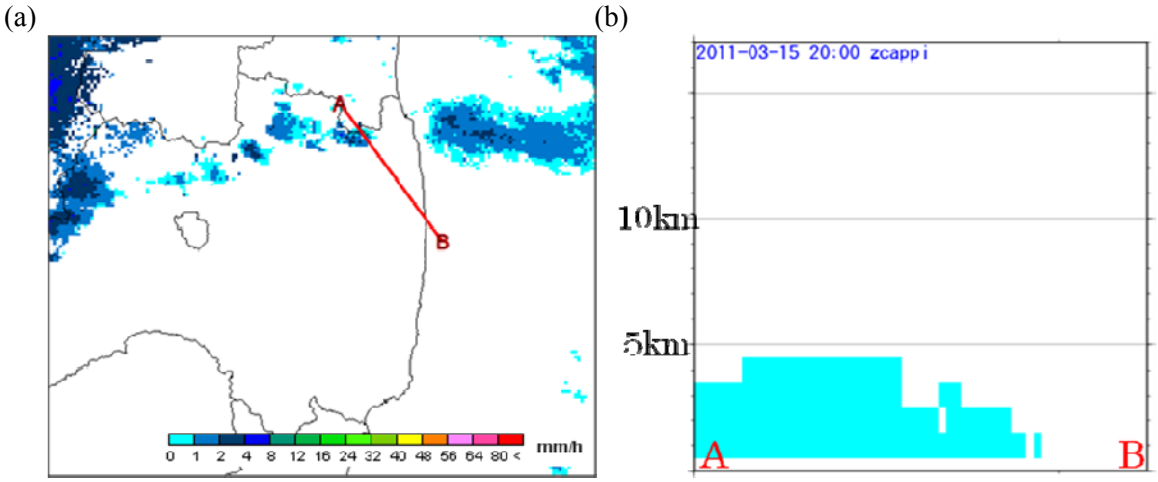

Fig. C-9-6. (a) Horizontal distribution of precipitation intensity estimated by JMA radar at 2000 JST 15 March 2011, and (b) vertical cross section of red line in (a).

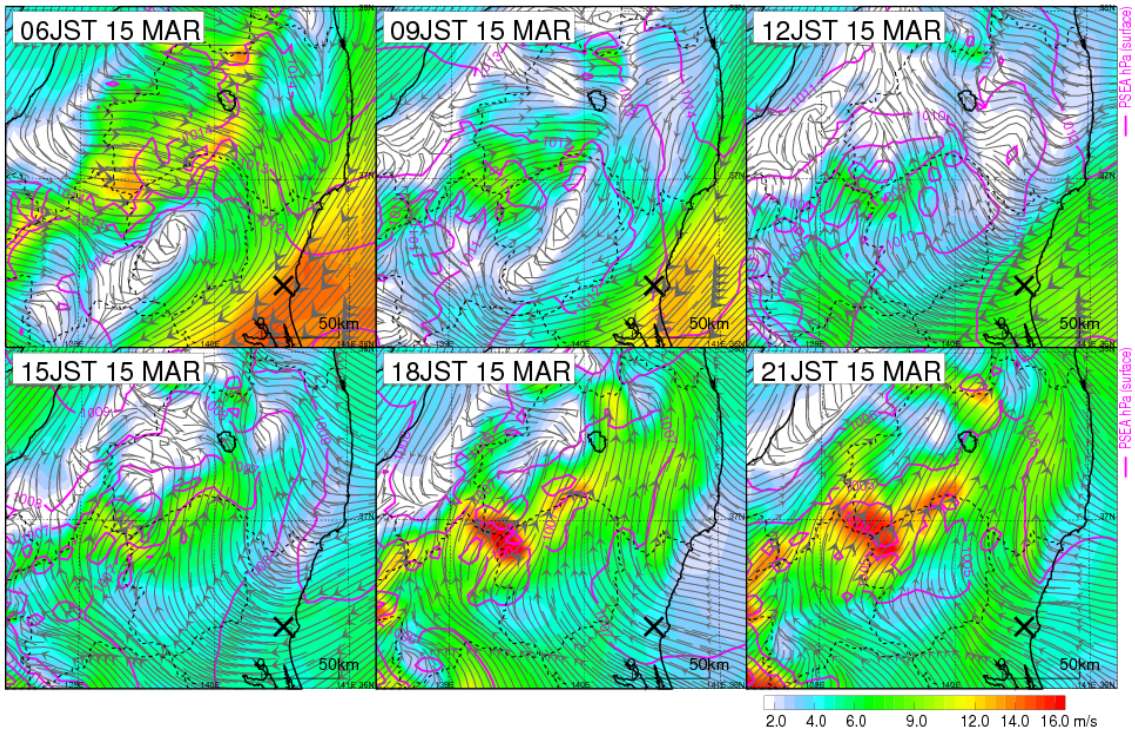

Fig. C-9-7. Horizontal winds at about a 540 m height above the model surface (stream lines), their speed (color shade) and sea level pressure (pink contours) depicted from mesoscale analysis of JMA between 2100 UTC, 14 (0600 JST, 15) and 1200 UTC (2100 JST), 15 March 2011. Black crosses show the location of Mito.

D. ATDM experiments

D-1. Design of the Task Team Experiment[1]

The ATDMs used by the WMO Task Team members included MLDP0 (*Modèle Lagrangien de Dispersion de Particules d'ordre 0* – Canada; D'Amours et al., 2010), HYSPLIT (Hybrid Single-Particle Lagrangian Integrated Trajectory Model - United States; Draxler and Hess, 1997), NAME (Numerical Atmospheric-dispersion Modelling Environment - United Kingdom; Jones et al. 2007), RATM (Regional Atmospheric Transport Model – Japan; Shimbori et al., 2010), and FLEXPART (Lagrangian Particle Dispersion Model – Austria; Stohl et al., 2005). All ATDMs were of a class of models called Lagrangian Particle Dispersion Models (LPDMs). The transport and dispersion of individual pollutant particles or gases are simulated in a computational framework that follows the position of the individual element by its mean motion from the wind fields and a turbulent component to represent the dispersion. These models are all run in off-line mode, meaning that the meteorological fields needed as input to the ATDM have to be made available before the runs are conducted.

There were four global meteorological analyses data sets (Canada, United States, European Center for Medium-Range Weather Forecasts, UK Met Office) and two regional high-resolution analyses (Japan) available for use by the ATDMs. These data sets are briefly described in Table D-1-1.

Table D-1-1. Summary of the meteorological analyses fields available for the ATDM calculations.

Meteorological Center's Product	Acronym	Space	Time	Vertical
CMC's Global Environmental Multiscale system	GEM	0.30°	6 h	Sigma
NOAA's Global Data Assimilation System	GDAS	0.50°	3 h	Hybrid sigma
The European Centre for Medium-Range Weather Forecasts	ECMWF	0.125° and 0.2°	3 h	Hybrid sigma
UKMET's operational global Unified Model	MetUM	0.23° by 0.35°	3 h	Height levels
JMA's mesoscale analyses fields	MESO	5 km	3 h	Hybrid height levels
JMA's radar-rain gauge-analyzed precipitation	RAP	1 km	30 min	Surface

Each participating modeling center used its own dispersion model with one or more of the meteorological data sets, resulting in 18 different combinations of dispersion models and meteorological input data for the initial analysis provided to UNSCEAR (Table D-1-2) using their preliminary source term. Subsequently, JMA revised its dispersion model and two additional simulations were available for the task team summary (Draxler et al., 2015) that used the Terada (2012) source term.

[1] R. Draxler

Table D-1-2. ATDM-Meteorology simulations completed (C) by each participating ATDM model (rows) with different meteorological data (columns) and also the ATDM simulations enhanced with the RAP data (R).

Data / Model	CMC	NOAA	ECMWF	MetUM	JMA
CMC-MLDP0	C				C
JMA-RATM					C,R
NOAA-HYSPLIT		C,R	C,R		C,R
UKMET-NAME			C	C	C,R
ZAMG-FLEXPART		C,R	C,R		

One critical aspect for the quantitative predictions of air concentration and deposition is the wet and dry scavenging that occurs along the particle's transport pathway. Since following a large number of radionuclides could be computationally prohibitive, only three generic species were tracked as surrogates for all of the radionuclides: a gas with no wet or dry scavenging (noble gas), a gas with a relatively large dry deposition velocity and wet removal to represent gaseous ^{131}I, and a particle with wet removal and a small dry deposition velocity to represent all the remaining radionuclide particles. There can be considerable variability in scavenging coefficients and deposition processes. Each ATDM had its own unique treatment of these processes which are described in more detail in Chapter F.

The ATDMs were all run "off-line" meaning that space and time varying meteorological data fields for the computational period must be available. The period of 11 – 31 March 2011 was determined to be the time window of greatest interest. Given the uncertainties in the emissions and the temporal frequency of meteorological analyses, the release periods were divided into three-hour duration segments. The emission rate is assumed to be a constant for each three-hour period. A separate 72 hour duration ATDM calculation was made for each radionuclide release period which was sufficiently long to permit particles to exit the regional sampling domain. After testing the ATDM calculations with several different particle number release rates and considering the regional nature and resolution of the concentration grid, the emissions were represented by the release of 100,000 particles per hour with a total mass of one unit per hour. Because of the uncertainty in the actual value of the time varying release height, particles were uniformly released from ground-level to 100 m.

The ATDM calculations were started every three hours from 11 March 0000 UTC through 31 March 2100 UTC, resulting in 168 independent calculations. All ATDMs used a predefined concentration/deposition grid configuration of 601 (west to east) and 401 (south to north) grid cells on a regular latitude-longitude grid at 0.05 degrees resolution (about 5 km) centred at 38N and 140E (Fig. D-1-1). The output was configured to provide 3-hour averages for air concentrations and 3-hour

deposition totals. Air concentration and deposition at any one point in space and time are computed by adding together the contribution of the each of the release period calculations (within that 72 hour window) contributing to desired sampling period.

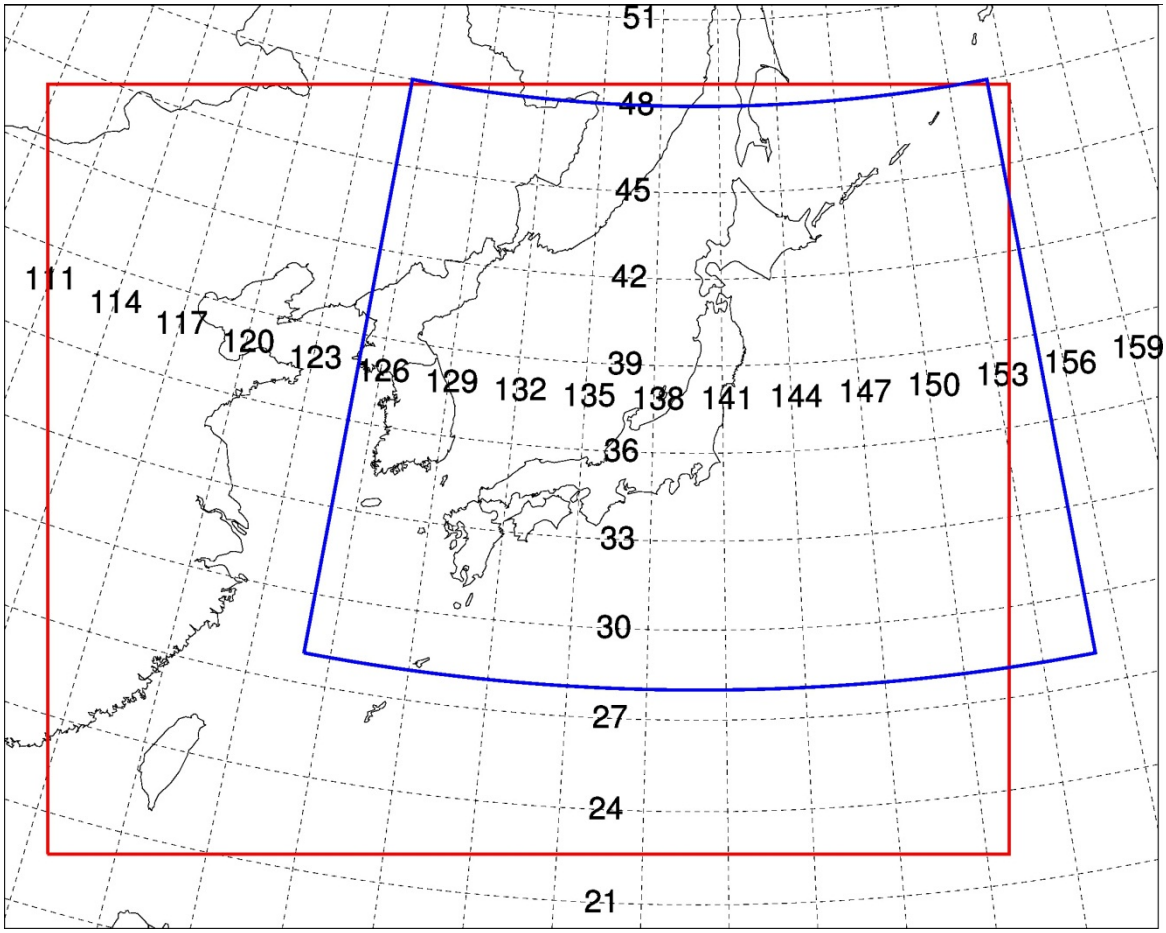

Fig. D-1-1. The air concentration and deposition grid (blue) and mesoscale analysis data grid (red).

Because of the fact that emissions were not finalized at the beginning of the TT study, and the undetermined number of radionuclides that might be required, all ATDM computations were done using a unit source emission rate. The calculation for each emission period provides the dispersion and deposition factors from the release point for that emission period to all downwind grid locations, defining what fraction of the emissions are transferred to each location for every output time period. The set of calculations for all emission times can be defined as the Transfer Coefficient Matrix (TCM). When quantitative results are required, the actual air concentrations and depositions are computed in a simple post-processing step by assigning the TCM computational surrogate to a specific radionuclide, multiplying the TCM by the appropriate time-varying emission rates and radioactive decay constant. The emissions that were provided had been decay-corrected to 0600 UTC 11 March. Therefore in the post-processing computation of air concentration and deposition, individual radionuclide decay rates are applied starting from the normalization time. Using this methodology, results for multiple

emission scenarios can easily be obtained without rerunning any of the ATDMs. A detailed description of this approach is given by Draxler and Rolph (2012). The TCM concept is a specific operational realization of the source receptor matrix concept and similar to the backtracking computations to create Source Receptor Sensitivity Fields (Wotawa et. al., 2002).

D-2. Reverse estimation of amounts of ^{131}I and ^{137}Cs discharged into the atmosphere[1]

During the Fukushima Daiichi Nuclear Power Plant (FDNPP) accident, an urgent task was to assess the radiological dose to the public resulting from the atmospheric release of radionuclides. This assessment was done by using both environmental monitoring data and computer simulations based on atmospheric dispersion modeling. However, source terms (e.g., the release rates and durations of radionuclides) essential to computer simulations of atmospheric dispersion were not available, although stack monitors or a severe accident analysis were expected to provide them. The Japan Atomic Energy Agency (JAEA), in cooperation with the Nuclear Safety Commission of Japan (NSC), has attempted to estimate the source terms of iodine and cesium discharged from FDNPP into the atmosphere by a reverse estimation method. In this method, the source terms are estimated by coupling environmental monitoring data with atmospheric dispersion simulations under the assumption of a unit release rate (1 Bq h^{-1}). We estimated the release rates and total amounts of ^{131}I and ^{137}Cs discharged from FDNPP from 12 March to 1 May 2011.

D-2-1. Reverse estimation method

The release rates of radionuclides (Bq h^{-1}) are calculated by dividing measured atmospheric activity concentrations of each radionuclide (^{131}I and ^{137}Cs) by simulated ones at each sampling point as follows:

$$Q_i = M_i / C_i , \qquad \text{(D-2-1)}$$

where Q_i is the release rate (Bq h^{-1}) of radionuclide i into the atmosphere, M_i is the measured atmospheric activity concentration (Bq m^{-3}) of radionuclide i, and C_i is the dilution factor (h m^{-3}) of radionuclide i, which is equal to the activity concentration simulated under the assumption of a unit release rate (1 Bq h^{-1}). Peak values from a time series of continuous measurement data were adopted for both the measured and calculated values used in Eq. (D-2-1). If concentration data for the source term estimation were available from two or more different measurement sites at the same time, only the highest value was used in the release rate calculation.

When atmospheric activity concentration data were not available, the release rates were estimated by comparing measured air dose rates due to radionuclides in plumes and/or on the ground surface with simulated rates derived from the simulations with a unit release rate, by assuming the radionuclide composition (iodine, cesium, etc.).

Total release amounts were estimated by time integration of the release rates as follows:

$$S_i = \sum \left[Q_{i,j} \times T_j \right], \qquad \text{(D-2-2)}$$

where S_i is the total released amount (Bq) of radionuclide i, $Q_{i,j}$ is the release rate (Bq h^{-1}) of radionuclide i at time j, and T_j (h) is the duration of the period when the release rate $Q_{i,j}$ was estimated to continue. When no monitoring data were available at time j, release rates obtained before or after time j were temporally interpolated or extrapolated.

[1] H. Terada and M. Chino

D-2-2. Environmental monitoring data

Environmental monitoring data of atmospheric activity concentrations of iodine and cesium (hereafter, dust sampling data) were mainly used for the source term estimation. We assumed that gaseous and particulate iodine were sampled according to the NSC's guidelines for environmental radiation monitoring (NSC, 2010), which recommends the use of dust samplers with charcoal cartridges for gaseous iodine. The data used in the estimation are available on the web sites of the Ministry of Education, Culture, Sports, Science and Technology (MEXT) (MEXT, 2011a), the Ministry of Economy, Trade and Industry (METI) (METI, 2011), the Japan Chemical Analysis Center (JCAC) (JCAC, 2011), and JAEA (Furuta et al., 2011). These data were collected in eastern Japan, mainly Fukushima Prefecture. Air dose rate monitoring data from MEXT (MEXT, 2011b) and Fukushima Prefecture (Fukushima Prefecture, 2011a, 2011b) indicated that the atmospheric release of radionuclides in the daytime of 15 March resulted in a large amount of ground deposition and, thus, high dose rates in the sector to the northwest of FDNPP. However, because no dust monitoring data were available in the daytime of 15 March, the release rates of ^{131}I and ^{137}Cs at that time were estimated by comparing measured air dose rate patterns due to ground shine with simulated patterns after the plume had moved away from this region. Similarly, the release amount on the afternoon of 12 March was also estimated from ground shine. The measurement data used for source term estimation are described in detail by Chino et al. (2011), Katata et al. (2012a, 2012b), and Terada et al. (2012).

D-2-3. Atmospheric dispersion simulation

The System for Prediction of Environmental Emergency Dose Information (SPEEDI) (MEXT, 2007), which is operated by the Nuclear Safety Technology Center of Japan, and the Worldwide version of SPEEDI (WSPEEDI-II) (Terada et al., 2008) developed by JAEA, were used for calculating atmospheric activity concentrations and air dose rates. The NSC provided the simulation results from SPEEDI to JAEA for the purpose of this source term estimation. Atmospheric dispersions of radionuclides were simulated by successive uses of the PHYSIC meteorological prediction model and the PRWDA21 atmospheric dispersion model in SPEEDI, and MM5 and GEARN in WSPEEDI-II. These models are described in detail by Nagai et al. (1999) and Terada and Chino (2008).

D-2-4. Results

Figure D-2-1 shows the estimated temporal variation in release rates of ^{131}I and ^{137}Cs (Terada et al., 2012) from 05:00 Japan Standard Time (JST = UTC + 9 h) on 12 March to 00:00 JST on 6 April 2011. Chino et al. (2011), Katata et al. (2012a, 2012b), and Terada et al. (2012) have described the source term estimation results in detail. Here, the estimation results are only outlined.

On the morning of 12 March, leakage of radionuclides from the Unit 1 primary containment vessel (PCV-U1) was detected, but the level of leakage was lower than that at later stages of the accident. At 15:36 JST on the afternoon of 12 March, a hydrogen explosion at Unit 1 increased the release rates of radionuclides. Between 15:30 and 16:00 JST, the estimated release rates were 3.0×10^{15} and 3.0×10^{14} Bq h^{-1} for ^{131}I and ^{137}Cs, respectively.

Venting operations were conducted to decrease the internal pressure of PCV-U3 at 09:24 and 12:30 JST on 13 March and at 05:20 JST on 14 March. However, the simulated plume mainly flowed toward the ocean on these days. In spite of these venting operations, a hydrogen explosion occurred at Unit 3 at 11:01 JST on 14 March. Because we had no sampling data from that time, we assumed that the release amounts were the same as those after the hydrogen explosion at Unit 1.

During the night of 14 March, dry venting was attempted at Unit 2. Though it is not clear whether the venting succeeded, the plume flowed south to south-southwest during this period. The observed air dose rates at Fukushima Daini Nuclear Power Plant (11.4 km to the south of FDNPP) and Kitaibaraki (80 km to the south) and atmospheric activity concentrations of ^{131}I and ^{137}Cs at JAEA-Tokai (100 km to the south) were high. By our source term estimation, the release rates of 3.5×10^{14} to 1.3×10^{15} Bq h^{-1} for ^{131}I and of 4.0×10^{13} to 1.3×10^{14} Bq h^{-1} for ^{137}Cs were estimated for the night of 14 March.

Between 07:00 and 12:00 JST on 15 March, the internal pressure of PCV-U2 decreased. This decrease corresponded to an extreme increase in the air dose rate to 1.5×10^{4} μGy h^{-1}, observed at the main gate from 07:00 to 10:00, which was clearly due to an increase in the release rate. The release rate from 07:00 to 10:00 was estimated to be 3.0×10^{15} for ^{131}I and 3.0×10^{14} Bq h^{-1} for ^{137}Cs. After this major release on the morning of 15 March, the internal pressure of PCV-U2 continued to decrease during the afternoon. The plume discharged during the afternoon of 15 March was carried directly toward Iitate village and Fukushima City by southeasterly winds, and a large amount of wet deposition occurred northwest of FDNPP. From 13:00 to 17:00 JST on 15 March, the estimated release rates of ^{131}I and ^{137}Cs increased again, to 4.0×10^{15} and 4.0×10^{14} Bq h^{-1}, respectively.

From 16 March to the early morning of 20 March, the plume was carried primarily toward the Pacific Ocean by westerly and northwesterly winds; consequently, too few monitoring data were available for estimating the source terms. Instead, we estimated the source terms during this period by temporal interpolation of those estimated during the period when observation data were available.

Beginning on 20 March, the direction of the plume again became landward. By this time, a systematic environmental monitoring had been established to measure atmospheric activity concentrations in Fukushima Prefecture. From 20 to 24 March, the estimated release rates of ^{131}I and ^{137}Cs were in the range of 1.4×10^{14} to 7.1×10^{14} Bq h^{-1} and 1.1×10^{12} to 3.5×10^{13} Bq h^{-1}, respectively.

After 25 March, the estimated release rates gradually decreased, although a temporary increase to the rate on 20 March occurred on 30 March. Subsequently, the release rates decreased continuously, and from the beginning of April estimation of the source terms by the reverse estimation method was difficult because no clear increases in atmospheric activity concentrations and the air dose rates were detected.

Using Eq. (D2-2), we estimated the total amounts of ^{131}I and ^{137}Cs discharged into the atmosphere from 05:00 JST on 12 March to 00:00 JST on 1 May to be approximately 1.2×10^{17} and 8.8×10^{15} Bq, respectively.

D-2-5. Future Tasks

The uncertainty of the estimated release rates is mainly due to that of the atmospheric dispersion calculations and the limited temporal and spatial coverage of the monitoring data. By comparing available observations and simulated results, we made the following simplified adjustments in the source term estimation.

- When there was a slight discrepancy in plume location between the simulation and the observations, the simulated plume distribution was rotated to reduce the discrepancy.
- When small differences were seen in plume arrival times between the simulation and the observations, the peak concentration values in the continuous measurement time series were used together with the simulated results for the release rate calculation.

Even after these adjustments, the error of the estimated release rates was at least a factor of 5. To estimate the total amounts of the radionuclides discharged into the atmosphere, the release rates were interpolated or extrapolated when no dust sampling data were available. The uncertainty due to this procedure cannot be assessed by using the presently available data. To estimate the temporal variation of release more accurately, further investigation of environmental data and technical evaluation by specialists of the reactor analysis and environmental fields are required.

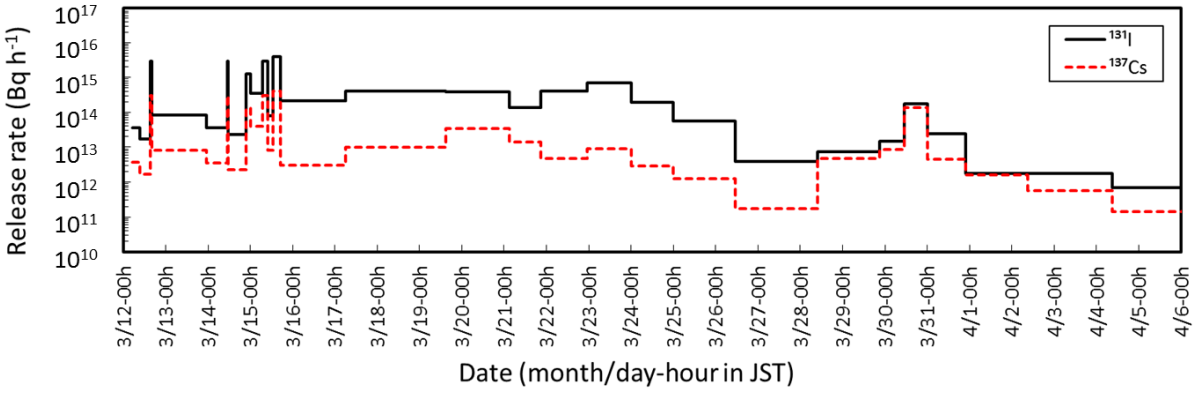

Fig. D-2-1. Estimated temporal variations of the release rates of ^{131}I and ^{137}Cs from 05:00 JST on 12 March to 00:00 JST on 6 April 2011.

D-3. Verification Methods[1]

The TT concluded that the most robust overall metric would be to evaluate the ATDM's performance by comparing the model predicted patterns of ^{137}Cs deposition to the available deposition measurements. The accumulated ^{137}Cs deposition field has the advantage of the availability of measurements over a wide region. However, one disadvantage is that the bulk of the deposition occurred during only a few time periods. There are also no deposition measurements over water, effectively excluding all episodes with westerly winds from the analysis. In addition to deposition, there is considerable interest in how well the ATDM-meteorology combinations can represent the air concentration data. However, in terms of radionuclide specific measurements, air concentration data were available at only a few locations. Air dose rate measurements could not be used for the TT analysis.

To perform a quantitative analysis of the ATDM-meteorology combinations, the TT used the ^{137}Cs deposition first reported by the Japanese Ministry of Education and Science and Technology (MEXT, 2011c). The ground-level results were merged with the observations by the U.S. Department of Energy's (USDOE, 2011) fixed-wing aircraft (C-12) from 2 April 2011 to 9 May 2011. The collected aircraft and ground based data points were averaged onto a grid (0.05 degree resolution) that was identical to the one used in the ATDM calculations. The aircraft based sampling covered 374 grid points and blending in the additional ground based MEXT data resulted in a total of 543 grid points for model verification. Note that the final deposition product shown in Fig. D-3-1 captures the heaviest deposition in the Fukushima prefecture, but does not include any of the deposition to the southwest.

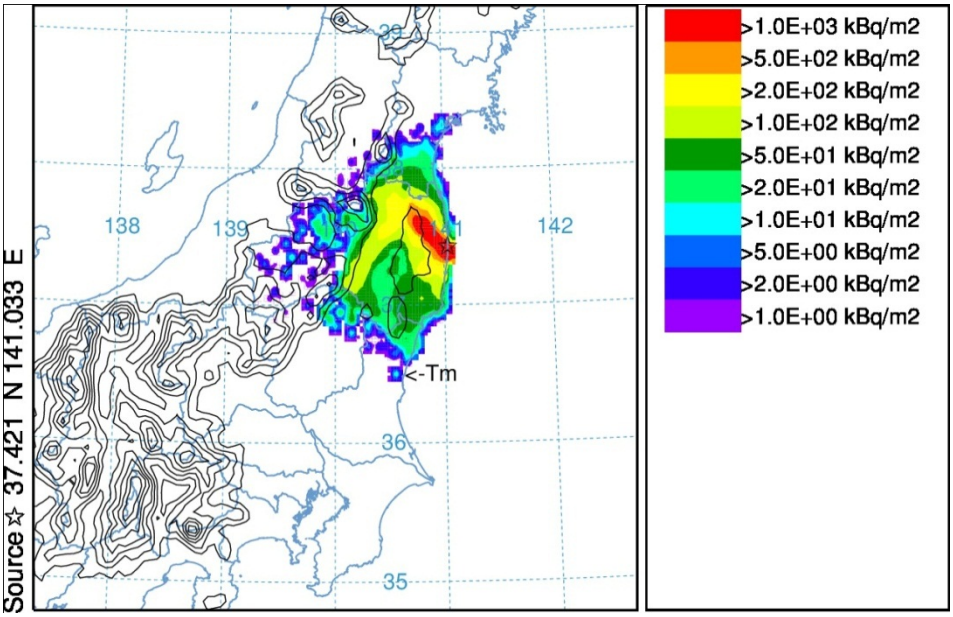

Fig. D-3-1. Averaged MEXT surface deposition and U.S. DOE aircraft based deposition measurements of ^{137}Cs and the location of the Toki-Mura air sampling site.

[1] R. Draxler

After the accident at the Fukushima Daiichi Nuclear Power Plant, radiation was monitored at the Nuclear Fuel Cycle Engineering Laboratories, Japan Atomic Energy Agency (JAEA) at their Tokai-Mura location (see Fig. D-3-1). Furuta et al. (2011) provides the monitoring results of dose rates, air concentrations, and deposition until 31 May 2011. The TT used the time series of ^{137}Cs and ^{131}I (aerosol and gas) air concentrations for the ATDM-meteorology evaluations for the 11-31 March period.

Procedures for evaluating ATDM calculations have a long history but the problem eludes simple solutions because the variability in atmospheric motions and processes cannot be deterministically represented in any model resulting in the inevitable mismatches between paired in space and time predicted and measured concentrations. The ATDM-meteorology evaluation protocol used here follows the procedure described by Draxler (2006), including a ranking method that gives equal weight to the normalized (0 to 1) sum of the correlation coefficient (R), the fractional bias (FB), the figure-of-merit in space (FMS), and the Kolmogorov-Smirnov parameter (KSP), such that the total model rank would range from 0 to 4 (from worst to best),

$$\text{Rank} = R^2 + 1 - |FB/2| + FMS/100 + (1 - KSP/100). \quad \text{(D-3-1)}$$

The correlation coefficient (R), also referred to as the Pearson's Correlation Coefficient (PCC), is used to represent the scatter among paired measured (M) and predicted (P) values:

$$R = \frac{\sum (M_i - \overline{M})(P_i - \overline{P})}{\sqrt{\sum (M_i - \overline{M})^2 \sum (P_i - \overline{P})^2}}, \quad \text{(D-3-2)}$$

where the summation is taken over the number of samples and the over-bar represents a mean value. A normalized measure of bias is the fractional bias (FB). Positive values indicate over-prediction and FB ranges in value from –2 to +2 and it is defined by:

$$FB = 2\frac{(\overline{P} - \overline{M})}{(\overline{P} + \overline{M})}. \quad \text{(D-3-3)}$$

The normalized mean square error (NMSE) is defined as:

$$NMSE = \frac{1}{\overline{M} \cdot \overline{P}} \cdot \frac{1}{N} \sum (M_i - P_i)^2 . \quad \text{(D-3-4)}$$

The NMSE provides information on the deviations and not on the overestimation or underestimation. This parameter is very sensitive to differences between measured and predicted values. Perfect model results would have a NMSE value of zero. A similar metric is the root mean square error (RMSE), which is the square root of NMSE without normalization by (M-P).

The spatial distribution of the calculation relative to the measurements can be determined from the Figure of Merit in Space (FMS), which is defined as the percentage of overlap between measured and predicted areas. Rather than trying to contour sparse measurement data, the FMS is calculated as the intersection over the union of predicted (p) and measured (m) concentrations in terms of the number (N) of samplers with concentrations greater than a pre-defined threshold (zero):

$$\mathrm{FMS} = 100\frac{N_P \cap N_M}{N_P \cup N_M}. \qquad \text{(D-3-5)}$$

Differences between the distribution of unpaired measured and predicted values is represented by the Kolmogorov-Smirnov parameter, which is defined as the maximum difference between two cumulative distributions when $M_k = P_k$, where

$$\mathrm{KSP} = Max\,|D(M_k) - D(P_k)|\,, \qquad \text{(D-3-6)}$$

and D is the cumulative distribution of the measured and predicted concentrations over the range of k values such that D is the probability that the concentration will not exceed M_k or P_k. It is a measure of how well the model reproduces the measured concentration distribution regardless of when or where it occurred. The maximum difference between any two distributions cannot be more than 100%.

D-4. The NOAA ARL Website[1]

As part of the evaluation process, the unit-source dispersion and deposition calculations from all the TT members were posted on a web page (http://ready.arl.noaa.gov/READY_fdnppwmo.php) hosted by the U.S. National Oceanic and Atmospheric Administration (Fig. D-4-1). The web interface provided a way for the TT members to evaluate their results, compare them to those of the other members, and permit the UNSCEAR emission group to test various emission scenarios and compare the results to measured deposition and air concentration data.

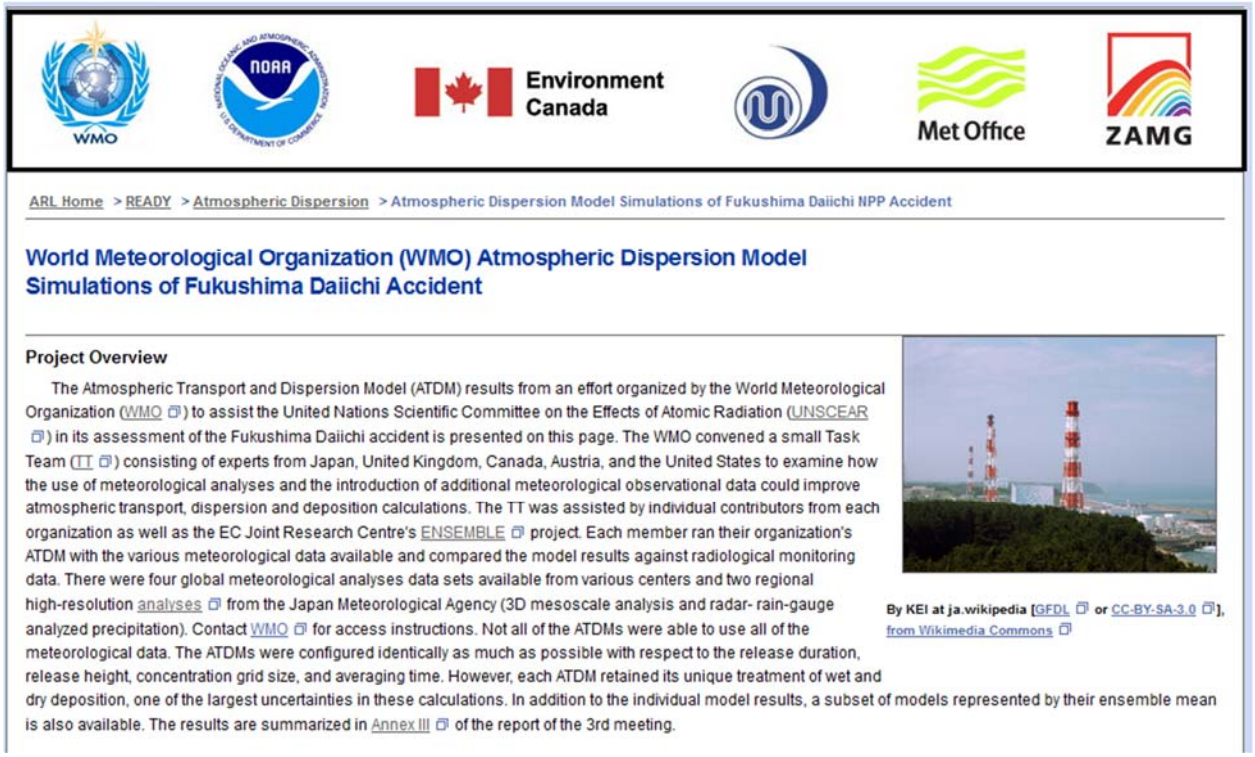

Fig. D-4-1. The home page for the WMO Fukushima meteorological evaluation results.

The web site provided access to all the ATDM-Meteorology combinations that were created during the Task Team's effort, various ensemble combinations of different members, as well as the results of additional calculations that were conducted by various members after the conclusion of the TT activities. The web site is still open to accept additional ATDM model results as long as they match the computational protocols. Upon selecting an ATDM-meteorology combination for analysis, a second web page is opened that permits the selection of a default source term (Fig. D-4-2). The available source terms may change from time to time, but the JAEA-Terada source term is the final one used by UNSCEAR. Various new source terms are under consideration.

[1] G. Rolph (NOAA) and R. Draxler

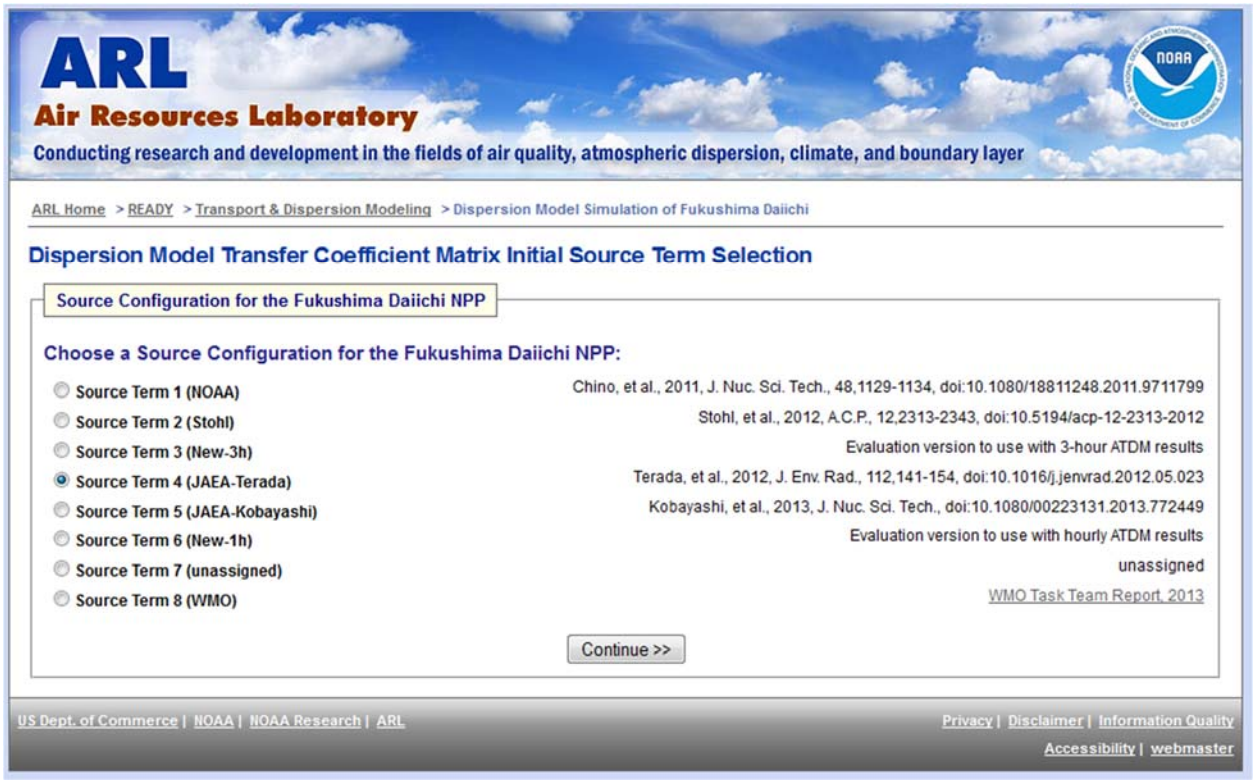

Fig. D-4-2. The source-term selection page.

Selection of any one source term just pre-populates the next page with 3-hourly values for ^{137}Cs, and gaseous and particulate ^{131}I (Fig. D-4-3). The web user may change the value of any of the pre-populated values to determine the effect on the final results. Although the source terms are defined for each 3-hour emission period, which corresponds to one ATDM simulation, the rate is given in Becquerels per hour. The emission entry page also permits the definition of any new species; the identification field is arbitrary, but the half-life and species type (noble gas, depositing gas, or particle) defines the subsequent calculation. The source term for each three-hour period is multiplied by the ATDM calculation for that time period and the air concentration and deposition grids from all ATDM simulations are added together for the same period to obtain the final values. Unless other species are requested to be included, the calculations will only be done for ^{137}Cs. Each species requires another pass through all the data files.

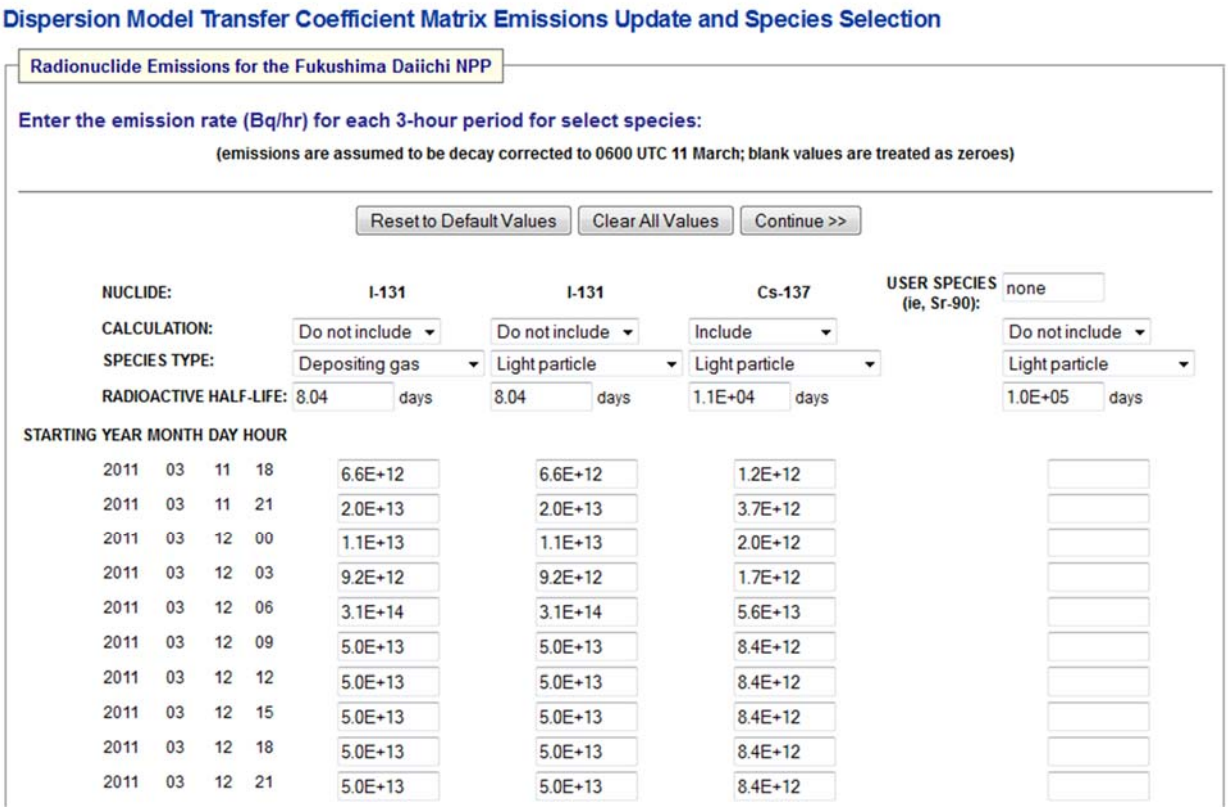

Fig. D-4-3. Source term entry page.

Pressing the continue button opens the verification selection page (Fig. D-4-4) where the air concentration or deposition measurements used for verification may be selected. Only two air concentration locations with measurement data are available for selection (Tokai-Mura and Takasaki), although other locations can be entered to extract model predictions at those locations. The default deposition is the one used for the WMO Task Team effort, the combination of DOE airborne and MEXT ground based measurements. However, recently added were the results of the MEXT airborne survey of May 2012, which includes results from all the prefectures, not just Fukushima.

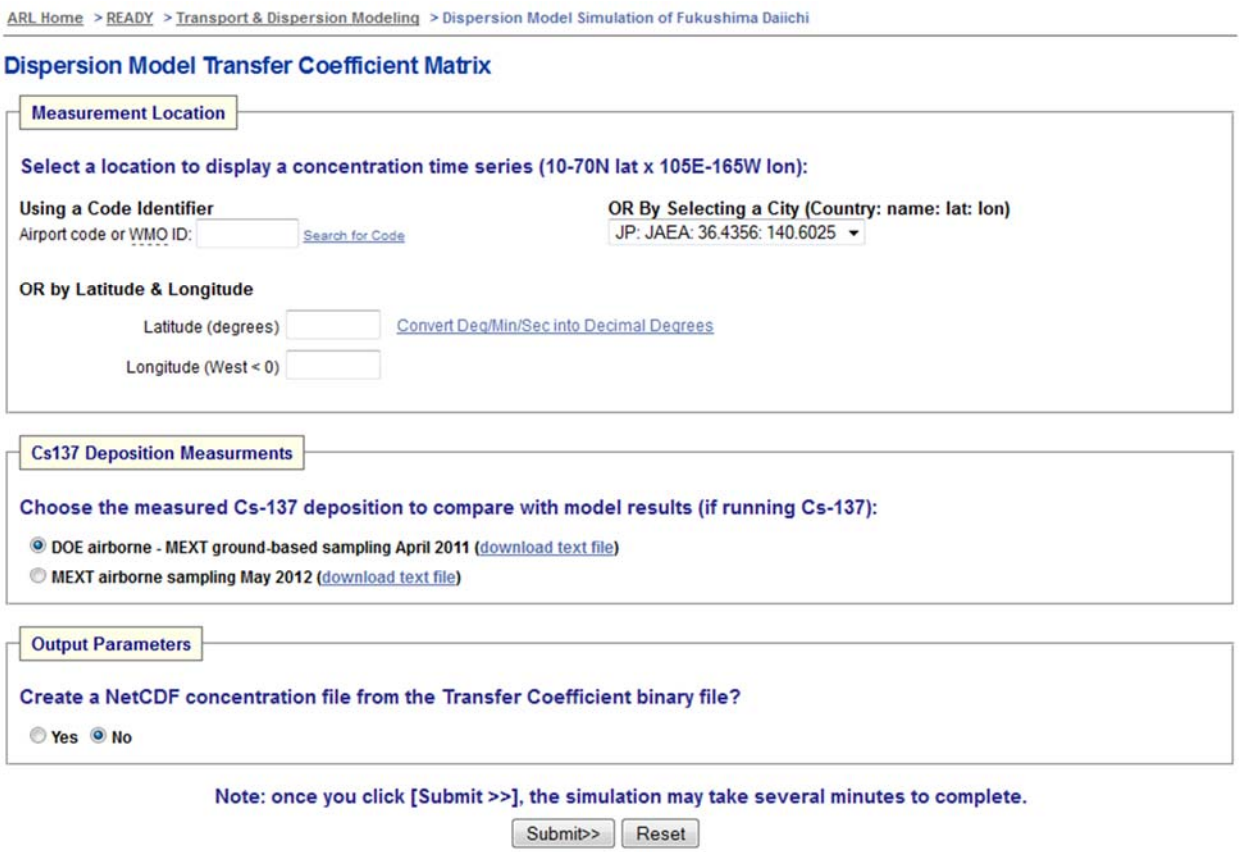

Fig. D-4-4. Verification selection page.

When the calculations have been completed, the model results page opens (not shown), which shows icons of the time series and scatter diagrams as well as text summaries of the statistical results. The deposition results have some text links rather than icons. Creating a deposition map requires a second step, where the time period as well as the contour intervals must be selected. Various output formats are available.

D-5. Task team final report and follow-up[1]

D-5-1. Task team final report and WMO technical publication

The final report of the Task Team was as uploaded as ANNEX III of the third meeting report on the website of WMO's CBS-DPFS/ERA related Meetings page (http://www.wmo.int/pages/prog/www/CBS-Reports/documents/WMO_fnpp_final_AnnexIII_4Feb2013_REVISED_17June2013.pdf), and published as WMO technical publication No. 1120 (Draxler et al. 2013a). The UNSCEAR (Fischer 2012) and JMAEA source terms (Section D-2) were used for verification. In Section 10 of the above mentioned reports, an ensemble analysis and discussion on ATDM uncertainty based on UNSCEAR source term is included. In addition, a more complete discussion of the ensemble analyses has been published by Solazzo and Galmarini (2015).

D-5-2. Presentations at the 93rd meeting of AMS and EMS and related publications

The 93rd American Meteorological Society annual meeting was held in Austin, Texas from January 6 to 10, 2013. A "Special Symposium on the Transport and Diffusion of Contaminants from the Fukushima Dai-Ichi Nuclear Power Plant: Present Status and Future Directions"; https://ams.confex.com/ams/93Annual/webprogram/FUKUSHIMASYMP.html) was organized there, and presentations were made on various topics such as an overview of the effects on the human body , emission source estimation, observations, limited model analysis, global ocean model analysis, and international cooperation. Draxler et al. (2013b) reported on the WMO Task Team results and Saito et al. (2013) presented JMA's contribution to the WMO Task Team activities. The presentations of the symposium are summarized by Kondo et al., 2013. Wotawa et al. (2013) also reported on some of the task Team's ATDM comparative experiments at the European Meteorological Society's annual meeting.

Five papers relating to the Task Team activities have been published in the Fukushima nuclear accident special issue of the Journal of Environmental Radioactivity (Draxler et al., 2015; Arnold et al., 2015; Saito et al., 2015; Leadbetter et al., 2015; Solazzo and Galmarini, 2015).

D-5-3. UNSCEAR 60th General session and its final report

The 60th General Assembly of UNSCEAR was held in Vienna from May 27 to 31, 2013 (http://www.unscear.org/unscear/en/about_us/sessions.html). The meeting report is available from the UNSCEAR website (http://daccess-ods.un.org/TMP/9420922.3985672.html). An UNSCEAR evaluation report on the Fukushima Daiichi nuclear power plant accident (UNSCEAR, 2014) was published separately in April 2014 as ANNEX A. From the task team final report, the results of the calculation of the NOAA ATDM and meteorological conditions were included in Appendix B.

[1] K. Saito and R. Draxler

E. JMA-RATM[1]

E-1. Original and Preliminary RATM

E-1-1. Description of RATM

The JMA-RATM (Japan Meteorological Agency Regional Atmospheric Transport Model, called the 'RATM' in this chapter) is a mesoscale tracer transport model, which can be driven by the JMA-MESO analysis GPVs (grid point values). The model takes a Lagrangian scheme (Iwasaki et al., 1998; Seino et al., 2004) with many computational particles that follow advection, horizontal and vertical diffusion, gravitational settling, wet scavenging and dry deposition processes. The RATM was originally developed at JMA for photochemical oxidant predictions (Takano et al., 2007) and volcanic-ash fall forecasts (Shimbori et al., 2009). In this section, we describe the original version of RATM (Shimbori et al., 2010) and a preliminary version of RATM to simulate radionuclides for the WMO technical Task Team (Saito et al., 2015). Flowchart of the RATM calculation for radionuclides is shown in Fig. E-1-1. Specifications of each version of the RATM are summarized in Table E-1-1.

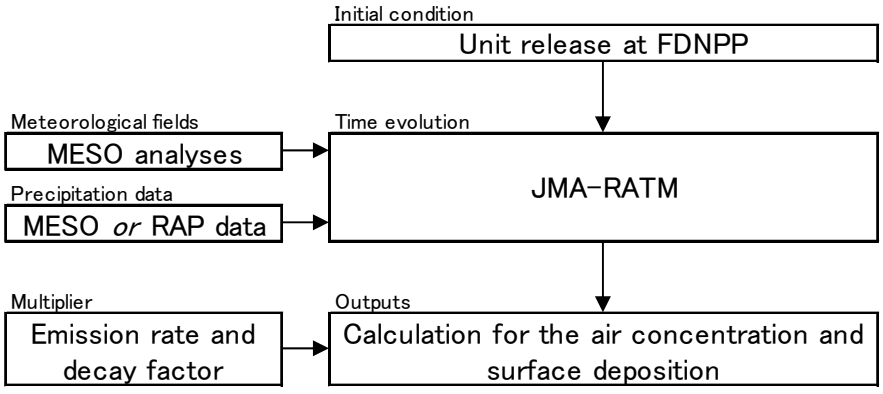

Fig. E-1-1. Flowchart of the JMA-RATM calculation for radionuclides.

a. Advection

We write the position $(x(t), y(t), z(t))$ for each computational particle at time t. The time evolution after the time step Δt is given by

$$x(t+\Delta t) = x(t) + \overline{u(t)}\Delta t + u'(t)\Delta t \quad \text{(E-1-1a)}$$

$$y(t+\Delta t) = y(t) + \overline{v(t)}\Delta t + v'(t)\Delta t \quad \text{(E-1-1b)}$$

$$z(t+\Delta t) = z(t) + \overline{w(t)}\Delta t + \sqrt{2K_{\mathrm{v}}\Delta t}\Gamma - V_{\mathrm{t}}\Delta t \quad \text{(E-1-1c)}$$

with the mean wind velocity $(\overline{u(t)}, \overline{v(t)}, \overline{w(t)})$. On the right-hand sides of above equations, the second and third terms represent advection and diffusion, respectively. The forth term of Eq. (E-1-1c) represents gravitational settling.

[1] T. Shimbori and K. Saito

Table E-1-1. Specifications of JMA-RATM.

Version		Original	Preliminary	Revised		Test
		for JMA Volcanic Ash Fall Forecast[1]	for WMO Task Team		for SCJ Working Group	
Model type		Lagrangian description				
Input meteorological field		Hourly outputs of MESO forecast GPVs	Three-hourly outputs of MESO analysis GPVs			
Number of particles		100,000/10 min.	100,000/3 h	300,000/3 h		
Time step		3 min.	10 min.		5 min.	
Advection	Horizontal	Forward difference with spherical triangle				
	Vertical	Not adjusted		Spatially-average and terrain-following at lowest model level		
Horizontal diffusion		Gifford (1982, 1984)				
Vertical diffusion		Louis et al. (1982)				
Gravitational settling[2] (grain-size distribution)		Vpar: Suzuki (1983) (log-normal with D_m=0.25 mm, σ_D=1.0)	Ngas: N/A Dgas: N/A Lpar: Stokes' law with Cunningham correction (log-normal with D_m=1 μm, σ_D=1.0)			
Wet scavenging[2]	Washout[3] (below-cloud)	Vpar: Kitada (1994) with MESO forecast (liquid rain)	Ngas: N/A Dgas: N/A Lpar: Kitada (1994) with MESO analysis (liquid rain) or RAP data below 3000 m a.s.l.	Ngas: N/A Dgas: N/A Lpar: same as left except application height below 1500 m a.s.l.	Ngas: N/A Dgas: N/A Lpar: same as left except using MESO analysis (liquid rain, solid snow and graupel)	
	Rainout (in-cloud)	Vpar: N/A	Ngas: N/A Dgas: Hertel et al. (1995) Lpar: N/A			Ngas: N/A Dgas: same as left Lpar: Hertel et al. (1995)
Dry-deposition[2]		Vpar: V_d=0.3 m s^{-1} (Shao, 2000)	Ngas: N/A Dgas: V_d=0.01 m s^{-1} (Draxler and Rolph, 2012) Lpar: V_d=0.001 m s^{-1} (Draxler and Rolph, 2012)			
Reflection on the ground		N/A	Iwasaki et al. (1998)			
Radioactive decay		N/A	Half-lifetime			
Output grid size		5 km				
References		Shimbori et al. (2010)	Draxler et al. (2013a), Saito et al. (2015)		Takigawa et al. (2013), Saito et al. (2015), SCJ (2014)	Saito et al. (2015)

[1] As of March 2011. JMA-RATM for volcanic ash was replaced on March 2013 (Shimbori et al., 2014).
[2] The abbreviations Ngas, Dgas, Lpar and Vpar mean noble gas, depositing gas, light aerosol and volcanic-ash particle, respectively.
[3] Below-scavenging coefficients Λ_w are listed in Table E-3-4.

b. Horizontal diffusion

Under the assumption of horizontally homogeneous turbulence, the $x-$ and y-components of subgrid-scale turbulent velocity in Eqs. (E-1-1a) and (E-1-1b) are given by Uliasz (1990):

$$u'(t) = R_{\mathrm{h}}(\Delta t)u'(t-\Delta t) + \sqrt{1 - R_{\mathrm{h}}\,(\Delta t)^2}\sigma_{u'}\Gamma \tag{E-1-2a}$$

$$v'(t) = R_{\mathrm{h}}(\Delta t)v'(t-\Delta t) + \sqrt{1 - R_{\mathrm{h}}\,(\Delta t)^2}\sigma_{v'}\Gamma \tag{E-1-2b}$$

with the initial conditions $u'(0) = u_0'\Gamma$ and $v'(0) = v_0'\Gamma$. The u_0' and v_0' are the magnitudes of turbulent horizontal velocities at the emission point and Γ is a normal random number with mean 0 and variance 1. R_{h} is the Lagrangian autocorrelation function of the turbulent velocity represented by

$$R_{\mathrm{h}}(\Delta t) = e^{-\Delta t/t_{\mathrm{Lh}}} \tag{E-1-3}$$

with Lagrangian time scale t_{Lh}. $\sigma_{u'}$ and $\sigma_{v'}$ are the standard deviations of u' and v', respectively, given by

$$\sigma_{u'}^2 \approx \sigma_{v'}^2 = \frac{K_{\mathrm{h}}}{t_{\mathrm{Lh}}} \tag{E-1-4}$$

with the horizontal diffusion coefficient K_{h} for $t \gg t_{\mathrm{Lh}}$. Substituting Eqs. (E-1-3) and (E-1-4) into (E-1-2a) and (E-1-2b), to the first order in Δt, we obtain the Langevin equation. Then the horizontal diffusion scheme represented by Eqs. (E-1-2a) and (E-1-2b) is the analogue of Brownian motion (Gifford, 1982, 1984).

For the three parameters in Eqs. (E-1-2a), (E-1-2b) - (E-1-4), we set as $u_0' = 0.253\ \mathrm{m\ s^{-1}}$, $t_{\mathrm{Lh}} = 5.0 \times 10^4\ \mathrm{s}$ and $K_{\mathrm{h}} = 5.864 \times 10^4\ \mathrm{m^2\ s^{-1}}$ according to Kawai (2002).

c. Vertical diffusion

The vertical diffusion coefficient in the third term on the right-hand side of Eq. (E-1-1c) are determined by Louis et al. (1982):

$$K_{\mathrm{v}} = l^2 \left|\frac{\partial \overline{\boldsymbol{U}}}{\partial z}\right| F_{\mathrm{v}}(R_{\mathrm{f}}) \tag{E-1-5}$$

where l is the mixing length in an analogy to the mean free path in molecular diffusion, $\overline{\boldsymbol{U}}$ is the mean horizontal wind velocity, and $F_{\mathrm{v}}(R_{\mathrm{f}})$ representing atmospheric stability is a function of flux

Richardson number R_f given by the level 2 scheme of Mellor and Yamada (1974, 1982). The mixing length takes the form (Blackadar, 1962)

$$l = \frac{kz}{1 + kz/l_0} \tag{E-1-6}$$

where k is the Kármán constant (≈0.4), z is height from ground surface and l_0 is maximum mixing length [m] given by Holtslag and Boville (1993):

$$l_0 = \begin{cases} 30 + 70 \exp\left(1 - \dfrac{z}{1000}\right), & z > 1000 \text{ m} \\ 100 , & z \leq 1000 \text{ m} \end{cases} \tag{E-1-7}$$

The upper limit of K_v is set to 50 $m^2 s^{-1}$ according to Yamazawa et al. (1998).

The above-mentioned schemes of advection and diffusion are used in original RATM and are also applied to radionuclides in the preliminary and revised RATM.

d. Gravitational settling

For dealing with light particles (Lpar) of radionuclides, i.e. radioactive matter or other accumulation-mode aerosol particles carrying some radioactive matter (e.g. ^{137}Cs), gravitational settling follows Stokes' law with a slip correction and the terminal velocity is given by (e.g., Sportisse, 2007)

$$V_t(D, z) = \frac{1}{18} \frac{\rho_p g D^2}{\eta_a / C_c} \tag{E-1-8}$$

where C_c is the Cunningham correction factor

$$C_c = 1 + Kn \left[a + b \exp\left(-\frac{c}{Kn}\right)\right], a = 1.257, b = 0.400, c = 1.100 \tag{E-1-9}$$

with the Knudsen number $Kn \equiv 2\lambda_a / D$. The viscosity η_a and the mean free path λ_a of air are calculated by

$$\eta_a(z) = \eta_0 \left[\frac{T_0 + C_S}{T_a(z) + C_S}\right] \left[\frac{T_a(z)}{T_0}\right]^{3/2} \tag{E-1-10}$$

$$\lambda_a(z) = \lambda_0 \frac{\eta_a(z)}{\eta_0} \left[\frac{p_a(z)}{p_0}\right]^{-1} \left[\frac{T_a(z)}{T_0}\right]^{1/2} = \lambda_0 \left[\frac{p_a(z)}{p_0}\right]^{-1} \left[\frac{T_0 + C_S}{T_a(z) + C_S}\right] \left[\frac{T_a(z)}{T_0}\right]^{2} \tag{E-1-11}$$

where p_a the air pressure, T_a the air temperature, C_S the Sutherland constant of air (=117 K) and $\eta_0 = 18.2\ \mu$Pa s, $\lambda_0 = 0.0662\ \mu$m are the standard values for the reference atmosphere ($T_0 = 293.15$ K, $p_0 = 1013.25$ hPa). The distribution of particle size D is assumed to be log-normal with mean diameter $D_m = 1$ μm and standard deviation $\sigma_D = 1.0$ (upper cutoff: 20 μm). The particle density ρ_p is 1 g cm^{-3} for all particle sizes.

Note that if a computational particle moves under the model surface by the vertical motion, it is numerically reflected to the mirror symmetric point above the surface.

e. Wet scavenging

(1) Washout (below-cloud scavenging)

Because the original RATM was not applied in predicting the dispersion and deposition of radionuclides, the wet scavenging schemes needed to be modified for this application. For Lpar, based on the original treatment of wet scavenging, only washout processes (below-cloud scavenging) are considered. The below-cloud scavenging rate by rain (liquid water) is given by Kitada (1994) (red solid line of Fig. E-1-2):

$$\Lambda_w = AP^B \quad \text{(E-1-12)}$$

$$A = 2.98 \times 10^{-5}\ (\mathrm{s}^{-1}), B = 0.75 \quad \text{(E-1-13)}$$

where P is the precipitation intensity [mm h^{-1}].

(2) Rainout (in-cloud scavenging)

On the other hand, wet deposition for a depositing gas (Dgas, e.g. ^{131}I) is considered only as a rainout process (in-cloud scavenging). The in-cloud scavenging rate for Dgas is given by Hertel et al. (1995):

$$\Lambda_r = \frac{1}{(1 - LWC)/HRT_a + LWC}\frac{P}{Z_r}\ [\mathrm{h}^{-1}] \quad \text{(E-1-14)}$$

where LWC the liquid water content, H the Henry constant (=0.08 M atm^{-1}; Sect. F-1), R the ideal-gas constant (=0.082 atm M^{-1} K^{-1}), and Z_r the height over which in-cloud scavenging takes place.

Wet scavenging is applied to Lpar or Dgas under the height of about 3000 m a.s.l. in the original and preliminary RATM (Shimbori et al. 2010). In the case of in-cloud scavenging for Dgas, however, we have not been able to calibrate the RATM results. Therefore the Sect. E-3 results are devoted to Lpar (^{137}Cs and particulate ^{131}I) verification.

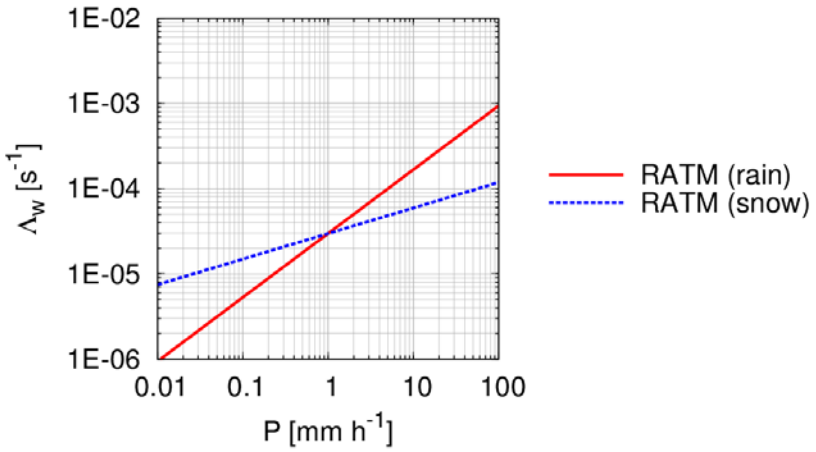

Fig. E-1-2. Below-cloud scavenging coefficients for rain (red solid line) and snow and graupel (blue dotted line) used in JMA-RATM. After Saito et al. (2015).

f. Dry deposition

Dry deposition is simply computed from the following deposition rate (e.g., Iwasaki et al., 1998):

$$\Lambda_{\mathrm{d}} = \frac{V_{\mathrm{d}}}{Z_{\mathrm{d}}} \tag{E-1-15}$$

where V_{d} is the dry-deposition velocity and Z_{d} is the depth of surface layer. The value of V_{d} is set to 0.001 m s^{-1} for Lpar and 0.01 m s^{-1} for Dgas (Sportisse, 2007; Draxler and Rolph, 2012), and Z_{d} is set to 100 m for both tracer types.

E-1-2. Use of MESO GPVs and RAP data

In Fig. E-1-1, the motion of computational particles in RATM is calculated in the same coordinate system as the MESO analysis (Lambert conformal mapping in the horizontal and a terrain-following hybrid in the vertical). The three-hourly 5-km MESO GPV data used to drive the RATM are momentum, potential temperature, pressure, density, accumulated precipitation and mixing ratio of cloud water. In the advection and diffusion steps, the mean wind velocities at each computational particle are calculated from the time-space interpolation of the density and momentum GPVs. To calculate the settling velocity, the temperature and pressure GPVs are used. For the wet scavenging process, the precipitation intensity is computed from the average of the three-hour accumulated precipitation GPVs. LWC for the in-cloud scavenging computation can be defined by the GPVs of mixing ratio of cloud water. However, due to limitations in the treatment of ice-phase deposition in the original RATM, only liquid rain was considered in the WMO Task Team calculation. Subsequently, we used the total precipitation in the SCJ (Science Council of Japan) Working Group calculations.

When using the RAP data, instead of the three-hourly accumulated precipitation by MESO GPVs, the RAP intensity at each MESO grid point (5-km resolution) is calculated from the spatial average of the surrounding 25-grid cells of RAP (1-km resolution) every 30 min. As noted above, because the original version of RATM cannot treat ice-phase deposition and RAP data do not distinguish solid and liquid precipitations, all RAP data were considered to be liquid rain in the calculation.

E-2. Revision of RATM[2]

As previously mentioned in Sect. B-3-2, the JMA-MESO analysis is produced by a three-hour forecast of the 5-km outer-loop of JMA-NHM (Saito et al., 2006, 2007, 2012) of JNoVA (Honda et al., 2005; Honda and Sawada, 2008). The stored values in the analysis field are not averaged in the assimilation window but are the instantaneous values predicted by the outer-loop model at the analysis time (the end of each three-hour assimilation window). Because the instantaneous vertical motion is affected by gravity waves and short-lived convection, a simple time interpolation of updrafts/downdrafts between the three-hourly analysis fields may yield an overestimation of the vertical advection of the air parcel, even if the magnitude of updrafts/downdrafts is small.

To compensate for the lack of temporal resolution, in the revised version of JMA-RATM, the vertical advection (the second term on the right-hand side of Eq. (E-1-1c)) is calculated using a spatially-averaged (nine-grid cells) value of the MESO vertical velocity and assumed to be terrain-following ($w(z^* = 40\ \mathrm{m}) = 0$) at the lowest model level. Figure E-2-1 compares the 24-h Lpar accumulated deposition for unit release (1 Bq/h) from 0000 UTC to 0300 UTC 14 March 2011. The upper-right panel shows the result where vertical motion of the particles is computed using the original MESO vertical velocity. Compared to the case without vertical advection (upper-left panel), the deposition over the sea off the east coast of Japan is reduced. The lower-left panel provides the result when the nine-grid cell averaged updraft/downdraft was applied to compute the vertical advection. The difference from the upper-right panel is not large but the deposition is slightly increased near the FDNPP (Fukushima Daiichi Nuclear Power Plant) site and slightly decreased at distant areas. In these simulations, Lpar emitted from the FDNPP site were first lifted up by the lowest level's small updraft in MESO GPVs. The lower-right panel is the result of when the lowest level vertical motion was assumed to be terrain following (i.e., the lowest level updraft/downdraft becomes zero over sea while the remaining vertical motion over land is just due to the terrain slope and the horizontal wind speed). The deposition off the east coast of Japan is increased.

In the preliminary version of RATM, wet scavenging was assumed to occur below about 3000 m in height, the same as in the original RATM (Table E-1-1), but deposition over Miyagi prefecture, to the north of Fukushima, was overestimated compared with the aircraft monitoring by the MEXT (Sect. D-3). In the revised RATM, this overestimation was reduced by limiting the level of wet scavenging to levels below about 1500 m (see Sect. E-3).

Some improper treatments of horizontal and vertical interpolations of the kinematic fields were found in the preliminary version of RATM. These computational bugs were corrected in the revised version. Also the number of computational particles was increased from 100,000/3 h to 300,000/3 h, but the impact was almost negligible (see Sect. E-3).

For the model intercomparison of the SCJ Working Group, we further modified RATM as noted previously: the time step was changed from 10 min. to 5 min. and in addition to rain, the precipitation

[2] The description is based on Sect. 3 of Saito et al. (2015).

intensity of snow and graupel in the MESO GPVs was used. For these calculations, the below-cloud scavenging coefficients of Lpar in Eq. (E-1-12) for snow and graupel are assumed (blue dotted line of Fig. E-1-2)

$$A = 2.98 \times 10^{-5}\ (\mathrm{s}^{-1}), B = 0.30 \qquad \text{(E-2-1)}$$

with reference to the B value of UKMET-NAME (Table F-2-1). The impacts of the modifications are shown in next section.

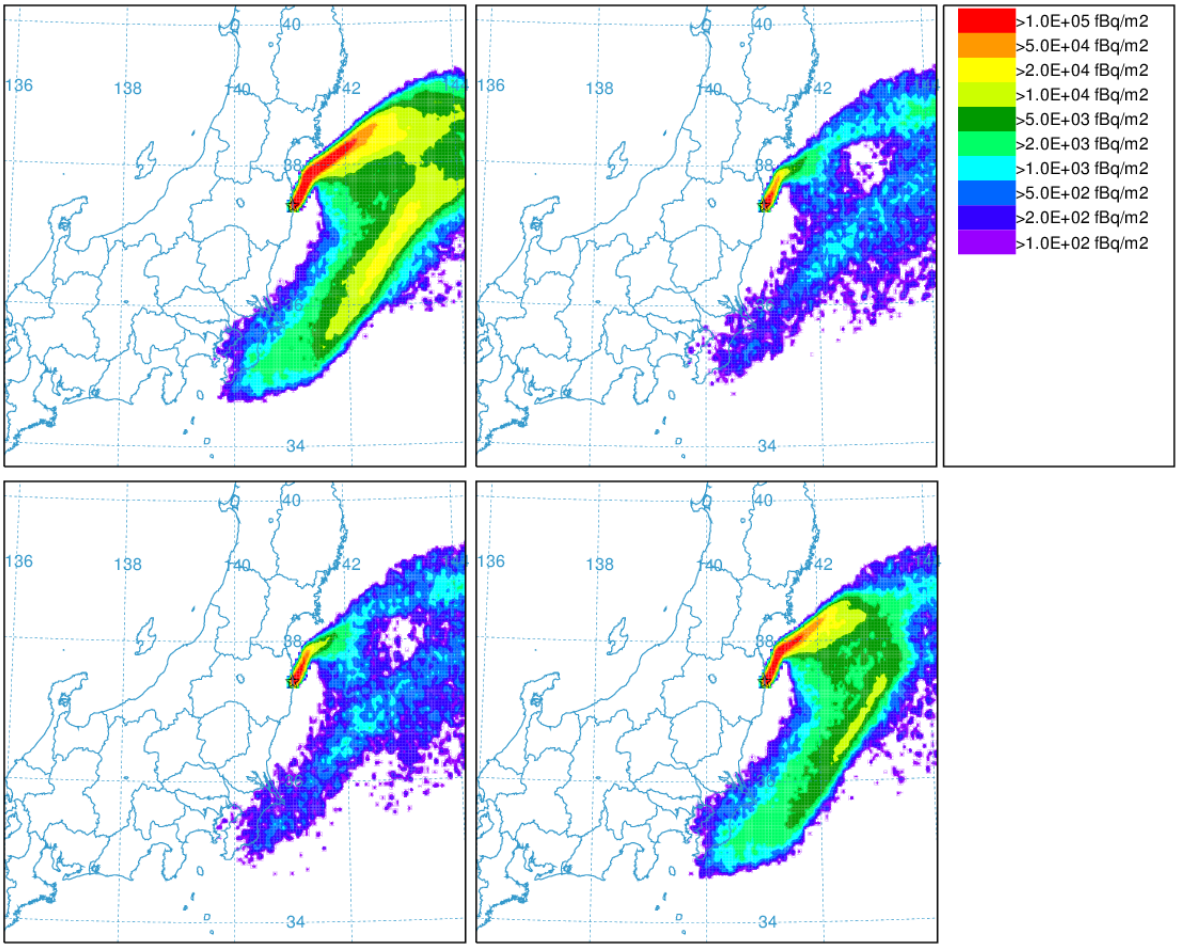

Fig. E-2-1. 24-h Lpar accumulated deposition by the JMA-RATM for unit release (1 Bq/h) at 0000-0300 UTC 14 March 2011. JMA-MESO GPV is used for precipitation. Upper left: without vertical advection. Upper right: vertical motion is computed by updraft/downdraft. Lower left: spatially-average is applied. Lower right: spatially-average and terrain-following at the lowest level. Star symbols indicate the location of FDNPP. These deposition maps are created by the drawing tool of the NOAA ARL website (Sect. D-4). After Saito et al. (2015).

E-3. Experiments with RATM[3]

E-3-1. Comparison with preliminary and revised RATM for the WMO Task Team

a. Experimental setting

According to the computational design described in Sect. D-1, JMA-RATM simulations were conducted by the WMO Task Team for the computational period of 1800 UTC 11 March through 2400 UTC 31 March, in three-hourly emission period increments using a unit source rate (1 Bq/h) for each discrete emission time segment. Emissions were uniformly distributed from the ground surface to 100 m a.g.l., and the concentration or deposition at any grid cell in the domain was given by the sum of the contribution from all the RATM emission segments after multiplying the resulting unit concentrations by the emission rate for each segment (Sect. D-1). The air concentration and deposition output fields were configured to use a regular latitude-longitude grid (601 by 401 grid cells) with the output averaged at three-hourly intervals at 0.05° (5 km) horizontal resolution and 100 m vertical resolution. In the post-processing step, the results from each of the 168 RATM simulations were multiplied by the actual emission rate at the release time of the simulation and decay constant for each radionuclide thereby permitting the RATM dispersion and deposition factors to be applied to multiple radionuclides. The estimated emission rates 'JAEA' (red solid line in Fig. 2 of Draxler et al. (2015)), originally derived by Chino et al. (2011) and later modified by Terada et al. (2012, in Sect. D-2) were used for the WMO Task Team simulations.

Figure E-3-1 compares ^{137}Cs accumulated deposition for 11 March to 3 April 2011 estimated using different computational methodologies. Here, rain in MESO GPVs was used for the calculations shown in the left panels while RAP data were used for those shown in the right panels. In the preliminary RATM (upper figures), deposition over Miyagi prefecture (north of Fukushima) and southern part of the Kanto Plain (west of Tokyo) was overestimated compared with observation as mentioned in the previous section E-2. In the revised RATM (lower figures), this overestimation was ameliorated. When RAP data is used for precipitation, an area with high deposition in the northwest of FDNPP becomes more distinctly reproduced (right figures), but the overestimation of deposition in the southern part of the Kanto Plain is also enhanced, even in the revised RATM.

b. Verifications against observation

The ^{137}Cs dispersion and deposition were verified against the observed time series of near ground level air concentrations at JAEA-Tokai (see Sect. D-2) and the deposition measurements taken by aerial and ground based sampling (Fig. D-3-1 in Sect. D-3). One of the characteristic features of the deposition pattern is the densely contaminated area extending to northwest from FDNPP. This area is bent to the south, east of Ou mountain range, and forms an inverse L-shaped pattern shown by the yellow shaded region in Fig. D-3-1. On the other hand, deposition in Miyagi prefecture, north of Fukushima, is relatively small.

[3] The description is based on Sects. 4 and 5 of Saito et al. (2015).

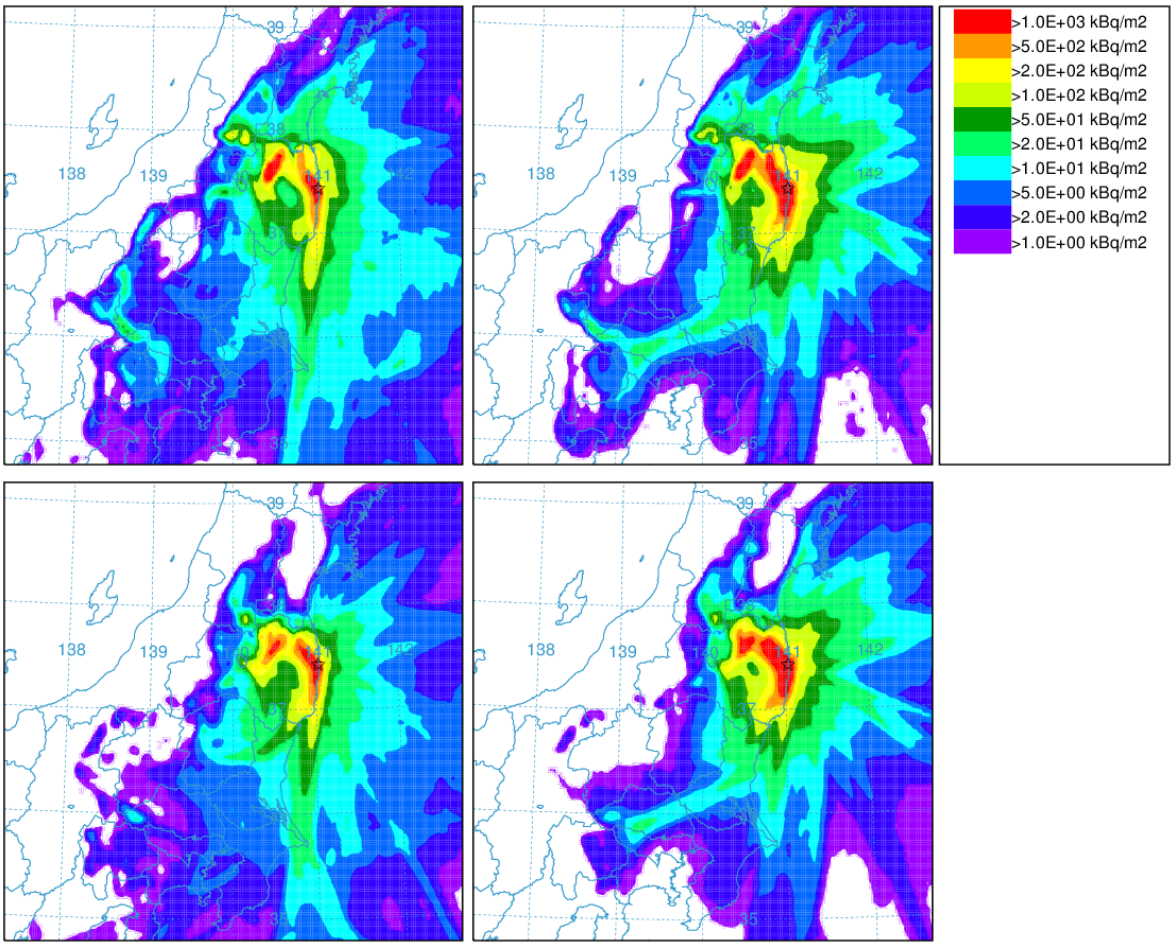

Fig. E-3-1. ^{137}Cs accumulated deposition for 11 March-3 April 2011 using the JAEA source. Upper left: preliminary RATM with MESO precipitation. Upper right: preliminary RATM with RAP precipitation. Lower: same as in upper panels but results by the revised RATM. After Saito et al. (2015).

The statistics of correlation coefficient ($-1 \leq R \leq 1$), fractional bias ($-2 \leq \mathrm{FB} \leq 2$), figure-of-merit in space (FMS [%]), Kolmogorov-Smirnov parameter (KSP [%]) mentioned in Sect. D-3 and the following two additional statistics used in Draxler et al. (2013a) were applied to the results of the preliminary and revised RATM.

i) Factor of two percentage (FA2 [%]), the percentage of calculations within a factor of two of the measured value.

ii) Factor of exceedance ($-50\% \leq \mathrm{FOEX} \leq 50\%$), the factor of the number of over-predictions in the pairs of predicted and measured values.

A ranking method was defined by giving equal weight to the normalized expressions of these statistics (Draxler et al., 2013a),

$$\mathrm{METRIC1} \equiv \mathrm{Rank} = R^2 + 1 - \left|\frac{\mathrm{FB}}{2}\right| + \frac{\mathrm{FMS}}{100} + \left(1 - \frac{\mathrm{KSP}}{100}\right) \quad \text{(E-3-1a)}$$

$$\mathrm{METRIC2} = R^2 + 1 - \left|\frac{\mathrm{FB}}{2}\right| + \frac{\mathrm{FA2}}{100} + \left(1 - \frac{\mathrm{KSP}}{100}\right) \quad \text{(E-3-1b)}$$

$$\mathrm{METRIC3} = \mathrm{METRIC1} + \left(1 - \left|\frac{\mathrm{FOEX}}{50}\right|\right)$$

$$= R^2 + 1 - \left|\frac{\mathrm{FB}}{2}\right| + \frac{\mathrm{FMS}}{100} + \left(1 - \left|\frac{\mathrm{FOEX}}{50}\right|\right) + \left(1 - \frac{\mathrm{KSP}}{100}\right) \quad \text{(E-3-1c)}$$

$$\mathrm{METRIC4} = \mathrm{METRIC3} + FA2/100$$

$$= R^2 + 1 - \left|\frac{\mathrm{FB}}{2}\right| + \frac{\mathrm{FMS}}{100} + \frac{\mathrm{FA2}}{100} + \left(1 - \left|\frac{\mathrm{FOEX}}{50}\right|\right) + \left(1 - \frac{\mathrm{KSP}}{100}\right) \quad \text{(E-3-1d)}$$

whose value would range from 0 to 4 (METRIC1 and 2), 5 (METRIC3), 6 (METRIC4) (from worst to best). Eq. (E-3-1a) is same as the Rank defined in Sect. D-3.

Two sets of calculations were examined, one where the precipitation was given by the MESO GPVs and the other using the RAP data. Table E-3-1 shows the verification statistics by RATM for ^{137}Cs deposition. Performance of the revised RATM (Rev. MESO) was significantly improved compared with the preliminary RATM (Pre. MESO) for all rank metrics. The most improvement was obtained in R, which increased from 0.45 in the preliminary version to 0.70 in the revised version. The use of RAP data for precipitation further improved the correlation coefficient to 0.84, while rank metrics became slightly worse due to the deterioration of FB and FOEX. These tendencies in the statistics in the use of RAP data can be understood by the area with high deposition in the northwest of FDNPP and the overestimation of deposition in the west of the Kanto Plain in right panels of Fig. E-3-1; in the aircraft monitoring by MEXT (Fig. 4 of Draxler et al. (2013a)), little or no deposition was observed in the western part of the Kanto Plain.

Table E-3-2 and Fig. E-3-2 show the time evolution and the corresponding statistics for ^{137}Cs concentration at the JAEA-Tokai observation site. Performance of the revised RATM using MESO precipitation was slightly improved in terms of the rank metrics, while the revision did not improve the metrics when the RAP data were used for precipitation. The reason for this deterioration in metrics in the use of RAP data is not obvious, but a similar tendency was also found in the other Task Team's model simulations (Chap. F). Arnold et al. (2015) inferred that the discrepancy of transport patterns by NWP (numerical weather prediction) analyses and the locations of the precipitation may result in a wrong description of the total wet scavenging. The quality of the RAP data itself is also arguable.

Table E-3-1. Statistical metrics for comparison of JMA-RATM simulations with observed deposition pattern of ^{137}Cs using the JAEA source. Bold values indicate best score for each simulation. Reproduced from Saito et al. (2015).

RATM	*R*	FB	FA2 (%)	FOEX (%)	FMS (%)	KSP (%)	METRIC 1	METRIC 2	METRIC 3	METRIC 4
Pre. MESO	0.45	**-0.02**	**51.01**	**-0.46**	**100.00**	**10**	3.09	2.60	4.08	4.59
Pre. RAP	0.77	0.54	41.99	9.67	**100.00**	11	3.22	2.63	4.02	4.44
Rev. MESO	0.70	-0.04	37.94	-0.83	99.63	**10**	**3.37**	**2.75**	**4.35**	**4.73**
Rev. RAP	**0.84**	0.56	35.73	9.12	99.08	13	3.28	2.65	4.10	4.46

Table E-3-2. Statistical metrics for comparison of JMA-RATM simulations with observed concentration time series of ^{137}Cs at JAEA-Tokai using the JAEA source. Bold values indicate best score for each simulation. Reproduced from Saito et al. (2015).

RATM	*R*	FB	FA2 (%)	FOEX (%)	FMS (%)	KSP (%)	METRIC 1	METRIC 2	METRIC 3	METRIC 4
Pre. MESO	0.51	-0.82	**21.43**	-21.43	**80.00**	**43**	2.22	1.63	2.79	3.01
Pre. RAP	**0.59**	-1.66	4.76	-45.24	57.50	64	1.46	0.93	1.55	1.60
Rev. MESO	0.39	**-0.40**	14.29	**-19.05**	77.50	**43**	**2.30**	**1.67**	**2.92**	**3.06**
Rev. RAP	0.07	-1.68	9.52	-42.86	62.50	67	1.12	0.59	1.26	1.36

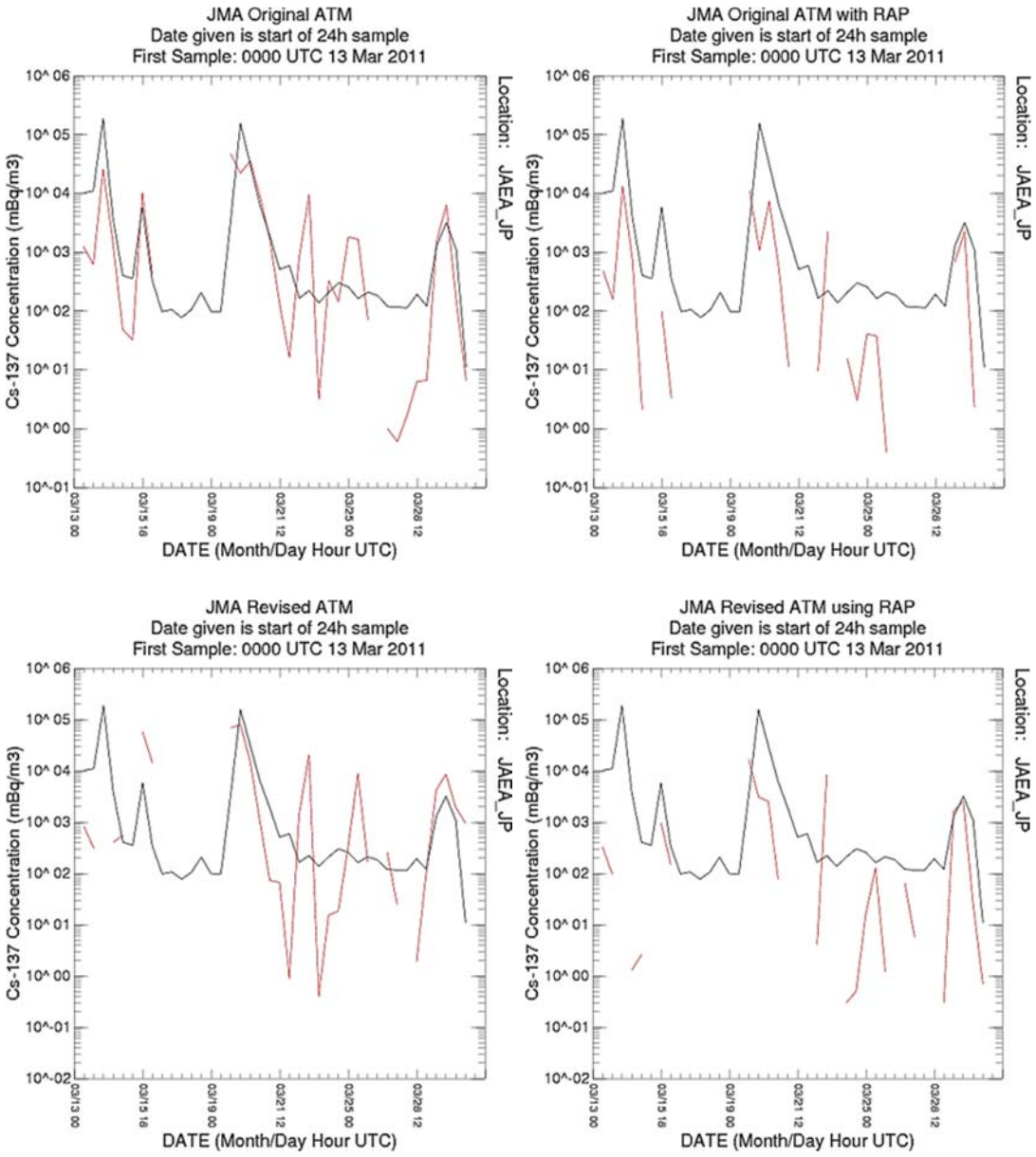

Fig. E-3-2. Same layout as in Fig. E-3-1 but time evolution of ^{137}Cs (logarithmic in the ordinate) at JAEA-Tokai for the period 13-31 March 2011. Black lines indicate observation. Red lines show results by the JMA-RATM with the JAEA source estimation. After Saito et al. (2015).

Table E-3-3. Statistical metrics for comparison of JMA-RATM simulations with observed concentration time series of particulate ^{131}I at JAEA-Tokai using the JAEA source. Bold values indicate best score for each simulation. Reproduced from Draxler et al. (2013a).

RATM	*R*	FB	FA2 (%)	FOEX (%)	FMS (%)	KSP (%)	METRIC 1	METRIC 2	METRIC 3	METRIC 4
Pre. MESO	0.47	-0.96	14.29	-30.95	**78.05**	43	2.09	1.45	2.47	2.62
Pre. RAP	**0.67**	-1.71	0.00	-45.24	60.98	60	1.60	0.99	1.70	1.70
Rev. MESO	0.14	**-0.54**	**16.67**	**-23.81**	75.61	**40**	**2.11**	**1.52**	**2.63**	**2.80**
Rev. RAP	0.02	-1.60	4.76	-42.86	60.98	65	1.16	0.60	1.30	1.35

Although the bright band is not likely critical in this experiment, radar echoes are scanned around the level of 1 km a.g.l. and solid waters are over-detected in the radar reflectivity. A lower limit of intensity around 0.4 mm h^{-1} is set in RAP, which means that very weak precipitation is not included. As mentioned in Sect. E-1-1, all RAP precipitation was considered to be liquid rain in the wet scavenging calculation in RATM, and this assumption also may yield some errors in the air concentration time evolution. Another possibility is that dispersion of radionuclides to the position of the JAEA site is somewhat uncertain. As suggested in Fig. C-9-7, the southward advection of radionuclides from FDNPP on 15 March 2011 was sensitive to small changes in the wind direction. Therefore, given the inherent limitations in the accuracy of wind direction in meteorological analyses, it may be unrealistic to expect that an RATM can precisely reproduce the time evolution of downwind air concentrations at JAEA-Tokai. In addition, the statistical results may also be affected by remaining uncertainties in the radionuclides release rate estimates which may never be finalized.

Table E-3-3 shows the verification statistics for particulate ^{131}I concentration at the JAEA-Tokai observation site. Similar tendency of the RATM results were confirmed for another type of radionuclides.

c. Sensitivity experiments to RATM parameters

In the revision of RATM, we tested some of the parameters with the greatest uncertainty to determine their impacts on the RATM calculations of the accumulated deposition patterns of ^{137}Cs from 1800 UTC 11 March to 2100 UTC 03 April 2011. A list of values of parameters used in the experiments and corresponding figures are given in Table E-3-4.

(1) Release height

In the WMO Task Teams' experiments, emissions of radionuclides were assumed to be distributed uniformly from the ground to 100 m a.g.l. But this release height may change depending on the atmospheric conditions and situation of the emission. The upper-left panel of Fig. E-3-3 shows the ^{137}Cs accumulated deposition when a lower release height of 30 m is applied. No significant difference was obtained in the dense deposited area compared with the case of the original release height of 100 m (lower-left panel of Fig. E-3-1). A small difference can be seen in the regions with weak deposition

over southern part of the Kanto plain, where the simulated deposition becomes slightly smaller by using the lower release height. This change corresponds to the observed deposition pattern (see Fig. 4 of Draxler et al. (2013a)), and small hotspot northeast of Tokyo is vaguely simulated in this experiment.

(2) Number of computational particles

The upper-right panel of Fig. E-3-3 shows the result when a smaller number of computational particles of 100,000/3 h were employed. Virtually the same result was obtained in the deposition patterns.

(3) Wet scavenging coefficient and application height

Wet scavenging is an important process for the deposition of radionuclides. The middle-left panel of Fig. E-3-3 indicates that when the wet scavenging process is not included in the simulation, the deposition becomes much less compared with the original calculation (lower-left panel of Fig. E-3-1). This result shows that the area with high deposition to the northwest of FDNPP was strongly affected by wet scavenging. However the treatments of scavenging caused by rain and/or snow have many ambiguities. The original version of RATM considered wet scavenging below 3000 m with the scavenging coefficient of Eqs. (E-1-12) and (E-1-13). The middle-right panel of Fig. E-3-3 shows the sensitivity of the results to changes in the below-cloud scavenging coefficient. Here, the scavenging coefficients of Eq. (E-1-13) is replaced by $A = 8.40 \times 10^{-5}\ (\mathrm{s}^{-1}), B = 0.79$, the values used in UKMET-NAME (Table F-2-1). When a lager value is applied, deposition of ^{137}Cs over west of the Kanto Plain is enhanced.

The lower-left panel of Fig. E-3-3 shows the result with the original scavenging application height of 3000 m. A distinct difference from the original simulation is seen over Miyagi prefecture, where overestimation of unobserved deposition is predicted. This result may suggest that the wet scavenging should be confined in lower levels in the case of the FDNPP accident.

(4) Dry deposition application height

Sensitivities to dry deposition surface-layer height and number of computational particles were also examined. Using a lower dry deposition surface layer height $Z_{\mathrm{d}} = 40$ m (the lowest model layer) had little impact on the deposition pattern (the lower-right panel of Fig. E-3-3).

Table E-3-4. List of values of parameters used in the JMA-RATM experiments and corresponding figures.

Source	Release height (m a.g.l.)	Number of comp. particles (per 3 h)	Time step (min.)	Below-cloud scav. coeff.		Scav. appl. height (m a.s.l.)	Dry-dep. appl. height (m a.g.l.)	Figures
				by rain	by snow			
JAEA	0-100	300,000	10	A=2.98x10^{-5}, B=0.75	N/A	<1500	<100	low.-left of Fig. E-3-1
JAEA	0-30	300,000	10	A=2.98x10^{-5}, B=0.75	N/A	<1500	<100	upp.-left of Fig. E-3-3
JAEA	0-100	100,000	10	A=2.98x10^{-5}, B=0.75	N/A	<1500	<100	upp.-right of Fig. E-3-3
JAEA	0-100	300,000	10	N/A	N/A	N/A	<100	mid.-left of Fig. E-3-3
JAEA	0-100	300,000	10	A=8.40x10^{-5}, B=0.79	N/A	<1500	<100	mid.-right of Fig. E-3-3
JAEA	0-100	300,000	10	A=2.98x10^{-5}, B=0.75	N/A	<3000	<100	low.-left of Fig. E-3-3
JAEA	0-100	300,000	10	A=2.98x10^{-5}, B=0.75	N/A	<1500	<40	low.-right of Fig. E-3-3
JAEA2	0-100	300,000	10	A=2.98x10^{-5}, B=0.75	N/A	<1500	<100	low.-left of Fig. E-3-4
JAEA2	0-100	300,000	5	A=2.98x10^{-5}, B=0.75	A=2.98x10^{-5}, B=0.30	<1500	<100	low.-right of Fig. E-3-4

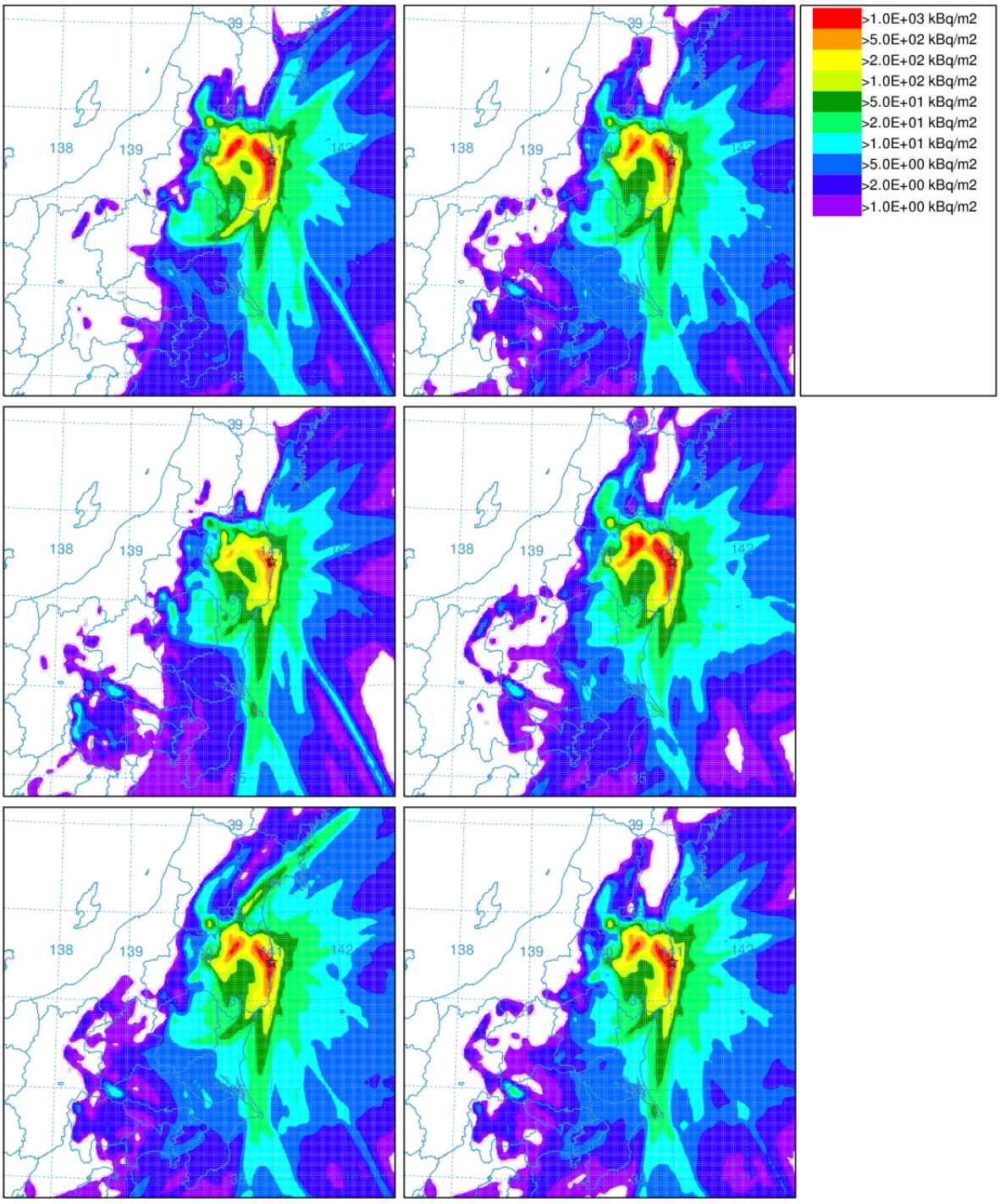

Fig. E-3-3. Same as in the lower-left panel of Fig. E-3-1, but following settings are different: Upper left: for the case with the release height 0-30 m a.g.l. Upper right: for the case with the number of computational particles 100,000/3 h. Middle left: for the case without wet scavenging. Middle right: for the case with the below-cloud scavenging coefficients of A=8.40x10^{-5} s^{-1} and B=0.79. Lower left: for the case with wet scavenging application height below about 3000 m a.s.l. Lower right: for the case with dry deposition application height less than 40 m. After Saito et al. (2015).

E-3-2. Results of revised RATM for the SCJ Working Group

The SCJ (2014) reviewed the modeling capability of the transport, dispersion and deposition of radioactive materials released to the environment as a result of the FDNPP accident. The primary purpose of this initiative was to assess the uncertainties in the simulation results through model intercomparisons (Sect. G-6). In participating in these model intercomparisons, we used the revised release rate 'JAEA2' by Kobayashi et al. (2013) and further modified RATM as mentioned at the end of Sect. E-2.

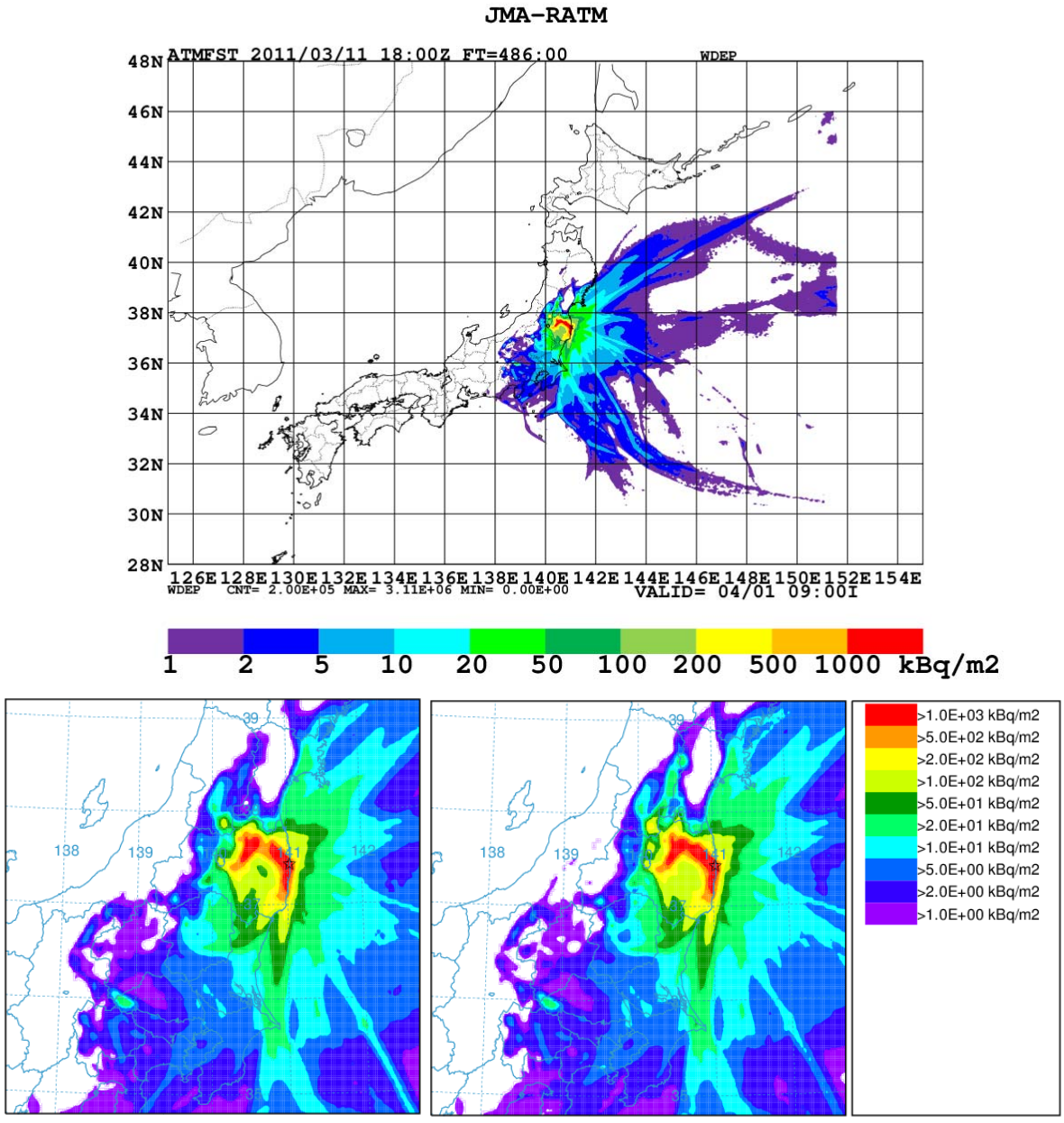

Fig. E-3-4. Upper: distribution of ^{137}Cs deposition by JMA-RATM in the SCJ model intercomparison. Lower left: Same as in the lower-left panel of Fig. E-3-1 (below-cloud scavenging is applied only to rain) but for the case that the release rate is given by JAEA2. Lower right: same as in the upper panel but an enlarged view for the same domain as in the lower-left panel of Fig. E-3-1. After Saito et al. (2015).

Figure E-3-4 shows the ^{137}Cs deposition distribution obtained by the SCJ experiment. As seen in its enlarged view (lower-right panel), the area with high deposition northwest of FDNPP is more enhanced relative to the previous RATM results and linked with the hotspot at Naka-dori valley, producing an inverse L-shaped pattern. Because the JAEA2 release rate is somewhat larger than that of JAEA (Fig. 4 of Kobayashi et al. (2013)), the enhancement of deposition was partly caused by the change of the release rate, while the modification of treatment of the wet scavenging (use of solid waters in MESO GPVs) likely contributed to modifying the shape of the area with high deposition. It is noteworthy that in this experiment, a small hotspot in Chiba prefecture (northeast of Tokyo, see Fig. 4 of Draxler et al. (2013a)) is better simulated compared with the previous RATM simulation (the lower-left panel of Fig. E-3-1).

To differentiate the impact of changes to the emission rate and model, we conducted additional experiments. The lower-left panel of Fig. E-3-4 is for the case when only the release rate is changed to JAEA2 source term and with application of below-cloud scavenging only to rain (the same model that in the lower-left panel of Fig. E-3-1). As indicated by these figures, both changes contribute to enhance the inverse L-shaped area with high deposition, but the change of the source term has a larger effect than inclusion of snow in the below-cloud scavenging in terms of the deposition distribution over the Kanto Plain.

E-3-3. Test version of RATM for in-cloud scavenging and future research

Another experiment with in-cloud scavenging for Lpar was conducted to test its impact. In this experiment, the three-dimensional distribution of cloud water analyzed by JNoVA was used to define cloud area and liquid water content. In an analogous form to Eq. (E-1-14), the in-cloud scavenging rate for Lpar is also given by Hertel et al. (1995):

$$\Lambda_{\mathrm{r}} = \frac{0.9}{LWC}\frac{P}{Z_{\mathrm{r}}} \ [\mathrm{h}^{-1}] \qquad \text{(E-3-2)}$$

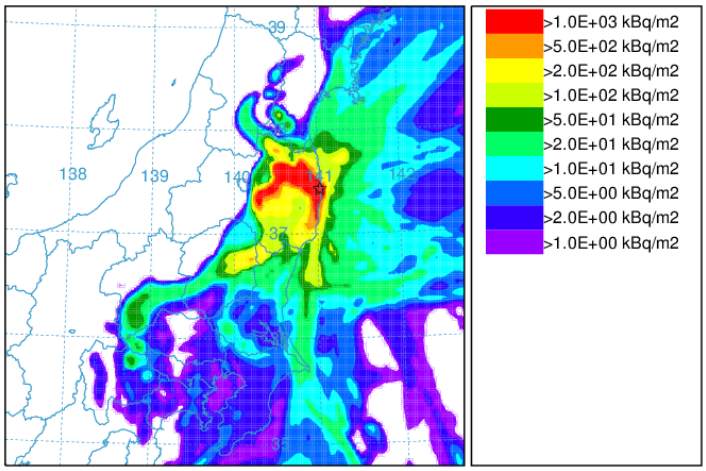

Fig. E-3-5. Same as in the lower-right panel of Fig. E-3-4 but for a test version of JMA-RATM that in-cloud scavenging for Lpar is considered. After Saito et al. (2015).

Figure E-3-5 shows the result when in-cloud scavenging of Eq. (E-3-2) is considered. A very large difference is seen in the north of Kanto Plain. An area with high deposition extends from the eastern part of Fukushima prefecture to west-southwest, resembling the observed hotspot in the northern Kanto Plain (Fig. 4 of Draxler et al. (2013a)). Although the simulated area with high deposition has a small (20-30 km) southward positional lag, this result suggests importance of considering in-cloud scavenging for Lpar.

In the WMO Task Team and the SCJ Working Group experiments, we used three-hourly MESO analysis as the meteorological field with linear interpolation in time and space to obtain input data for RATM at every 5 or 10 min. time step. The time interval of the meteorological field may not be sufficient to properly treat the upward motion of the radionuclides and to characterize their finer spatiotemporal scale transport due to changes of the wind speed and direction. To obtain more temporally resolved meteorological fields, additional mesoscale model simulations are needed. On the progress of this subject, Sekiyama et al. (2015) conducted the RATM experiments (the same version for SCJ Working Group) using the one-hourly 15 km, 3 km and 500 m NHM-LETKF GPVs (see Sect. G-4).

Use of a lower below-cloud scavenging application height yielded slightly better results in the revised version in some respects, but the same effect could be obtained by reducing the scavenging coefficient itself or changing the source emissions. The results of the additional test of an in-cloud scavenging scheme for Lpar suggested the importance of its consideration for future model improvements. More sophisticated method should be developed for in-cloud scavenging so that the three-dimensional distribution of rain and snow in the MESO analysis can be used more effectively. In addition, changes of the assumed grain-size distribution and particle density will also have an effect on the surface deposition. These points are all subjects for future research.

F. ATDM simulations by TT members

F-1. The NOAA ATDM experiments[1]

The calculation of the transport and dispersion from the source was done using the Hybrid Single-Particle Lagrangian Integrated Trajectory (HYSPLIT – Draxler and Hess, 1998) model. A detailed description of the computational aspects of the model can be found in Draxler and Hess (1997) and its configuration is reviewed in the User's Guide (Draxler, 1999).

The special extract of the NOAA GDAS meteorological data archive used for the HYSPLIT ATDM calculations was available on the native hybrid sigma levels. Approximately 15 levels occur below 850 hPa with the remainder extending up to approximately 10 hPa. The three dimensional fields included the horizontal winds, temperature, and humidity. When using the GDAS data for calculations, vertical velocities were computed in HYSPLIT by integrating the divergence. The other fields used in the calculations include the surface heat and momentum fluxes for the computation of vertical mixing, the boundary layer depth, and the precipitation rate.

The ECMWF data fields had a comparable number of data fields and vertical resolution to the GDAS but included the vertical velocity field.

When using the JMA mesoscale analysis, a minimum amount of pre-processing was applied to the data which contained pressure, potential temperature, horizontal winds, moisture, and vertical velocity. The 3D pressure fields was used directly to map the data at each level to the HYSPLIT vertical sigma coordinate, potential temperature was converted to ambient temperature, and the vertical velocities were remapped to a terrain following coordinate system consistent with the HYSPLIT computational framework. A vertical velocity correction,

$$\sigma (u\, \partial\eta/\partial x + v\, \partial\eta/\partial y) \qquad \text{(F-1-1)}$$

was applied at all levels based upon the slope of the terrain surface (η) and decreasing with height (σ). With respect to the wet deposition, HYSPLIT calculations used the precipitation fields without adjustment: the MESO analysis 3-hour accumulated precipitation and calculations with the RAP used the precipitation at the grid point nearest in space (~ 1 km) and time (~ 30 min) to each particle at each integration time step.

In HYSPLIT, scavenging is parameterized through removal constants β (s^{-1}), where the deposition D over time step Δt for each particle of mass M is

$$D = M \{1-\exp[-\Delta t (\beta_{dry}+\beta_{gas}+\beta_{inc}+\beta_{bel})] \}. \qquad \text{(F-1-2)}$$

The particle mass is reduced by D each time step. The time constant for within-cloud removal for particulate pollutants is

$$\beta_{inc} = S\, P\, \Delta Z_p^{-1}, \qquad \text{(F-1-3)}$$

[1] R. Draxler

where S is the ratio of the pollutant's concentration in water to its concentration in air ($4x10^4$), ΔZ_p is the depth of the pollutant layer, and the precipitation rate P is the value predicted by the meteorological model used in the calculation. Below-cloud removal is defined directly as a rate constant ($\beta_{bel} = 5x10^{-6}$), independent of the precipitation rate. The wet deposition of gases depends upon their solubility and for inert non-reactive gases it is a function of the Henry's Law constant (H - Molar atm^{-1}), the ratio of the pollutant's equilibrium concentration in water to that in air. Therefore, the gaseous wet removal time constant is

$$\beta_{gas} = H\ R\ T\ P\ \Delta Z_p^{-1}, \qquad \text{(F-1-4)}$$

where R is the universal gas constant (0.082 atm $M^{-1}\ K^{-1}$), T is temperature, and the wet removal of gases is applied at all levels from the ground to the top of the cloud-layer. The dry deposition calculation is limited to particles within the surface layer (ΔZ_s is usually about 75 m), and the time constant is

$$\beta_{dry} = V_d\ \Delta Z_s^{-1}. \qquad \text{(F-1-5)}$$

One critical aspect for quantitative predictions of air concentration is the wet and dry scavenging that occurs along the transport pathway. Three generic species were tracked as surrogates for the radionuclides: a gas with no wet or dry scavenging, a gas with a relatively large dry deposition velocity (0.01 m/s) and wet removal (Henry's constant = 0.08) to represent gaseous I^{131}, and a particle with a small deposition velocity (0.001 m/s). There can be considerable variability in scavenging coefficients and the wet scavenging coefficients used in these calculations are lower than the original model default values (Draxler and Hess, 1997) but these lower values are consistent with the results from more recent deposition studies using the HYSPLIT scavenging parameterizations.

F-2. The Met Office ATDM Experiments[1]

NAME (Numerical Atmospheric-dispersion Modelling Environment) is the UK Met Office's Lagrangian particle dispersion model and it is used to model the atmospheric transport and dispersion of a range of gases and particles (Maryon et al., 1999 and Jones et al. 2007). It was originally developed to model the transport of radioactive material following the Chernobyl accident but now has a wide range of applications including simulating releases of hazardous materials (chemical, biological, radiological and nuclear) (Leadbetter et al 2013, Draxler et al 2012, Becker et al 2007, Ryall and Maryon 1998), modelling the transport of ash clouds from volcanic eruptions (Webster 2012), modelling the airborne transmission of diseases (Burgin 2012), forecasting air quality, analyzing air pollution episodes and identifying source locations and source strengths.

In NAME, large numbers of model particles are released into the model atmosphere, where each particle represents a certain mass of the material (gases or aerosols) being released. These particles are advected within the model atmosphere by input three-dimensional winds from numerical weather prediction models and turbulent dispersion is simulated by random walk techniques; particle velocities are correlated in time at short ranges while the more simple Wiener process is applied for longer range problems. Gravitational settling of particles and loss processes, such as wet and dry deposition, radioactive decay, cloud gamma (Bedwell 2011) and chemical transformations, are calculated when required.

NAME is typically run using NWP data from the Met Office or ECMWF but can be configured to use data in GRIB format from any model provided a suitable variable set is available. In addition, NAME can use radar rainfall observations in place of NWP rainfall estimates. NAME can use both limited area and global deterministic data as well as ensemble data (through an in-built ensemble framework). These NWP data sets can be nested both in space and time.

For the WMO Task Team work NAME was run with Met Office, ECMWF and JMA Mesoscale NWP with and without JMA Radar Rainfall observations sample deposition results for ^{137}CS are shown in Figure F-2-1. In order to use the JMA Mesoscale data it was necessary to pre-process the data to reformat it into a coordinate system supported by NAME and also to generate a number of additional fields required by NAME: converting potential temperature to temperature, converting accumulated rainfall to mean rates, estimating cloud cover, boundary layer depth and the estimation of surface fluxes of heat and momentum. Surface roughness was also absent and values from ECMWF were used in their place.

Dry deposition is modelled in NAME using the concept of the deposition velocity, v_d (Webster and Thomson, 2011). The flux of pollutant to the ground, F, is proportional to the concentration, C, of pollutant and is given by

$$F = v_d C \qquad \text{(F-2-1)}$$

[1] M. C. Hort and S. J. Leadbetter

where v_d is the constant of proportionality. The deposition velocity can either be specified by the user, which was the case for all the calculations discussed in this report, or is calculated using a resistance analogy

$$v_d = \frac{1}{R_a + R_b + R_c}, \qquad \text{(F-2-2)}$$

where R_a is the aerodynamic resistance, R_b is the laminar layer resistance and R_c is the surface resistance. The aerodynamic resistance represents the efficiency with which material is transported to the ground by turbulence and is independent of the material. The laminar layer resistance is used to specify the resistance to transport by diffusion across the thin quasi-laminar layer adjacent to the surface. Different parameterizations for R_b are used for gases and particles. The surface resistance characterizes the resistance to capture by the surface and is dependent on both the pollutant and the underlying surface. For particles, the surface resistance is taken to be zero. For gases, a fixed surface resistance can be specified by the user or, for a selection of gases, a complex land use dependent surface resistance parameterization can be invoked.

The removal of material from the atmosphere by wet deposition is based on the depletion equation

$$\frac{dC}{dt} = \Lambda C \qquad \text{(F-2-3)}$$

where C is the air concentration and Λ is the scavenging coefficient. The scavenging coefficient is given by

$$\Lambda = Ar^B \qquad \text{(F-2-4)}$$

where r is the rainfall rate (in mm hr^{-1}) and A and B are coefficients which vary for different types of precipitation (i.e., large-scale/convective and rain/snow) and for different wet deposition processes (i.e., rainout, washout and the seeder-feeder process) (see Table F-2-1) (Maryon et al., 1999). Within NAME, wet deposition due to convective and large-scale precipitation are computed separately and summed to give total wet deposition. Material located above the cloud top is not subject to wet deposition. Enhanced wet deposition (due to the seeder-feeder process) is applied to material close to the ground in regions of elevated orography.

Table F-2-1. Scavenging coefficients used in NAME

	Rain		Snow/Ice	
	Large-Scale	Convective	Large-Scale	Convective
Orographic enhancement (seeder-feeder)	$A = 3.36 \times 10^{-4}$ $B = 0.79$	$A = 3.36 \times 10^{-4}$ $B = 0.79$	$A = 1.0 \times 10^{-3}$ $B = 0.79$	$A = 1.0 \times 10^{-3}$ $B = 0.79$
Below-cloud (washout)	$A = 8.4 \times 10^{-5}$ $B = 0.79$	$A = 8.4 \times 10^{-5}$ $B = 0.79$	$A = 8.0 \times 10^{-5}$ $B = 0.305$	$A = 8.0 \times 10^{-5}$ $B = 0.305$
In-cloud (rainout)	$A = 8.4 \times 10^{-5}$ $B = 0.79$	$A = 3.36 \times 10^{-4}$ $B = 0.79$	$A = 8.0 \times 10^{-5}$ $B = 0.305$	$A = 3.36 \times 10^{-}$ $B = 0.79$

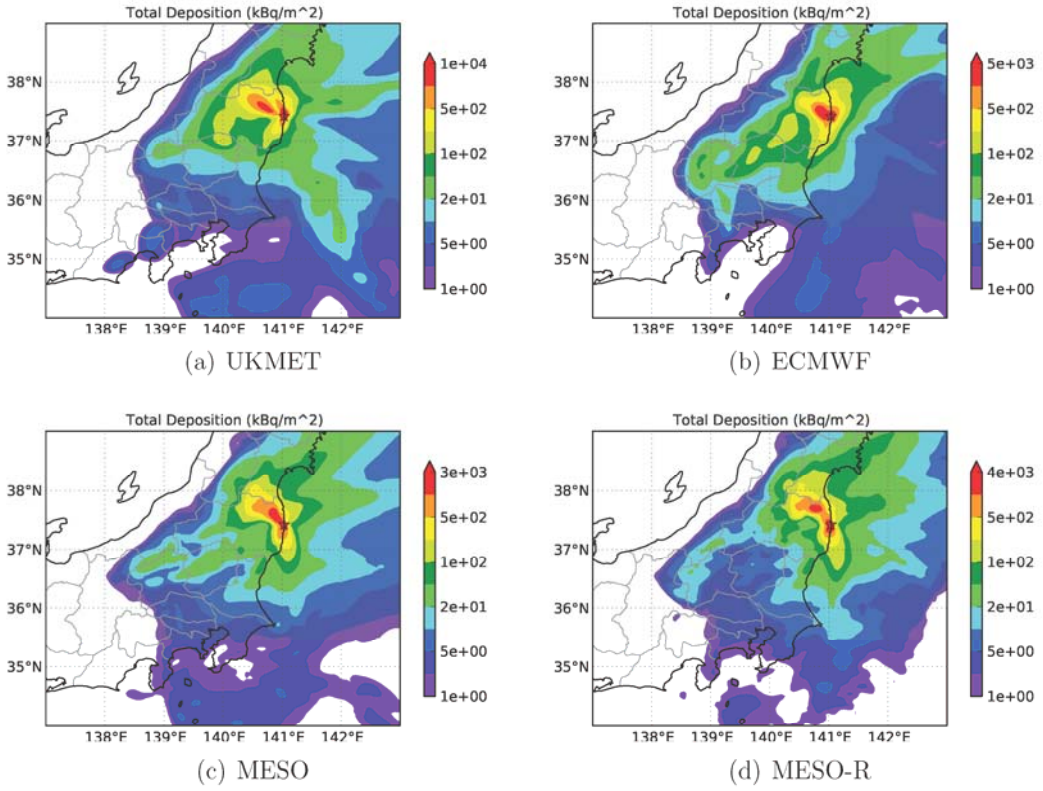

Fig. F-2-1. Deposition maps from NAME using 4 different meteorological data sets. UK (UKMET), European Centre (ECMWF), JMA Mesoscale (MESO) and JAM Mesoscale plus radar rainfall (MESO-R).

F-3. Impact of different meteorological input on ATM with FLEXPART[1]

F-3-1. Introduction and data

The work focuses on the influence of different meteorological input data (from JMA, ECMWF and NCEP), especially with regard to precipitation, on atmospheric transport modeling (ATM) simulations of aerosol-bound radionuclides with the Lagrangian particle dispersion model FLEXPART, version 8.23 (Stohl et al. 1998, 2005). Precipitation is known to be the most decisive factor for ground-level contamination (e.g. Clark and Smith, 1988) due to the efficiency of wet deposition processes (below-cloud and in-cloud scavenging). High resolution total precipitation fields from the operational Japanese Mesoscale analysis (~ 5 km horizontal resolution) and a radar-rain gauge analysis product (~ 1 km horizontal resolution) supplied by the JMA (JMA, 2012; Saito et al., 2015) offered a unique opportunity to assess the influence of spatially highly resolved precipitation input data in ATM for the particular case of the Fukushima Dai-ichi accident. In a pragmatic, yet limited, approach the latter fields were used to replace precipitation in the global or regional ECMWF (~0.125° native resolution) and global NCEP (~0.5° native resolution) data (see http://www.ecmwf.int/research/ifsdocs/CY37r2/index.html and http://www.emc.ncep.noaa.gov/GFS/doc.php) bearing in mind that there may be inconsistencies between the wind and precipitation fields. However, as precipitation is often not well modeled by NWP models but of high importance for deposition it was felt that it was important to investigate the impact of this potential off-line method for improving the precipitation fields used in ATM. The publicly available gridded ^{137}Cs deposition map (USDOE, United States Department of Energy, 2011; MEXT, 2011c) for land in area surrounding the Fukushima NPP and ^{137}Cs air concentration measurements from the International Monitoring System (IMS) of CTBTO were used for verification. For this study the ^{137}Cs source term by Terada et al. (2012) was used.

F-3-2. Atmospheric transport modeling

FLEXPART version 8.23 (which differentiates between in-cloud and below-cloud scavenging) includes a disadvantage that needs to be tackled. This disadvantage consists of the fact that clouds are diagnosed according to the exceedance of 80% relative humidity and that values are interpolated spatially and temporally using nearest neighbor interpolation. Thus, a particle may encounter precipitation, where no cloud is present, which leads to zero wet deposition for this grid point, a problem which is especially relevant for convective clouds/precipitation. A fix to this problem was proposed by Seibert et al. (2012) and tested within this evaluation. It includes a stepwise reduction of the relative humidity threshold (from 90% down to 25%) for diagnosing clouds if precipitation is present. Cloud base and height are interpolated from surrounding grid points in time and in space. If no clouds can be found there and precipitation is present the previous bulk parameterization for in cloud and below cloud scavenging is used.

---

[1] C. Maurer, D. Arnold and G. Wotawa

In line with Draxler and Heffter (1981) and as described in Draxler et al (2013a), independent forward runs with a unit source emission rate for 3 hourly release periods were performed every 3 hours to yield the source-receptor sensitivities for each release segment. These runs were finally scaled by the source strength in the corresponding release segment and summed up to give the actual modeled values at each time step and grid point. Following Draxler (2006) the statistical parameters correlation (R), fractional bias (FB), figure-of-merit in space (FMS) and the Klomogorov-Smirnov parameter (KSP) were used individually and in combination in a single measure called RANK (ranging from 0, worst, to 4, best) to quantitatively assess the model performance of the local runs.

F-3-3. Results

A summary of results can be found in **Table F-3-1**.

a. NCEP-0.5° versus ECMWF-0.5°

The differences between NCEP-0.5° and ECMWF-0.5° (abbreviated in **Table F-3-1** as NC-0.5 and EC-0.5) are worth mentioning. Maxima for the EC-0.5 driven run are around five times larger than for NC-0.5. The overall deposition is larger for EC-0.5 and the measured maximum with depositions over 500 kBqm^{-2} to the Northwest of the power plant is clearly better represented using ECMWF input data (**Fig. F-3-1**). All statistical scores mentioned above (**Table F-3-1**) as well as a scatter diagram (not shown) confirm the view that the ECMWF run ranks better than the NCEP run.

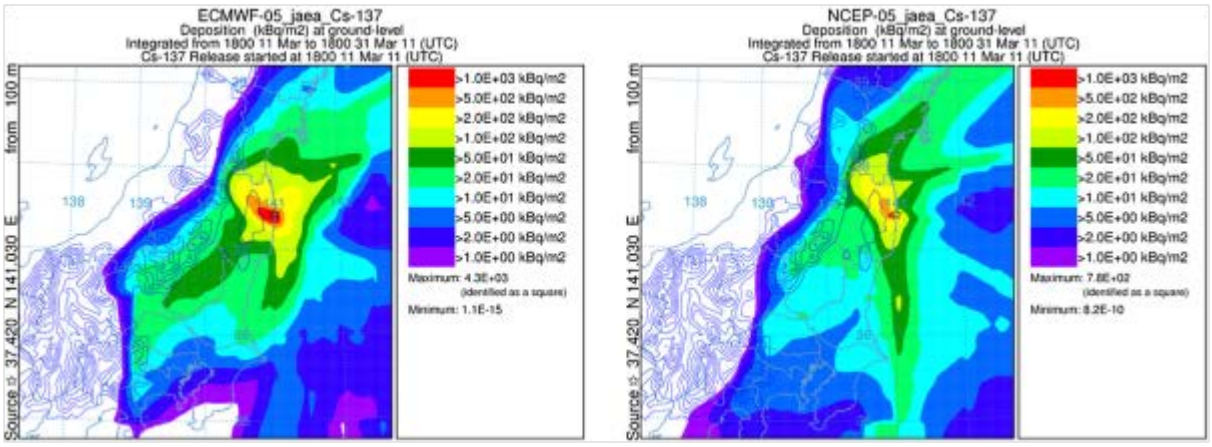

Fig. F-3-1.: Total accumulated deposition running FLEXPART with ECMWF (left) and NCEP (right) data both at 0.5° horizontal resolution. From Arnold et al. (2015), Fig.3.

b. ECMWF-0.2/0.1° versus ECMWF-0.5°

Increasing the horizontal resolution in the ECMWF fields used in the dispersion simulations from 0.5° to 0.2° (runs EC-0.2 and EC-0.5° in **Table F-3-1**) leads to the expected increase in structure and a more realistic appearance (**Fig. F-3-2**). The lower resolution input results in a smoother deposition field and larger area covered with smaller values in the plume axis northwest of Fukushima. Another important outcome is the increased deposition on the slope of the mountain district of Northern Japan as well west of the Kanto plain. This increase is carried forward if the resolution in the ECMWF field

gets enhanced to 0.1° (**Fig. F-3-2**). Performance metrics showed some slight improvements with the increase in horizontal resolution from 0.5° to 0.2°. However, using 0.1° input data lessens the Rank, which fits many experiences for model-to-point comparisons, where with increasing resolution of the meteorological input small dislocations between modeled patterns and measurements increasingly deteriorate statistical scores. Nevertheless it is advisable to use input data of 0.2° instead of 0.5° for ATM applications.

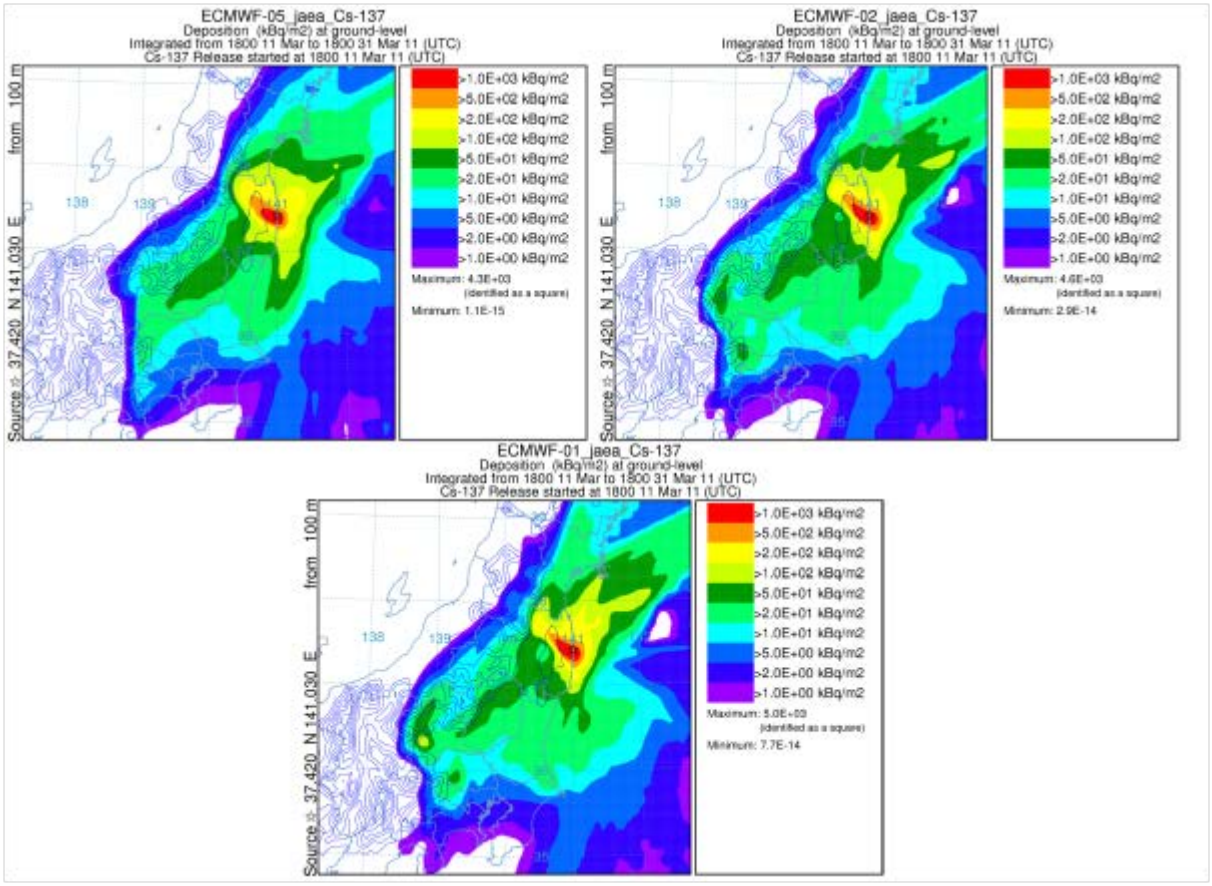

Fig. F-3-2.: Total accumulated deposition running FLEXPART with ECMWF at 0.5° (left), 0.2° (right) and 0.1° (center) horizontal resolution. Partly from Arnold et al. (2015), Fig.5.

c. ECMWF-0.2° versus ECMWF-0.2° with inserted JMA products

When replacing model precipitation with the radar-rain gauge analysis data in the 0.2°-ECMWF fields (ECRA-0.2 run in **Table F-3-1**) scores worsen slightly, whereas they improve when ingesting the Mesoscale precipitation analysis (ECME-0.2 run in **Table F-3-1**). In the first case the continuous maxima northwest of the NPP changes to a two-maxima pattern (**Fig. F-3-3**), in the second case the area with the greatest deposition extends a bit further north, thereby matching better the measurements. The regions with lower deposition to the south-west are also better represented. Maximum values turn out to be larger in both cases compared to plain ECMWF input data. The ingestion procedure was also applied to NCEP data, but resulted in a general worsening of results for both kinds of JMA-precipitation data (see results for NCME-0.5 and NCRA-0.5 in **Table F-3-1**). In this case the

elongated maximum to the northwest of the NPP is not reproduced. The results indicate an inconsistency between NCEP wind fields and observed precipitation, which in turn hints at a weaker performance of NCEP wind fields compared to those from ECMWF.

When the above described fix for wet deposition is applied to the FLEXPART source code, modeled depositions tend to worsen for plain ECMWF input data (regardless of the resolution) by 2-3% (see **Table F-3-1**). For example, the main deposition area becomes overestimated by the EC-0.2MC run, deposition onshore and inland towards the south also exceed the observations. Contrariwise, the runs with the ingested JMA-products (ECME-0.2MC and ECRA-0.2MC) show ranks improved by 2.3 and 5% respectively, mainly due to enhanced scavenging to the northwest of the NPP. It looks as if the consistency between precipitation fields and other meteorological input data, which is questionable in case of the ingestion of JMA precipitation products, is more important for the currently applied deposition scheme in FLEXPART version 8.23. This becomes understandable when one bears in mind that wet deposition for a grid point is only activated in this scheme if a cloud is diagnosed from relative humidity. With independent precipitation data the scheme is even more problematic than with dependent one.

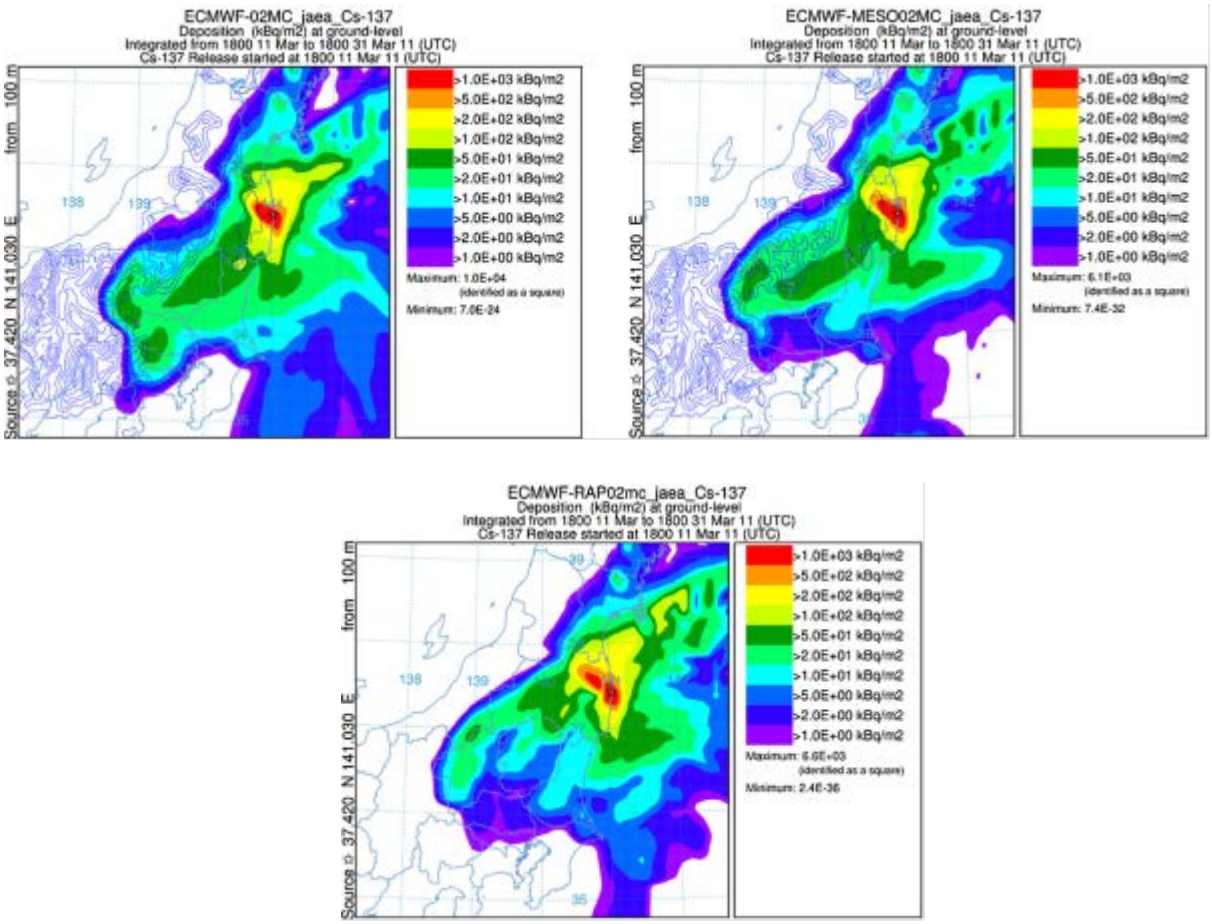

Fig. F-3-3.: Deposition patterns obtained with the quick fix for the wet deposition scheme in FLEXPART for the EC-0.2MC (upper left), the ECME-0.2MC (right) and the ECRA-0.2MC (center) runs.

Name	Met. precip. info.	Resolution (deg)	Corr	FB	FMS	KSP	Rank
EC-0.2	ECMWF	0.2	0.80	−0.08	100.00	15.00	3.44
EC-0.2MC	ECMWF	0.2	0.69	0.08	100.00	7.00	3.36
EC-0.5	ECMWF	0.5	0.71	−0.07	100.00	9.00	3.38
EC-0.5MC	ECMWF	0.5	0.68	0.09	97.24	10.00	3.28
ECRA-0.2	ECMWF + RAP	0.2	0.72	0.02	100.00	11.00	3.39
ECRA-0.2MC	ECMWF + RAP	0.2	0.83	0.13	100.00	6.00	3.57
ECME-0.2	ECMWF + MESO	0.2	0.81	0.00	100.00	15.00	3.50
ECME-0.2MC	ECMWF + MESO	0.2	0.83	0.05	100.00	9.00	3.58
NC-0.5	NCEP	0.2	0.66	−0.59	100.00	10.00	3.05
NCME-0.5	NCEP + MESO	0.5	0.65	−0.76	100.00	16.00	2.88
NCRA-0.5	NCEP + RAP	0.5	0.66	−0.84	100.00	20.00	2.82

Table F-3-1.: Statistical scores for the individual FLEXPART runs with different meteorological input data. MC label indicates the wet deposition FLEXPART quick fix was implemented. From Arnold et al. (2015), Fig.8 and Table 2.

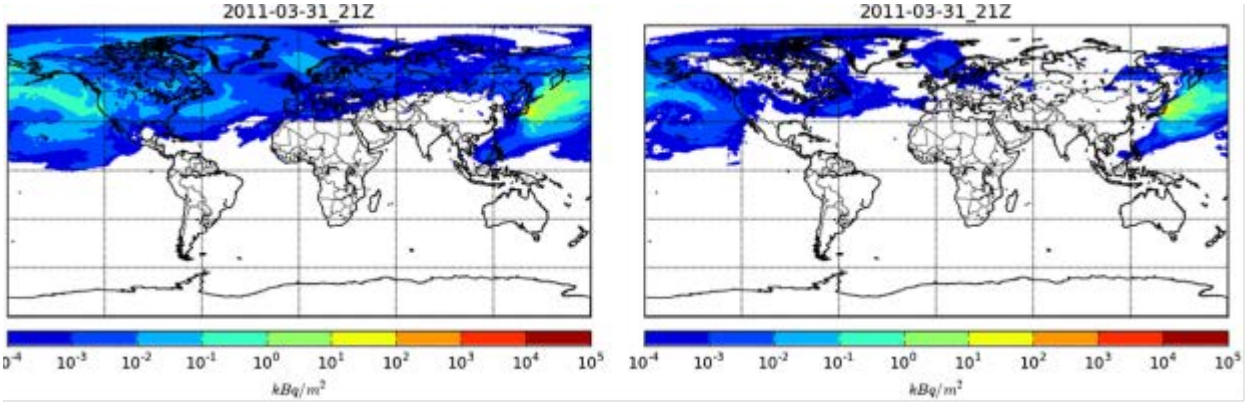

Fig. F-3-4.: Total global deposition on the 31st of March at 21 UTC for NCEP driven run (left) and ECMWF driven run (right). From Arnold et al. (2015), Fig.10.

d. Hemispheric run

Finally two hemispheric runs were evaluated with releases being tracked until the 31st of March. The runs were driven by global 0.5°-ECMWF data with a 0.2° nest (ECME-0.2 data) over Japan and by global 0.5°-NCEP data. Modeled ^{137}Cs depositions (**Fig. F-3-4**, however not comparable to any measurements) as well as ambient air concentrations (**Fig. F-3-5**) are generally higher using NCEP data as input. The plume arrival time and the two maxima pattern are quite well reproduced by FLEXPART at the IMS stations USP78 and USP79 (both located in the Central Pacific) both for ECMWF and NCEP input data. However, for ECMWF input the simulated concentrations are clearly underestimated, reaching up to a difference of two orders of magnitude. Overall uncertainties in patterns and magnitudes grow with increasing distance to the release location.

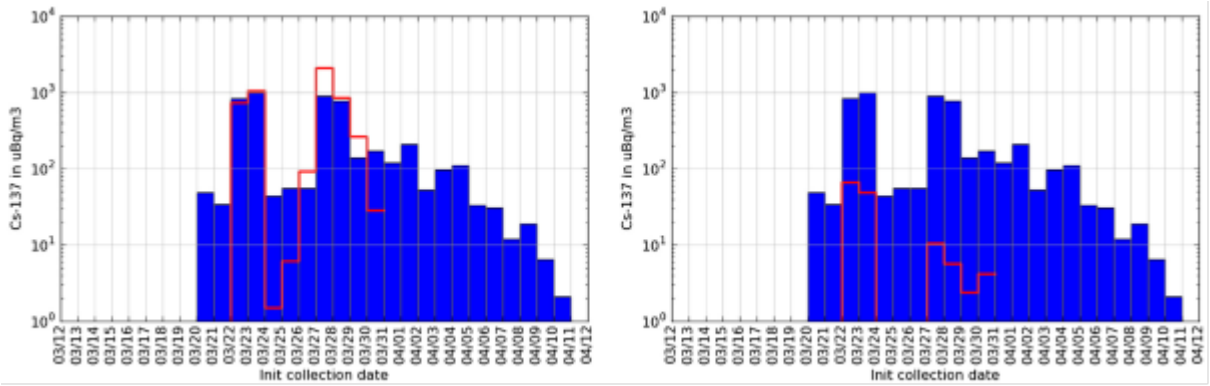

Fig. F-3-5: Time series of ^{137}Cs concentration at the USP78 IMS station. Measurements (blue) compared to modeled (red) concentrations with NCEP (left) and ECMWF (right) data. From Arnold et al. (2015), Fig.11.

F-3-4. Summary

The local model performance is clearly superior for 0.5° ECMWF fields compared to 0.5° NCEP fields given the Fukushima accident and the specific source term due to a systematic underestimation in NCEP results. Increasing the resolution from 0.5° to 0.2° for the ECMWF data seems beneficial. Inserting the Japanese Mesoscale precipitation analysis in 0.2°-ECMWF fields yielded the best result, especially when a wet deposition fix was applied. For the radar-gauge product things are different. They lead to a worsening in deposition when no fix is applied and to a bettering if it is applied, since the fix makes the model more robust to inconsistencies between wind and precipitation fields. Hemispheric runs yield more realistic concentration amplitudes (see Arnold et al. (2015) for more results) if driven by NCEP data.

F-4. The CMC ATDM experiments[1]

MLDP0 (*Modèle Lagrangien de Dispersion de Particules d'ordre 0*) is a Lagrangian particle dispersion model of zeroth order designed for long-range dispersion problems occurring at regional and global scales and is described in details in D'Amours and Malo (2004) and D'Amours et al. (2010). Dispersion is estimated by calculating the trajectories of a very large number of air particles (also called parcels or fluid elements). Large scale transport is described by calculating the displacement due to the synoptic component of the wind field and diffusion through discretized stochastic differential equations to account for the unresolved turbulent motions. Vertical mixing caused by turbulence is handled through a random displacement equation (RDE) based on a diffusion coefficient K_z. The calculation of the diffusion coefficient combines two formulations following Delage (1997), for the surface layer, and O'Brien (1970), for the above layers, in order to produce a vertical profile of K_z consistent with the depth of the ABL (due to the reflection condition at the top of the ABL). This coefficient is calculated in terms of a mixing length, stability function, and vertical wind shear. Lateral mixing (horizontal diffusion) is modelled according to a first order Langevin Stochastic Equation for the unresolved components of the horizontal wind (mesoscale fluctuations).

MLDP0 is an off-line model that uses the full 3-D meteorological fields provided by a numerical weather prediction (NWP) system, i.e. fields of wind, moisture, temperature and geopotential heights must be provided to the model. These are normally obtained from the GEM model forecasts and objective analysis systems in either global, regional or high resolution configuration.

In MLDP0 a computational particle (or parcel) is assumed to represent the ensemble average of a large number of "real" air constituents (aerosols or gases). At the emission, it is assigned a mass which depends on the total quantity of material emitted and the total number of particles. The effect of radioactive decay, wet scavenging, dry deposition and gravitational settling can be simulated by calculating the amount of material removed from the carrier particle, when it travels in regions of the atmosphere where such processes are active.

Dry deposition occurs when a particle is subjected to a reflection at the ground surface. It is modelled in terms of a dry deposition velocity v_d and an absorption probability P. The absorption probability is calculated according to Wilson et al. (1989) as

$$P = 1 - R\,, \quad R = \frac{1-a}{1+a}\,, \quad a = \left(\frac{\pi}{2}\right)^{1/2} \frac{v_d}{\sigma_w}\,, \tag{F-4-1}$$

[1] A. Malo and R. Servranckx

where R is the reflection probability and σ_w is the standard deviation of the vertical turbulent wind component. Since a particle represents the mean of an ensemble of particles, the fraction of the mass removed by dry deposition is equal to P. The deposition rate is calculated by assuming that a particle contributes to the total surface deposition flux in proportion to the tracer material it carries when it is found in a layer adjacent to the ground surface. Dry deposition increment dm_d for particle p over a model time step dt can be expressed as

$$dm_d = P \cdot m_p = (1 - R) \cdot m_p \,, \tag{F-4-2}$$

where m_p is the particle mass. The new particle mass m'_p is then adjusted accordingly

$$m'_p = R \cdot m_p \,. \tag{F-4-3}$$

Wet deposition is treated with a simple scheme and will occur when a particle is presumed to be in a cloud (*in-cloud scavenging*) and is modelled in terms of a wet scavenging rate. Below-cloud scavenging is not considered yet in the operational version of MLDP0. The tracer removal rate is proportional to the local cloud fraction f_c and the particle mass m_p. Wet deposition increment dm_w for particle p over a model time step dt and updated particle mass are calculated using the following relationships

$$dm_w = m_p \cdot \left[1 - \exp(-s_w f_c dt)\right], \tag{F-4-4}$$

$$m'_p = m_p \cdot \exp(-s_w f_c dt), \tag{F-4-5}$$

where s_w is the wet scavenging rate (s^{-1}). Local cloud fraction is parameterized according to Pudykiewicz (1989) as a function of relative humidity following

$$f_c = \frac{U - U_t}{U_s - U_t}, \quad \text{if } U \geq U_t \,, \tag{F-4-6}$$

where f_c is the cloud fraction, U is the relative humidity, U_t is the threshold value of the relative humidity above which the subgrid scale condensation occurs (75% is the default value in MLDP0), U_s is the relative humidity for the saturation state (100%). Local cloud fraction can be estimated in both hindcast and forecast modes, using analysed and forecast NWP meteorological fields.

Gravitational settling in the trajectory calculations is computed according to Stokes' law for fine particles. By default, MLDP0 is run neglecting gravitational settling effects. However, this optional removal process can be included accounting together for a particle size distribution and density of a particle. This process represents an important removal mechanism in atmospheric transport modelling and can modify significantly modelled airborne concentrations and total ground deposition at short scale (near the source) as well as at very long range. This impact is related especially to the particle size

distribution used in the modelling. In order to properly model this physical process, it is therefore necessary to have a good knowledge of particle size distribution, something that is rarely known or available.

In MLDP0, tracer concentrations at a given time and location are obtained by assuming that particles carry a certain amount of tracer material. The concentrations are then obtained by calculating the average residence time of the particles, during a given time period, within a given sampling volume, and weighting it according to the material amount carried by the particle. Concentrations can be estimated more accurately close to the source with a Lagrangian model as compared to an Eulerian model. It is important to note that in MLDP0, all concentrations are averaged in space and time. The concentrations are averaged in the vertical layers and in the horizontal (surrounding grid points weighting algorithm) for smoothing effects and artificial noise attenuation as well as over the output time period/step/resolution specified by the modeller. For example, concentration outputs at 3-h time steps would correspond to average values over that 3-h period.

Three generic species were modelled as surrogates for the radionuclides: a gas with no wet or dry scavenging to mimic noble gases (such as ^{133}Xe), a gas with a relatively large dry deposition velocity (1 cm/s) and wet removal rate (3×10^{-4} s^{-1}) to represent a depositing gas (such as gaseous ^{131}I), and a particle with a small dry deposition velocity (0.1 cm/s) and wet scavenging rate (3×10^{-5} s^{-1}) to represent light particles (such as ^{137}Cs or particulate ^{131}I). Details are shown in Table F-4-1.

Table F-4-1. Different physical removal processes accounted in MLDP0 simulations (Draxler et al., 2013a).

Type	Species Name	v_d [cm/s]	s_w [s^{-1}]	Dry Deposition	Wet Scavenging	Radioactive Decay	Gravitational Settling	Surrogate for
Gas	Ngas	0	0	No	No	No	No	Noble gases (Kr, Xe, Rn)
Particle, light	Lpar	0.1	3×10^{-5}	Yes	Yes	No	No	^{137}Cs, ^{131}I
Gas, depositing	Dgas	1	3×10^{-4}	Yes	Yes	No	No	^{131}I

F-5. Results of ATDM simulations[1]

F-5-1. ATDM simulations using UNSCEAR source term

The ATDM simulation results from the task team are summarized in WMO (2012b) and Draxler et al. (2013a). The experiments were conducted according to the experimental design protocol described in D-1.

Figure F-5-1 shows a sample of the calculated ^{137}Cs deposition patterns from NOAA-HYSPLIT (top) and UKMET-NAME (bottom) using the UNSCEAR source term. Here, the left panels show the predicted deposition patterns using the ECMWF meteorology, while the right panels show the model results using the JMA MESO meteorology. The UKMET results tend to be smoother than the NOAA calculation which is especially striking for the calculations using the finer resolution MESO data.

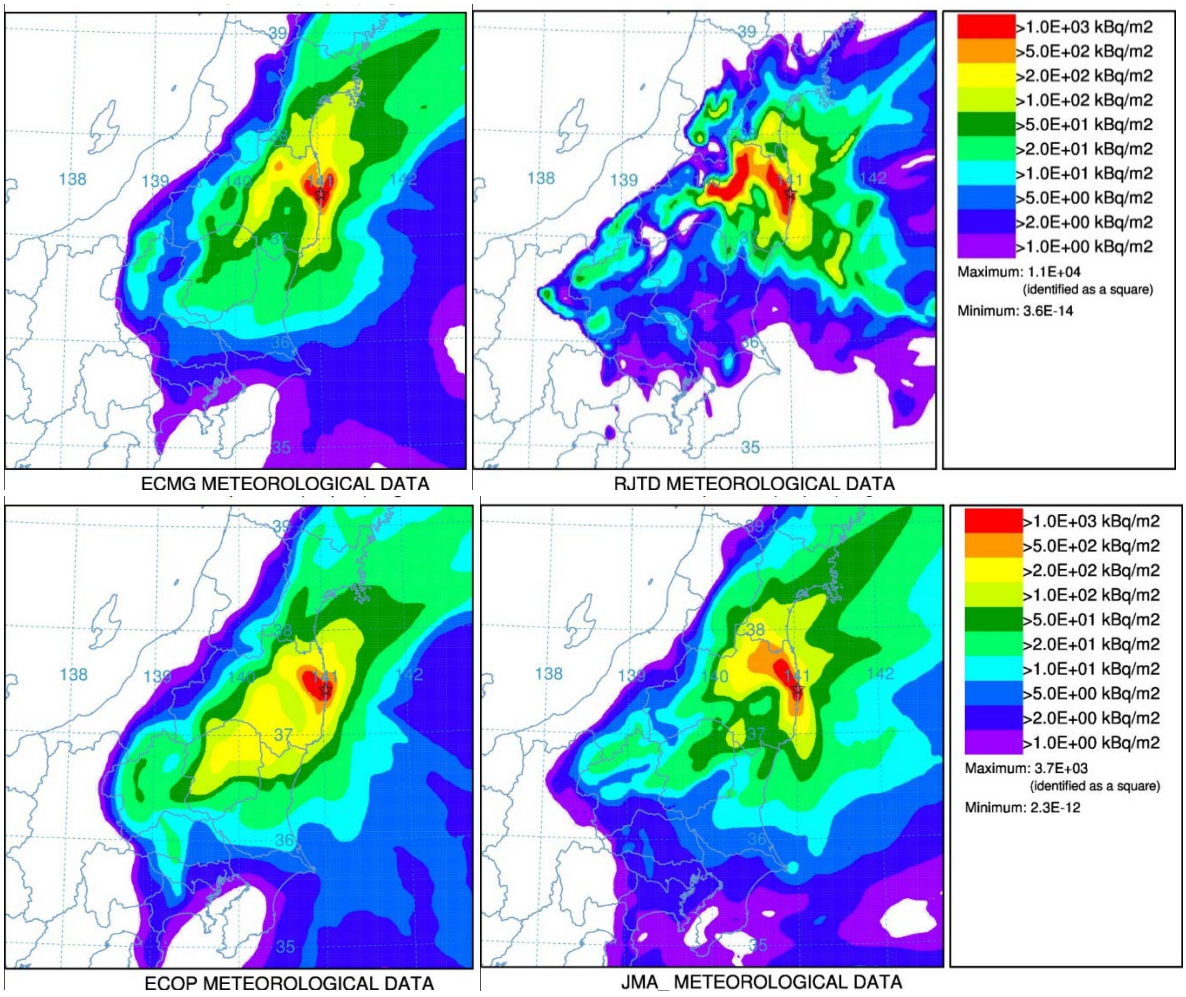

Fig. F-5-1. Upper: Calculated ^{137}Cs deposition using NOAA-HYSPLIT ATDM with ECMWF data (left) and with the JMA-MESO analysis (right). Bottom: UKMET-NAME ATDM with ECMWF data (Left) and with the JMA-MESO analysis (right). Reproduced from Draxler et al. (2013a).

[1] K. Saito, R. Draxler, T. Shimbori, M. Hort, G. Wotawa, A. Malo and R. Servranckx

An example of the computed ^{137}Cs deposition pattern for the ensemble mean of ten selected members (Draxler et al., 2013a) from all task tem ATDMs is shown in Fig. F-5-2. The computed high deposition region shows a comparable downwind direction to the measurements (Fig. D-3-1), including the turn to the southwest, less transport to the north, and a much smoother pattern, more consistent with the measurements.

Detailed verification results for the case using UNSCEAR source term is given in Draxler et al. (2013a).

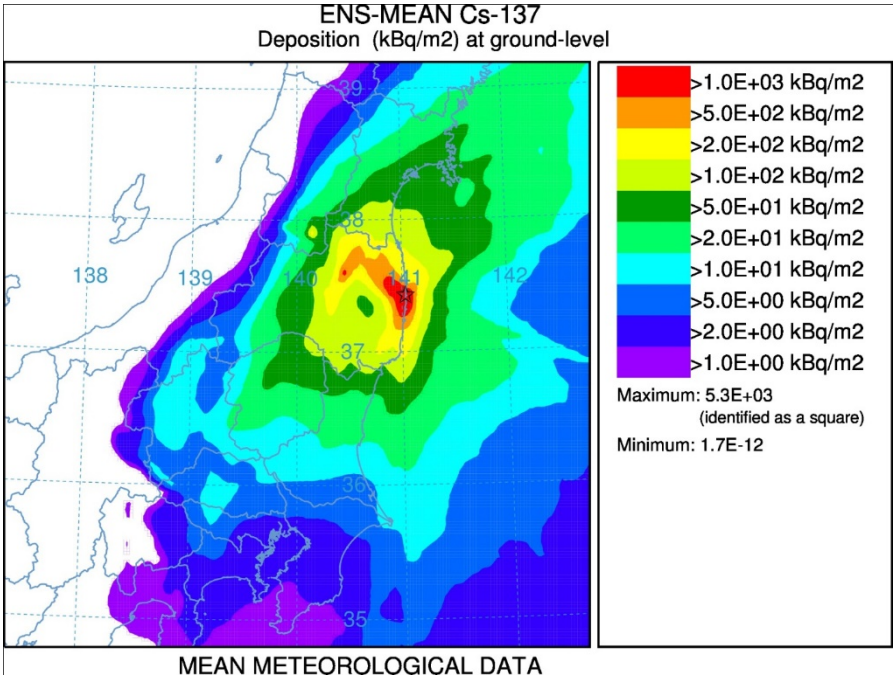

Fig. F-5-2. Calculated ^{137}Cs deposition using the mean of ten selected ATDM-meteorology combinations. After Draxler et al. (2013a).

F-5-2. Verification results using JAEA source term

The results of ATDM simulations and their verifications have been published in WMO (2012b) and Draxler et al. (2013a). In this subsection, verification results using JAEA source term are briefly summarized from the above publications.

Table F-5-1 shows ATDM verification results for ^{137}Cs deposition using JAEA source term. In this table, JMA (PRE) shows the results from the preliminary JMA-RATM simulations before the modifications described in Section E-2 were applied. METRIC1 is the total model rank defined by the Eq. (D-3-1). Here, the value of METRIC1 is positive and becomes 4.0 for a perfect case. For ^{137}Cs deposition, NOAA-HYSPLIT using GDAS showed the best score for METRIC1. ZAMG-FLEXPART and, NOAA-HYSPLIT using ECMWF analysis and, UKMET-NAME using JMA-MESO also scored a relatively high performance. In NOAA-HYSPLIT, the use of JMA MESO analysis did not improve

the METRIC1, while the results of CMC-MLDP0 and UKMET-NAME were improved by the use of JMA MESO.

Table F-5-2 shows ATDM verification results for air concentrations at JAEA. Including the best score by CMC and the second best by JMA-RATM, all the top five ranked models used the JMA Meso analysis for their computations.

Replacing the JMA Mesoscale analysis precipitation fields with JMA precipitation observation analysis (MESO-R) did not improve the ATM calculations of deposition and even deteriorated the scores for air concentration. The reason for this is not clear. It should be noted that the air concentration verification was for a single location (JAEA) thus it does not reflect the horizontal distribution of radionuclides. The southward advection of radionuclides from Fukushima Daiichi NPP on March 15th was sensitive to small changes in the wind direction. As for deposition, ZAMG-FLXPART using ECMWF analysis slightly improved its score when the precipitation analysis was used. Saito et al. (2015) suggested the following reasons that the precipitation analysis did not improve the performance of ATM calculations:

The discrepancy of the transport patterns created using numerical weather prediction (NWP) analyses and the locations of the actual precipitation may result in a wrong description of the total wet scavenging. The quality of the RAP data itself is also arguable. Although the bright band (shown in Fig. B-3-2) is not likely critical in this experiment, radar echoes are scanned around the level of 1 km AGL and solid waters are over-detected in the radar reflectivity. A lower detection limit of around 0.4 mm h^{-1} applies to the RAP, which means that very weak precipitation is not included. In case of JMA-RATM, all RAP precipitation was considered to be liquid rain in the wet scavenging calculation (see Section E-2), and this assumption also may yield some errors in the time evolution.

Table F-5-1. ATDM verification results for ^{137}Cs deposition using JAEA source term. First to fifth values of METRIC1 are indicated by bold type. In analysis, '-R' means that JMA precipitation analysis is used. Reproduced from Draxler et al. (2013a).

Organization	Analysis	R	FB	FMS	FOEX	%FA2	KSP	METRIC1
CMC	GEM	0.76	-0.32	100.00	11.69	48.99	19.00	3.22
CMC	MESO	0.76	-0.44	100.00	-4.33	45.12	6.00	3.30
JMA (PRE)	MESO	0.45	-0.02	100.00	-0.46	51.01	10.00	3.09
JMA (PRE)	MESO-R	0.77	0.54	100.00	9.67	41.99	11.00	3.22
NOAA	GDAS	0.87	-0.08	100.00	8.01	48.25	6.00	**3.65**
NOAA	GDAS-R	0.68	-0.57	100.00	-16.48	31.86	23.00	2.94
NOAA	MESO	0.55	0.38	100.00	-8.01	41.07	15.00	2.97
NOAA	MESO-R	0.48	0.43	100.00	-4.14	35.54	16.00	2.85
NOAA	ECMWF	0.83	-0.30	100.00	-12.06	46.96	10.00	**3.45**
NOAA	ECMWF-R	0.55	-0.74	100.00	-20.35	21.92	33.00	2.60
UKMET	UM	0.44	0.24	100.00	30.48	42.36	30.00	2.77
UKMET	ECMWF	0.80	0.11	100.00	19.06	54.70	25.00	3.34
UKMET	MESO	0.76	0.04	100.00	5.80	45.12	11.00	**3.45**
UKMET	MESO-R	0.66	0.03	100.00	6.35	34.62	9.00	3.33
ZAMG	GDAS	0.66	-0.59	100.00	-6.17	45.12	10.00	3.05
ZAMG	GDAS-R	0.66	-0.84	100.00	-16.85	28.36	20.00	2.82
ZAMG	ECMWF	0.78	-0.08	100.00	9.85	59.67	15.00	**3.41**
ZAMG	ECMWF-R	0.83	0.13	100.00	5.99	52.12	6.00	**3.57**

Table F-5-2. Same as in Table F-5-1, but for particulate ^{131}I air concentrations at JAEA. Reproduced from Draxler et al. (2013a).

Organization	Analysis	R	FB	FMS	FOEX	%FA2	KSP	METRIC1
CMC	GEM	0.07	-1.37	73.17	-30.95	7.14	53.00	1.52
CMC	MESO	0.23	-0.09	80.49	-4.76	16.67	34.00	**2.47**
JMA (PRE)	MESO	0.51	-0.82	80.00	-21.43	21.43	43.00	**2.22**
JMA (PRE)	MESO-R	0.59	-1.66	57.50	-45.24	4.76	64.00	1.46
NOAA	GDAS	0.10	-1.37	60.00	-42.86	7.14	69.00	1.24
NOAA	GDAS-R	0.10	-1.38	60.00	-42.86	7.14	67.00	1.25
NOAA	MESO	0.15	-1.63	62.50	-40.48	11.90	67.00	1.16
NOAA	MESO-R	0.15	-1.63	60.00	-40.48	9.52	67.00	1.14
NOAA	ECMWF	0.27	-1.33	62.50	-35.71	11.90	60.00	1.43
NOAA	ECMWF-R	0.27	-1.35	62.50	-35.71	16.67	60.00	1.43
UKMET	UM	0.06	-1.42	65.85	-30.95	19.05	53.00	1.42
UKMET	ECMWF	0.13	-0.93	68.29	-28.57	21.43	53.00	1.70
UKMET	MESO	0.24	-0.50	80.00	-28.57	16.67	52.00	**2.09**
UKMET	MESO-R	0.24	-0.53	80.00	-30.95	16.67	52.00	**2.07**
ZAMG	GDAS	0.17	-0.37	57.50	-35.71	14.29	57.00	**1.85**
ZAMG	GDAS-R	0.18	-0.43	57.50	-35.71	14.29	55.00	1.84
ZAMG	ECMWF	0.12	-0.54	52.50	-35.71	11.90	60.00	1.67
ZAMG	ECMWF-R	0.08	-0.55	42.50	-35.71	7.14	69.00	1.46

G. Relevant modeling at MRI and JMA

G-1. Numerical Atmospheric Transport and Dispersion Models[1]

Numerical atmospheric transport dispersion and deposition models (ATDMs) are capable of simulating air and ground surface contamination with radioactive materials from nuclear accidents. Given the time and place of emission sources, ATDMs calculate the advection, diffusion, and dry and wet deposition processes of radioactive materials. Many ATDMs are driven by meteorological parameters provided by numerical weather prediction (NWP) models. They range from high-resolution limited-area models to low-resolution global models, depending on their purposes and the available computational resources.

Although predictions by ATDMs are very informative, they have some uncertainty, which results from limited information about emission sources and incomplete model representation of transport and deposition processes, in addition to the uncertainty of NWP products. In general, the products of ATDMs should not be used for quantitative comparison with some threshold densities of radioactive materials for evacuation, but they are suitable for assessing the worst case scenario.

Although ATDMs were not used for mitigating risks of radiation exposure in the case of the accident at the Fukushima Dai-ichi Nuclear Power Plant (Iwasaki, 2013), a working group of the Meteorological Society of Japan has pointed out some ways in which numerical predictions of the atmospheric dispersion of accidentally released radioactive materials can be utilized (WGMSJ, 2014). In particular, ATDMs may be useful along with monitoring data in the following environmental emergencies:

(i) Radioactive materials floating near the ground surface:

People become internally exposed to floating radioactive materials through inhalation. For example, radioactive iodine tends to concentrate in the thyroid gland, where it may cause thyroid cancer. ATDMs are expected to provide information about contaminated air near the ground surface.

(ii) Radioactive materials deposited on the ground:

Airborne radioactive materials contaminate the ground surface through dry and wet deposition. Wet deposition, in which falling raindrops gather radioactive materials between the clouds and the ground, can cause severe radioactive contamination of the ground even far away from the emission source. Unfortunately, the performance of ATDMs in simulating wet deposition processes is not satisfactory because of NWP errors in predicting precipitation, together with the errors arising from the ATDM itself, degrade the quality of wet deposition predictions. However, ATDMs can be used to estimate the vertically integrated amount of airborne radioactive materials, which is the maximum potential wet deposition.

[1] T. Iwasaki

G-2. WMO emergency response activities and operational atmospheric transport modelling at JMA[1]

G-2-1. Introduction

The Japan Meteorological Agency (JMA) was designated by the World Meteorological Organization (WMO) as a Regional Specialized Meteorological Centre (RSMC) for Atmospheric Transport Modelling (ATM) for radiological Environmental Emergency Response (EER). RSMCs-ATM are responsible for providing ATM products in response to requests by the International Atomic Energy Agency (IAEA) and members of WMO. This section briefly describes the WMO EER service and the operational atmospheric transport model used by JMA.

Table G-2-1. List of current WMO RSMCs-ATM for radiological EER.

	Organization (country)	Start year	WMO Regional Association
RSMC Tokyo	Japan Meteorological Agency (Japan)	1997	WMO Regional Association II (Asia)
RSMC Beijing	Chinese Meteorological Administration (China)	1997	
RSMC Obninsk	Roshydromet* (Russia)	1997	
RSMC Montréal	Canadian Meteorological Center (Canada)	1989	WMO Regional Associations III and IV (South, Central, and North America, and the Caribbean)
RSMC Washington	National Environmental Prediction Center (USA)	1993	
RSMC Melbourne	Bureau of Meteorology (Australia)	1995	WMO Regional Association V (South-West Pacific)
RSMC Exeter	UK Met Office (UK)	1989	WMO Regional Associations I and VI (Africa and Europe)
RSMC Toulouse	Meteo France (France)	1989	

* The Russian Federal Service for Hydrometeorology and Environmental Monitoring

G-2-2. WMO RSMCs-ATM

After the Chernobyl nuclear power plant accident in April 1986, the Commission for Basic Systems (CBS) of WMO held a series of discussions and decided to launch an ATM EER service to meet the broad interest in the atmospheric dispersion of toxic radiological materials. The national meteorological and hydrological services of the United Kingdom, France, and Canada started their ATM services in 1989. Table G-2-1 lists the current RSMCs-ATM. JMA was designated an RSMC at the 49th session of the WMO executive council in 1997 and initiated its service on 1 July 1997. Two other RSMCs (Beijing and Obninsk) in Regional Association (RA) II (Asia) also began operation then. The German Weather Service (Deutscher Wetterdienst) has been contributing by acting as the WMO Regional Telecommunications Hub (RTH) for EER. In this role, it receives nuclear and radiological emergency messages from IAEA and disseminates early warning messages through the WMO Global Telecommunication System (GTS).

Each RSMC is responsible for providing forecasts within its region of responsibility (see Table G-2-1). RSMSs provide their ATM products not only to IAEA but also to WMO members within their

[1] M. Sakamoto

region of responsibility. For example, if a WMO member in RA II asks for support, RMSCs Tokyo, Beijing, and Obninsk serve this request. If RSMC Tokyo receives a request from a WMO member in RA V (South-West Pacific), which is adjacent to RA II and includes part of Southeast Asia, RSMC Tokyo replies to the member and forwards the request to RSMC Melbourne, the responsible center of RA V, which services the request.

More than one RSMC is allocated to each RA so that RSMCs can compare and evaluate the accuracy of their products before presenting a concise statement of ATM forecast results and the meteorological situation within the region. In the case of RA V, where there is only one center, RSMCs Montréal and Washington provide services in support of RSMC Melbourne.

G-2-3. International coordination by the CBS expert team

CBS formed an expert team to organize emergency responses and related activities, and the team is currently called the Expert Team on Emergency Response Activities. This team, which is composed of representatives from the RSMCs, RTH, WMO, and IAEA secretariats and other related international organizations, meets once every two years to discuss issues regarding ATM services at related WMO centers.

The team reports to the CBS Open Programme Area Group on Data-Processing and Forecasting System, which then conveys the contribution through CBS to the WMO Executive Council and the World Meteorological Congress. For instance, the issues and activities discussed at the team meeting in Vienna in 2011 were contributed to CBS-15 in Jakarta in 2012 and the 65th Executive Council meeting in 2013.

G-2-4. Standard EER products

The standard set of EER products, as defined in Appendix II-7 of the Manual on the Global Data-processing and Forecasting System (WMO, 2010), consists of seven charts (Fig. G-2-1) and a joint statement on weather and atmospheric dispersion forecasts within the region.

(a) Trajectory chart (Fig. G-2-1 (a))

Trajectories of three tracers released at 500, 1500, and 3000 m above the surface are shown in the chart. The tracers are released at the start release time of radioactive material and move with the wind stream, without considering disturbance by atmospheric diffusion and viscosity. The forecast extends to 72 hours after the forecast initial time. Changes in the height of each tracer with time are shown below the map in the figure.

(b) Time-integrated concentration charts (Fig. G-2-2 (b))

The 24 hour time-integration concentration of the radioactive material by 24, 48, and 72 hours after the forecast initial time are presented in three charts. The distributions shown in Fig. G-2-2 (b) is the average from the surface to an altitude of 500 m. The unit of radioactivity in the charts is Bq s / m^3, and indicates the number of radiological decays in the 24 hour period per cubic meter of atmosphere.

(c) Total deposition charts (Fig. G-2-3 (c))

The distribution of radioactive materials that have accumulated through dry and wet deposition processes on the surface from the initial release time is shown in three charts, for 24, 48, and 72 hours after the forecast initial time. The unit of deposition is Bq / m^2, which is the number of radiological decays per second per square meter of surface.

(d) Joint Statement

A concise consensual plain text description of weather conditions and the atmospheric dispersion forecast of the radioactive material is prepared by the RMSCs within each region. For example, RSMCs Tokyo, Beijing, and Obninsk prepare this statement whenever documentation for RA II is needed. The statement basically includes a synopsis of the current situation and the forecast of meteorological conditions in the area of concern, along with the transport modelling results, including the differences and similarities among the models.

The impact of an accident depends not only on the amount of radioactive material released but also on the types of radionuclides and on the exposure pathway. The products produced by the WMO RSMCs consist only of weather forecast and atmospheric transport information; they do not address the consequences of the release of toxic materials in the region. Therefore, expertise in nuclear science and in biology, including knowledge of the characteristics of nuclear decay and the impact of radiation exposure on the bodies of humans and animals, is needed to interpret any impacts from the products.

WMO RSMCs present their ATM products to IAEA and the registered organizations of WMO member states. The ATM results should be analyzed by specialized international organizations such as IAEA and WHO, and by relevant national governmental organizations of the influenced member states.

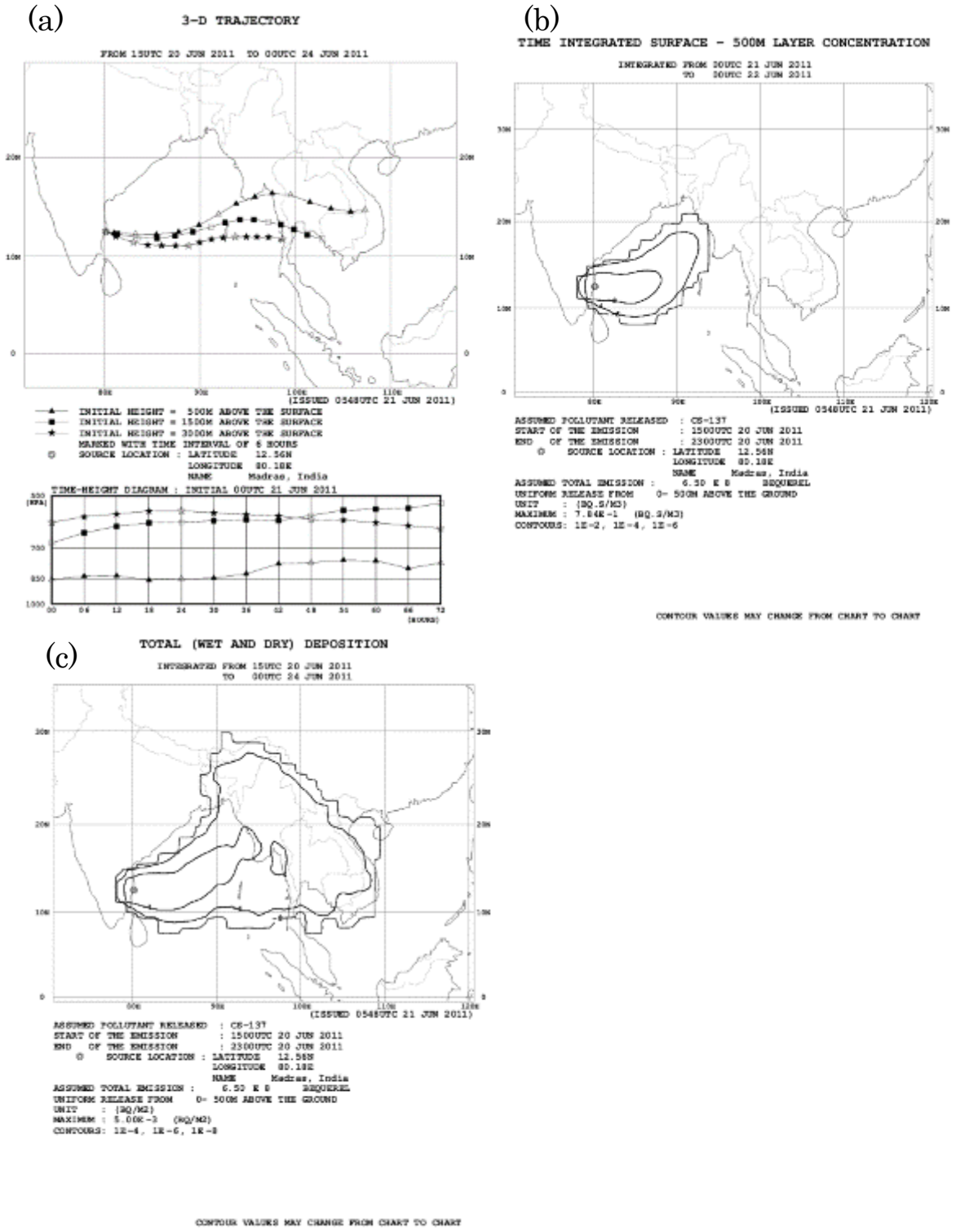

Fig. G-2-1. Examples of the standard EER products: (a) trajectory chart and time–height diagram for the three tracers, (b) time-integrated concentration chart, (c) total deposition chart.

G-2-5. JMA's ATM for EER

The atmospheric transport model for EER by JMA uses a Lagrangian approach in which many tracer particles are released at the time and location of the pollutant emissions and the model simulates the displacement of the tracers. The tracers move by advection and diffusion, and they may descend and settle onto the surface through dry or wet deposition. Table G-2-2 shows the specifications of the atmospheric transport model. The effects of advection, diffusion and deposition are simulated by using 3-hourly grid point values from JMA's operational global numerical weather prediction. Tracer particles are also removed by nuclear decay. Iwasaki et al. (1998) described the development of the ATM and the results of an international comparison experiment, and Sakamoto (2013) gave a detailed description of the model.

Lagrangian ATMs have the advantage that they conserve the total amount of released tracers. There is neither a fictitious loss nor a gain if the treatment of deposition and of radiological decay is appropriate. Almost all RSMCs[2] use Lagrangian atmospheric transport models.

Table G-2-2. Specifications of the ATM for the radiological EER at RSMC Tokyo.

Type of ATM	Lagrangian
Vertical diffusion scheme	Louis et al. (1982)
Dry deposition scheme	Kitada et al. (1986)
Wet deposition scheme	Kitada (1994)
Number of tracer particles	100,000
Horizontal grid cell size for concentration and deposition	1° × 1°
Weather forecast system	JMA's Operational Global Forecast (TL959L60 Global Spectral Model)*
Grid point data used in the ATM	Lower Resolution (TL319L40) Grid Point Data prepared for ATM. The ATM uses gridded wind velocity, precipitation, specific humidity, temperature, surface pressure, and horizontal pressure gradient data.

* When the start release time is earlier than the forecast initial time, the operational global analysis data are also used as for the period before the forecast initial time.

G-2-6. A case study of a wildfire event

To demonstrate the performance of JMA's ATM for EER, a case study of a wildfire event, during which the distributions of the tracers were optically observed by a satellite imager, is presented in this subsection.

According to the fire and smoke products produced by the Office of Satellite and Product Operations of the U.S. National Environmental Satellite, Data, and Information Service (NESDIS), on 28 April 2011 wildfires were started by lightning around the Okefenokee National Wildlife Refuge (ONWR) in Georgia, USA. The fires continued for months, and smoke was clearly observed, especially during the period from 19 to 23 June. Visible and infrared images acquired by the MODIS instrument on the AQUA satellite were published on the NESDIS website. Although there were other wildfires during the same period, the large wildfires around ONWR produced the most smoke.

In the visible image acquired by the AVHRR sensor on NOAA-18 at 17:00 UTC on 23 June (Fig. G-2-2a), a broad thick band of clouds covers parts of the central and eastern United States and southern Canada, but there is little cloud cover over the western Atlantic Ocean at around 30°N. In the

[2] The only exception is the ATM of RSMC Toulouse, which uses an Eulerian approach.

differential infrared image acquired at the same time (Fig. G-2-2b), the broad gray area spreading over the Atlantic from the U.S. east coast was identified as smoke released by the ONWR wildfires. Because emittance of infrared (IR) radiation of smoke is heavily dependent on the wavelengths, a differential IR image is used to reveal the presence of the smoke.

Figure G-2-3 shows the result of the ATM forecast, in which tracers are uniformly released from the surface in the ONWR from 00:00 UTC on 15 June to 00:00 UTC on 23 June 2011. To simulate the broad distribution for the long forecast period, the number of the tracers was set to be two million. The distribution of the total column amount of tracers at 00:00 UTC on 23 June in the forecast results, presented using a log-scale in Fig. G-2-3, generally corresponds to the area of smoke shown in Fig. G-2-2b. Few tracers are below the thick cloud area seen in Fig. G-2-2a because the considerable amount of precipitation predicted by the global forecast washed out the tracers. In fact, NESDIS reported that there was no smoke identified north of Virginia because of heavy rain. A thick area of tracers also extends from the northeastern Labrador-Ungava Peninsula to the north Atlantic. JMA's global analyses of geopotential height at 500 hPa and wind distribution at 700 hPa at 00:00 UTC on 23 June 2011 (Fig. G-2-4) show a cutoff low pressure system around Newfoundland. The tracers over the Labrador-Ungava Peninsula followed the counterclockwise air circulation around this low, and their distribution corresponds well to the smoke distribution in Fig. G-2-2b. The tracers were relatively high because of upwelling flow around the low.

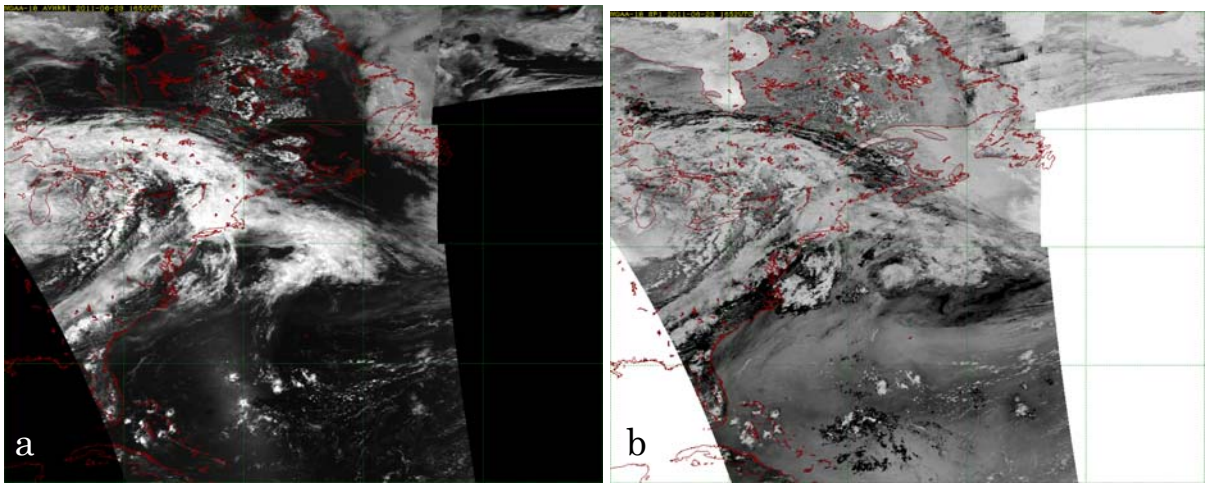

Fig. G-2-2. Images acquired by NOAA-18 / AVHRR at 17:00 UTC on 23 June 2011: (a) visible image, (b) differential infrared image.

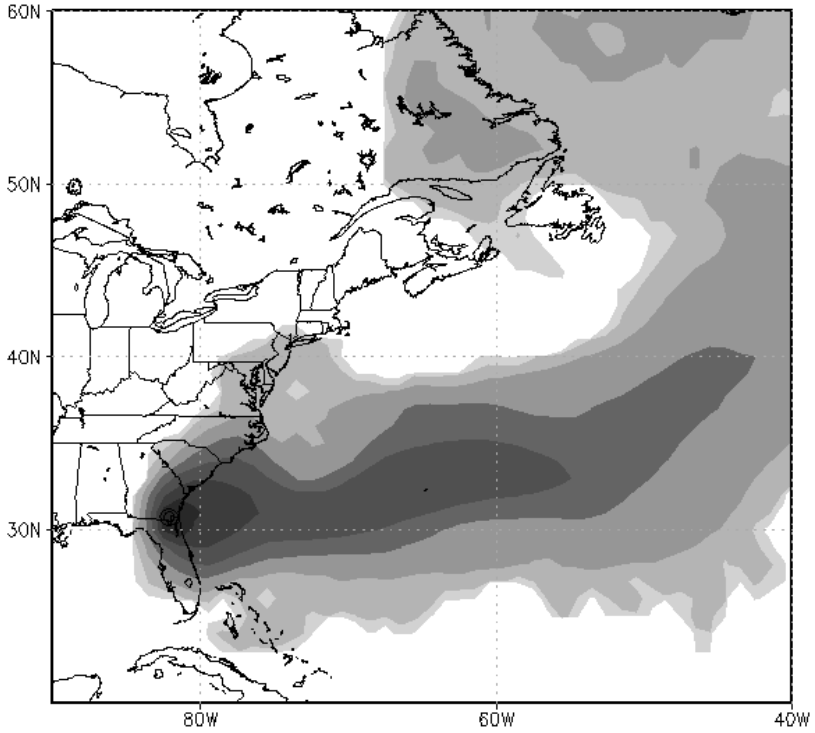

Fig. G-2-3. Distribution of the total column amount of tracers in the ATM forecast for 00:00 UTC on 23 June 2011.

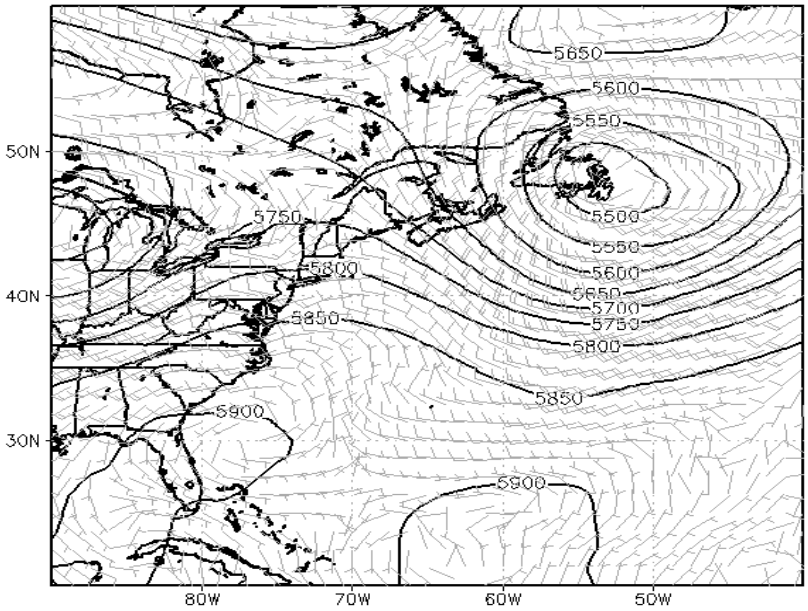

Fig. G-2-4. Analysis of the geopotential height at the 500 hPa level (contour interval, 50 m), and wind barbs at 700 hPa at 00:00 UTC on 23 June 2011.

G-3. NHM-Chem: Sensitivity of Cs deposition to the size and hygroscopicity of Cs-bearing aerosols[1]

G-3-1. Abstract

The emission, transport, and deposition of ^{137}Cs released by the Fukushima Daiichi Nuclear Power Plant (FDNPP) accident were simulated with consideration of the microphysical properties (i.e. size and hygroscopicity) of the Cs-bearing aerosols (carrier aerosols of radioactive Cs). The sensitivity of the simulated deposition of ^{137}Cs to the size and hygroscopicity of the carrier aerosols was assessed and compared with the sensitivity to meteorological fields simulated using different dynamics and physics modules. Two types of Cs-bearing aerosols were considered in the simulation, supermicron water-insoluble and submicron water-soluble particles, in accordance with previously published observational evidence (Adachi et al., 2013 and Kaneyasu et al., 2012). Even though the same transport model was used, the simulated depositions were very different when meteorological models with different dynamics and physics modules were used. The sensitivity of ^{137}Cs deposition to the carrier aerosol size and hygroscopicity, in which the proportion of water-insoluble aerosol emission ranged from 10% to 90%, during the early stage ranged from March. 11-12 to Mar. 12-20, was found to be lower but still as important as the sensitivity to meteorological fields simulated using different dynamics and physics modules. To better understand the environmental behavior of the radioactive Cs discharged from the FDNPP, knowledge of the carrier aerosol microphysical properties is as important as the accuracy of the meteorological simulation and the emission scenario.

G-3-2. Introduction

Three months after the FDNPP accident, Chino et al. (2011) estimated the emission amounts of radioactive ^{137}Cs and ^{131}I associated with the accident by using a reverse estimation method in which both the environment monitoring data and an atmospheric dispersion simulation were used (see section D-2). Since then, many modeling studies have been conducted to assess the emission, dispersion, and deposition amounts of radionuclides associated with the accident (Morino et al. 2011; Yasunari et al., 2011; Schöppner et al. 2011; Takemura et al., 2011; Sugiyama et al., 2012; Stohl et al., 2012; Terada et al., 2012; Katata et al., 2012a, 2012b; Morino et al., 2013; Adachi et al., 2013; Hu et al., 2014; Katata et al., 2015; Sekiyama et al., 2015).

Because numerical models use uncertain parameters and rough assumptions, model inter-comparison and intra-comparison (or sensitivity) studies are essential to assess the uncertainties of numerical simulations. In fact, previous model inter-comparison studies have shown that simulation results vary substantially among models (Draxler et al., 2013a; Katata et al., 2015; SCJ, 2014). Although model inter-comparison studies can show how the simulation results of models using different dynamics, physics, and chemistry modules and emission scenarios differ overall, the reasons for the differences cannot be easily identified. In contrast, model intra-comparison (or sensitivity)

[1] M. Kajino

studies can identify the modules or parameters that are responsible for different results, but under limited conditions that the simulations are performed only by a single model.

Morino et al. (2013) investigated the sensitivity of radioactive Cs dispersion and deposition to the wet-scavenging modules and emission scenarios. Like most previous studies, for the meteorological field they used the output of only one meteorology model. In this study, we used several different meteorology models and simulation techniques to evaluate sensitivity of the transport model results to different meteorological simulations as well.

Another important aspect of this study is that we examined the sensitivity of the simulated deposition to the microphysical properties of Cs-carrying aerosols for the first time. Adachi et al. (2013) reported that in the early stage of the accident, the carrier aerosols of radioactive Cs were spherical, water-insoluble particles (hereafter, Cs-balls), and they predicted that the atmospheric behavior of these aerosols would be different from that of the submicron water-soluble particles described by Kaneyasu et al. (2012). Washout (or below-cloud scavenging) of aerosol particles (i.e., of both types described in this paragraph) is not usually efficient because of their small inertia and slow Brownian motion. In contrast, the submicron water-soluble particles are efficiently scavenged via rainout (or in-cloud scavenging) because the Kelvin (curvature) effect is enough small. Washout is probably the dominant scavenging process of water-insoluble aerosols, because very high supersaturation conditions are needed for rainout of water-insoluble aerosols to occur.

The purpose of this study was to assess the sensitivities described above in order to evaluate the uncertainties of the simulated deposition of ^{137}Cs caused by aerosol microphysical properties (i.e., aerosol size and hygroscopicity) and to compare it to the uncertainty caused by the use of different meteorological simulations.

G-3-3. NHM-Chem

NHM-Chem is a chemical transport model, offline- or online-coupled with Japan Meteorological Agency's non-hydrostatic model (JMA-NHM; Saito et al., 2007). NHM is a numerical weather prediction model of JMA. An Eulerian regional chemical transport model, Regional Air Quality Model 2 (RAQM2) (Kajino et al., 2012a), is used to simulate emission, transport, and deposition of trace gases and aerosols. RAQM2 implements a triple-moment modal aerosol microphysics module that assumes a log-normal size distribution of aerosol populations. This model describes the nature of aerosol dynamical processes, such as nucleation, condensation, coagulation, hygroscopic growth, dry deposition, grid-scale rainout (cloud condensation and ice nuclei activation and subsequent mixed-phase cloud microphysical processes) and washout (coagulation between aerosols and settling hydrometeors) processes, and sub-grid-scale convection and scavenging processes. In the study, the offline-coupled NHM-Chem was used in order to use different meteorological models alternatively, such as the Weather Research and Forecasting (WRF) model (Skamarock et al., 2008) to drive RAQM2.

G-3-4. Simulation settings

In this study, meteorology simulations were performed with NHM and WRF with two different cloud microphysics modules, Morrison et al. (2009) and Lim and Hong (2010), referred to as WRF-MORR and WRF-WDM6, respectively. The two WRF simulations were used so that the sensitivity to just the cloud microphysical process (grid-scale) could be assessed, because wet deposition of ^{137}Cs over Japan dominated over dry deposition in this study.

NHM, WRF, and RAQM2 shared the same domain, which consisted of 215 × 259 grid cells with a 3 km horizontal resolution; this model domain is slightly larger than the area shown in Fig. G-3-1. There were 50 vertical layers up to 50 hPa in NHM, 28 layers up to 100 hPa in WRF, and 20 layers up to 10 km in RAQM2. JMA Meso-Regional Objective Analysis data sets (3 hourly, 5 km × 5 km) were used for the initial and boundary conditions of NHM and WRF. The same analysis data sets were used for the spectral nudging in NHM and for the grid nudging in WRF.

The radionuclide transport version of NHM-Chem was developed for simulations of nuclear power plant accidents such as the FDNPP accident (Adachi et al., 2013; Sekiyama et al., 2015). This version of NHM-Chem uses an aerosol dynamics module that is simplified from that described by Kajino et al. (2012a) because aerosol hygroscopicity and the particle size distribution are assumed to be constant during transport. The nature of the aerosol dynamics such as dry deposition and grid-scale rainout/washout processes are thus described on the basis of the prescribed size distribution and hygroscopicity. Details of the dry and wet deposition processes are described by Kajino et al. (2012a; their sections 2.2.7 and 2.2.8). Even aerosols that are completely water-insoluble (i.e., hygroscopicity κ = 0) can act as cloud condensation nuclei under highly supersaturated conditions. Although water-insoluble aerosols can coagulate with cloud droplets within a cloud (this is also rainout process), for simplicity, in this study we did not consider rainout of Cs-balls and only washout in their wet deposition modeling. Sub-grid scale convection and scavenging processes were not considered. The fog deposition process of Katata et al., (2015) was considered.

We used the emission scenario for ^{137}Cs discharged from the FDNPP from Terada et al. (2012), and considered Cs-bearing aerosols to be of two types. Supermicron water-insoluble particles (Cs-balls) had a lognormal size distribution, number equivalent geometric mean dry diameter $D_{g,n,dry}$ = 2.3 μm, geometric standard deviation σ_g = 1.3, particle density ρ_p = 2.0 g/cm^3, and κ = 0 (Adachi et al., 2013), and submicron water-soluble particles (Kaneyasu et al., 2012) had a lognormal size distribution, $D_{g,n,dry}$ = 0.1 μm, σ_g = 1.6, ρ_p = 1.83 g/cm^3, and κ = 0.4.

For the sensitivity studies, taking into consideration the findings of Adachi et al. (2013), we allowed the proportion of early-stage emissions consisting of Cs-balls during the early stage to range from 10% to 90%, and the ending date of the early stage to range from 12 to 20 March 2011.

The analysis period was from 00:00 UTC on 11 March to 00:00 UTC on 1 April, with a spin-up period of 3 days. Thus, the entire simulation period was from 8 March to 1 April 2011.

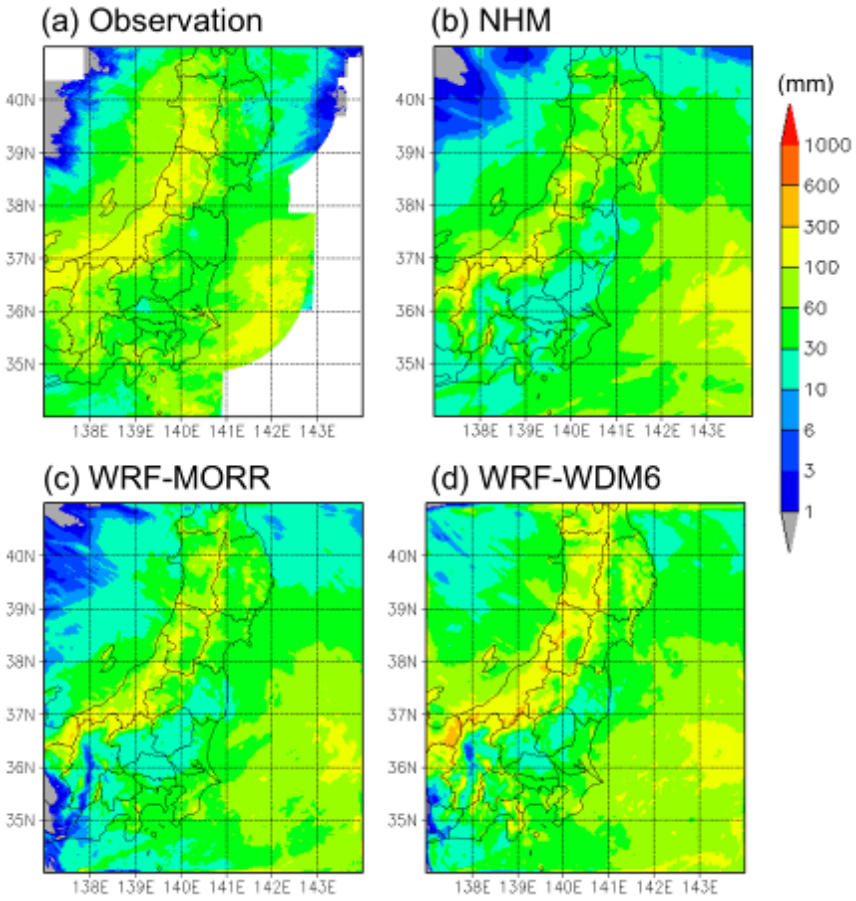

Fig. G-3-1. Cumulative precipitation (mm) from 11 March to 1 April: (a) Radar/rain gauge-analyzed precipitation (RAP) data and precipitation simulated by (b) NHM, (c) WRF-MORR, and (d) WRF-WDM6.

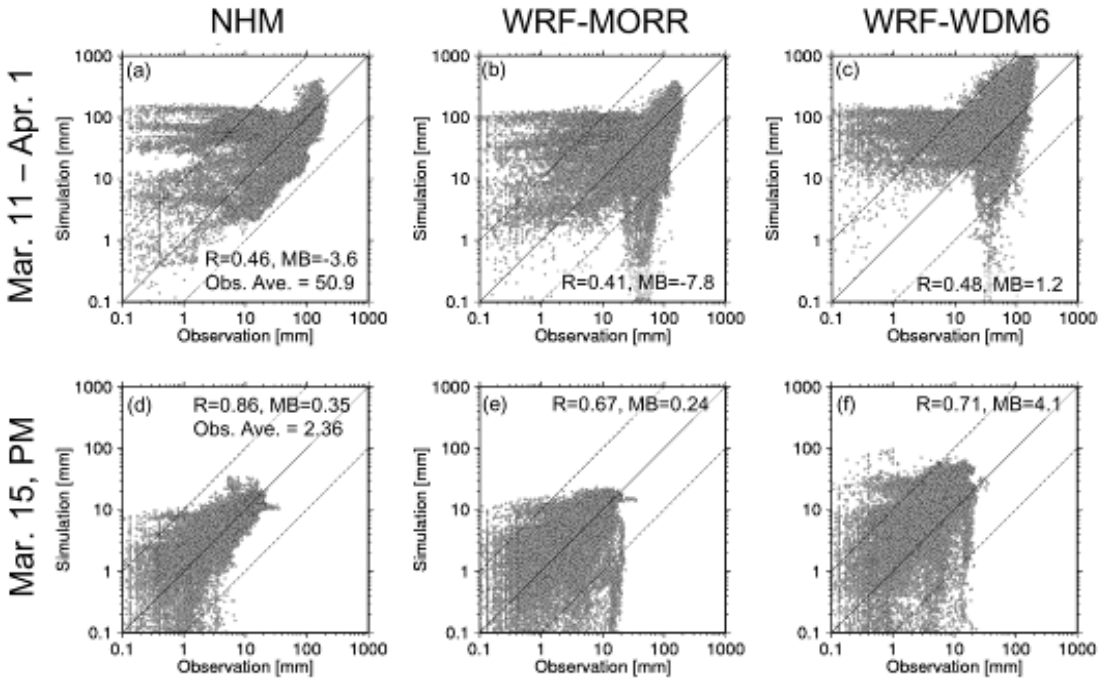

Fig. G-3-2. Scattergrams of simulated and observed (RAP) cumulative precipitation: (a–c) from 11 March to 1 April and (d–f) in the afternoon of 15 March. Simulations were by (a, d) NHM, (b, e) WRF-MORR, and (c, f) WRF-WDM6. The plotted data are for all grids for which both observation and simulation data were available. Although the data are plotted on a log-log scale, the statistics *R*, mean bias (MB), and the observation average (Obs. Ave.) were calculated on a linear-linear basis.

G-3-5. Results and discussion

We compared observed and simulated cumulative precipitation from 11 March to 1 April among the three meteorology models (Figs. G-3-1 and G-3-2). For observed data, we used JMA's radar/rain gauge-analyzed precipitation (RAP) data, which were interpolated to the 3 km resolution grid. We also compared observed and simulated cumulative precipitation on the afternoon of 15 March (Fig. G-3-2, lower panels), when substantial deposition occurred on land (e.g., Morino et al., 2013). All three simulations overestimated precipitation over the ocean by a factor of more than 10 (data points above the 10:1 simulation:observation line in Fig. G-3-2), and the two WRF simulations also underestimated precipitation in the southwestern part of the domain by a factor of more than 10 (data points below the 1:10 simulation:observation line in Fig G-3-2). Our focus was on land regions where the ^{137}Cs deposition was large (>10 kBq/m^2) (see Fig. G-3-3), and we did not expect the large discrepancies between the simulated and observed precipitation over the ocean to substantially affect the modeling of ^{137}Cs deposition in land areas.

The differences due to the different cloud microphysics modules were notable. The simulated precipitation spatial distribution patterns of the two WRFs were similar and different from the NHM pattern, whereas the precipitation amounts in WRF-MORR were fairly close to those in NHM, and those in WRF-WDM6 were much larger than the amounts in the other two simulations (Fig. G-3-2). WRF-WDM6 overestimated precipitation substantially over high-altitude regions (corresponding to locations where the simulated precipitation was >600 mm; Fig. G-3-1d). In the afternoon of 15 March, the overestimation of WRF-WDM6 was substantial; the mean bias (MB) was 4.1 mm and the observation average was 2.36 mm. Judging from the values of the correlation coefficient (R), the performance of NHM was best among the three meteorological simulations (R = 0.86, MB = 0.35 mm). The MB of WRF-MORR was smallest (MB = 0.24 mm), but owing to the square shape of the plotted data, R was 0.67.

Comparison of cumulative ^{137}Cs deposition amounts between aircraft observations (Torii et al., 2012) and simulations by NHM, WRF-MORR, and WRF-WDM6 (Fig. G-3-3), performed under the assumption that 100% of ^{137}Cs was carried by water soluble particles, showed that NHM simulated too much deposition in northern areas (Yamagata, Miyagi, and Iwate prefectures). This deposition was caused by rainout of ice phase precipitation (snow and graupel). For accurate simulation of rainout of ^{137}Cs, the vertical distribution of the ^{137}Cs and the hydrometeor mixing ratio must be accurately predicted. However, because no observations of the vertical profiles of ^{137}Cs are available for the time period of this study, the reason for this overestimation is impossible to identify.

WRF-MORR also simulated too much deposition in Yamagata and Miyagi prefectures, but WRF-WDM6 simulated less deposition in this area. The two WRF simulations reasonably reproduced depositions in the highest deposition areas (>1000 kBq/m^2), but depositions in those areas were underestimated by NHM. The two WRF simulations also reasonably reproduced the higher depositions in the mountainous regions of Tochigi and Gunma prefectures, but they overestimated depositions in the southern area (Tokyo, Kanagawa, Shizuoka, and Chiba prefectures). The NHM

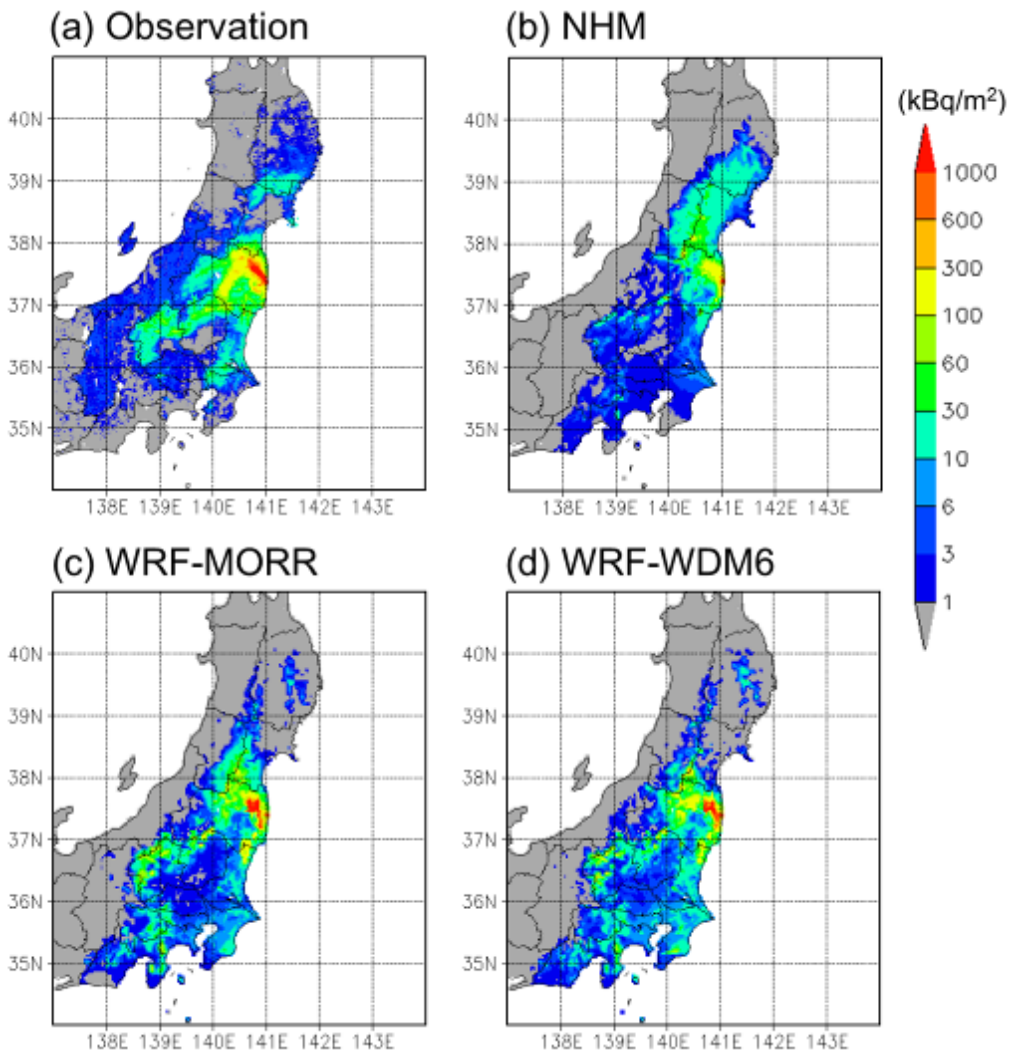

Fig. G-3-3. Cumulative ^{137}Cs deposition amounts (kBq/m^2) in (a) aircraft observations and (b) NHM, (c) WRF-MORR, and (d) WRF-WDM6 simulations. Simulated depositions are shown only for land areas to facilitate visual comparison with the observed deposition.

simulation underestimated deposition in all of these areas (i.e., in Tochigi and Gunma prefectures as well as in Tokyo, Kanagawa, Ibaraki, and Chiba prefectures). It is notable that, even though the transport model was the same, the simulated depositions varied substantially among the different meteorological simulations.

Figure G-3-4 shows depositions of water-soluble and water-insoluble particles simulated by using the three meteorological fields on both land and ocean areas. We compared the simulated depositions with aircraft observation data (Fig. G-3-3a) interpolated to the 3 km resolution grids of the models in Fig. G-3-5. Note that following Morino et al. (2013) and Katata et al. (2015), *R* and MB were calculated only when the observed values were larger than 10 kBq/m^2.

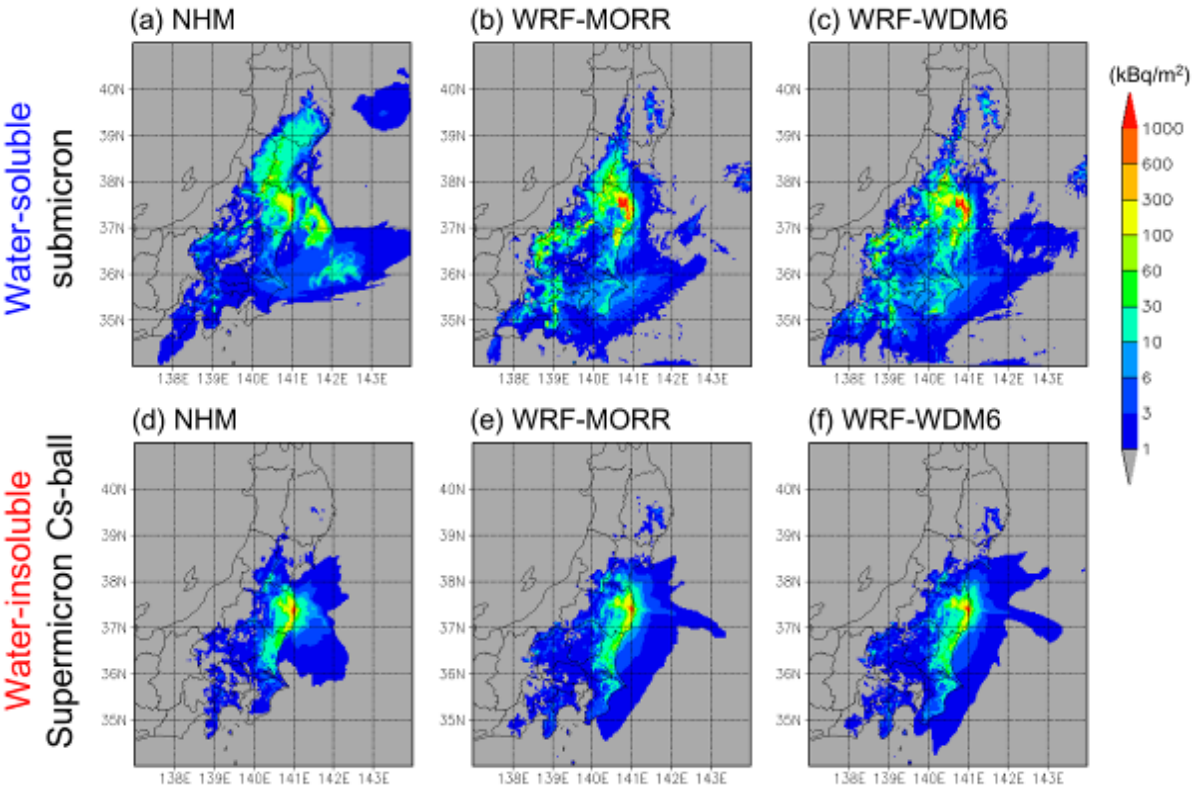

Fig. G-3-4. Cumulative depositions (kBq/m^2) simulated using the meteorological fields of (a, d) NHM, (b, e) WRF-MORR, and (c, f) WRF-WDM6 under the assumption that 100% of Cs was carried by (a–c) water soluble or (d–f) water insoluble particles.

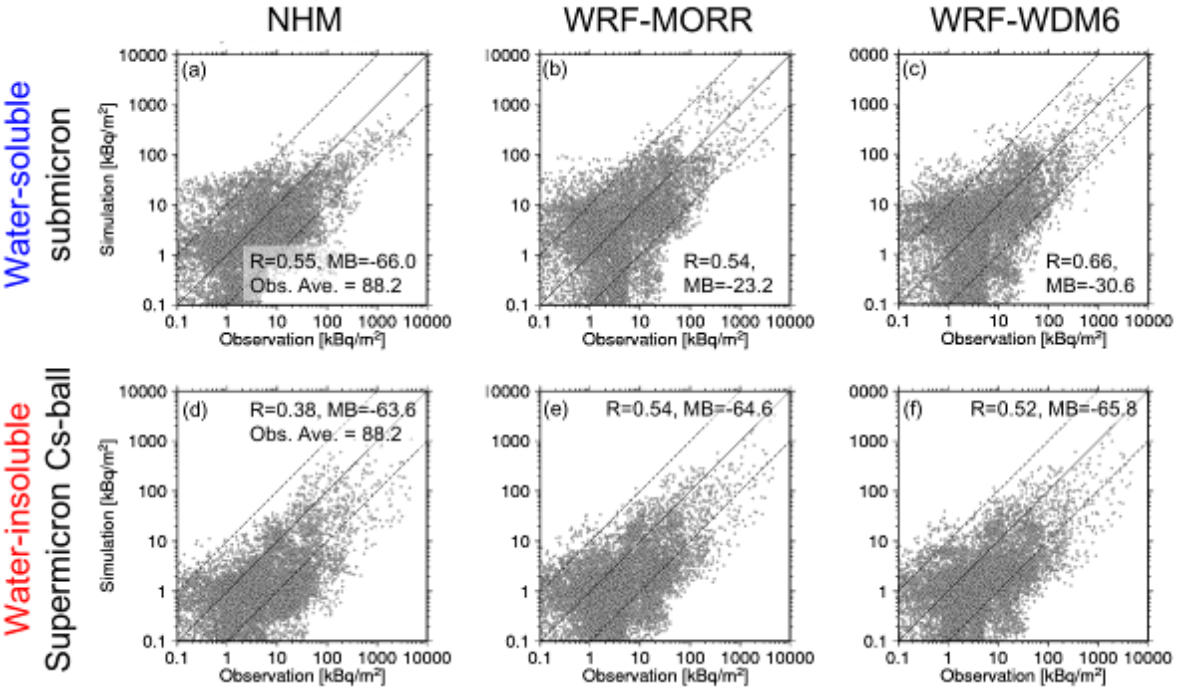

Fig. G-3-5. Scattergrams of cumulative deposition between the (a, d) NHM, (b, e) WRF-MORR, and (c, f) WRF-WDM6 simulations and aircraft observations. The simulations were performed under the assumption that 100% of Cs was carried by (a–c) water soluble or (d–f) water insoluble particles. Although the data are plotted on a log-log scale, the statistics *R* and mean bias (MB) were calculated on a linear-linear basis.

The simulated results were substantially different between Cs-bearing particles assumed to be 100% water soluble or water insoluble, because rainout of the Cs-balls was not considered to occur (compare upper and lower panels in Figs. G-3-4 and G-3-5), whereas the dry deposition velocity of Cs-balls was approximately four times that of the water-soluble submicron aerosols. It is interesting that although the simulation of precipitation by NHM/WRF-WDM6 was good/poor, the simulation of deposition by NHM/WRF-WDM6 was poor/good.

Adachi et al. (2013) detected Cs-balls only in samples collected during the early stage of the accident (14–15 March), but they reported that radioactive Cs was carried by water-soluble aerosols later (20–22 March). Kaneyasu et al. (2012), who analyzed samples collected from 28 April to May 12 and during 12–26 May (i.e., after the later sampling period of Adachi et al., 2013), also reported the radioactive Cs to be carried by water-soluble aerosols. Therefore, the assumption of 100% water-insoluble or water-soluble particles (Figs. G-3-4 and G-3-5) was not realistic; rather, reality must lie somewhere in between. Therefore, under the assumption that Cs-balls, as indicated by Adachi et al. (2013), were emitted only in the early stage of the accident, we used the following settings to test the sensitivity to aerosol microphysical properties:

1. We set the proportion of Cs-ball emissions to values from 10% to 90% during the early stage.
2. We started the early stage on 11 March but varied its ending date between 12 and 20 March 2011 (i.e., before the later sampling of Adachi et al., 2013).

We next compared cumulative depositions simulated using the meteorological fields calculated by NHM and the two WRF simulations between two extreme cases: 10% Cs-ball emission until 12 March and 90% Cs-ball emission until March 20 (Fig. G-3-6). The statistics (MB, root mean square error (RMSE) and *R*) of these comparisons are presented in Table G-3-1, together with the statistics for the three meteorological simulations when emissions were assumed to consist of 100% water-soluble submicron particles.

It is notable that even when the transport model settings and aerosol properties were the same, the fractional bias (MB divided by the observation average) ranged from 0.25 to 0.74, differing by approximately threefold, among the three different meteorological simulations. This difference is marked, because it means, for example, that the emission amount estimated by an inverse model from the deposition amount could vary threefold, depending on the meteorological model used. The ranges of MB, RMSE and *R* in the sensitivity to aerosol properties test results were smaller than their ranges in the sensitivity to meteorology test results (Table G-3-1), but the differences were similarly marked. The fractional bias range differed by approximately twofold between WRF-MORR and WRF-WDM6 (0.35–0.74 and 0.38–0.66, respectively). Therefore, the sensitivity of ^{137}Cs deposition to aerosol microphysical properties was as important as its sensitivity to the meteorological simulation used.

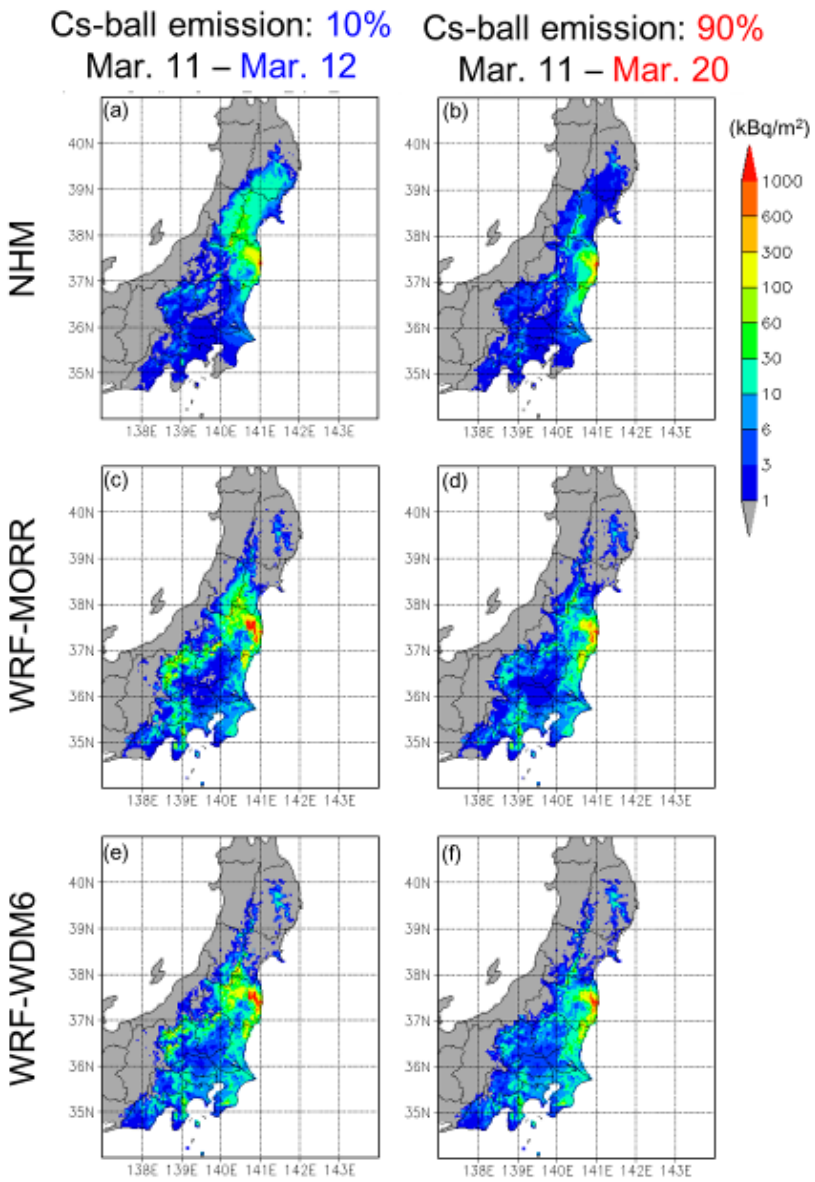

Fig. G-3-6. Simulated cumulative depositions (kBq/m^2) using the meteorological fields calculated by (a, b) NHM, (c, d) WRF-MORR, and (e, f) WRF-WDM6 between the two extreme aerosol microphysical assumptions: (a, c, e) 10% Cs-ball emission from 11 to 12 March and (b, d, f) 90% Cs-ball emission from 11 to 20 March.

Table G-3-1. Ranges of the statistics between observed and simulated cumulative depositions between the two extreme sensitivity tests (10% or 90% Cs-balls and 12 or 20 March as the ending date of the early stage) with each meteorological simulation (first to third row). The bottom row shows the same statistics among the meteorological simulations when no Cs-balls were assumed.

Sensitivity to	MB[1] (min:max) (kBq/m^2)	RMSE[1] (min:max) (kBq/m^2)	R[1] (min:max) (–)	Obs. Ave. (kBq/m^2)	Simulation settings		
					Meteorological simulation	Cs-ball fraction	Ending date of early stage
Aerosol properties	−68.5 : −65.5	274.3 : 295.0	0.39 : 0.55	88.2	NHM	10–90%	Mar.12 – 20
Aerosol properties	−57.2 : −22.8	251.1 : 272.5	0.53 : 0.59	88.2	WRF–MORR	10–90%	Mar.12 – 20
Aerosol properties	−54.6 : −30.2	225.9 : 244.2	0.65 : 0.70	88.2	WRF–WDM6	10–90%	Mar.12 – 20
Meteorology simulations	−66.0 : −23.2	233.0 : 274.9	0.54 : 0.66	88.2	NHM, WRF–MORR, WDM6	0%	–

[1] linear–linear statistics

G-3-6. Summary

We simulated the emission, transport, and deposition of ^{137}Cs released due to the FDNPP accident. The sensitivity of the simulated depositions of radioactive Cs to the size and hygroscopicity of the carrier aerosols was assessed and compared with the sensitivity to the meteorological simulation.

Two types of Cs-bearing aerosols, water-insoluble supermicron particles (Cs-balls) and water-soluble submicron particles were considered in the simulation. The simulated depositions of the two aerosols were significantly different because rainout was not considered to occur with Cs-balls, and the dry deposition velocities of Cs-balls were approximately four times those of the water-soluble particles.

Even when the transport model was used with exactly the same settings, the simulated depositions were very different among the different meteorological simulations: The fractional bias (MB divided by observation average) ranged from 0.25 to 0.74, an approximately threefold difference. The sensitivity of ^{137}Cs deposition to particle size and hygroscopicity (determined by adjusting the proportion of water-insoluble Cs emission between 10% and 90% and the ending date of the early stage between 12 and 20 March 2011) was smaller but just as important as the sensitivity to the meteorological simulation (in which 100% of Cs was assumed to be water soluble, as in previous studies). To better understand the environmental behavior of radioactive Cs discharged from the FDNPP, knowledge of the aerosol microphysical properties is as important as the accuracy of the meteorological simulations and emission scenarios.

In future work, several new wet deposition modules and emission scenarios, together with new meteorological simulations (for example, NHM-LETKF as in Sekiyama et al., 2015), will be added to the current sensitivity analysis study to provide a more robust uncertainty estimation of the numerical simulation techniques. It would also be interesting to estimate the sensitivity to the modeling approach (Lagrangian or Eulerian), because the both approaches have been used in FDNPP accident simulation studies.

G-4. NHM-Chem-LETKF[1]

G-4-1. Introduction

Generally, it is difficult to tell how high a model's resolution needs to be to simulate the atmospheric transport and deposition of radionuclides. Japan has a complex topography, and Fukushima is well known as a mountainous region. Although the Fukushima Daiichi Nuclear Power Plant (FDNPP) is located on the Pacific Ocean coastal plain, the Abukuma Mountains (up to 1000 m in elevation) are located just behind the FDNPP. Beyond the Abukuma range, Fukushima City is located in a long narrow basin, called the Naka-dori Valley, about 70 km from the FDNPP, and Mt. Azuma, a 2000-m peak, rises just behind the city. This topography is well depicted by a grid with a 500-m horizontal resolution (Fig. G-4-1c). In contrast, it is difficult to recognize these features on a grid with a 15-km horizontal resolution (Fig. G-4-1a). Most regional models used to simulate radiation from the Fukushima nuclear accident have used a 3-km horizontal resolution (Fig. G-4-1b) (e.g., Chino et al., 2011; Sugiyama et al., 2012; Morino et al., 2013; Adachi et al., 2013; Hu et al., 2014), but it is not clear that a horizontal resolution of 3 km allows the advection and deposition of radionuclides from the FDNPP accident to be properly reproduced. Furthermore, global simulation models of the FDNPP accident (e.g., Yasunari et al., 2011; Takemura et al., 2011; Schöppner et al., 2011; Stohl et al., 2012) commonly have had horizontal resolutions much lower than 15 km, too low to depict Fukushima's complex topography in detail.

In this study, we investigated whether models using a 3-km grid (the typical regional model resolution) or a 15-km grid (representative of the global model resolution) are suitable for simulating the radioactive pollution from the FDNPP accident by comparing simulation results obtained with such models with those obtained with a very high resolution model (500-m grid). We performed tests with both Eulerian and Lagrangian chemistry transport models, but both models were driven by the same meteorological analyses. However, we encountered difficulties in obtaining meteorological analyses with an arbitrary horizontal resolution; an interpolated, extrapolated, or nudged meteorological analysis is likely to be a mixture of different resolution analyses. Therefore, we conducted our own data assimilation to obtain analysis data with an arbitrary resolution, independent of any model or analysis with another resolution.

[1] T. T. Sekiyama and M. Kunii

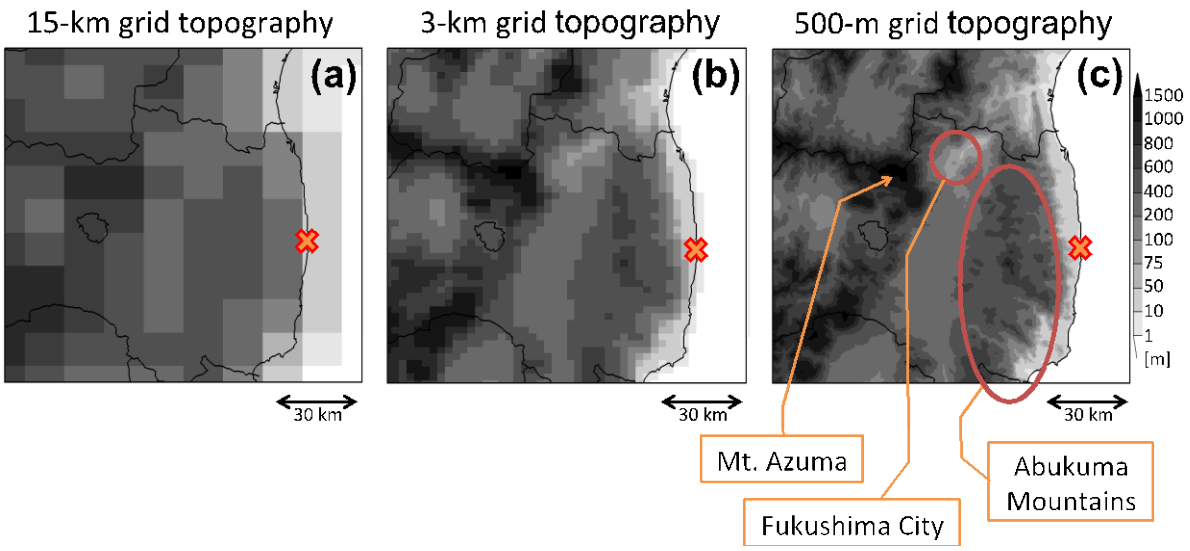

Fig. G-4-1. Fukushima topography depicted at three different scales: (a) 15-km grid, (b) 3-km grid, and (c) 500-m grid. The cross mark indicates the location of FDNPP. The Abukuma Mountains are up to about 1000 m high, and Fukushima City is located in a narrow basin 70 m above sea level (asl). The highest of the several peaks of Mt. Azuma is 2035 m asl.

G-4-2. Model Description

Before performing the radionuclide transport calculations, we prepared meteorological analyses with three different horizontal resolutions by using a flow-dependent data assimilation system assembled and validated by Kunii (2013). This data assimilation system consists of the Japan Meteorological Agency's nonhydrostatic model (JMA-NHM; Saito et al., 2006, 2007) and a local ensemble transform Kalman filter (LETKF; Hunt et al., 2007) called NHM-LETKF. The system calculated all of the necessary meteorological variables, which were stored after every 10 minutes of simulation time and used subsequently to drive the radionuclide transport models. In this study, the horizontal resolutions were set to 15 km, 3 km, and 500 m. A one-way nested data assimilation scheme was implemented, in which the first guess of a lower resolution model was used for the boundary conditions for the integration with a finer resolution model (cf. Kunii, 2013). Each nested inner model ran independently of the outer coarse-resolution model except for the boundary conditions. Operationally, JMA-NHM is initialized by the JMA non-hydrostatic model four-dimensional variational data assimilation system (JNoVA, Honda et al., 2005; see also section C-8). Most regional simulation models used in Japan and some models used by the World Meteorological Organization Task team for the FDNPP accident use JNoVA grid-point-value (GPV) data as initial/boundary conditions or pseudo-observations (e.g., Chino et al., 2011; Morino et al., 2013; Adachi et al., 2013; Draxler et al., 2013a; Saito et al., 2015). In contrast, we calculated our meteorological analyses using our own data assimilation system (NHM-LETKF) instead of JNoVA GPV data.

The 15-km-grid analysis was calculated by the outermost NHM-LETKF; its domain covered East Asia and it consisted of 20 ensemble members. The initial and boundary conditions of the NHM-LETKF cycle were obtained from the JMA operational global prediction system. The covariance localization parameters were set to 150 km in the horizontal, 0.2 natural-logarithmic

pressure-coordinate in the vertical, and 3 hours in time. As observation data for assimilation, we used JMA's operational dataset, which is integrated and quality-controlled for JNoVA mesoscale weather prediction, as described by Kunii (2013). The JNoVA dataset contains observations acquired by radiosondes, weather observatories, pilot balloons, wind profilers, aircraft, ships, buoys, and satellites, but satellite radiances and radar precipitation analyses were not assimilated in this study. Instead, we assimilated additional surface wind observations acquired by JMA's Automated Meteorological Data Acquisition System (AMeDAS) and Tokyo Electric Power Company's (TEPCO) monitoring posts. The TEPCO monitoring posts are located at FDNPP and at Fukushima Dai-ni Nuclear Power Plant, which is 12 km south of FDNPP.

The 3-km-grid analysis was calculated by the first nested NHM-LETKF, the domain of which covered eastern Japan. The lateral boundary conditions were supplied by the output of the outer (15-km-grid) NHM-LETKF cycle. This NHM-LETKF was implemented with almost the same configuration of JMA-NHM as the 15-km simulation, but the convective parameterization scheme was not activated. We used the same observation data (i.e., JNoVA, AMeDAS, and TEPCO datasets) as in the 15-km data assimilation. Next, the 500-m grid analysis was calculated by the second nested NHM-LETKF, the domain of which domain mostly covered most of Fukushima Prefecture. The lateral boundary conditions were supplied from the outputs of the 3-km NHM-LETKF cycle. Basically, The same configuration of the 500-m-grid JMA-NHM s were was basically implemented the same in the 500-m grid spacing JMA-NHM as that of the 3-km simulation. Again, the same observation data were assimilated during the second nested NHM-LETKF cycle.

We conducted Eulerian simulations with NHM-Chem. NHM-Chem is a meteorology model (JMA-NHM; Saito et al., 2007) coupled offline with a chemical transport model (Regional Air Quality Model 2; RAQM2) that was developed by Kajino et al. (2012a). The details of RAQM2 are described in Chapter G-3. The meteorological analyses were taken into RAQM2 every 10 minutes and linearly interpolated within that 10 minute interval. RAQM2 and NHM-LETKF shared the same model domains and horizontal grid resolutions, but their vertical resolutions were converted from NHM-LETKF's original number of layers to RAQM2's 20 layers. The combined system is called NHM-Chem-LETKF. We used the ^{137}Cs emission scenario from FDNPP estimated by the Japan Atomic Energy Agency (JAEA) (cf. Chino et al., 2011). For comparison, we also conducted Lagrangian simulations using the JMA operational Regional Atmospheric Transport Model (JMA-RATM), which was developed by Shimbori et al. (2009, 2010). The details of JMA-RATM are described in Chapter E. The meteorological analyses were taken into JMA-RATM every 1 hour. After the model calculations, the hourly concentration and deposition outputs were multiplied by the JAEA hourly ^{137}Cs emission rate.

G-4-3. Results and discussion

We focus here on the simulation of ^{137}Cs on 15 March 2011 (UTC) because we were interested in the radioactive plumes that moved landward. The standard experiment with the JAEA emission scenario performed by Morino et al. (2013) showed that most of the ^{137}Cs deposition on land (mainly in Fukushima Prefecture) occurred from 15 to 16 March (Japanese Standard Time; JST). This period accounted for 72% of the total amount deposited on land from 10 March to 20 April 2011. We found large differences among the analyses in the horizontal winds in the planetary boundary layer (PBL) (Fig. G-4-2). The 15-km analysis (Fig. G-4-2a) did not represent the northerly winds along the Naka-dori Valley around Fukushima City because the 15-km-grid model could not represent the Abukuma Mountains or the Naka-dori Valley. In the 3-km (Fig. G-4-2b) and 500-m (Fig. G-4-2c) analyses, the wind fields were roughly the same, but only the 500-m analysis reproduced the fine wind structure over the mountains and valleys.

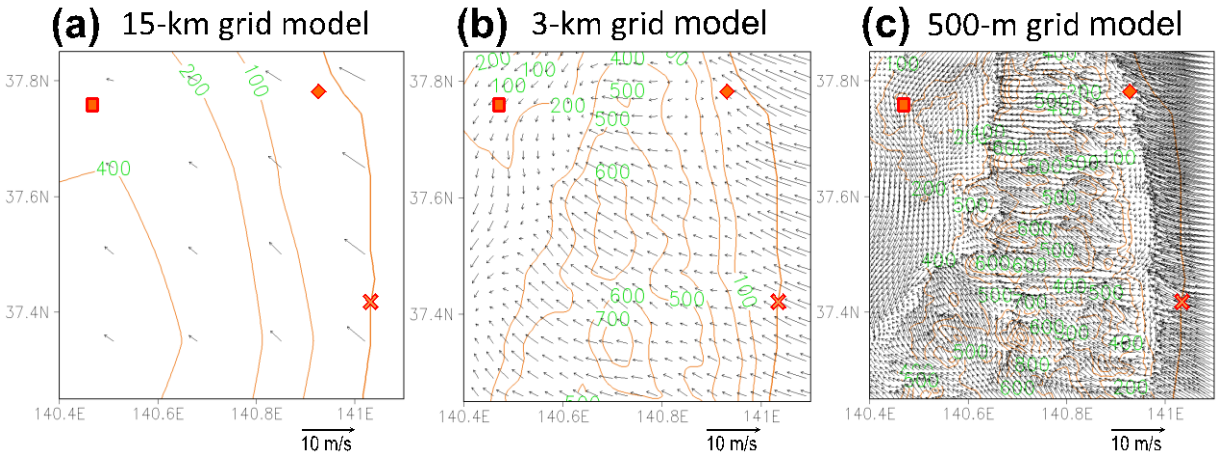

Fig. G-4-2. Lowest model level (20 m above ground level) wind direction and speed (10-minute mean) in the northern Abukuma Mountain area, Fukushima Prefecture, at 15:00 UTC on 15 March 2011, simulated by (a) the 15-km-grid JMA-NHM, (b) the 3-km-grid JMA-NHM, and (c) the 500-m-grid JMA-NHM. The cross mark indicates the location of FDNPP, the diamond indicates the location of the AMeDAS Souma observatory, and the square indicates the location of the AMeDAS Fukushima City observatory.

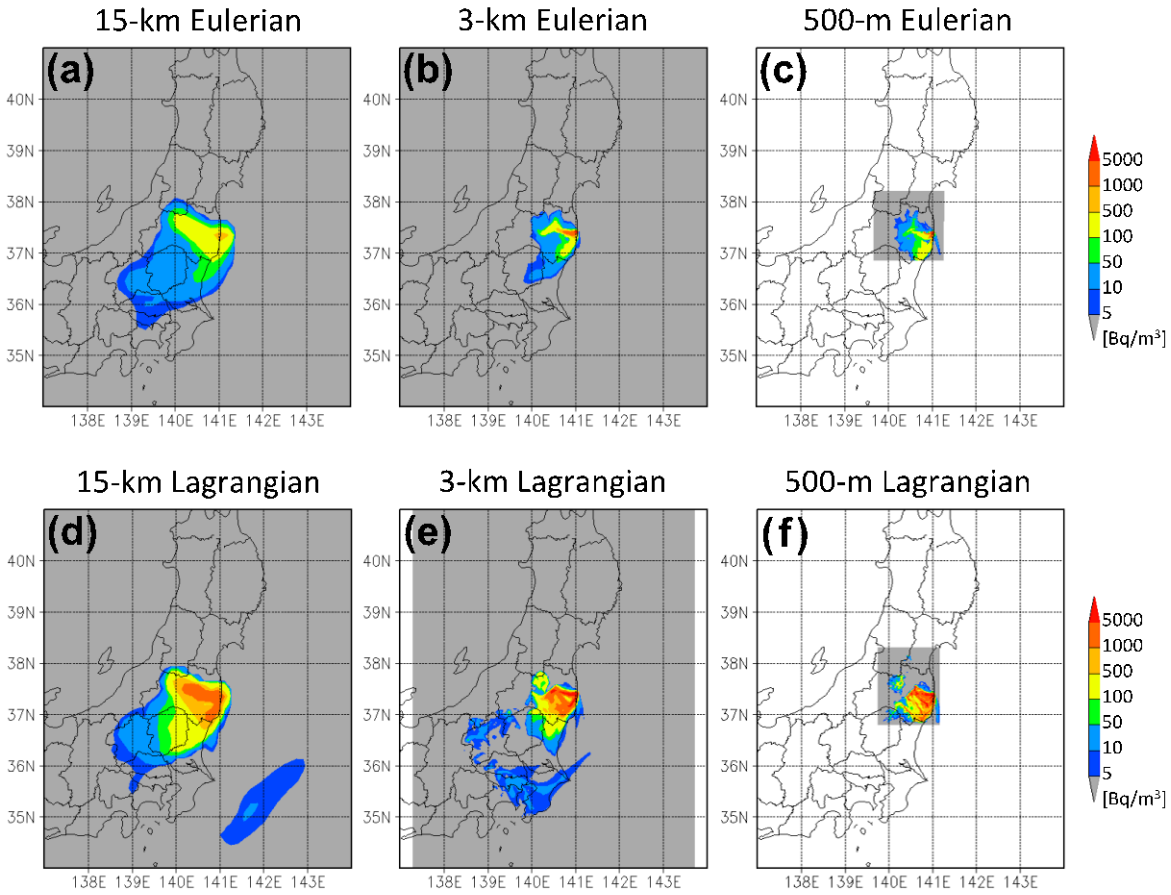

Fig. G-4-3. Surface ^{137}Cs concentrations averaged from 00:00 UTC on 15 March to 00:00 UTC on 16 March 2011 as simulated by the Eulerian model (RAQM2) using the (a) 15-km, (b) 3-km, and (c) 500-m meteorological analysis, and by the Lagrangian model (JMA-RATM) using (d) 15-km, (e) 3-km, and (f) 500-m meteorological analysis.

According to the TEPCO monitoring post data, the wind in the vicinity of FDNPP gradually changed in a clockwise direction from northerly to southeasterly between 06:00 JST (21:00 UTC the day before) and 12:00 JST (03:00 UTC) on 15 March 2011. The wind continued southeasterly for more than 10 hours, blowing inland from the coastal FDNPP site. During that time, the radioactive plume would have been carried across Fukushima and neighboring prefectures. In the Eulerian simulation results, the ^{137}Cs distributions showed good agreement between the 3-km (Fig. G-4-3b) and 500-m (Fig. G-4-3c) simulations. The ^{137}Cs plume crossed over the Abukuma Mountains but was mostly blocked by Mt. Azuma and other mountains west of the Naka-dori Valley. However, the 15-km Eulerian simulation (Fig. G-4-3a) could not represent this blockage of the ^{137}Cs plume, which spread broadly through the Naka-dori Valley as far as Yamagata Prefecture in this simulation. Thus, as expected from the PBL wind errors, the behavior of the plume in the 15-km simulation was unnatural. The results of the Lagrangian simulations were similar. The behavior of the plume in the Lagrangian 15-km simulation (Fig. G-4-3d) was completely different from that in the 3-km (Fig. G-4-3e) and 500-m (Fig. G-4-3f) Lagrangian simulations. Similar to the Eulerian simulations, the 3-km and 500-m grid Lagrangian simulations showed good agreement, and both successfully reproduced the blockage of the ^{137}Cs plume along the Naka-dori Valley. In addition, the 15-km Lagrangian (Fig. G-4-3d) and

Eulerian (Fig. G-4-3a) simulations showed very similar ^{137}Cs distributions, although the simulated concentrations were quantitatively different.

In both the 15-km transport model results (Fig. G-4-4a and G-4-4d) for the total one-day accumulated deposition of ^{137}Cs on 15 March 2011 UTC, a highly polluted area extended broadly beyond Mt. Azuma and other mountains, across the Naka-dori Valley, and as far as Yamagata and Niigata prefectures. This distribution is similar to the surface concentration distribution (Fig. G-4-3a and G-4-3d). In addition, the most polluted area was not located near FDNPP but in the vicinity of the inland border between Fukushima and Yamagata prefectures. This unrealistic distribution was caused by wet deposition of the ^{137}Cs-137 plume after it passed the mountains beyond the Naka-dori Valley and extended into a heavy precipitation area. Such hot-spot pollution was not detected by the JAEA aerial observations. In contrast, both the 3-km (Fig. G-4-4b and G-4-4e) and 500-m (Fig. G-4-4c and G-4-4f) models showed that the heavily polluted area was mostly limited to eastern Fukushima Prefecture near FDNPP, consistent with the JAEA aerial observations.

G-4-4. Conclusion

A large difference was found in the PBL wind field between the 15-km resolution meteorological analysis and the analyses with 3 km and 500 m resolutions. The 15-km analysis could not reproduce Fukushima's mountainous topography in detail. Consequently, it failed to depict the complex wind structure over mountains and valleys. This error in the wind field caused large differences in the radionuclide transport and deposition simulation. In the real world, the ^{137}Cs plume from FDNPP, after crossing over the Abukuma Mountains, was apparently mostly blocked by Mt. Azuma and other mountains along the Naka-dori Valley. However, the 15-km grid simulations could not represent this blockage of the plume, which spread out unnaturally across the Naka-dori Valley. In contrast, the 3-km and 500-m simulations successfully reproduced the ^{137}Cs plume blockage along the Naka-dori Valley, and the two simulations produced highly similar distributions of ^{137}Cs surface concentrations and deposition. The behaviors simulated by the Eulerian and Lagrangian models were the same qualitatively, but the two models yielded quantitatively different results even when they were driven by the same meteorological analysis. More detailed information about these simulations is available in Sekiyama et al. (2015).

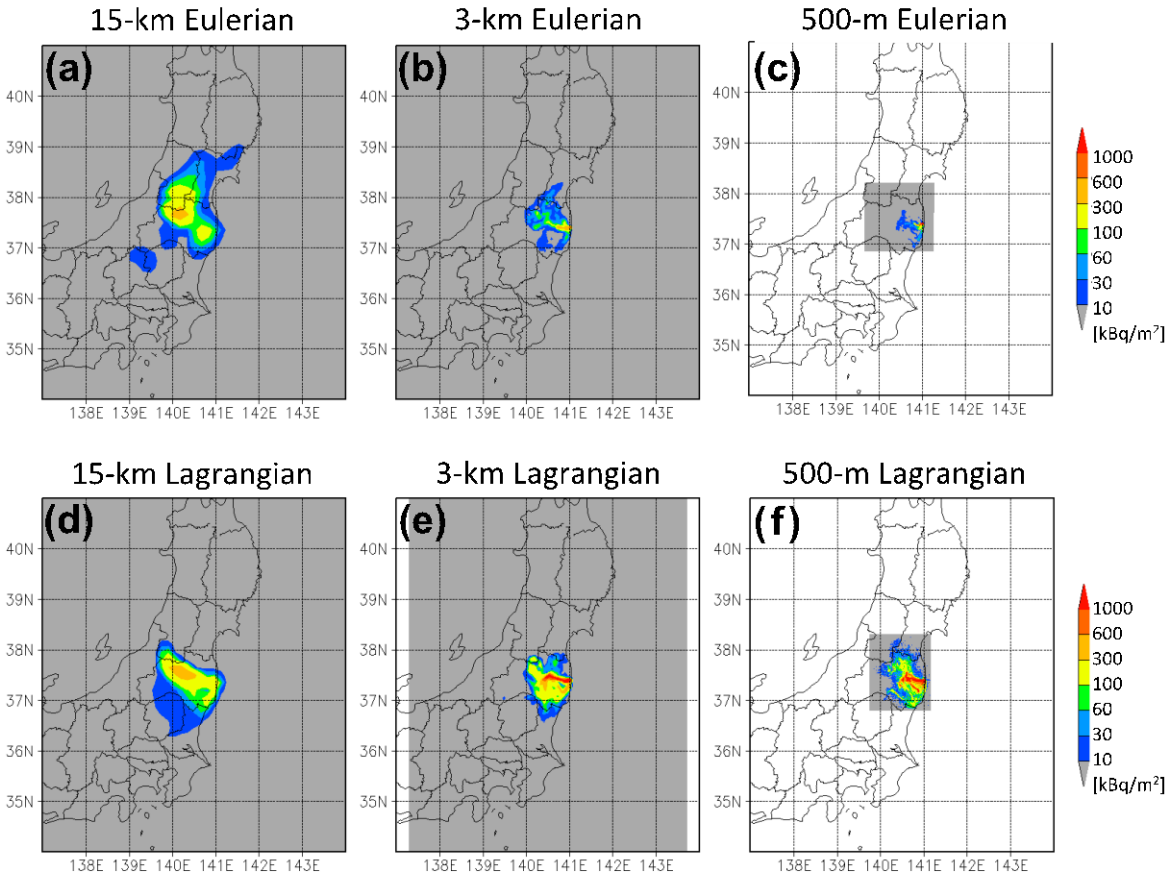

Fig. G-4-4. Total deposition of Cs-137 accumulated from 00:00 UTC 15 March to 00:00 UTC 16 March 2011 simulated by the Eulerian model RAQM2 with (a) 15-km grid meteorological analysis, (b) 3-km grid meteorological analysis, and (c) 500-m grid analysis. The same as simulated by the RAQM2, but simulated by the Lagrangian model JMA-RATM with (d) 15-km grid analysis, (e) 3-km grid analysis, and (f) 500-m grid analysis.

G-5. Emission source estimation by an inverse model[1]

G-5-1. Introduction

Results of tracer transport simulations of radionuclides vary substantially depending on the source term conditions. Although more than four years have passed since the accident at the Fukushima Dai-ichi Nuclear Power Plant (FDNPP), robust source term estimates have still not been obtained.

Chino et al. (2011) and Terada et al. (2012) used a reverse method in which they compared radionuclide observational data with regional tracer transport model (SPEEDI) simulation results to obtain emission time series of ^{137}Cs and ^{131}I. Chino et al. (2011) reported a preliminary estimate for the ^{137}Cs total emission amount from the FDNPP from 11 March to 6 April 2011 of 13.0 PBq and suggested that the maximum emissions occurred on 14 and 15 March. They also reported that large emission events occurred on 21–22 and 30–31 March. The Japan Atomic Energy Agency (JAEA) revised this estimate of the total release amount of ^{137}Cs for the period from 11 March to 19 April to 8.8 PBq (Terada et al., 2012). An important limitation of these analyses was that only data from Japanese land observation sites were used; therefore, they could not constrain radionuclide plumes transported over the Pacific Ocean.

Stohl et al. (2012) carried out a Bayesian synthesis inversion in which the results of a tagged global tracer transport model (FLEXPART) were used with observation data obtained mainly by the global radionuclide monitoring network operated by the preparatory commission for the Comprehensive Nuclear Test Ban Treaty Organization (CTBTO). They estimated the total ^{137}Cs emission amount from 11 March to 20 April to be 36.6 PBq, which is larger than the estimate reported by Terada et al. (2012) by a factor of 4. Their analysis included assessments of the radionuclide plumes that were transported over the Pacific Ocean because they used observation data from a wide area of the Northern Hemisphere and a global transport model. However, Stohl et al. (2012) used a Lagrangian transport model, which simulated the transport, diffusion, and deposition of large numbers of tracer particles released at the accident site. Although Lagrangian models are able to precisely calculate transport processes, they cannot estimate diffusion processes, such as turbulent, cumulus, and planetary boundary layer diffusion, or deposition processes (wet or dry) in detail, even though diffusion and deposition are the most important processes affecting the long-range transport of aerosol tracers. As a result, diffusion and deposition amounts might be affected.

In this section, we present a new estimate of the ^{137}Cs source term obtained by a Bayesian synthesis inversion method that coupled global observation network data with a global semi-Lagrangian aerosol transport model.

G-5-2. Analysis Method

The analysis method used tagged simulation results from the global semi-Lagrangian aerosol model MASINGAR (Tanaka and Chiba, 2005) with a TL319 horizontal resolution (approximately 60 km). Tagged tracers (^{137}Cs) from the lowest model layer (surface to 50 m) were released every 3 hours at a

[1] T. Maki

rate of 1 Tg/h. It was assumed that the released ^{137}Cs was attached to hydrophilic aerosols with an effective radius of 0.7 μm and was removed by dry and wet deposition. One of the merits of a tagged tracer simulation is that once ^{137}Cs source term emission time series are obtained, the ^{137}Cs atmospheric concentrations and depositions can be determined simply by calculating the linear combination of the source term estimations and the tagged tracer simulation results, without re-calculation of the aerosol model. As a result, we could construct a near-real-time prediction system by combining a properly distributed observation network and the operational tagged tracer transport model system (an emission prediction scenario is required when using such a system operationally). We used daily mean observation data of 51 global sites (CTBTO, Hoffmann et al., 2000; RING OF FIVE, Masson et al., 2011; University of California, Smith et al., 2014; Academia Sinica, Hsu et al., 2012; and Meteorological Research Institute, Igarashi et al., 2009) (Fig,. G-5-1) and an analysis period of 40 days, from 11 March to 19 April. We tested two prior emission estimates. The first prior estimate was the JAEA posterior emission (Terada et al., 2012). For the second, we used the Norwegian Institute for Air Research prior emission (not posterior; Stohl et al., 2012) because our observational data were similar to theirs. The observational error, which included the spatial representation error, was set to 20%. The prior flux uncertainty is treated as a tuning parameter which shows the ratio between the observation and prior flux uncertainty, and several sensitivity tests were conducted by changing the prior emission flux uncertainties from 10% to 5000%.

G-5-3. Results and discussion

We selected the source term estimate of Stohl et al. (2012) as our prior emission estimate by comparing the mismatch between the observation data and the estimated concentrations. On the basis of the sensitivity test results, we set the prior flux uncertainty to 100%. The total ^{137}Cs emission amount from the FDNPP for the period from 11 March to 19 April was 19.4 PBq, and the estimated uncertainty was 3.0 PBq. In the present inverse analysis, the emission height level had only a small effect on the estimated time series of the source term. The maximum ^{137}Cs emission, which occurred on 15 March, was larger than the prior estimate emission estimate. Our results suggest that emission events occurred during 18–22 March and 28–30 March (Fig. G-5-2); however, the emission amount during 28–30 March was smaller than the estimates of Chino et al. (2011) and Terada et al. (2012).

In our analysis, which used tagged tracer simulation results, global observation data, and an inverse model, we obtained a total flux that was intermediate between the fluxes estimated by Stohl et al. (2012) and Terada et al. (2012) and consistent with other analysis results (Table G-5-1). We evaluated the atmospheric ^{137}Cs concentrations and deposition amounts by combining our estimate of total flux with the tagged simulation results.

However, to evaluate the results of our analysis several issues need to be addressed. One of the most important is that we used only one model, and the bias of the model transport could directly affect the estimated source term. For robust source term estimation, we should compile tagged model simulation results obtained with multiple models using the same experimental settings and compare their estimated

source terms. Another issue is the relatively coarse horizontal resolution of the model. To obtain a finer horizontal and temporal resolution, we should use a regional chemical transport model and collect hourly observation data. In addition, the available observation data for the Pacific Ocean are insufficient; therefore, to improve the analysis we should make use of marine deposition observation data.

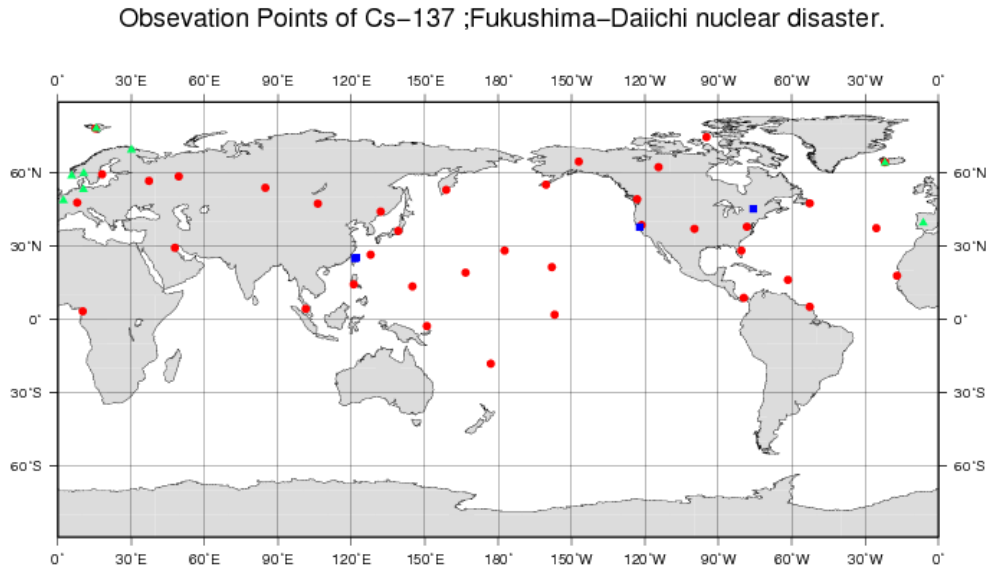

Fig. G-5-1. Locations of the observation data collection sites used in this study. Red, green, and blue circles show CTBTO, RING OF FIVE, and other observation sites, respectively.

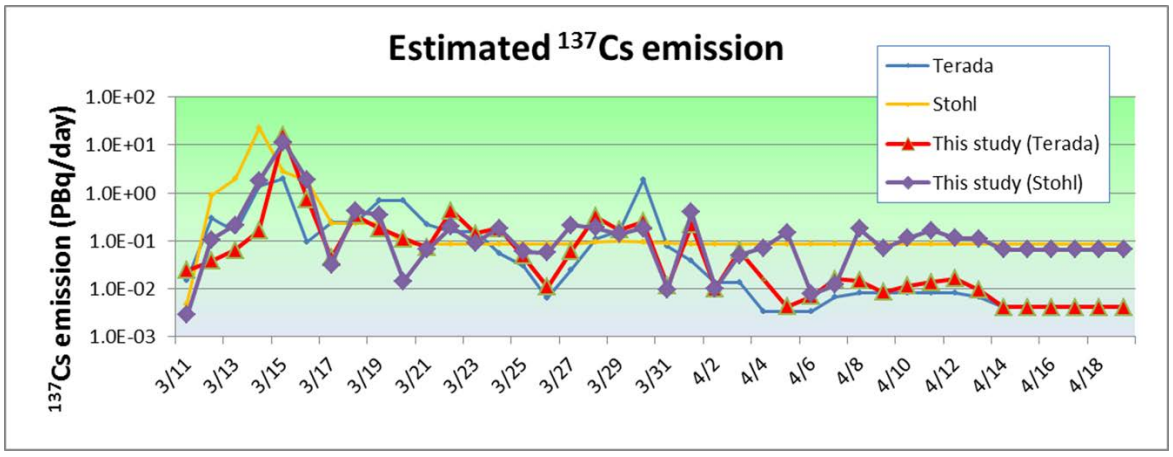

Fig. G-5-2. Estimated time series of ^{137}Cs emission from the FDNPP. The blue and orange lines show the source term time series obtained by Terada et al. (2012) and Stohl et al. (2012), respectively. The thick red and thick purple lines show the inversed posterior ^{137}Cs emission time series obtained by using emissions data of Terada and Stohl, respectively, as our prior emission estimate.

Table G-5-1. Recent ^{137}Cs source term estimations for the FDNPP accident.

Author	Total Flux	Remarks
This study	19.4 PBq (±3.0 PBq)	(11 March–19 April)
JAEA (Terada et al., 2012)	8.8 PBq	(10 March–19 April)
Stohl et al. (2012)	36.6 PBq (207–537)	(10 March–20 April)
Winiarek et al. (2014)	10–15 PBq	(11 March–26 March)
MEXT (2011d) and Chino et al. (2011)	14–17 PBq	From obs. and numerical model analysis
MELCOR analysis (Gauntt et al. (2001))	16 PBq	From Stohl et al. (2012)
IRSN (Institut de radioprotection et de sûreté nucléaire)	30 PBq	From Stohl et al. (2012)
ZAMG (Zentralanstalt für Meteorologie und Geodynamik)	67 PBq	From Stohl et al. (2012)

G-6. Science Council of Japan atmospheric transport model intercomparison[1]

G-6-1. Introduction

In this section, we describe the model intercomparison project of the Science Council of Japan (SCJ) and the contributions of the Meteorological Research Institute (MRI) to the intercomparison. SCJ launched a working group for model intercomparison under the Subcommittee of Investigation on the Environmental Contamination Caused by the Nuclear Accident in the Sectional Committee on Nuclear Accident, Committee on Comprehensive Synthetic Engineering, in July 2012. The objective of the SCJ working group was to assess the uncertainties in the results of experiments simulating the transport of radioactive materials from the Fukushima Daiichi Nuclear Power Plant accident by comparing existing model results.

The chair of the working group, Prof. Teruyuki Nakajima of the University of Tokyo, invited individuals from several research institutions and universities who had conducted research on the transport of radionuclides to be members. In October 2012, the working group issued a call for participation in the SCJ intercomparison, including to the World Meteorological Organization (WMO) Task Team. The members of the Task Team discussed the matter and decided that the Task Team would not participate as a whole team, but that the decision as to whether to participate would be left to individual members. Following this decision, the Japan Meteorological Agency (JMA) chose to participate; thus, JMA's Task Team and researchers in MRI participated in the SCJ intercomparison.

G-6-2. Brief description of the model intercomparison

The SCJ model intercomparison consisted of four parts: regional atmospheric transport, global-scale atmospheric transport, oceanic transport of radionuclides, and emission source estimation by inversion methods. The contributing groups were asked to provide their best simulation results as of spring 2013. Because the objective of the intercomparison was to evaluate the characteristics and accuracies of the currently available simulated results, uniform conditions were not imposed. Therefore, there were large differences in model setup (e.g., grid resolution and integration time interval) and the data (meteorological field data and emission scenarios) used to constrain each simulation. However, this no-constraint policy made it difficult to investigate the causes of the differences in the simulation results.

In total, 9 regional atmospheric models, 6 global atmospheric models, and 11 oceanic models were included in the SCJ model intercomparison. In this section, the contributions of JMA to the intercomparison of regional and global-scale atmospheric transport models are presented. JMA also contributed to the SCJ intercomparison by using an inverse model to estimate the emission flux by an inversion method; these results are described in section G-5 of this technical report.

[1] T.Y. Tanaka

G-6-3. Regional atmospheric transport model intercomparison

For the regional atmospheric transport intercomparison, nine contributing groups provided nine sets of simulated results (Takigawa et al., 2013). The contributing groups were the Centre d'Enseignement et de Recherche en Environnement Atmosphérique (Winiarek et al., 2014), the Central Research Institute of Electric Power Industry (Hayami et al., 2012), the Institut de radioprotection et de sûreté nucléaire (Korsakissok et al., 2013), the Japan Atomic Energy Agency (JAEA) (Terada et al., 2008), the Japan Agency for Marine-Earth Science and Technology (JAMSTEC), JMA (Saito et al., 2014), MRI (Kajino et al., 2012a, 2012b; Adachi et al., 2013; Sekiyama et al., 2015), the National Institute for Environmental Studies (Morino et al., 2011, 2013), and Seoul National University (Park et al., 2013).

MRI contributed results obtained with the regional chemistry transport models NHM-Chem (Kajino et al., 2012a, 2012b; Sekiyama et al., 2013, 2015) and JMA-RATM (Saito et al., 2014) to the intercomparison of regional transport. Detailed descriptions of NHM-Chem and its results are given in sections G-3 and G-4 of this technical report. The version of JMA-RATM used for the SCJ regional atmospheric model intercomparison was slightly modified from the WMO Task Team version. The main differences were (1) the radionuclide emission scenario was changed to "JAEA2" (Kobayashi et al., 2013), (2) the time step of the integration was shortened to 5 minutes, and (3) snow and hail as well as rain from the meso-analysis of accumulated precipitation were used. JMA-RATM and its results are described in detail in section E of this technical report. The horizontal distribution of the accumulated ^{137}Cs deposition during March 2011 simulated by JMA-RATM is shown in Fig. G-6-1a.

The regional atmospheric model intercomparison results showed that the land area deposition was 27 ± 10% of total emissions. However, MEXT aircraft observations on 31 May 2012 showed on-land deposition to be 2.7 PBq (Torii et al., 2012). This observed value and the total emissions estimated by inverse analysis (17.8 ± 8.9 PBq; section G-5) lead to a land area deposition of 18 ± 7% of total emissions, but to a value of 20 ± 6% if a total emission of 14.6 ± 3.5 PBq, which is within two standard deviations of the mean, is used. These differences in the land area deposition percentage are due to model simulation errors, and errors in the total emission estimate and in the estimate of the land-deposited amount from aircraft observations.

G-6-4. Global atmospheric transport model intercomparison

The intercomparison of global-scale transport models included 5 global transport models, 1 large-scale regional transport model, and 12 simulated results. Four of the five global models, SPRINTARS (Takemura et al., 2011), EMAC (Christoudias and Lelieveld, 2013), Model of Aerosol Species IN the Global AtmospheRe (MASINGAR)-1 (Tanaka et al., 2003), and MASINGAR mk-2 (Tanaka et al., 2012), are global aerosol models that are coupled online with general circulation models. The remaining models are the TM5 global transport model (Huijnen et al., 2010) and the MRI Passive-tracers Model for radionuclides (MRI-PM/r) regional transport model (Kajino et al., 2012a, 2012b; Adachi et al., 2013), which are off-line models that use assimilated meteorological fields or meteorological fields previously calculated by another model. All of the participating models in the SCJ intercomparison were grid point

Eulerian or semi-Lagrangian advection models.

MRI contributed three models to the global atmospheric transport model intercomparison: MASINGAR-1 (Tanaka et al., 2003), MASINGAR mk-2 (Tanaka et al., 2012) and MRI-PM/r. The simulated results of two versions of MASINGAR were submitted for the intercomparison. MASINGAR-1 was coupled with an atmospheric general circulation model (AGCM) called MRI/JMA 98, which has been used as JMA's operational dust forecasting model since January 2004 (Tanaka et al., 2003). The model resolutions were set to a T106 Gaussian horizontal grid (approximately 1.125° × 1.125°) and 30 vertical layers from the surface to a height of 0.4 hPa. A newer version of this aerosol model, called MASINGAR mk-2, was coupled with an AGCM called MRI-AGCM3, which is a component of MRI's earth system model MRI-ESM1 (Yukimoto et al., 2011, 2012). MASINGAR mk-2 was also used as the global aerosol model for the CMIP5 climate change experiment. For the intercomparison, the model resolutions were set to a TL319 horizontal grid (approximately 0.5625° × 0.5625°) and 40 vertical layers from the ground surface to a height of 0.4 hPa. In this intercomparison experiment, the horizontal wind fields were assimilated from six-hourly 1.25° ×1.25° JMA Climate Data Assimilation System (JCDAS) global reanalysis data (Onogi et al., 2007) using a Newtonian relaxation nudging technique. The JCDAS reanalysis was also used for sea-surface temperature data. The released ^{137}Cs was assumed to be readily attached to ambient aerosols with a unimodal lognormal distribution (mode radius, 0.07 μm; dispersion, 2.0) (Tanaka et al., 2012). For the intercomparison, the ^{137}Cs results simulated with the source terms of JAEA (Terada et al. 2012) and Stohl et al. (2012) were submitted. For the ^{133}Xe experiment, the inversely estimated source term of Stohl et al. (2012) was used.

MRI-PM/r is a large-scale regional off-line chemistry transport model. The regional domain used was 107°E–252°E and 3°N–61°N with 234 × 120 grids (Mercator map projection), which corresponded to a horizontal resolution of approximately 60 km × 60 km. The vertical coordinates were terrain-following with 13 vertical layers up to 10 hPa. The Advanced Research Weather Research and Forecasting model (WRF; Skamarock et al., 2008) was used to simulate the meteorological field. The U.S. National Centers for Environmental Prediction six-hourly, 1° × 1° final operational global analysis dataset ds083.2 (http://rda.ucar.edu/datasets/ds083.2/) was used for the initial and boundary conditions of WRF and also for the analysis nudging method. The aerosol module used a category approach to represent the interaction between radionuclides and environmental species (Kajino and Kondo, 2011). The aerosol particles were grouped into six categories: primary hot particles (PRI), Aitken mode (ATK), accumulation mode (ACM), dust particles (DU), sea-salt particles (SS), and pollen (POL). The aerosol chemical and dynamical processes, such as nucleation, condensation, coagulation and deposition, were calculated by a modal moment dynamics approach (Kajino and Kondo, 2011; Kajino, 2011; Kajino et al. 2012a, 2012b). The emission inventory of environmental species with anthropogenic, biogenic, and biomass burning origins was the same as that used by Kajino and Kondo (2011). Five percent of the Cs was assumed to form radioactive primary particles (PRI), and the remaining 95% was assumed to condense onto pre-existing particles of the other five types with the mass fluxes proportional to the

surface area concentrations of each aerosol category. A revised version of the JAEA inventory (Terada et al., 2012) was used for the emissions of ^{134}Cs and ^{137}Cs.

The simulated horizontal distributions of the accumulated ^{137}Cs deposition through the end of March 2011 obtained with the MRI global-scale models are shown in Fig. G-6-1b–f. All of the simulated results show the ^{137}Cs deposited over a wide area of the Northern Hemisphere, with the highest concentrations in the Northwest Pacific region. The global-scale model intercomparison results indicate that the global wet deposition accounted for 93 ± 5% of the total ^{137}Cs deposition. The JMA-RATM results (Fig. G-6-1a), however, showed that 46% of ^{137}Cs was removed by wet deposition in the simulation region, and the regional atmospheric model intercomparison results showed that 68 ± 20% of ^{137}Cs was removed by wet deposition over the simulation regions. The cause of these differences between the global and regional simulations was mainly the different simulation regions, because dry deposition was dominant in the vicinity of the power plant where concentrations of ^{137}Cs were high. However, another non-negligible cause was differences among the models in the treatment of dry and wet deposition and in the meteorological fields used.

G-6-5. Summary

The SCJ intercomparison of regional and global atmospheric transport model simulation results showed that the models were capable of depicting the main features of the observed radioactive material distributions. Quantitative comparisons of the simulation results, however, revealed large uncertainties, especially in the amount of wet deposition. The skill of the models depends on the performance of the dynamic frameworks, chemical transportation processes, dry and wet deposition processes and other elements. Therefore, the models can be significantly improved through collaboration among the different modeling communities. The full report of the SCJ model intercomparison project was published by the Sectional Committee on Nuclear Accident, Committee on Comprehensive Synthetic Engineering, of SCJ on 2 September 2014 (SCJ, 2014).

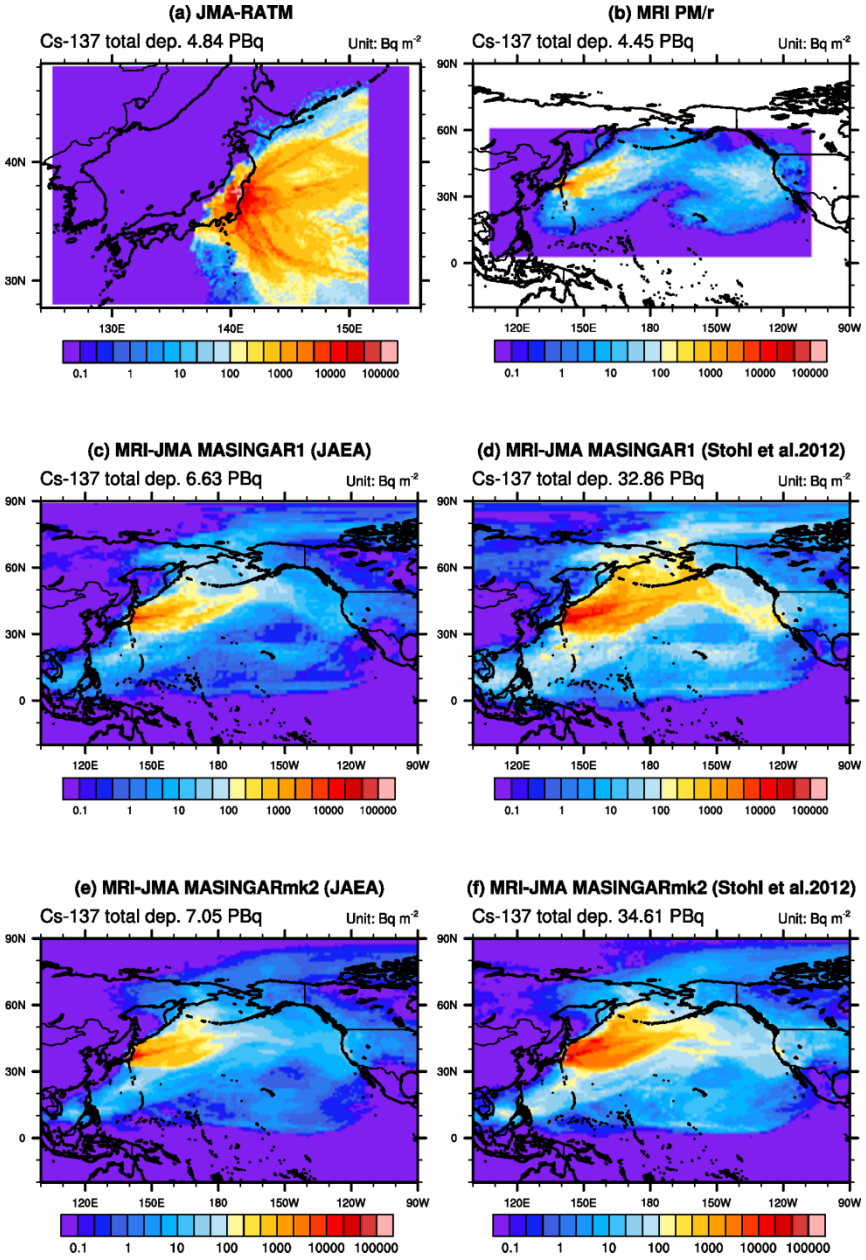

Fig. G-6-1. Horizontal distributions of the accumulated ^{137}Cs deposition from 11 to 31 March 2011 by (a) JMA-RATM, (b) NHM-Chem, (c) MASINGAR-1 using the JAEA source term, (d) MASINGAR-1 using the Stohl et al. (2012) source term, (e) MASINGAR mk-2 using the JAEA source term, and (f) MASINGAR mk-2 using the Stohl et al. (2012) source term. Units are Bq m^{-2}.

H. References

Adachi, K., M. Kajino, Y. Zaizen, and Y. Igarashi, 2013: Emission of spherical cesium-bearing particles from an early stage of the Fukushima nuclear accident. *Nature Scientific Reports*, **3**, 2554, doi:10.1038/srep02554.

Araki, K., 2000: Six-hour forecasts of precipitation. *Reports of the Numerical Prediction Division*, **47**, 36–41. (in Japanese)

Arnold, D., C. Maurer, G. Wotawa, R. Draxler, K. Saito, and P. Seibert, 2015: Influence of the meteorological input on the atmospheric transport modelling with FLEXPART of radionuclides from the Fukushima Daiichi nuclear accident. *J. Environ. Radioact.*, **139**, 212–225.

Becker, A., G. Wotawa, L-E De Geer, P. Seibert, R. Draxler, C. Sloan, R. D'Amours, M. Hort, H. Glaab, P. Heinrich, Y. Grillon, V. Shershakov, K. Katayama, Y. Zhang, P. Stewart, M. Hirtl, M. Jane, and P. Chen, 2007: Global backtracking of anthropogenic radionuclides by means of a receptor oriented ensemble dispersion modelling system in support of Nuclear-Test-Ban Treaty verification. *Atmos. Environ.*, **41**, 4520–4534.

Bedwell, P., J. Wellings, S. M. Haywood, A. R. Jones, and M. C. Hort, 2011: Cloud gamma modelling in the UK Met Office's NAME III model. *AGU Chapman Conference*.

Blackadar, A. K., 1962: The vertical distribution of wind and turbulent exchange in a neutral atmosphere. *J. Geophys. Res.*, **67**, 3095–3102.

Browning, K. A., and F. F. Hill, 1981: Orographic Rain. *Weather*, **35**, 326–329.

Burgin, L. E., J. Gloster, C. Sanders, P. S. Mellor, S. Gubbins, and S. Carpenter, 2012: Investigating incursions of bluetongue virus using a model of long-distance culicoides biting midge dispersal. *Transboundary and Emerging Diseases*, doi:10.1111/j.1865-1682.2012.01345.x.

Chino, M., H. Nakayama, H. Nagai, H. Terada, G. Katata, and H. Yamazawa, 2011: Preliminary estimation of release amounts of ^{131}I and ^{137}Cs accidentally discharged from the Fukushima Daiichi Nuclear Power Plant into the atmosphere. *J. Nucl. Sci. Technol.*, **48**, 1129–1134.

Christoudias, T., and J. Lelieveld, 2013: Modelling the global atmospheric transport and deposition of radionuclides from the Fukushima Dai-ichi nuclear accident. *Atmos. Chem. Phys.*, **13**, 1425–1438.

Clark, M. J., and F. B. Smith, 1988: Wet and dry deposition of Chernobyl releases. *Nature*, **332**, 245–249.

Courtier, P., J.-N. Thépaut, and A. Hollingsworth, 1994: A strategy for operational implementation of 4D-Var, using an incremental approach. *Q. J. Roy. Met. Soc.*, **120**. 1367–1387.

D'Amours, R., and A. Malo, 2004: A zeroth order Lagrangian particle dispersion model MLDP0. *Internal publication*, Canadian Meteorological Centre, Environmental Emergency Response Section, Dorval, QC, Canada, 19 pp. (available online at http://eer.cmc.ec.gc.ca/publications/DAmours.Malo.2004.CMC-EER.MLDP0.pdf)

D'Amours, R., A. Malo, R. Servranckx, D. Bensimon, S. Trudel, and J.-P. Gauthier, 2010: Application of the atmospheric Lagrangian particle dispersion model MLDP0 to the 2008 eruptions of Okmok

and Kasatochi volcanoes. *J. Geophys. Res.*, **115**, D00L11, 11 pp, doi:10.1029/2009JD013602.

Delage, Y., 1997: Parameterising sub-grid scale vertical transport in atmospheric models under statically stable conditions. *Bound.-Layer Meteor.*, **82**, 23–48.

Draxler, R. R., 1999: HYSPLIT_4 User's Guide. *NOAA Tech. Memo, ERL ARL-230, Air Resources Laboratory, Silver Spring, MD,* 35 pp. (available online at http://www.arl.noaa.gov/documents/reports/hysplit_user_guide.pdf)

Draxler, R. R., 2006: The Use of global and mesoscale meteorological model data to predict the transport and dispersion of tracer plumes over Washington, D.C. *Wea. Forecasting*, **21**, 383–394.

Draxler, R., and J. L. Heffter, 1981: Workbook for estimating the climatology of regional-continental scale atmospheric dispersion over the United States. *NOAA Tech. Memo.* ERL ARL-96. NOAA, Air Resour. Lab. Silver Spring, Md.

Draxler, R. R., and G. D. Hess, 1997: Description of the HYSPLIT_4 modeling system. *NOAA Tech. Memo. ERL ARL-224, Air Resources Laboratory, Silver Spring, MD,* 24 pp., NTIS PB98-116593.

Draxler, R. R., and G. D. Hess, 1998: An overview of the HYSPLIT_4 modelling system for trajectories, dispersion, and deposition. *Aust. Meteor. Mag.*, **47**, 295–308.

Draxler, R. R., and G. D. Rolph, 2012: Evaluation of the Transfer Coefficient Matrix (TCM) approach to model the atmospheric radionuclide air concentrations from Fukushima. *J. Geophys. Res.*, **117**, 10 pp, doi:10.1029/2011JD017205.

Draxler, R., D. Arnold, S. Galmarini, M. Hort, A. Jones, S. Leadbetter, A. Malo, C. Maurer, G. Rolph, K. Saito, R. Servranckx, T. Shimbori, E. Solazzo, and G. Wotawa, 2013a: Evaluation of meteorological analyses for the radionuclide dispersion and deposition from the Fukushima Daiichi Nuclear Power Plant accident. *WMO Technical Publication*, **1120**, 64 pp. (available online at https://www.wmo.int/e-catalog/detail_en.php?PUB_ID=669)

Draxler, R., P. Chen, M. Hort, A. Malo, K. Saito, and G. Wotawa, 2013b: World Meteorological Organization's evaluation of the radionuclide dispersion and deposition from the Fukushima Daiichi Nuclear Power Plant accident. *Proceeding, Special Symposium on the Transport and Diffusion of Contaminants from the Fukushima Dai-Ichi Nuclear Power Plant.* (available online at https://ams.confex.com/ams/93Annual/webprogram/Paper215372.html)

Draxler, R., D. Arnold, M. Chino, S. Galmarini, M. Hort, A. Jones , S. Leadbetter, A. Malo, C. Maurer, G. Rolph, K. Saito, R. Servranckx, T. Shimbori, E. Solazzo, and G. Wotawa, 2015: World Meteorological Organization’s model simulations of the radionuclide dispersion and deposition from the Fukushima Daiichi Nuclear Power Plant accident. *J. Environ. Radioact.*, **139**, 172–184.

Fischer, B., 2012: Radionuclide emissions for the Fukushima Daiichi accident prepared for the UNSCEAR assessment. (private communication)

Fukushima Prefecture, 2011a: http://www.pref.fukushima.lg.jp/sec_file/monitoring/m-3/20-50km0312-0331.pdf (in Japanese)

Fukushima Prefecture, 2011b: http://www.pref.fukushima.lg.jp/sec_file/monitoring/m-1/7houbu0311-0331.pdf (in Japanese)

Furuta, S., S. Sumiya, H. Watanabe, M. Nakano, K. Imaizumi, M. Takeyasu, A. Nakada, H. Fujita, T. Mizutani, M. Morisawa, Y. Kokubun, T. Kono, M. Nagaoka, H. Yokoyma, T. Hokama, T. Isozaki, M. Nemota, Y. Hiyama, T. Onuma, C. Kato, and T. Kurachi, 2011: Results of the Environmental Radiation Monitoring Following the Accident at the Fukushima Daiichi Nuclear Power Plant - Interim Report (Ambient Radiation Dose Rate, Radioactivity Concentration in the Air and Radioactivity Concentration in the Fallout), Radiation Protection Department, Nuclear Fuel Cycle Engineering Laboratories, Tokai Research and Development Center, Japan Atomic Energy Agency Tokai-mura, Naka-gun, Ibaraki-ken, *JAEA-Review* 2011-035, August, 89 pp. (in Japanese, available online at http://jolissrch-inter.tokai-sc.jaea.go.jp/search/servlet/search?5031728)

Gauntt, R. O., R. K. Cole, C. M. Erickson, R. G. Gido, R. D. Gasser, S. B. Rodriguez, M. F. Young, S. Ashbaugh, M. Leonard, and A. Hill, 2001: MELCOR Computer Code Manuals, Vol. 3: Demonstration Problems, Version 1.8.5 May 2001, Sandia National Laboratories, SAND2001-0929P, Albuquerque, USA.

Gifford, F. A., 1982: Horizontal diffusion in the atmosphere: A Lagrangian-dynamical theory. *Atmos. Environ*., **16**, 505–512.

Gifford, F. A., 1984: The random force theory: Application to meso and large-scale atmospheric diffusion. *Bound.-Layer Meteor*., **30**, 159–174.

Hayami, H., A. Sato, M. Tsuzaki, and H. Shimadera, 2012: Atmospheric transport and deposition modeling of radioactive materials released from the Fukushima Daiichi nuclear power plant. *CRIEPI report*, V11054. (in Japanese)

Hertel, O., J. Christensen, E. H. Runge, W. A. H. Asman, R. Berkowicz, and M. F. Hovmand, 1995: Development and testing of a new variable scale air pollution model—ACDEP. *Atmos. Environ*., **29**, 1267–1290.

Hoffmann, W., R. Kebeasy, and P. Firbas, 2000: Introduction to the verification regime of the Comprehensive 5 Nuclear-Test-Ban Treaty. *Phys. Earth Planet. Inter*., **113**, 5–9.

Holtslag, A. A. M., and B. A. Boville, 1993: Local versus nonlocal boundary-layer diffusion in a global climate model. *J. Climate*, **6**, 1825–1842.

Honda, Y., and K. Sawada, 2008: A new 4D-Var for mesoscale analysis at the Japan Meteorological Agency. *CAS/JSC WGNE Res. Act. Atmos. Ocea. Model.*, **38**, 01.07–01.08.

Honda, Y., and K. Sawada, 2009: Upgrade of the operational mesoscale 4D-Var system at the Japan Meteorological Agency. *CAS/JSC WGNE Res. Act. Atmos. Ocea. Model.*, **39**, 01.11–01.12.

Honda, Y., M. Nishijima, K. Koizumi, Y. Ohta, K. Tamiya, T. Kawabata, and T. Tsuyuki, 2005: A pre-operational variational data assimilation system for a non-hydrostatic model at the Japan Meteorological Agency: Formulation and preliminary results. *Q. J. Roy. Meteorol. Soc.*, **131**, 3465–3475.

Hsu, S.-C., C.-A. Huh, C.-Y. Chan, S.-H. Lin, F.-J. Lin, and S. C. Liu, 2012: Hemispheric dispersion of radioactive plume laced with fission nuclides from the Fukushima nuclear event. *Geophys. Res.*

Lett., **39**, L00G22, doi:10.1029/2011GL049986.

Hu, X., D. Li, H. Huang, S. Shen, and E. Bou-Zeid, 2014: Modeling and sensitivity analysis of transport and deposition of radionuclides from the Fukushima Daiichi accident. *Atmos. Chem. Phys. Discuss.*, **14**, 2113–2173.

Huijnen, V., J. Williams, M. van Weele, T. van Noije, M. Krol, F. Dentener, A. Segers, S. Houweling, W. Peters, J. de Laat, F. Boersma, P. Bergamaschi, P. van Velthoven, P. Le Sager, H. Eskes, F. Alkemade, R. Scheele, P. Nédélec, and H.-W. Pätz, 2010: The global chemistry transport model TM5: description and evaluation of the tropospheric chemistry version 3.0. *Geosci. Model Dev.*, **3**, 445–473.

Hunt, B. R., E. J. Kostelich, and I. Szunyogh, 2007: Efficient data assimilation for spatiotemporal chaos: A local ensemble transform Kalman filter. *Physica D*, **230**, 112–126.

Igarashi, Y., Y. Inomata, M. Aoyama, K. Hirose, H. Takahashi, Y. Shinoda, N. Sugimoto, A. Shimizu, and M. Chiba, 2009: Plausible change in Asian dust source suggested by atmospheric anthropogenic radionuclides-observation of single wet deposition events during spring of 2007. *Atmos. Environ*, **43**, 2971–2980.

Ikuta, Y., and Y. Honda, 2011: Development of 1D+4DVAR data assimilation of radar reflectivity in JNoVA. *CAS/JSC WGNE Res. Activ. Atmos. Ocea. Model*., **41**, 01.09–01.10.

Ishikawa, Y., 2010: Data assimilation of GPS precipitable water vapor into the JMA mesoscale numerical weather prediction model. *CAS/JSC WGNE Res. Act. Atmos. Ocea. Model.*, **40**, 01.13–01.14.

Iwasaki, T., 2013: What happened from the accidental release of radioactive materials from the Fukushima Dai-Ichi Nuclear Power Plant on 3.11 in 2011? *Extended abstract, Special Symposium on the Transport and Diffusion of Contaminants from the Fukushima Dai-Ichi Nuclear Power Plant*, 4 pp. AMS annual meeting on 5th of January at Austin. (available online at https://ams.confex.com/ams/93Annual/webprogram/Manuscript/Paper220977/AMS-Extended%20Abstract.Iwasaki.2013.pdf)

Iwasaki, T., T. Maki, and K. Katayama, 1998: Tracer transport model at Japan Meteorological Agency and its application to the ETEX data. *Atmos. Environ.*, **32**, 4285–4295.

JCAC, 2011: http://www.jcac.or.jp/site/senryo/taiki-kouka-back-list.html (in Japanese)

JMA, 2013: Outline of the operational numerical weather prediction at the Japan Meteorological Agency (March 2013), 188 pp. (available online at http://www.jma.go.jp/jma/jma-eng/jma-center/nwp/outline2013-nwp/pdf/outline2013_all.pdf)

JMA, 2014: Specifications of the JMA's NWP models and Ensemble Prediction Systems. (available online at http://www.jma.go.jp/jma/jma-eng/jma-center/nwp/specifications_models.pdf)

Jones, A. R., D. J. Thomson, M. C. Hort, and B. Devenish, 2007: The U.K. Met Office's next-generation atmospheric dispersion model, NAME III. In C. Borrego and A.-L. Norman, editors, Air Pollution and its Applications XVII. *Proceedings of the 27th NATO/CCMS International Technical Meeting on Air Pollution Modelling and its Application*, Springer,

580–589.

Kajino, M., 2011: MADMS: Modal Aerosol Dynamics model for multiple Modes and fractal Shapes in the free-molecular and near-continuum regimes. *J. Aerosol Sci.*, **42**, 224–248.

Kajino, M., and Y. Kondo, 2011: EMTACS: Development and regional-scale simulation of a size, chemical, mixing type, and soot shape resolved atmospheric particle model. *J. Geophys. Res.*, **116**, D02303, 28 pp, doi:10.1029/2010JD015030.

Kajino, M., M. Deushi, T. Maki, N. Oshima, Y. Inomata, K. Sato, T. Ohizumi, and H. Ueda, 2012a: Modeling wet deposition and concentration of inorganics over Northeast Asia with MRI-PM/c. *Geosci. Model Dev.*, **5**, 1363–1375.

Kajino. M, Y. Inomata, K. Sato, H. Ueda, Z. Han, J. An, G. Katata, M. Deushi, T. Maki, N. Oshima, J. Kurokawa, T. Ohara, A. Takami, and S. Hatakeyama, 2012b: Development of the RAQM2 aerosol chemical transport model and predictions of the Northeast Asian aerosol mass, size, chemistry, and mixing type. *Atmos. Chem. Phys.*, **12**, 11833–11856.

Kaneyasu, N., H. Ohashi, F. Suzuki, T. Okada, and F. Ikemori, 2012: Sulfate aerosol as a potential transport medium of radiocesium from the Fukushima nuclear accident. *Environ. Sci. Technol.*, **46**, 5720–5726.

Katata, G., M. Ota, H. Terada, M. Chino, and H. Nagai, 2012a. Atmospheric discharge and dispersion of radionuclides during the Fukushima Dai-ichi Nuclear Power Plant accident. Part I: source term estimation and local-scale atmospheric dispersion in early phase of the accident. *J. Environ. Radioact*. **109**, 103–113.

Katata, G., H. Terada, H. Nagai, and M. Chino, 2012b: Numerical reconstruction of high dose rate zones due to the Fukushima Daiichi Nuclear Power Plant accident. *J. Environ. Radioact.*, **111**, 2–12.

Katata, G., M. Chino, T. Kobayashi, H. Terada, M. Ota, H. Nagai, M. Kajino, R. Draxler, M. C. Hort, A. Malo, T. Torii, and Y. Sanada, 2015: Detailed source term estimation of the atmospheric release for the Fukushima Daiichi Nuclear Power Station accident by coupling simulations of atmospheric dispersion model with improved deposition scheme and oceanic dispersion model. *Atmos. Chem Phys.*, **15**, 1029–1070.

Kawai, H., 2002: Forecast of sulfur dioxide flow from Miyake volcano with a high resolution regional transport model. *CAS/JSC WGNE Res. Act. Atmos. Ocea. Model*., **32**, 05.24–05.25.

Kitada, T., 1994: Modelling of transport, reaction and deposition of acid rain. *Kishou Kenkyu Note*, **182**, 95–117. (in Japanese)

Kitada, T., G. R. Carmichael, and L. K. Peters 1986: Effects of dry deposition on the concentration-distribution of atmospheric pollutants within land- and sea-breeze circulations. *Atmos. Environ*., **20**, 1999–2010.

Kobayashi T., H. Nagai, M. Chino, and H. Kawamura, 2013: Source term estimation of atmospheric release due to the Fukushima Dai-ichi Nuclear Power Plant accident by atmospheric and oceanic dispersion simulations. *J. Nucl. Sci. Technol*,, **50**, 255–264.

Kondo, H., T. Satomura, T. Takemura, H. Yamazawa, and A. Watanabe, 2012: A report of the special topic session “Current status and issues of numerical models for the transport of radioactive substances” at the 2011 Autumn Meeting. *Tenki*, **59**, 239–250. (in Japanese)

Kondo, H., T. Yamada, M. Chino, T. Iwasaki, G. Katata, T. Maki, K. Saito, H. Terada, and H. Tsuruta, 2013: Report of the Special Symposium on the Transport and Diffusion of Contaminants from the Fukushima Dai-Ichi Nuclear Power Plant: Present Status and Future Directions. *Tenki*, **60**, 723–729. (in Japanese)

Korsakissok, I., A. Mathieu, and D. Didier, 2013: Atmospheric dispersion and ground deposition induced by the Fukushima Nuclear Power Plant accident: a local-scale simulation and sensitivity study. *Atmos. Environ.*, **70**, 267–279.

Kunii, M., 2013: Mesoscale data assimilation for a local severe rainfall event with the NHM-LETKF system. *Wea. Forecasting*, **29**, 1093–1105.

Leadbetter, S, M. Hort, A, Jones, H. Webster, and R. Draxler, 2015: Sensitivity of the deposition of Caesium-137 from Fukushima Dai-ichi nuclear power plant on the wet deposition parameterisation in NAME. *J. Environ. Radioact.,* **139**, 200–211.

Lim, K.-S. S., and S.-Y. Hong, 2010: Development of an effective double-moment cloud microphysics scheme with prognostic cloud condensation nuclei (CCN) for weather and climate models. *Mon. Wea. Rev.*, **138**, 1587–1612.

Louis, J. F., M. Tiedtke, and J. F. Geleyn, 1982: A short history of the operational PBL parameterization at ECMWF. *Workshop on planetary boundary layer parameterization*. ECMWF, 59–79.

Makihara, Y., 2000: Algorithms for precipitation nowcasting focused on detailed analysis using radar and raingauge data, Study on the Objective Forecasting Techniques. *Tech. Rep. MRI*, **39**, 63–111.

Maryon, R. H., D. B. Ryall, and A. L. Malcolm, 1999: The NAME 4 dispersion model: Science documentation. *Technical report, UK Meteorological Office*. Turbulence Diffusion Note, **262**.

Masson, O., A. Baeza, J. Bieringer, K. Brudecki, S. Bucci, M. Cappai, F. P. Carvalho, O. Connan, C. Cosma, A. Dalheimer, D. Didier, G. Depuydt, L. E. De Geer, A. De Vismes, L. Gini, F. Groppi, K. Gudnason, R. Gurriaran, D. Hainz, Ó. Halldórsson, D. Hammond, O. Hanley, K. Holeý, Zs. Homoki, A. Ioannidou, K. Isajenko, M. Jankovic, C. Katzlberger, M. Kettunen, R. Kierepko, R. Kontro, P. J. M. Kwakman, M. Lecomte, L. Leon Vintro, A.-P. Leppänen, B. Lind, G. Lujaniene, P. Mc Ginnity, C. Mc Mahon, H. Malá, S. Manenti, M. Manolopoulou, A. Mattila, A. Mauring, J. W. Mietelski, B. Møller, S. P. Nielsen, J. Nikolic, R. M. W. Overwater, S. E. Pálsson, C. Papastefanou, I. Penev, M. K. Pham, P. P. Povinec, H. Ramebäck, M. C. Reis, W. Ringer, A. Rodriguez, P. Rulík, P. R. J. Saey, V. Samsonov, C. Schlosser, G. Sgorbati, B. V. Silobritiene, C. Söderström, R. Sogni, L. Solier, M. Sonck, G. Steinhauser, T. Steinkopff, P. Steinmann, S. Stoulos, I. Sýkora, D. Todorovic, N. Tooloutalaie, L. Tositti, J. Tschiersch, A. Ugron, E. Vagena, A. Vargas, H. Wershofen, and O. Zhukova, 2011: Tracking of airborne radionuclides from the damaged Fukushima Dai-Ichi nuclear reactors by European networks. *Environ. Sci. Technol.,* **45**,

7670–7677.

Mellor, G. L., and T. Yamada, 1974: A hierarchy of turbulence closure models for planetary boundary layers. *J. Atmos. Sci*., **31**, 1791–1806.

Mellor, G. L., and T. Yamada, 1982: Development of a turbulence closure model for geophysical fluid problems. *Rev. Geophys. Space Phys*., **20**, 851–875.

METI, 2011: http://www.meti.go.jp/press/2011/06/20110603019/20110603019.html (in Japanese)

MEXT, 2007: SPEEDI System for Prediction of Environmental Emergency Dose Information, *Pamphlet of SPEEDI*.

MEXT, 2011a: Monitoring information of environmental radioactivity level, Readings of dust sampling, http://radioactivity.nsr.go.jp/en/list/200/list-1.html

MEXT, 2011b: Monitoring information of environmental radioactivity level, Readings of Environmental Radiation Level by emergency monitoring, http://radioactivity.nsr.go.jp/en//list/207/list-1.html

MEXT, 2011c: Results of analyses of radionuclides (Cs-134 and Cs-137) in soil. (Retrieved from http://www.mext.go.jp/b_menu/shingi/chousa/gijyutu/017/shiryo/__icsFiles/afieldfile/2011/09/02/1310688_1.pdf)

MEXT, 2011d: Results of airborne monitoring by the Ministry of Education, Culture, Sports. Science and Technology and the U.S. Department of Energy. Available online at http://radioactivity.nsr.go.jp/ja/contents/4000/3710/24/1305820_20110506.pdf, http://radioactivity.nsr.go.jp/ja/contents/5000/4858/24/1305819_0708.pdf, http://radioactivity.nsr.go.jp/ja/contents/5000/4901/24/1910_1216.pdf

Morino, Y., T. Ohara, and M. Nishizawa, 2011: Atmospheric behavior, deposition, and budget of radioactive materials from the Fukushima Daiichi nuclear power plant in March 2011. *Geophys. Res. Lett.*, **38**, doi:10.1029/2011GL048689.

Morino, Y., T. Ohara, M. Watanabe, S. Hayashi, and M. Nishizawa, 2013: Episode analysis of deposition of radiocesium form the Fukushima Daiichi Nuclear Power Plant accident. *Environ. Sci. Technol.*, **47**, 2314–2322.

Morrison, H., G. Thompson, and V. Tatarskii, 2009: Impact of cloud microphysics on the development of trailing stratiform precipitation in a simulated squall line: compassion of one- and two-moment schemes. *Mon. Wea. Rev.*, **137**, 991–1007.

Nagai, H., M. Chino, and H. Yamazawa, 1999: Development of scheme for predicting atmospheric dispersion of radionuclides during nuclear emergency by using atmospheric dynamic model. *J. At. Energy. Soc. Japan*, **41**, 777–785. (in Japanese with English abstract)

Nagata, K., 2011: Quantitative precipitation estimation and quantitative precipitation forecasting by the Japan Meteorological Agency. *RSMC Tokyo – Typhoon Center Technical Review*, **13**, 37–50. (available online at http://www.jma.go.jp/jma/jma-eng/jma-center/rsmc-hp-pub-eg/techrev/text13-2.pdf)

NSC, 2010: The guideline for environmental radiation monitoring. (in Japanese, available online at

http://www.bousai.ne.jp/vis/shiryou/pdf/kankyou_monitor_h2204.pdf)

O'Brien, J. J., 1970: A note on the vertical structure of the eddy exchange coefficient in the planetary boundary layer. *J. Atmos. Sci*., **27**, 1213–1215.

Onogi, K., J. Tsutsui, H. Koide, M. Sakamoto, S. Kobayashi, H. Hatsushika, T. Matsumoto, N. Yamazaki, H. Kamahori, K. Takahashi, S. Kadokura, K. Wada, K. Kato, R. Oyama, T. Ose, N. Mannoji, and R. Taira, 2007: The JRA-25 Reanalysis. *J. Meteor. Soc. Japan*, **85**, 369–432.

Park, S.-U., A. Choe, and M.-S. Park, 2013: Atmospheric dispersion and deposition of radionuclides (^{137}Cs and ^{131}I) released from the Fukushima Dai-ichi Nuclear Power Plant. *Comput. Water, Energy, Environ. Eng.*, **2**, 61–68.

Pudykiewicz, J., 1989: Simulation of the Chernobyl dispersion with a 3-D hemispheric tracer model. *Tellus B*, **41**, 391–412.

Ryall, D. B., and R. H. Maryon, 1998: Validation of the UK Met. Office's name model against the ETEX dataset. *Atmos. Environ.* **32**, 4265–4276.

Saito, K., 2012: The Japan Meteorological Agency nonhydrostatic model and its applications to operation and research. *Atmospheric Model Applications*, 85–110, doi:10.5772/35368.

Saito, K., T. Fujita, Y. Yamada, J. Ishida, Y. Kumagai, K. Aranami, S. Ohmori, R. Nagasawa, S. Kumagai, C. Muroi, T. Kato, H. Eito, and Y. Yamazaki, 2006: The operational JMA nonhydrostatic mesoscale model. *Mon. Wea. Rev.*, **134**, 1266–1298.

Saito, K., J. Ishida, K. Aranami, T. Hara, T. Segawa, M. Narita, and Y. Honda, 2007: Nonhydrostatic atmospheric models and operational development at JMA. *J. Meteor. Soc. Japan*, **85B**, 271–304.

Saito, K., T. Shimbori, and R. Draxler, 2013: JMA's regional ATM calculations for the WMO technical Task Team on meteorological analyses for Fukushima Daiichi Nuclear Power Plant accident. *Extended abstract, Special Symposium on the Transport and Diffusion of Contaminants from the Fukushima Dai-Ichi Nuclear Power Plant*, 5 pp. (available online at https://ams.confex.com/ams/93Annual/webprogram/Manuscript/Paper219086/AMS_ExtAbs_JMARATM.pdf)

Saito, K., T. Shimbori, T. Hara, E. Toyoda, T. Kato, T. Fujita, K. Nagata, and Y. Honda, 2014: The WMO Technical Task Team on meteorological analyses for Fukushima Daiichi Nuclear Power Plant accident. *Sokko-jiho* (Japanese bulletin on operations at JMA), **81**, 1–30. (in Japanese, available online at http://www.jma.go.jp/jma//kishou/books/sokkou/81/vol81p001.pdf)

Saito, K, T. Shimbori, and R. Draxler, 2015: JMA's regional atmospheric transport model calculations for the WMO technical task team on meteorological analyses for Fukushima Daiichi Nuclear Power Plant accident. *J. Environ. Radioact.*, **139**, 185–199.

Sakamoto, M., 2013: Atmospheric Transport Model. Outline of the Operational Numerical Weather Prediction at the Japan Meteorological Agency, 95–98. (available online at http://www.jma.go.jp/jma/jma-eng/jma-center/nwp/outline2013-nwp/pdf/outline2013_03.pdf)

Schöppner, M., W. Plastino, P. P. Povinec, G. Wotawa, F. Bella, A. Budano, M. De Vincenzi, and F. Ruggieri, 2011: Estimation of the time-dependent radioactive source-term from the Fukushima

nuclear power plant accident using atmospheric transport modelling. *J. Environ. Radioact.*, **114**, 10–14.

SCJ, 2014: A review of the model comparison of transportation and deposition of radioactive materials released to the environment as a result of the Fukushima Daiichi Nuclear Power Plant accident. *Report of working group for model intercomparison, Subcommittee to Review the Investigation on Environmental Contamination Caused by the Nuclear Accident, Committee on Comprehensive Synthetic Engineering, Science Council of Japan.* (available online at http://www.scj.go.jp/ja/info/kohyo/pdf/kohyo-22-h140902-e1.pdf)

Seibert, P., D. Arnold, M. Gabriele, N. Arnold, K. Gufler, H. Kromp-Kolb, W. Kromp, P. Sutter, and A. Wenisch, 2012: Severe accidents of nuclear power plants in Europe: possible consequences and mapping of risk. *4th International Disaster and Risk Conference IDRC*, Davos, 26-30 August. (available online at http://www.slideshare.net/GRFDavos/severe-accidents-of-nuclear-power-plants-in-europe-possible-consequences-and-mapping-of-risk)

Seino, N., H. Sasaki, J. Sato, and M. Chiba, 2004: High-resolution simulation of volcanic sulfur dioxide dispersion over the Miyake Island. *Atmos. Environ.*, **38**, 7073–7081.

Sekiyama, T. T., M. Kajino, and M. Kunii, 2013: Ensemble simulation of the atmospheric radionuclides discharged by the Fukushima nuclear accident. *Geophys. Res. Abstracts*, 15, EGU2013-1695. (available online at http://meetingorganizer.copernicus.org/EGU2013/EGU2013-1695.pdf)

Sekiyama, T. T., M. Kunii, M. Kajino, and T. Shimbori, 2015: Horizontal resolution dependence of atmospheric simulations of the Fukushima nuclear accident using 15-km, 3-km, and 500-m grid models. *J. Meteor. Soc. Japan*, **93**, 49–64.

Shao, Y., 2000: Physics and Modelling of Wind Erosion. *Kluwer Academic Pub.*, Dordrecht, pp. 268–270.

Shimbori, T., Y. Aikawa, and N. Seino, 2009: Operational implementation of the tephra fall forecast with the JMA mesoscale tracer transport model. *CAS/JSC WGNE Res. Act. Atmos. Ocea. Model*, **39**, 05.29–05.30.

Shimbori, T., Y. Aikawa, K. Fukui, A. Hashimoto, N. Seino, and H. Yamasato, 2010: Quantitative tephra fall prediction with the JMA mesoscale tracer transport model for volcanic ash: A case study of the eruption at Asama volcano in 2009. *Pap. Met. Geophys.*, **61**, 13–29, doi:10.2467/mripapers.61.13. (in Japanese with English abstract and figure captions)

Shimbori T., R. Kai, Yo. Hayashi, Yu. Hayashi, A. Sugai, Y. Hasegawa, A. Hashimoto, A. Takagi, T. Yamamoto, and K. Fukui, 2014: Tephra fall predictions with the JMA regional atmospheric transport model: A case study of the eruptions at Shinmoe-dake volcano in 2011. *Pap. Met. Geophys.*, **65**, 75–107, doi:10.2467/mripapers.65.75. (in Japanese with English abstract and figure captions)

Shoji, Y, 2009: A study of near real-time water vapor analysis using a nationwide dense GPS network

of Japan. *J. Meteor. Soc. Japan*, **87**, 1–18.

Skamarock, W. C., J. B. Klemp, J. Dudhia, D. O. Jill, D. M. Barker, M. G. Duda, X. Y. Huang, W. Wang, and J. G. Powers, 2008: A description of the advanced research WRF version 3. *Tech. Note, NCAR/TN-475+STR*, 125 pp., Natl. Cent. For Atmos. Res., Boulder, Colo.

Smith, A. R., K. J. Thomas, E. B. Norman, D. L. Hurley, B. T. Lo, Y. D. Chan, P. V. Guillaumon, and B. G. Harvey, 2014: Measurements of fission products from the Fukushima Daiichi incident in San Francisco Bay Area air filters, automobile filters, rainwater, and food. *J. Environ. Protect.*, **5**, 207–221.

Solazzo, E., and S. Galmarini, 2015: The Fukushima-Cs137deposition case study: properties of the Multi-Model ensemble. *J. Environ. Radioact.*, **139**, 226–233.

Sportisse, B., 2007: A review of parameterizations for modelling dry deposition and scavenging of radionuclides. *Atmos. Environ.*, **41**, 2683–2698.

Stohl, A., M. Hittenberger, and G. Wotawa, 1998: Validation of the Lagrangian particle dispersion model FLEXPART against large-scale tracer experiment data. *Atmos. Environ*. **32**, 4245–4264.

Stohl, A., C. Forster, A. Frank, P. Seibert, and G. Wotawa, 2005, Technical note: The Lagrangian particle dispersion model FLEXPART version 6.2. *Atmos. Chem. Phys.*, **5**, 2461–2474.

Stohl, A., P. Seibert, G. Wotawa, D. Arnold, J. F. Burkhart, S. Eckhardt, C. Tapia, A. Vargas, and T. J. Yasunari, 2012: Xenon-133 and caesium-137 releases into the atmosphere from the Fukushima Dai-ichi nuclear power plant: determination of the source term, atmospheric dispersion, and deposition. *Atmos. Chem. Phys.*, **12**, 2313–2343.

Sugiyama, G., J. Nasstrom, B. Pobanz, K. Foster, M. Simpson, P. Vogt, F. Aluzzi, and S. Homann, 2012: Atmospheric dispersion modeling: challenges of the Fukushima Daiichi response. *Health Phys.*, **102**, 493–508.

Suzuki, T., 1983: A theoretical model for dispersion of tephra: Arc Volcanism: Physics and Tectonics, D. Shimozuru and I. Yokoyama, Eds., *TERRAPUB*, Tokyo, pp. 95–113.

Takano, I., Y. Aikawa, and S. Gotoh, 2007: Improvement of photochemical oxidant information by applying transport model to oxidant forecast. *CAS/JSC WGNE Res. Act. Atmos. Ocea. Model*., **37**, 05.35–05.36.

Takemura, T., H. Nakamura, M. Takigawa, H. Kondo, T. Satomura, T. Miyasaka, and T. Nakajima, 2011: A numerical simulation of global transport of atmospheric particles emitted from the Fukushima Daiichi Nuclear Power Plant. *SOLA*, **7**, 101–104.

Takigawa, M., H. Nagai, Y. Morino, T. T. Sekiyama, H. Hayami, T. Tanaka, T. Nakajima, and T. Shibata, 2013: International intercomparison of atmospheric simulations of radionuclides. *Proceedings, the 54th Annual Meeting of Japan Society for Atmospheric Environment*, 136 p. (in Japanese)

Tanaka, T. Y., and M. Chiba, 2005: Global simulation of dust aerosol with a chemical transport Model, MASINGAR. *J. Meteor. Soc. Japan*, **83A**, 255–278.

Tanaka, T. Y., K. Orito, T. T. Sekiyama, K. Shibata, M. Chiba, and H. Tanaka, 2003: MASINGAR, a

global tropospheric aerosol chemical transport model coupled with MRI/JMA98 GCM: Model description. *Pap. Met. Geophys.*, **53**, 119–138, doi:10.2467/mripapers.53.119.

Tanaka, T. Y., M. Kajino, T. Maki, T. T. Sekiyama, Y. Igarashi, M. Chiba, and M. Mikami, 2012: Numerical simulation of atmospheric transport of radionuclides in Meteorological Research Institute. Japan Geoscience Union Meeting 2012.

Terada, H., and M. Chino, 2008: Development of an atmospheric dispersion model for accidental discharge of radionuclides with the function of simultaneous prediction for multiple domains and its evaluation by application to the Chernobyl nuclear accident. *J. Nucl. Sci. Technol.*, **45**, 920–931.

Terada, H., H. Nagai, A. Furuno, T. Kakefuda, T. Harayama, and M. Chino, 2008: Development of Worldwide Version of System for Prediction of Environmental Emergency Dose Information: WSPEEDI 2nd version. *Trans. At. Energy Soc. Japan*, **7**, 257–267. (in Japanese with English abstract)

Terada, H., G. Katata, M. Chino, and H. Nagai, 2012: Atmospheric discharge and dispersion of radionuclides during the Fukushima Dai-ichi Nuclear Power Plant accident. Part II: verification of the source term and analysis of regional-scale atmospheric dispersion. *J. Environ. Radioact.*, **112**, 141–154.

Torii, T., Y. Sanada, T. Sugita, A. Kondo, Y. Shikaze, M. Takahashi, M. Ishida, Y. Nishizawa, and Y. Urabe, 2012: Investigation of radionuclide distribution using aircraft for surrounding environmental survey from Fukushima Dai-ichi Nuclear Power Plant. *JAEA-Technologoy 2012-036*, Japan Atomic Energy Agency, 182 pp. (in Japanese with English abstract)

Uliasz, M., 1990: Development of the mesoscale dispersion modeling system using personal computers. Part I: Models and computer implementation. *Z. Meteor*., **40**, 110–120.

UNSCEAR, 2013: Report of the United Nations Scientific Committee on the Effects of Atomic Radiation to the General Assembly. 17 pp. (available online at http://www.unscear.org/docs/reports/2013/13-85418_Report_2013_GA_Report.pdf)

UNSCEAR, 2014: Levels and effects of radiation exposure due to the nuclear accident after the 2011 great east-Japan earthquake and tsunami. *UNSCEAR 2013 Report, Vol. 1, Scientific Annex A.* 321 pp. (available online at http://www.unscear.org/docs/reports/2013/13-85418_Report_2013_Annex_A.pdf)

USDOE, 2011: US DOE/NNSA Response to 2011 Fukushima Incident, *United States Department of Energy*. (available online at https://explore.data.gov/d/prrn-6s35)

Webster, H. N., and D. J. Thomson, 2011: Dry deposition modeling in a Lagrangian dispersion model. *Int. J. Environ. Pollut.*, **47**, 1–9.

Webster, H. N., D. J. Thomson, B. T. Johnson, I. P. C. Heard, K. Turnbull, F. Marenco, N. I. Kristiansen, J. Dorsey, A. Minikin, B. Weinzierl, U. Schumann, R. S. J. Sparks, S. C. Loughlin, M. C. Hort, S. J. Leadbetter, B. J. Devenish, A. J. Manning, C. S. Witham, J. M. Haywood, and B. W. Golding, 2012: Operational prediction of ash concentrations in the distal volcanic cloud from

the 2010 Eyjafjallajökull eruption. *J. Geophys. Res.*, **117**, D00U08, 17pp, doi:10.1029/2011JD016790.

WGMSJ (Working Group on Emergency Response to Atmospheric Dispersion of Accidental Release of Radioactive Materials, Meteorological Society of Japan), 2014: Utilization of numerical prediction of atmospheric dispersion of accidentally released radioactive materials (in Japanese, available online at http://www.metsoc.jp/default/wp-content/uploads/2014/12/teigen-201412.pdf)

Wilson, J. D., F. J. Ferrandino, and G. W. Thurtell, 1989: A relationship between deposition velocity and trajectory reflection probability for use in stochastic Lagrangian dispersion models. *Agric. For. Meteor.*, **47**, 139–154.

Winiarek, V., M. Bocquet, O. Saunier, and A. Mathieu, 2012: Estimation of errors in the inverse modeling of accidental release of atmospheric pollutant: Application to the reconstruction of the cesium-137 and iodine-131 source terms from the Fukushima Daiichi power plant. *J. Geophys. Res.*, **117**, D05122, 16 pp, doi:10.1029/2011JD016932.

Winiarek, V., M. Bocquet, N. Duhanyan, Y. Roustan, O. Saunier, and A. Mathieu, 2014: Estimation of the caesium-137 source term from the Fukushima Daiichi nuclear power plant using a consistent joint assimilation of air concentration and deposition observations. *Atmos. Environ.*, **82**, 268–279.

WMO, 2010: Manual on the Global Data-processing and Forecasting System. WMO, **485**.

WMO, 2011, Final report of the Meeting of the WMO Task Team on Meteorological Analyses for Fukushima Daiichi Nuclear Power Plant Accident, Geneva, Switzerland, 30 November – 2 December 2011. 27 pp. (available online at http://www.wmo.int/pages/prog/www/CBS-Reports/documents/FinalRep_TT_FDnpp_v6.pdf)

WMO, 2012a, Final report of the Second Meeting of the WMO Technical Task Team on Meteorological Analyses for Fukushima-Daiichi Nuclear Power Plant Accident, London, UK , 1 – 3 May 2012. 13 pp. (available online at http://www.wmo.int/pages/prog/www/CBS-Reports/documents/FinalReport_TTMetAnalyFDnpp.pdf)

WMO, 2012b, Final report of the Third Meeting of the WMO Technical Task Team on Meteorological Analyses for Fukushima-Daiichi Nuclear Power Plant Accident, Vienna, Austria , 3 – 5 December 2012. 76 pp. (available online at http://www.wmo.int/pages/prog/www/CBS-Reports/documents/FINAL-REPORT-Vienna-Dec2012.pdf and http://www.wmo.int/pages/prog/www/CBS-Reports/documents/WMO_fnpp_final_AnnexIII_4Feb2013_REVISED_17June2013.pdf)

Wotawa, G., L.-E. De Geer, P. Denier, M. Kalinowski, H. Toivonen, R. D'Amours, F. Desiato, J.-P. Issartel, M. Langer, P. Seibert, A. Frank, C. Sloan, and H. Yamazawa, 2002: Atmospheric transport modeling in support of CTBT verification—overview and basic concepts. *Atmos. Environ.*, doi:10.1016/S1352-2310(03)00154-7.

Wotawa, G., R. Draxler, D. Arnold, S. Galmarini, M. Hort, A. Jones, S. Leadbetter, A. Malo, C.

Maurer, G. Rolph, K. Saito, R. Servranckx, T. Shimbori, and E. Solazzo, 2013: Transport and deposition of radionuclides after the Fukushima nuclear accident: international model inter-comparison in the framework of a WMO Task Team. *Geophys. Res. Abstracts*, **15**, EGU2013-3193. (available online at http://meetingorganizer.copernicus.org/EGU2013/EGU2013-3193.pdf)

Yamazawa, H., A. Furuno, and M. Chino, 1998: Evaluation of a long-range Lagrangian dispersion model with ETEX. *Atmos. Environ.*, **32**, 4343–4349.

Yasunari, T. J., A. Stohl, R. S. Hayano, J. F. Burkhart, S. Eckhardt, and T. Yasunari, 2011: Cesium-137 deposition and contamination of Japanese soils due to the Fukushima nuclear accident. *Proc. Natl. Acad. Sci.*, **108**, 19530–19534.

Yukimoto, S., H. Yoshimura, M. Hosaka, T. Sakami, H. Tsujino, M. Hirabara, T. Y. Tanaka, M. Deushi, A. Obata, H. Nakano, Y. Adachi, E. Shindo, S. Yabu, T. Ose, and A. Kitoh, 2011: Meteorological Research Institute-Earth System Model Version 1 (MRI-ESM1) ―Model Description―. *Tech. Rep. MRI*, **64**, 88 pp, doi:10.11483/mritechrepo.64.

Yukimoto, S., Y. Adachi, M. Hosaka, T. Sakami, H. Yoshimura, M. Hirabara, T. Y. Tanaka, E. Shindo, H. Tsujino, M. Deushi, R. Mizuta, S. Yabu, A. Obata, H. Nakano, T. Koshiro, T. Ose, and A. Kitoh, 2012: A New Global Climate Model of the Meteorological Research Institute: MRI-CGCM3 ―Model Description and Basic Performance―. *J. Meterol. Soc. Japan*, **90A**, 23–64.

I. Appendix

I-1. Final report of the first meeting of WMO Task Team (Geneva, Switzerland, 30 November - 2 December 2011)

I-2. Final report of the second meeting of WMO Task Team (London, UK, 1 - 3 May 2012)

I-3. Final report of the third meeting of WMO Task Team (Vienna, Austria, 3 - 5 December 2012)

WORLD METEOROLOGICAL ORGANIZATION

COMMISSION FOR BASIC SYSTEMS

MEETING OF THE WMO TASK TEAM ON METEOROLOGICAL ANALYSES FOR FUKUSHIMA DAIICHI NUCLEAR POWER PLANT ACCIDENT

GENEVA, SWITZERLAND, 30 NOVEMBER – 2 DECEMBER 2011

FINAL REPORT

Kazuo Saito, Alice Soares, Roland Draxler, Matthew Hort, Geoff Love, Peter Chen, Gerhard Wotawa

EXECUTIVE SUMMARY

The first meeting of WMO Technical Task Team (TT) on Meteorological Analyses for Fukushima Daiichi NPP accident took place at the WMO Headquarters, in Geneva, Switzerland, from 30 November to 2 December 2011. The TT's work is to examine how the use of meteorological analyses, and the introduction of additional meteorological observational data, could improve the atmospheric transport, dispersion and deposition calculations as validated against radiological monitoring data, which at a minimum should contribute to the requirements which the United Nations Scientific Committee on the Effects of Atomic Radiation (UNSCEAR) stated in its request for assistance from WMO. At the same time, this work should contribute to the review and possible enhancements to the nuclear emergency response system, presently in place.

The TT reviewed and adopted its Terms of Reference, and reported on each of its terms, including: (a) meteorological observational data, (b) meteorological NWP analyses data, (c) gaps in the meteorological analyses, (d) meteorological conditions during the nuclear accident, (e) evaluation of the observational data and analyses, (f) uncertainty of the atmospheric dispersion and deposition calculations, (g) liaison with UNSCEAR, (h) proposal fro enhancements of the WMO EER system. Mr Roland Draxler (RSMC Washington, USA) is named as the Chairperson of the TT.

The TT agreed to focus its work on the period 11 March to 20 April 2011. It developed a bibliography of relevant publications and presentations, stated its current point of view regarding arrangements for sharing of information, and agreed a tentative work plan to the planned completion of the final UNSCEAR study in 2013.

GENERAL SUMMARY OF THE WORK OF THE SESSION

1. Opening

1.1 The first meeting of the Technical Task Team (TT) on Meteorological Analyses for Fukushima Daiichi NPP Accident was opened by Dr Geoffrey Love, Director of the WMO Weather and Disaster Risk Reduction Services Department, on behalf of the Secretary-General of WMO. He expressed appreciation to the experts and their respective organizations for agreeing to contribute to this important work. He noted that while the WMO Environmental Emergency Response (EER) system responded well to the NPP accident during the response phase with real-time meteorological systems, including meteorological analyses and forecasts, and atmospheric dispersion predictions, the current task is to examine how the use of meteorological analyses and the introduction of additional meteorological observational data could improve the atmospheric dispersion calculations as validated against radiological monitoring data. The work of the TT should at a minimum contribute to the requirements which the United Nations Scientific Committee on the Effects of Atomic Radiation (UNSCEAR) has stated in its request for assistance from WMO. At the same time, this work should contribute to the review and possible enhancements to the EER system, which was essentially designed following the Chernobyl nuclear accident of 25 years ago.

2. Adopting of agenda and working arrangements

2.1 Mr Peter Chen of the Secretariat, introduced the Expanded Provisional Agenda, and suggested to the meeting to consider who could act as Chairperson for the Task Team. Mr Roland Draxler (USA), with the unanimous agreement of the participants, agreed to chair the TT and this first meeting.

2.2 The meeting revised and adopted the agenda, which is found in Annex I.

2.3 The list of participants is found in Annex II. The meeting was informed that Mr René Servranckx (Canada), Chairperson of the CBS Coordination Group for Nuclear Emergency Response Activities, had notified the Secretariat that he was unable to attend this meeting.

3. Introduction

3.1 The Secretariat provided background information related to the work of the TT, in particular the request of UNSCEAR to participate in its study on the levels and effects of the radiation released from the nuclear accident at the Fukushima Daiichi NPP.

3.2 This report adopted the acronym “ATM” to refer to “atmospheric transport, dispersion and deposition modelling”, including the numerical simulation systems, and their outputs.

4. Terms of Reference

4.1 The meeting reviewed and revised the TT’s draft Terms of Reference, which is found in Annex III.

5. Relevant period of interest

5.1 Although most of the known atmospheric emissions occurred in the last half of March 2011, the meeting noted that it was difficult to predict the future evaluations that will be performed and that the meteorological data requirements should cover a period from the time of the earthquake - tsunami until the situation had stabilized, 11 March through 20 April, 2011.

5.2 Discharges into the ocean may have occurred over a different time period. Therefore meteorological data may be required by the ocean modeling groups (marine dispersion experts) for a longer period. Other UNSCEAR groups, such as those studying land contamination, may also

require data for longer periods. Clarification is needed from the relevant groups. At this point no request was made to the Japan Meteorological Agency (JMA) or other meteorological services, regarding data provision for a more extensive period.

6. Response to the Terms of Reference (ToR)

(a) Meteorological observational data

a.1 The meeting reviewed the meteorological observational data, including from surface, upper-air radiosonde, upper-air wind profiler data, collected by JMA as summarized by K. Saito in Annex IV and determined that all of the data are potentially useful in evaluating the meteorological analyses, and any subsequent dispersion and deposition calculations using the analysis data, and possibly for use by other groups involved in the UNSCEAR assessment. It was proposed that the observational data be supplied in their native JMA binary format along with a description of this format. The archive location is to be determined after consultation with UNSCEAR data working group.

a.2 The meeting agreed that perhaps the most critical element in the deposition calculations was getting the precipitation correct. In this aspect, JMA agreed to provide their Radar/Rain Gauge analyzed precipitation fields available every 30 minutes at 1-km resolution (latitude-longitude, LL, grid), in GRIB2, as summarized by K. Saito in Annex IV.

(b) Meteorological NWP Analyses Data

b.1 The meeting reviewed the meteorological NWP analysis data created by JMA as summarized by K. Saito in Annex V and determined that:

- The 4D-VAR mesoscale analysis, including surface, at 3-hour intervals and 5-km 50-hybrid level resolution (Lambert Conformal, LM, projection), would be the most suitable for local and regional scale atmospheric transport, dispersion and deposition modeling (ATM).
- In addition hourly analysis data from the JMA nowcasting model (3D-Var) (LM projection / 5-km resolution / hourly / GRIB2 / U V T, including AWS data) would also be useful for certain studies.

b.2 JMA has agreed to reprocess these data sets from their internal archive format to GRIB2. The data will remain in the native Lambert Conformal horizontal coordinates on the original model levels.

b.3 Initially these data would be provided to Task Team participants for evaluation purposes and subsequently to UNSCEAR after consultation with their data working group. The archive location is to be determined after consultation with UNSCEAR data working group.

b.4 Although other groups are also creating high resolution meteorological analyses, it is uncertain whether these analyses can approach the level of observational data assimilated by the JMA products. However, other mesoscale analyses could possibly be used in the assessment of uncertainty limits to the critical meteorological fields and their inclusion into any future data archive is encouraged.

b.5 With respect to the global analyses fields, i.e. JMA (Japan), Met Office (UK), NOAA (US), CMC (Canada), and ECMWF (to be provided by ZAMG, Austria) agreed to make their model fields available, initially from their respective centers, but potentially at a common repository after consultation with UNSCEAR. See Annex V.

(c) Gaps in the meteorological analyses

c.1 The meeting agreed that it was difficult to determine what is required to improve the analyses used for the dispersion calculations prior to actually having evaluated these data in any

detail. However, one obvious problem emerged in the discussion that the long-range results were very sensitive to precipitation fields and the dispersion model scavenging coefficients.

c.2 NOAA provides estimated precipitation fields derived from CMORPH, see: (http://www.cpc.ncep.noaa.gov/products/janowiak/cmorph.shtml), and ftp://ftp.cpc.ncep.noaa.gov/precip/global_CMORPH/30min_8km/

CMORPH is a technique for generating global precipitation analyses at very high spatial and temporal resolutions (8-km horizontal resolution at hourly intervals) using precipitation estimates that have been derived from low orbiter satellite microwave observations, but there are known retrieval issues over land, problems with frozen precipitation and limitations in orbital coverage. Mr Draxler agreed to investigate their availability and provide these data to the Task Team and UNSCEAR.

c.3 The CMORPH data as well as similar global datasets could potentially be used by ATMs to better represent the precipitation encountered by the plume for long range studies. However, the value of these data has not been tested for atmospheric deposition applications, considering their known limitations.

(d) Meteorological conditions during the nuclear accident

d.1 The meeting reviewed a summary of the meteorological conditions in East Japan for the March 11-26 (2011) period, provided by K. Saito (see Annex VI for an extended discussion). He noted that the primary contribution to the Japan land areas may have occurred within two periods: March 15-16 and March 20-23. The meeting discussed that a preliminary report to UNSCEAR (May 2012) could incorporate an expanded discussion of these events building upon the material already provided by JMA.

(e) Evaluation of the observational data and analyses

e.1 The meeting discussed how the suitability of the existing meteorological analyses for ATM calculations could be assessed. The meeting assumed that these calculations would primarily rely upon the meteorological analyses produced by major weather centres rather than the meteorological observations. The meeting decided that the best approach would be to compare radiological plume calculations based upon the different analyses with each other and meteorological and radiological observations. This can be achieved through comparison of predicted and measured patterns or correlations which do not rely upon exact knowledge of the radiological source term beyond what is already established.

e.2 The WMO Secretariat will arrange with CTBTO for radiological measurement data availability and sharing under the framework of cooperation with UNSCEAR. In this context, the task team members assume that radiological data obtained by UNSCEAR will be available to the team for the support task as well as any scientific papers that result from these evaluations.

e.3 The meeting agreed that the mesoscale analysis provided by JMA (see b.1) would be used to run their ATM calculations in addition to their existing simulations with global analyses (ECMWF, NCEP, CMC, Met Office UK). Because wet deposition was recognized as a major source of uncertainty, consideration will be given on how to best use the JMA high resolution precipitation analysis (1-km, 30-min).

e.4 The chairperson presented to the meeting a possible framework for conducting the ATM simulations independent of any emission assumptions. The computational scheme was based upon creating multiple ATM runs for specific time intervals using a unit emission rate that can later be multiplied with any time varying emission scenario without having to rerun the ATMs. The meeting agreed to use this framework as a reference and produce output fields in accordance with the scheme. Technical details are provided by the chairperson, included in Annex VII. Mr Draxler

also agreed to host a web page (see: http://ready-testbed.arl.noaa.gov/READY_fdnpp.php for a prototype) that will include the modeling results from the other participants.

e.5 The meeting discussed possible ways to evaluate the different ATM results against the measurements. It was agreed that the DATEM framework (http://www.arl.noaa.gov/DATEM.php) created by NOAA would be the most efficient approach to perform this comparison. ZAMG agreed to convert the radiological measurement data to the DATEM format, and NOAA agreed to investigate how these measurement data could be incorporated into the computational framework.

(f) Uncertainty of the atmospheric dispersion and deposition calculations

f.1 The meeting discussed the various uncertainties involved in the calculation of dispersion and deposition. Although suitable meteorological analysis data sets have been identified, there will always be some uncertainty regarding the meteorological parameters at any one point in space and time because the data analysis fields are snapshots in time which are averaged over grid cells with underlying complex terrain. Most of the time, the prevailing flow direction was offshore away from the existing land-based monitoring network. The remaining significant releases with on-shore flow were related to complex meteorological situations (see Section 6 (d)) with rapidly changing wind direction and variable precipitation patterns. Model derived wet deposition calculations carry large uncertainties and therefore observed precipitation fields need to be incorporated into the calculations.

f.2 The meeting proposed the use of the results from the framework discussed in the previous section to address uncertainties described above. The framework allows for the comparison of multiple model results either with different meteorological analyses using the same ATM model or, the same meteorological analysis using different ATMs. This would provide an estimate of the range of possible air concentration and deposition values,

(g) Liaison with UNSCEAR

g.1 The meeting noted that the proposed modeling framework did not require a precise knowledge of the emissions and in fact could be used by UNSCEAR to optimize the emissions to match the measurement data. However for certain model comparisons, it would be desirable to have an estimate of the temporal variation of the emissions. The Task Team would rely upon advice from UNSCEAR source term group to propose a scenario that can be used for meteorological model evaluations.

g.2 As was already discussed in the previous section, the most appropriate way to evaluate meteorological analyses in this case is to compare the ATM outputs based upon these analyses with radiological measurement data. In that aspect, the Task Team would rely upon the UNSCEAR data group to provide access to the appropriate measurement data.

g.3 The group agreed to provide UNSCEAR access to the model comparison framework and/or to the individual ATM calculations.

g.4 The working arrangements between UNSCEAR Expert Group B and the WMO Task Team will initially be coordinated through the chairpersons from each group. However, it is expected that the groups would meet as needed to discuss technical issues, either through Telecon or Webex meetings if possible.

(h) Proposal for enhancements of the WMO EER system

h.1 The meeting agreed that the results of the Task Team are important in the consideration of future EER products and services.

7. Bibliography

Source Estimation

- Chino, M. et al., 2011. Preliminary Estimation of Release Amounts of 131 I and 137 Cs Accidentally Discharged from the Fukushima Daiichi Nuclear Power Plant into the Atmosphere. *Journal of NUCLEAR SCIENCE and TECHNOLOGY*, 48(7), pp.1129–1134.
- Stohl, A. et al., 2011. Xenon-133 and caesium-137 releases into the atmosphere from the Fukushima Dai-ichi nuclear power plant: determination of the source term, atmospheric dispersion and deposition. *Atmos. Chem. Phys. D.*

Radiological Observations

- Masson, O. et al., 2011. Tracking of Airborne Radionuclides from the Damaged Fukushima Dai-Ichi Nuclear Reactors by European Networks. *Environmental Science & Technology*, 45(18), pp.7670–7677.
- Tagami, K. et al., 2011. Specific activity and activity ratios of radionuclides in soil collected about 20km from the Fukushima Daiichi Nuclear Power Plant: Radionuclide release to the south and southwest. *Science of the Total Environment*, 409(22), pp.4885–4888.
- Kinoshita, N. et al., 2011. Assessment of individual radionuclide distributions from the Fukushima nuclear accident covering central-east Japan. *Proceedings of the National Academy of Sciences*.

Dispersion and Deposition Modeling

- Yasunari, T. et al., 2011. Cesium-137 deposition and contamination of Japanese soils due to the Fukushima nuclear accident. In *Proceedings of the National Academy of Sciences*. Proceedings of the National Academy of Sciences.

Presentations

- *EUROSAFE Forum 2011, Brussels, November 5th to 6th, 2012. http://www.eurosafe-forum.org/eurosafe-forum-2011*
- *Presentations at the special session "Current status and subjects of the radionuclide transport models" at the autumn meeting of the Meteorological Society of Japan (MSJ, http://msj.visitors.jp/notification/pdf/A2011oral_20110909.pdf), including:*

    - Tanaka, T. et al., Global transport model using MASINGAR.
    - Kajino, M. et al., MRI regional chemical transport model using NHM-Chem.
    - Maki, T. et al., Emission flux estimation by inverse model.
    - Tsuruta, H. et al., Regional Deposition of Radioactive Cs and I by the Accident of the Fukushima Daiichi NPP.
    - Takemi, T. and H Ishikawa, High-Resolution modeling analyses of wind and diffusion fields over Fukushima.
    - Kondo, H. et al., Transport and deposition analysis by AIST-MM.
    - Takigawa, M. et al., Deposition estimation using WRF/Chem.
    - Kato, M. et al., Transport and diffusion simulation using CReSS.

8. Arrangements for sharing information

8.1 The meeting noted that the creation of a central data repository for all meteorological and ATM products considered by the Task Team is not currently feasible. The Task Team noted that UNSCEAR would address the data repository issue in their data sharing plan.

8.2 With respect to the data, it is expected that all data collected and generated in this effort will be shared between UNSCEAR and the Task Team.

8.3 The meeting noted that all results generated by the Task Team will become publicly available, either through the web or scientific publications.

9. Work plan and timetable

16 January 2012 - Task Team Meeting Report (Draxler and Secretariat)

30 January – 3 Feb 2012 – UNSCEAR work group meeting

Week of 6 February - TT teleconference (to revise work plan and timetable)

March 2012 – sample mesoscale analysis available from JMA (Saito)

April 2012 – TT to provide preliminary ATM results for the full period (11 March to 20 April 2011) to NOAA (Draxler) in the model evaluation framework format.

23 April 2012 – TT meeting

14 May 2012 - Preliminary TT report to UNSCEAR on meteorological analyses and ATM results

21 May 2012 – 59th session UNSCEAR progress and preliminary report

June 2012 - meteorological data and NWP analyses from TT members will be ready for sharing within TT

July 2012 – ZAMG (Wotawa) to provide available measurement data in DATEM format

October 2012 – TT to complete and provide ATM results using JMA meso-analyses within TT

November 2012 – NOAA (Draxler) to provide DATEM statistical results linked with model evaluation framework

December 2012 – TT meeting

March 2013 – TT to provide draft final report on meteorological analyses and ATM results

April 2013 – Final TT report provided to UNSCEAR on meteorological analyses and ATM results

May 2013 – 60th session UNSCEAR report

10. Closing

10.1 The first meeting of the Technical Task Team (TT) on Meteorological Analyses for Fukushima Daiichi NPP Accident closed at 17:15 on Friday, 2 December 2011.

ANNEX I

Agenda

1. **Opening**
2. **Adopting of agenda and working arrangements**
3. **Introduction**
4. **Terms of Reference**
5. **Relevant period of interest**
6. **Response to the Terms of Reference (ToR)**
7. **Bibliography**
8. **Arrangements for sharing information**
9. **Work plan and timetable**
10. **Closing**

ANNEX II

List of Participants

Dr Gerhard **WOTAWA** Zentralanstalt für Meteorologie und Geodynamik (ZAMG) Hohe Warte 38 A-1191 VIENNA **Austria**	Tel: Fax: Email:	+(43 1) 36026 2007 +(43 1) 369 12 33 gerhard.wotawa@zamg.ac.at
Dr Kazuo **SAITO** Meteorological Research Institute Japan Meteorological Agency (JMA) 1-1, Nagamine, Tsukuba Ibaraki 305-0052 **Japan**	Tel: Fax: Email:	+(81 29) 853 8638 +(81 29) 853 8649 ksaito@mri-jma.go.jp
Dr Matthew **HORT** Met Office UK Fitzroy Road Exeter EX13PB Devon **United Kingdom**	Tel: Fax: Email:	(+44 1392) 886 242 (+44 1392) 885 681 matthew.hort@metoffice.gov.uk
Mr Roland **DRAXLER** Air Resources Laboratory NOAA – Office of Oceanic and Atmospheric Research SSMC3, Room 3350 1315 East-West Highway SILVER SPRING, Maryland (MD) 20910-6233 **United States of America**	Tel: Fax: Email:	+(1 301) 713 0295 ext 117 +(1 301) 713 0119 roland.draxler@noaa.gov
WMO Secretariat 7 bis avenue de la Paix Case postale 2300 1211 GENEVE 2 **Switzerland**		
Mr Peter **CHEN**	Tel: Fax: Email:	+(41 22) 730 8231 +(41 22) 730 8128 pchen@wmo.int
Ms Alice **SOARES**	Tel: Fax: Email:	+(41 22) 730 8449 +(41 22) 730 8128 asoares@wmo.int
Dr Geoffrey **LOVE**	Tel: Fax: Email:	+(41 22) 730 8264 +(41 22) 730 8128 glove@wmo.int

ANNEX III

WMO Technical Task Team on Meteorological Analyses – Fukushima Daiichi NPP Accident

Terms of Reference

Membership and Chairperson

- Roland Draxler, Chairperson (RSMC Washington, USA)
- Matthew Hort (RSMC Exeter, UK)
- Gerhard Wotawa (RSMC Vienna, Austria)
- Kazuo Saito (Meteorological Research Institute, Japan Meteorological Agency, Japan)
- René Servranckx (Chairperson of CBS Coordination Group on Nuclear ERA, RSMC Montreal, Canada)

Terms of work

(a) Determine the relevant meteorological observational data sets and related information required to support the meteorological analyses and identify their archive location and availability;

(b) Determine which of the existing meteorological analyses are of sufficient spatial and temporal detail that can be used to estimate the atmospheric transport, dispersion, and surface deposition of radionuclides that were released from the nuclear accident and identify their archive location and availability;

(c) Identify gaps in the existing meteorological analyses that if addressed would make them more suitable for estimating atmospheric transport, dispersion, and deposition and in coordination with the WMO Secretariat, identify which members will provide updated analyses;

(d) Based upon the observational data and analyses, prepare a report on the temporal and spatial variations in atmospheric conditions during the nuclear accident;

(e) Evaluate the suitability and quality of the observational data and meteorological analyses for computing atmospheric transport, dispersion, and surface deposition by comparing the computational results with radiological measurements;

(f) Estimate the uncertainty in the atmospheric transport, dispersion and deposition (ATM) computations by comparing the results from several different ATMs and using different meteorological analyses;

(g) Liaise and assist where possible with the UN Scientific Committee on the Effects of Atomic Radiation (UNSCEAR), in their study on the levels and effects of exposure due to the Fukushima Daiichi nuclear accident.

(h) Propose possible enhancements to the WMO EER system, including additional products and/or additional modes of operation with the relevant international organizations.

Duration and working arrangements

It is anticipated that the work of the Task Team would commence immediately, and span a period of 12 -18 months. The Team will work mainly by e-correspondence, and meet face-to-face, as needed. WMO Secretariat will facilitate the work of the team.

ANNEX IV

Table A4.1 - Meteorological observational data collected by JMA

Data name	Number of point	Duration	Data amount	levels	Elements
AWS (Fig. A4.1)	1300	10-minute: hourly, daily	Total amount of data 10-minute: 18GB (2003-2011) hourly & daily: 22GB (1976-2011) Shorter time periods are available	1	Precipitation amount (10-minute, hourly, daily), daily maximum precipitation (10-minute, hourly)
	800			1	temperature, wind speed/direction, sunshine duration (10-minute),
	300			1	Snow depth (hourly), snowfall depth (hourly, daily), maximum snow depth (daily)
Note of precipitation	150		16MB/month	1	Kinds of precipitation phenomenon, start/end time of the phenomenon, etc. (written in Japanese)
Radiosonde (Fig. A4.2)	16	twice a day	2MB/month	25	altitude, temperature, relative humidity, wind direction, wind speed and passing time at 25 standard level
			temperature/relative humidity: 8MB/month wind direction/speed: 5MB/month	variable	temperature/relative humidity, wind direction/speed at significant level
Wind profiler (Fig. A4.2)	31	every 10 minutes	50KB/day	variable	Wind direction, Wind speed, Vertical speed Signal to noise ratio

Table A4.2 - Precipitation analysis of radar and raingauge observations

Data name	Domain size	Map projection	Resolution	Duration	Data amount (Daily)	levels	Elements
Radar /Rain gauge-Analyzed Precipitation	2560x3360 (SW:20N 118E, NE:48N 150E)	LL	1km (0.0125x0.008333)	Twice an hour	0.375MB (18MB)	SURF	RAIN

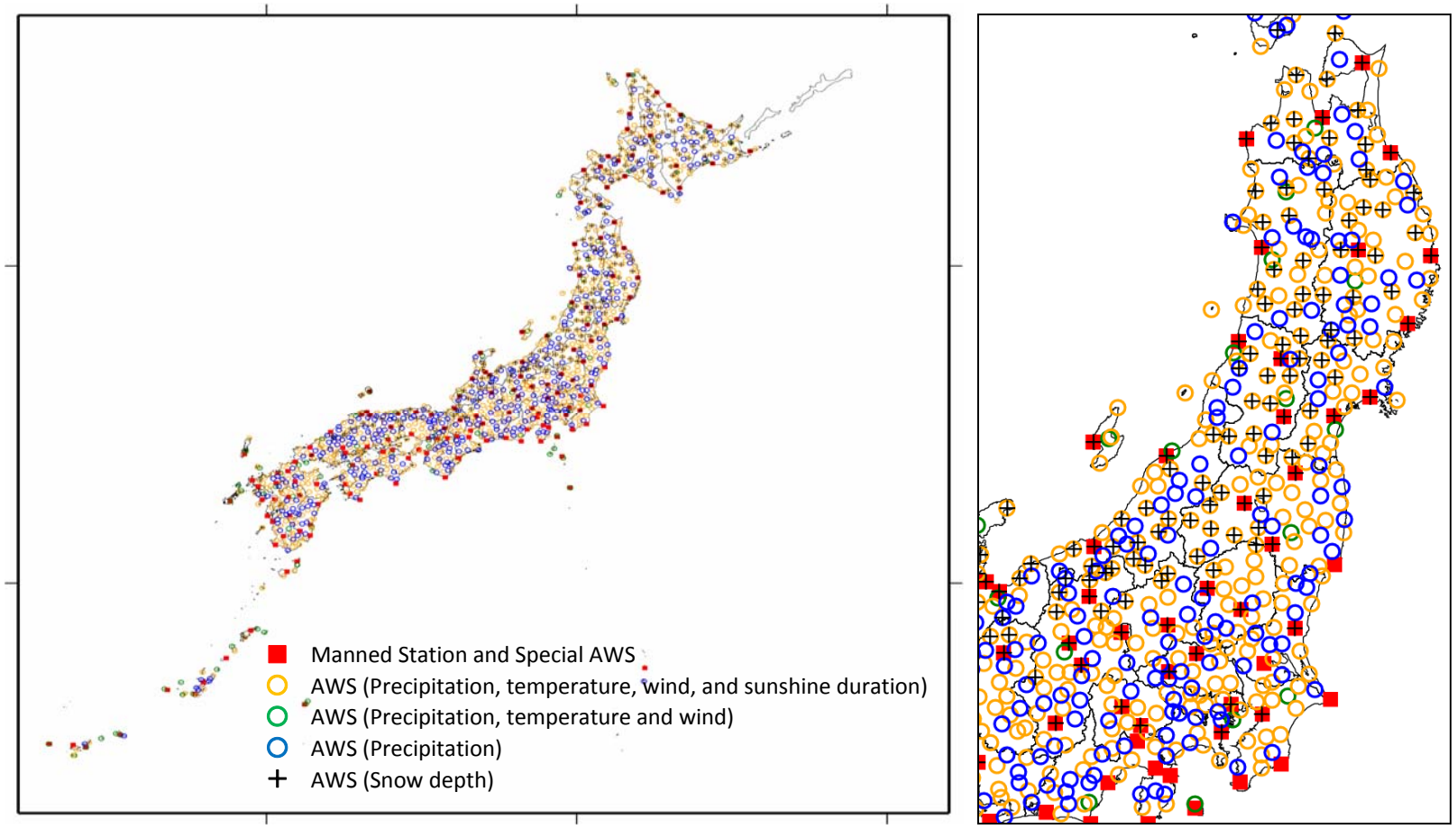

Fig. A4.1 - Left: Distribution of surface stations in Japan. Right: Enlarged view in East Japan.

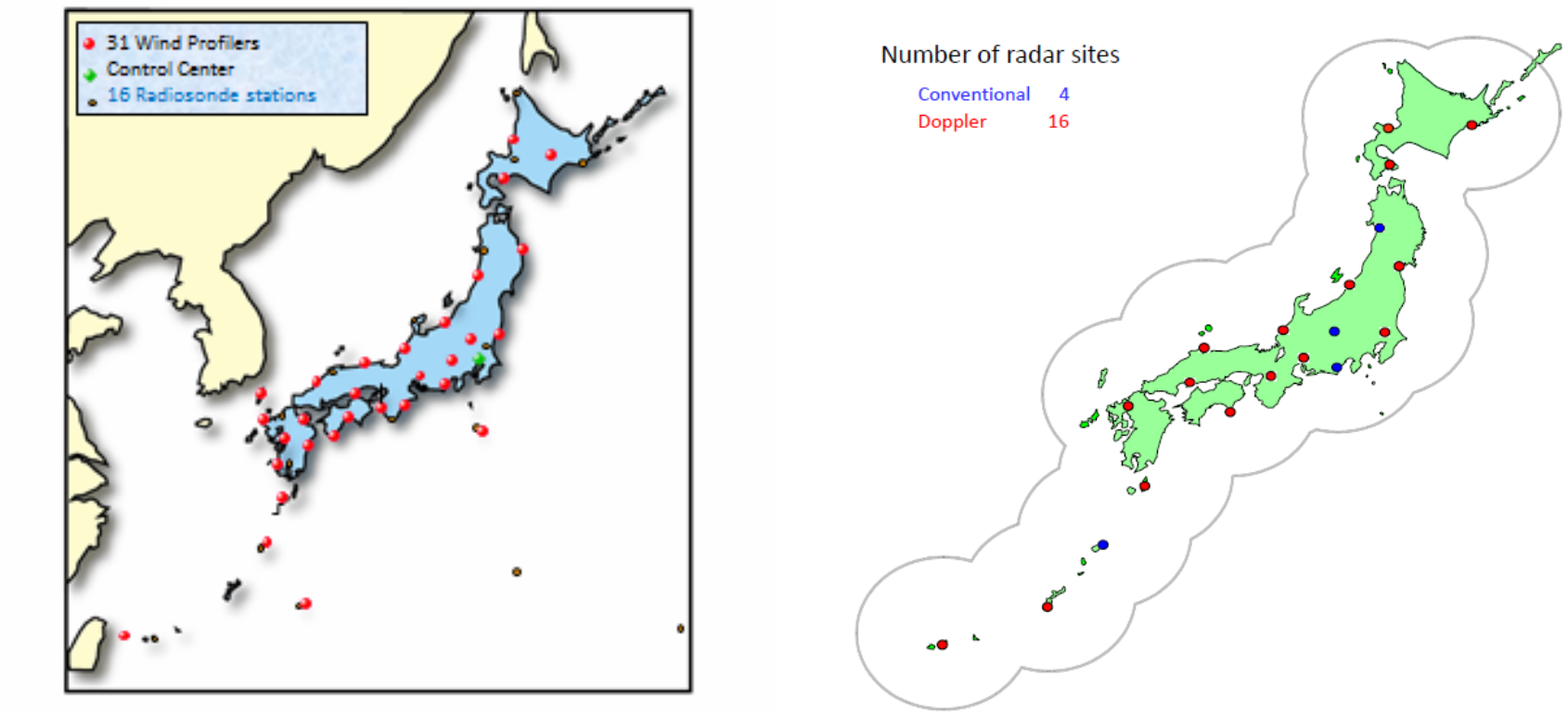

Fig. A4.2 - Left: Upper observations in Japan. Right: Radar observations by JMA.

ANNEX V

Meteorological NWP Analysis Data

Table A5.1 - Regional Meteorological NWP analysis data created by JMA

Data name	Plane	Num of layers	Method	Domain size	Map projection	Resolution	Output interval	Data amount (Daily)	Levels	Elements
Meso analysis	Model	50	4DVAR	721x577 (SW:19.66N 117.74E, NE:47.71N 156.16E)	LM (Lambert conformal)	5km	3 hourly	600MB (4800MB)	z*-z hybrid coordinate (lowest level: 20m, model top: 21.8km)	ZS SL FLAT FLON PAIRF DNSG2 RU RV RW PT TIN(4 layers) QV QC QR QCI QS QG ETURB PRS PSEA
Meso surface analysis	Surface	1		721x577 (SW:19.66N 117.74E, NE:47.71N 156.16E)	LM	5km	3 hourly	15MB (120MB)	SURF	TUGDG(4 layers) KINDG SST KIND TUGD(4 layers) JFLG HRAIN CLD TBB CVT ETOP PARM
Hourly analysis	P	17	3DVAR	721x577 (SW:19.66N 117.74E, NE:47.71N 156.16E)	LM	5km	hourly	43MB (1032MB)	SURF 1000 975 950 925 900 850 800 700 600 500 400 300 250 200 150 100	U V T

Table A5.2 - Global Meteorological NWP analysis data

Centre + Data name	Plane	Num of layers	Method	Domain size	Map projection	Resolution (Long-Lat degrees)	Output interval	Data amount (Daily)	Lowest 10 levels	Elements
JMA, Global analysis (Global)	Hybrid sigma-pressure	60 up to 0.1 hPa (16 input for ATM)	4DVAR	T_L959 (TL319 input for ATM)	LL	0.1875 (0.5625 input for ATM)	6 hourly	132MB (input for ATM)	SURF, 1000, 925, 850, 700, 600, 500, 400, 300, 250 hPa (input for ATM)	U V T Z RH OMG P(surface) PHI(surface)
ECMWF, Global analysis	Hybrid pressure	91 up to 0.01 hPa	4DVAR	T1279	LL (for standard products)	0.125 (for standard products). Fields can be requested at lower res	3 hourly	Depends on area, res and field set	1012, 1009, 1005, 1000, 993, 986, 977, 966, 954, 940 hPa (w.r.t. reference surface pressure of 1013.25 hPa)	All standard 3-d and 2-d fields required by a dispersion model + wide variety of other fields.
UK Met Office, Global UM analysis	Hybrid height above ground	70 up to 80km	4DVAR	1024 x 769	LL	0.3515625, 0.234375	3 hourly	354 Mb (12 Gb un compressed)	SURF, 10.0, 36.7, 76.7, 130.0, 196.7, 276.7, 370.0, 476.7, 596.7 m agl	3d: U, V, W, T, Q, QCL, QCF, P + variety of 2d fields
NOAA, Global analysis	Hybrid sigma-pressure	56	3DVAR	720x361	LL	0.5	3 hourly	500 MB	Delta hPa: 4, 5, 7, 8, 9,10,11,12,14,16,18	U V T Z Q + variety of 2-d surface fields
CMC, Global analysis	Eta	58	4DVAR	801 x600	LL	0.3	6 hourly	1.0 GB (for 4 cycles)	1.0 .995 .985 .9733 .9606 .9477 .9316 .9151 .8973 .8780	U V T GZ P0 HU HR ES WE + variety of surface fields
	Hybrid	80	4DVAR	801 x600	LL	0.3	6 hourly	1.6 GB (for 4 cycles)	1.0 .995 .985 .974 .961 .947 .932 .916 .898 .879	U V T GZ P0 HU HR ES WE + variety of surface fields

ANNEX VI

Meteorological conditions in East Japan for the March 11-26, 2011

1) Synoptic weather pattern:

After the passage of a weak pressure trough over East Japan from 9th to 11th a high pressure system moved eastward along the south coast of the main island of Japan from 11th to 13th. A weak low pressure system moved eastward off the south coast of the main island from 13th to 15th, and moved toward the northeast while developing rapidly after 15th. A low pressure system passed from 20th to 22nd over main island. (Fig. A6.1)

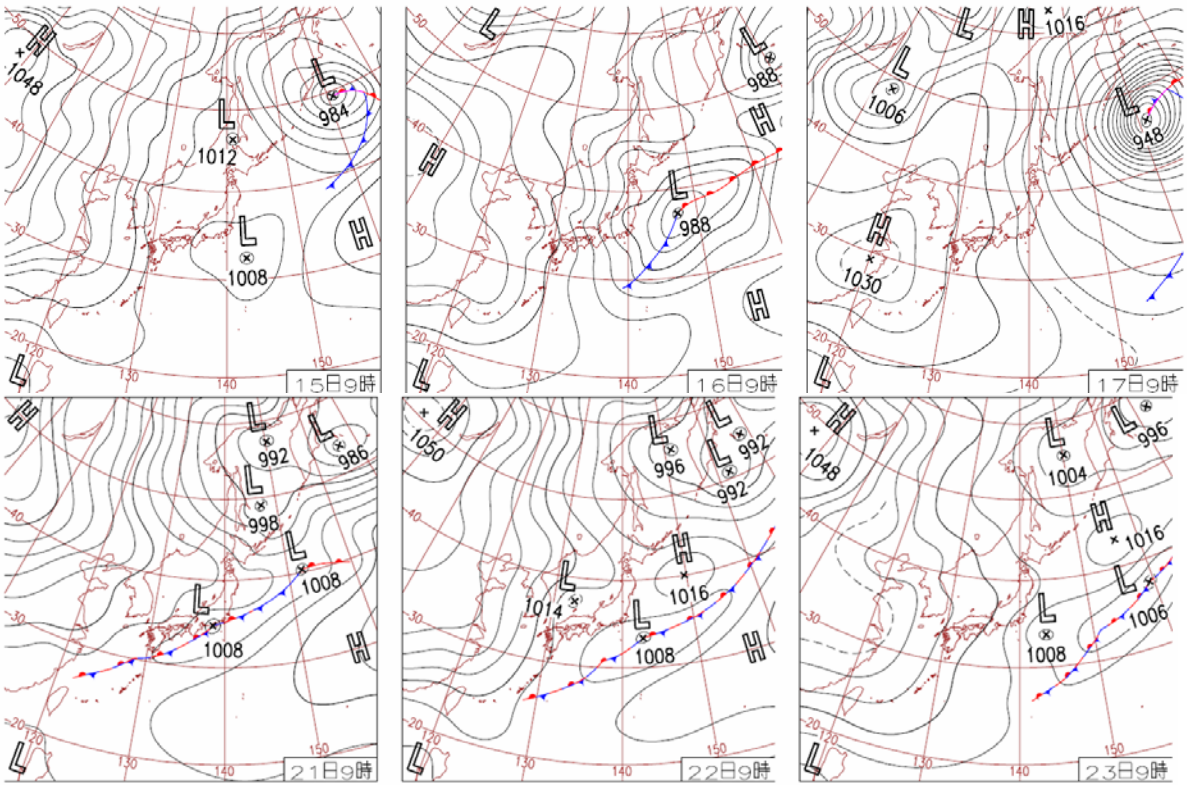

Fig. A6.1 - Surface weather chart at 0000 UTC (0900 JST) from 15 to 17 (upper) and from 21 to 23 (lower), March 2011.

2) Precipitation over east Japan:

Light rains were observed from 9th to 12th morning due to passage of a weak pressure trough over East Japan. Light rains were also observed from 15th to 17th morning due to a weak low pressure system which moved eastward off the south coast of the main. Moderate rains were given in the Kanto area from 20th to 23rd by a low pressure system which passed over the main island of Japan. (Fig. A6.2)

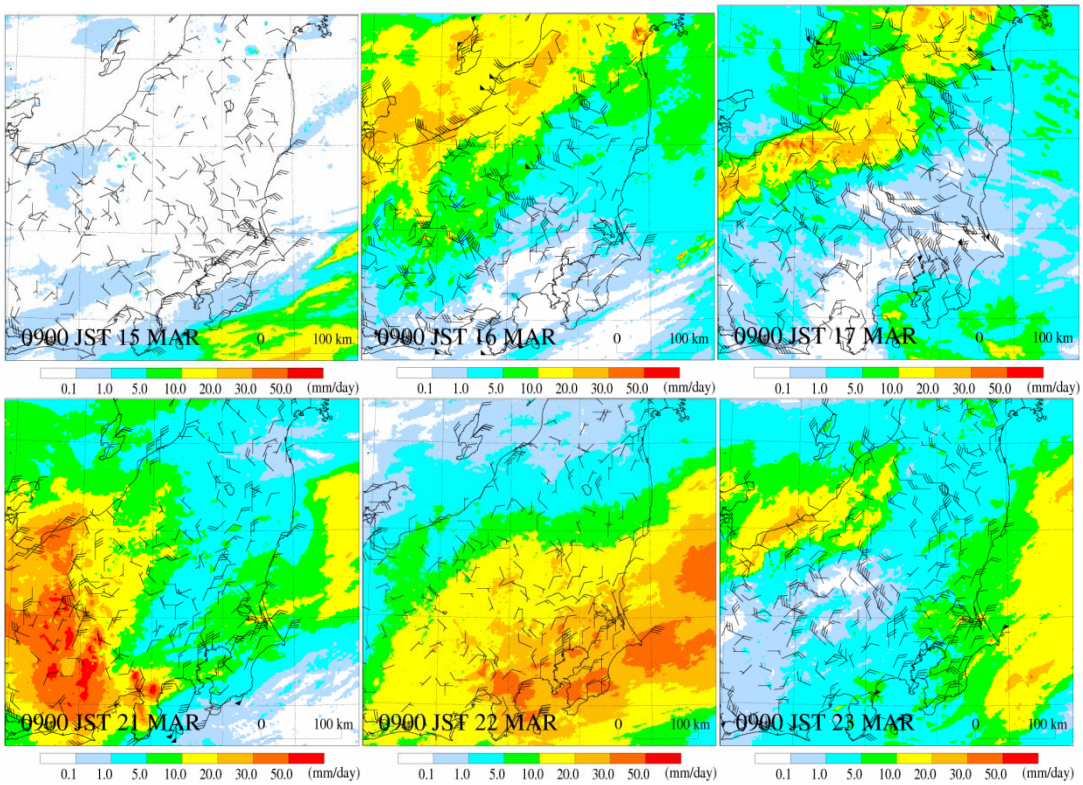

Fig. A6.2 – 24-hour accumulated precipitation amount and observed surface winds at 0000 UTC (0900 JST) for 15-17 (upper) and for 21-23 (lower), March 2011.

3) 950 hPa winds on March 15 by the mesoscale analysis of JMA:

The 950 hPa winds were westerly until the morning of 15th, but changed to NN-Easterly during the daytime of the 15th. After 1500 JST, the winds turned ES-Easterly, and then changed to Northerly after 0000 JST on the 16th (Fig. A6.3).

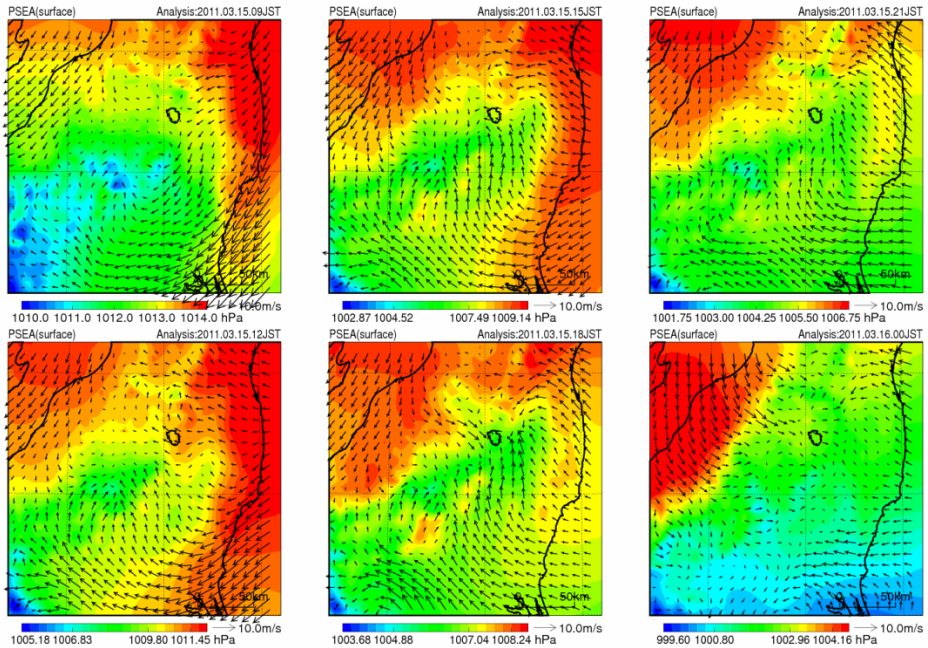

Fig. A6.3 – 950hPa winds (arrows) and mean sea level pressure (colour shade) by mesoscale analysis of JMA for 0000 UTC (0900 JST) – 1500 UTC (0000 JST), 15 March 2011.

4) Winds below 7 km observed at the wind profiler (Mito) nearest to the NPP during the period March 12-20:

The wind direction was southerly below 1 km while westerly above 1 km in the afternoon of March 12 when the hydrogen explosion occurred at the No. 1 reactor. Low level wind was southwesterly during the morning of the 14th when the hydrogen explosion occurred at the No. 3 reactor. Winds below 1 km were N-Easterly during the morning of the 15th when the reactor container burst occurred at the No. 2 reactor (Fig. A6.4).

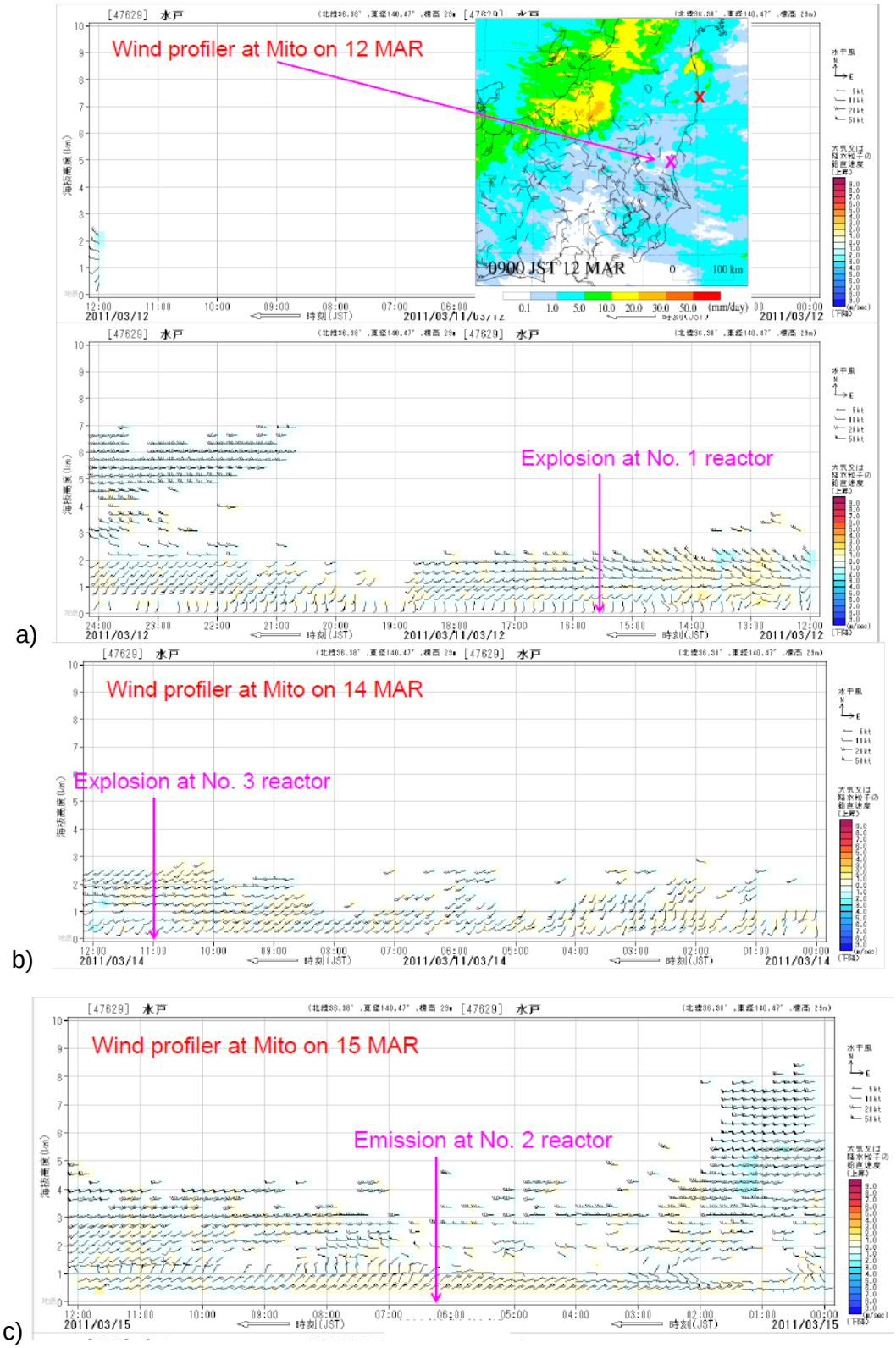

Fig. A6.4 – Time series of winds below 7 km observed by a JMA wind profiler at the nearest point (Mito). a) From 1200 JST to 2400 JST, March 14. b): From 0000 JST to 2400 JST, March 14. C) From 0000 JST to 2400

JST, 15 March. Horizontal wind direction (barbs) and vertical speed of precipitation or air (colour shade).

5) Summary

The radionuclides were dispersed due to winds and other conditions, and this has been monitored (Fig. A6.5) and confirmed by Ministry of Education and Science and Technology (MEXT). The following two periods may have been the primary contributors to the observed deposition pattern:

- Southwestward transport by northeasterly low level winds from midnight of the 14th to early morning of the 15th and northwestward transport that resulted in the high density deposition pattern during the afternoon of the 15th

- Northward transport in the afternoon of the 20th and southward transport from midnight of the 21st to the early morning of the 22nd.

Modeling results by researchers in Japan generally support the above speculation *(e.g., Yasunari et al., 2011; Kajino et al., 2011; Kondo et al., 2011; Takigawa et al., 2011; Kato et al., 2011)*, but a high deposition area over the middle of the Fukushima prefecture has not yet been well simulated.

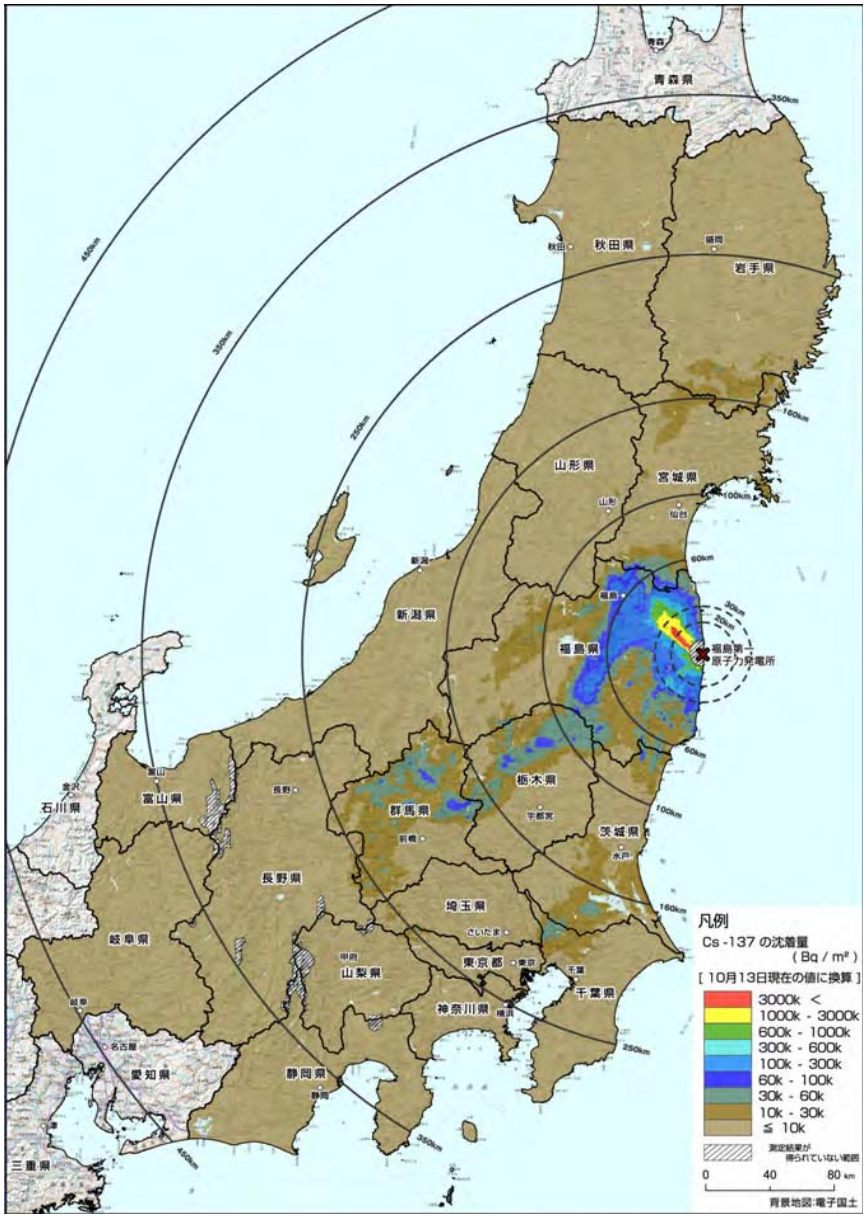

Fig. A6.5 – Regional deposition map of ^{137}Cs in surface soils observed by aircraft monitoring by MEXT (from home page of the Ministry of Education, Culture, Sports, Science and Technology (MEXT), Japan). (http://radioactivity.mext.go.jp/ja/1910/2011/11/1910_111112.pdf).

ANNEX VII

Computational Framework for the Fukushima Daiichi NPP Accident Simulations

The basic approach to the dispersion-deposition calculations to create an ATM calculation using a unit source rate (1/hr) for discreet emission time segments from the beginning to the end of the computational period. The concentration or deposition at any grid cell in the domain will be the sum of the contribution from each ATM emission segment after multiplying the resulting unit concentrations by the actual emission rate for each segment. Radioactive decay is also applied during this processing step.

- Computational period: 0000Z 11 March 2011 through 0000Z 21 April 2011
- Emission periods: 3-hour segments, 0000-0300; 0300-0600; ...
- Concentration & Deposition: 3-hour average & total, 0000-0300; 0300-0600; ...

The computational period consists of 41 days, each day has 8 emission periods, and therefore 328 independent simulations are required:

- Simulation #1: Emissions 0000Z-0300Z 11 March; Output 0000Z 11 March through 0000Z 21 April (328 output periods)
- Simulation #2: Emissions 0300Z-0600Z 11 March; Output 0300Z 11 March through 0000Z 21 April (327 output periods)
- Simulation # ...
- Simulation #328: Emissions 2100Z-0000Z 21 April; Output 2100Z 20 April through 0000Z 21 April (1 output period)

Three generic species should be tracked as surrogates for the radionuclides: a gas with no wet or dry scavenging, a gas with a relatively large dry deposition velocity and wet removal, and a particle with a small dry deposition velocity and wet removal.

Table A7.1 Summary the computational species

Type	Name	Wet Removal	Dry Deposition	Surrogate for
Gas	Ngas	No	No	Noble gases
Gas, depositing	Dgas	Yes	Yes	I-131
Particle, light	Lpar	Yes	Yes	Cs-137; I-131

The output concentration grid should be a regular spaced latitude-longitude grid where the latitude and longitude grid spacing may be different if desired. Although multiple output levels are possible, to limit the size of the output files, it is proposed that only the data from two levels and three computational species be submitted for evaluation: a level at height "0" m AGL defines the deposition, and a level at "100" represents the average concentration from the ground to 100 m AGL. Two concentration grids are suggested, one for regional simulations and one for global simulations:

Domain	Center Latitude	Center Longitude	Latitude Span	Longitude Span	Spacing Deg Lat	Spacing Deg Lon
Regional	38N	140E	20	30	0.05	0.05
Global	0	0	181	360	0.50	0.50

The file size issues can be significant. For example, a coarser resolution global calculation using a 6-hour emission frequency and a one-degree concentration grid with only one output data level resulted in a space requirement for all files of about 2 GB. For the global grid defined above, one could expect a much larger (4x horizontal, 2x vertical, 2x temporal) space requirement of about 32 GB. The regional grid is expected to require about 10 GB. Output files should be named according to the start of the release time: {Base_Name}_${MM}${DD}${HH}.

The proposed concentration file format follows the convention used by the NOAA ATM (HYSPLIT) and the resulting files would be compatible with all the current web based post-processing routines as well as numerous graphics and other output file manipulation programs available for Windows PC or Mac applications. Concentration files may be written in either packed or unpacked format. Concentration file packing does not write the same information in fewer bytes, but rather writes the same information using twice as many bytes. The packed files are generally smaller because only concentration values at the non-zero grid points are written to the output file by the model. However this requires the grid point location to be written with the concentration, hence the additional bytes. If most of the grid is expected to have non-zero concentrations, then the unpacked format will save space. The output files should be written as unformatted big-endian binary according to the following specification (a sample program will be provided):

Record #1

- CHAR*4 Meteorological *MODEL* Identification
- INT*4 Meteorological file start (*YEAR, MONTH, DAY, HOUR, FORECAST-HR*)
- INT*4 *NUMBER* of starting locations
- INT*4 Concentration packing flag (0=no 1=yes)

Record #2 Loop to record: Number of starting locations

- INT*4 Release starting time (*YEAR, MONTH, DAY, HOUR*)
- REAL*4 Starting location and height (*LATITUDE, LONGITUDE, METERS*)
- INT*4 Release starting time (*MINUTES*)

Record #3

- INT*4 Number of (*LATITUDE-POINTS, LONGITUDE-POINTS*)
- REAL*4 Grid spacing (*DELTA-LATITUDE,DELTA-LONGITUDE*)
- REAL*4 Grid lower left corner (*LATITUDE, LONGITUDE*)

Record #4

- INT*4 *NUMBER* of vertical levels in concentration grid
- INT*4 *HEIGHT* of each level (meters above ground)

Record #5

- INT*4 *NUMBER* of different pollutants in grid
- CHAR*4 Identification *STRING* for each pollutant

Record #6 Loop to record: Number of output times

- INT*4 Sample start (*YEAR MONTH DAY HOUR MINUTE FORECAST*)

Record #7 Loop to record: Number of output times

- INT*4 Sample stop (*YEAR MONTH DAY HOUR MINUTE FORECAST*)

Record #8 Loop to record: Number levels, Number of pollutant types

- CHAR*4 Pollutant type identification *STRING*
- INT*4 Output *LEVEL* (meters) of this record

No Packing (all elements)

- REAL*4 Concentration output *ARRAY*

Packing (only non-zero elements)

INT*4 Number of non-zero elements

- INT*2 First (I) index value
- INT*2 - Second (J) index value
- REAL*4 - Concentration at (I,J)
- ... repeat the above three values: times the number of non-zero elements

WORLD METEOROLOGICAL ORGANIZATION

COMMISSION FOR BASIC SYSTEMS

MEETING OF THE WMO TASK TEAM ON METEOROLOGICAL ANALYSES FOR FUKUSHIMA DAIICHI NUCLEAR POWER PLANT ACCIDENT

LONDON, UK, 1-3 MAY 2012

FINAL REPORT

Olivier Isnard, Peter Bedwell, Gerhard Wotawa, Matt Hort, Florian Gering, Roland Draxler, Peter Chen, Alain Malo, Kazuo Saito.

GENERAL SUMMARY OF THE WORK OF THE SESSION

1. Opening

1.1 The second meeting of the WMO Technical Task Team (TT) on Meteorological Analyses for Fukushima Daiichi NPP Accident was held at the offices of the Met Office UK, at Gray's Inn House, London, UK, and opened by the TT's chairperson, Mr Roland Draxler. Mr Draxler welcomed and expressed appreciation to all the participants. Mr Peter Chen, the representative of the WMO Secretariat recalled that the current task is to examine how the use of meteorological analyses and the introduction of additional meteorological observational data could improve the atmospheric dispersion calculations as validated against radiological monitoring data. The work of the TT will contribute to the requirements which the United Nations Scientific Committee on the Effects of Atomic Radiation (UNSCEAR) has stated in its request for assistance from WMO. In this regard, two experts of the UNSCEAR Study were invited to participate at this meeting: Mr Olivier Isnard of the French Institut de Radioprotection et de Sûreté Nucléaire (IRSN), and Mr Florian Gering of the German Bundesamt für Strahlenschutz (BfS). As well, UNSCEAR Study's UK experts of the Health Protection Agency, who are working in the UNSCEAR dose assessment group, were also invited to participate on one part of the agenda.

2. Adopting of agenda and working arrangements

2.1 Mr Draxler introduced the provisional agenda, which meeting adopted, and is found in Annex I.

2.2 The list of participants is found in Annex II. The meeting was informed that Mr René Servranckx (Canada), Chairperson of the CBS Coordination Group for Nuclear Emergency Response Activities, had notified the Secretariat that he was unable to attend this meeting. Instead, the work of RSMC Montréal contributing to the output of the TT was represented by Mr Alain Malo.

2.3 Daily working arrangements were agreed by the meeting.

3. Review of preliminary ATM runs for 11 – 31 March 2011

3.1 Mr Draxler provided a summary of the outcomes of the first meeting of the TT (Geneva, Dec. 2011), and also a summary of the progress made on the preliminary ATM runs for the period 11 – 31 March 2011, carried out by NOAA, JMA, Met Office UK, CMC. ZAMG (Austria) will soon provide its computations. JMA provided a regional ATM run using its high resolution mesoanalyses, while the other used their respective global analyses.

3.2 As per agreement from the first TT meeting, all members implemented the computational scheme for ATM simulations (Draxler, 2012). The meeting discussed various issues around the configuration of the ATM runs, including the source term and species, and the release height(s).

3.3 While waiting for the conclusion of the work of the UNSCEAR source term expert sub-group, these ATM runs were based on a source sequence following Chino (2011). Mr Isnard indicated that he was using a different source sequence, and agreed to provide the TT with a 3-hourly sequence of emissions and release height.

3.4 The group discussed as to whether the published source term data were valid at the time of release or at the time the fission reaction stopped. There was some uncertainty about this matter as Mr Wotawa indicated that for all their source term inversion calculations using measured data, the release amounts were decay corrected back to the time of the earthquake. Mr Isnard and Mr Gering will check with the UNSCEAR source term group and report back to the TT.

3.5 As for the release height, the different ATMs used different values for the releases, while Mr Isnard had computed with time varying release heights. While the TT agreed that it would be best to use a point release at a height of 100 metres above ground level, there was interest to understand the sensitivity of the results to varying release heights (to reflect explosive releases), and Mr Isnard agreed to also provide these data to the TT so that they could conduct sensitivity tests.

3.6 Mr Isnard noted that not all events are equally important and that getting the meteorological conditions correctly simulated on high emission days is critical in the assessment.

3.7 The meeting agreed that at this time the ATM results should be computed at 3-hourly intervals and at 5-km horizontal resolution. In addition to the graphical output and text based time series, the UNSCEAR representatives expressed the desire to have the ATM output also available in a binary format such as in NetCDF. Mr Draxler agreed to provide this option through the web interface and make the converter available to the TT members.

3.8 All ATM runs have accounted for wet deposition with NWP estimated rainfall rate, but have not as yet used the JMA high resolution precipitation analyses (derived from radar and raingauge data). These data will be available soon to TT members from a WMO, and from a JMA ftp site.

3.9 Mr Saito presented the Cs-137 deposition results from the JMA ATM using their mesoscale analyses, currently the only ATM to use these high-resolution data, which showed considerably more spatial structure than any of the other ATM calculations that used lower resolution global meteorological fields. He noted that the results are very sensitive to the source term and slight adjustments to the release rate could have a significant effect on the deposition pattern. The TT is awaiting the updated source term information that will be provided by UNSCEAR Group-B.

3.10 The meeting discussed the JMA results using their mesoscale analyses which suggested sensitivity of the ATM calculations to the vertical motion field. The JMA ATM results for Cs-137 deposition are shown below for calculations without (top panel) and with (bottom panel) vertical motion. Mr Saito noted that the observed pattern lies somewhere between the two calculations.

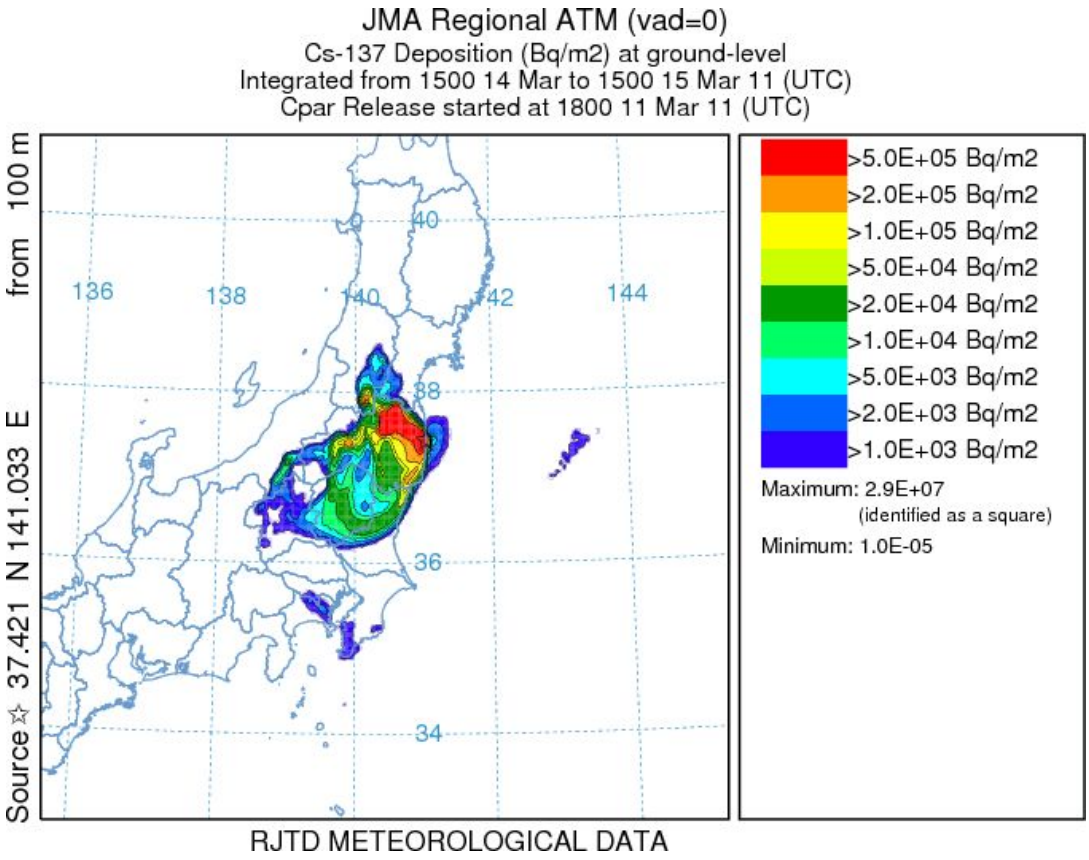
JMA Regional ATM (vad=0)
Cs-137 Deposition (Bq/m2) at ground-level
Integrated from 1500 14 Mar to 1500 15 Mar 11 (UTC)
Cpar Release started at 1800 11 Mar 11 (UTC)
Source ☆ 37.421 N 141.033 E from 100 m
136
138
140
142
144
40
38
36
34
>5.0E+05 Bq/m2
>2.0E+05 Bq/m2
>1.0E+05 Bq/m2
>5.0E+04 Bq/m2
>2.0E+04 Bq/m2
>1.0E+04 Bq/m2
>5.0E+03 Bq/m2
>2.0E+03 Bq/m2
>1.0E+03 Bq/m2
Maximum: 2.9E+07
(identified as a square)
Minimum: 1.0E-05
RJTD METEOROLOGICAL DATA

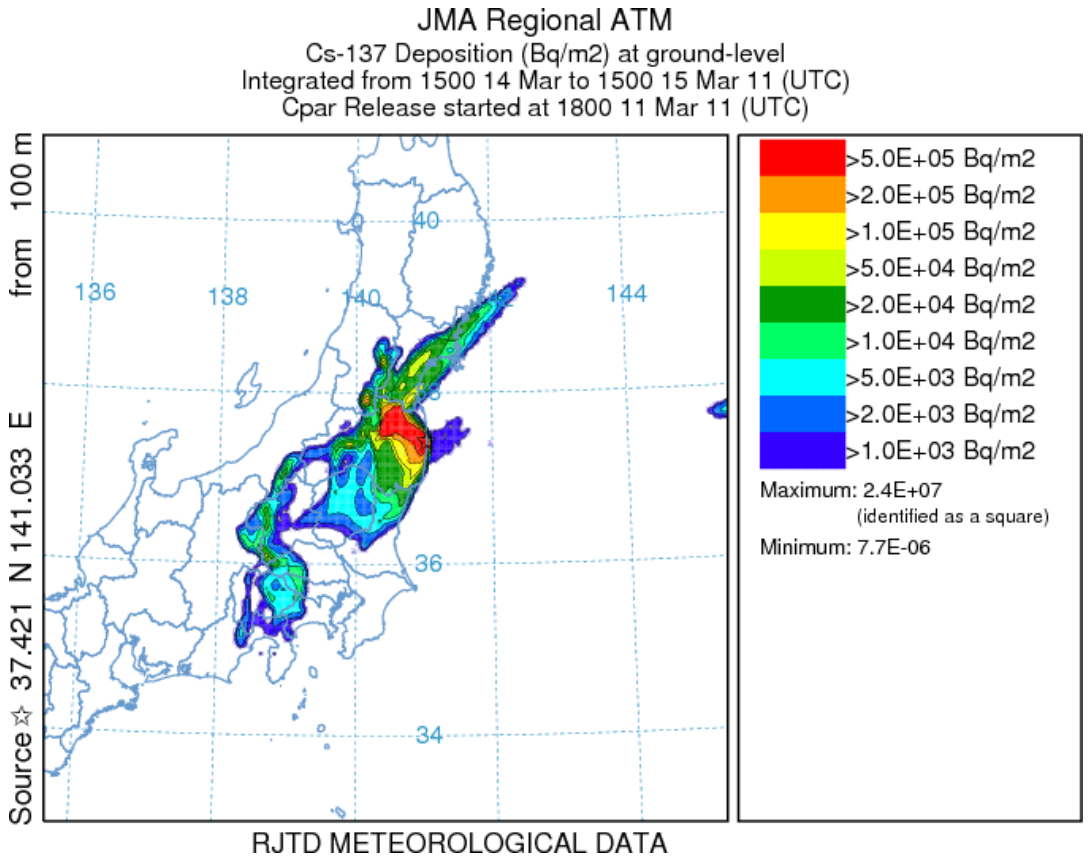
JMA Regional ATM
Cs-137 Deposition (Bq/m2) at ground-level
Integrated from 1500 14 Mar to 1500 15 Mar 11 (UTC)
Cpar Release started at 1800 11 Mar 11 (UTC)
Source ☆ 37.421 N 141.033 E from 100 m
136
138
140
144
40
36
34
>5.0E+05 Bq/m2
>2.0E+05 Bq/m2
>1.0E+05 Bq/m2
>5.0E+04 Bq/m2
>2.0E+04 Bq/m2
>1.0E+04 Bq/m2
>5.0E+03 Bq/m2
>2.0E+03 Bq/m2
>1.0E+03 Bq/m2
Maximum: 2.4E+07
(identified as a square)
Minimum: 7.7E-06
RJTD METEOROLOGICAL DATA

3.11 The following table summarizes the ATM runs that have been carried out.

Preliminary ATM Calculations (11-31 March 2011)

Center	Meteorology	ATM	Release	Output
CMC	GEM 0.30d 30 levels 6-hourly	MLDP0 dt=5min	1 unit/h 0-100 m AGL 300K p/3h	601x401 grid 0.05d x 100m 3-hr averaged
NOAA	GDAS 0.50d 56 levels 3-hourly	HYSPLIT dt=6min	1 unit/h 100 m AGL 300K p/3h	601x401 grid 0.05d x 100m 3-hr averaged
JMA	Meso Analysis 5-km 50 levels 3-hourly	Regional dt=10min	1 unit/h 0-100 m ASL 100K p/3h	721x577 grid 0.05d x 100m 3-hr averaged
UKMet	Unified 0.35x0.23 deg 70 levels 3-hourly	NAME dt=10min	1 unit/h 0-100 m AGL 300K p/3h	600x400 0.05d x 100m 3-hr averaged
ZAMG	ECMWF 0.2x0.2 deg 92 levels 3-hourly	FLEXPART dt=variable	1 unit/h 0-100 m AGL 300K p/3h	

3.12 The task team members agreed to provide a short technical document describing their ATM calculations which will be posted on the web site linked to each ATM. Mr Isnard and Mr Gering also agreed to provide to the TT members a short description of their atmospheric transport and dispersion model ATMs.

4. Evaluation of the sample JMA mesoscale meteorological analysis data files

4.1 Mr Saito presented the details of the JMA meso-analyses produced by a 4DVar system (ref. JMA, also see report of first TT meeting), and provided to members the entire dataset for the period 11 – 31 March 2011, at 3-hourly and 5-km horizontal resolution, in Lambert conformal map projection, which he had brought on memory sticks. The total dataset size is approximately 57 GB in GRIB2 format; a description of the dataset is included with the dataset. These data will also be made available to the larger UNSCEAR community from a WMO Internet accessible site, the exact URL is to be determined and provided by WMO Secretariat.

4.2 The meeting welcomed the offer of Mr Saito to provide a software tool to convert these files to latitude-longitude grid, while retaining the vertical hybrid terrain-following grid and also with an option to convert these data to pressure-level surfaces. Mr Saito indicated that this tool could be made available by the end of June 2012.

4.4 Mr Isnard and Mr Gering agreed that this JMA mesoanalyses dataset was probably very suitable for use by their own ATM and dose calculation systems, and will attempt to use it for their own ATM trials, compare their results with those produced by TT members and communicate these results with the TT.

4.5 The meeting noted that the intent of the TT was to provide guidance to UNSCEAR about the best meteorology to use for ATM calculations in their assessment. The issue was no longer a question of which meteorological analyses was most suitable to use, but how can the ATM models be optimized to work with the JMA data, whether computing vertical motion, stability, mixing, or deposition. Several TT members noted they will have to make changes to use these data which should provide valuable feedback to UNSCEAR groups planning to use the mesoscale analyses.

5. Status of verification data for ATM and meteorological evaluation

5.1 The meeting discussed the potential usefulness of CTBTO/IMS/RN data for verification of ATM results. Mr Wotawa explained to the meeting regarding CTBTO's data policy for these data, through informal consultations with the CTBTO/PTS. Aside from publishing actual data values, all other information generated from the use of such data may be made openly available to the public. While these data would be very useful for validating regional/global scale ATM results, there is only monitoring data from one such RN station (Takasaki) in Japan, located approximately 220 km west-southwest of Fukushima-Daiichi. The meeting agreed that they would not pursue this matter further with respect to verification of ATM calculations over Japan, but it might be useful for global calculations. Several TT members agreed to pursue this matter further, outside and independently of the current WMO TT ToR.

5.2 Mr Isnard will investigate the availability of other air concentration measurements at selected sites that could be used for verification.

5.3 Another approach is to use the deposition monitoring data that has been used to show the complex deposition pattern around the accident site. Mr Gering described sampling data from Japan, of 2000 data points, that are available from a high density of soil sampling sites within 100-200 km of the NPP, and he agreed to provide these data to the TT to evaluate the ATM outputs. Mr Draxler has already put in place a statistics package to compute the overall performance and ranking of the ATM outputs compared to measurement data which could then be added to the existing web interface and distribute to TT members.

6. Discussion on UNSCEAR requirements

6.1 Mr Peter Bedwell from the UK Health Protection Agency presented an overview of the work HPA conducted for the World Health Organization's assessment and the requirements that the UNSCEAR dose assessment group-C would need from the UNSCEAR dispersion modeling group-B. He noted that all the initial ATM calculations for WHO showed large under-predictions of particulate air concentrations outside of Japan with under-predictions increasing with distance. This was attributed to either excessive wet scavenging or uncertainty in the source term. Several TT members have reached similar conclusions using their own ATMs. This confirmed the TT focus on integrating higher resolution precipitation analysis with the ATM calculations

6.2 Mr Bedwell reviewed some of the ATM technical requirements for UNSCEAR's dose calculations. Although he expressed a desire for higher spatial resolution, the TT's configuration of 3-hourly and 5-km horizontal resolution was consistent with their requirements.

6.3 The meeting discussed the relationship of the TT ToR with the UNSCEAR requirements and clarified their respective roles. The WMO TT will be providing the higher resolution meteorological fields for UNSCEAR ATM calculations and technical guidance on how to use these analyses. WMO TT will not be doing any dose calculations for UNSCEAR. However, the UNSCEAR dispersion modeling group may access the TT ATM calculations to provide uncertainty estimates to their ATM calculations within the existing evaluation framework.

7. Review of the Terms of Reference of the WMO Task Team

The TT members reviewed and made one modification to its Terms of Reference, which is found in Annex III.

8. Revised Work plan and timetable

The TT reviewed and updated its work plan and time table as follows:

1 - 3 May 2012 – TT meeting, and meeting report

23 May 2012 - 59th session UNSCEAR progress and preliminary report (TT input provided from TT meeting of Dec. 2011)

31 May 2012 - TT members provide ATM model configuration summary

31 May 2012 - Mr Gering agreed to investigate the provision of surface measurement data; Mr Isnard agreed to investigate the provision of surface air concentration measurement data.

June 2012 - JMA high-resolution precipitation analyses and the JMA mesoscale analysis data converter be shared with TT members

June 2012 - TT discuss via email or teleconference the verification potential of measurement data

Early July 2012 - (before UNSCEAR all-experts meeting) – teleconference on progress of TT activities

July 2012 - NOAA (Draxler) to provide DATEM statistical results linked with model evaluation framework

September 2012 - TT to complete and provide ATM results using JMA meso-analyses. JMA to provide a comparison of the JMA mesoanalyses of precipitation with the JMA high-resolution precipitation analyses

December 2012 - third TT meeting, drafting final TT report

May 2013 – 60th session UNSCEAR report

9. Closing

The meeting was closed at 15:00, Thursday 3 May 2012.

Reference

- Chino, M., Nakayama, H., Nagai, H., Terada, H., Katata, G., Yamazawa, H., 2011. Preliminary Estimation of Release Amounts of ^{131}I and ^{137}Cs Accidentally Discharged from the Fukushima Daiichi Nuclear Power Plant into the Atmosphere. *Journal of NUCLEAR SCIENCE and TECHNOLOGY*, 48(7), pp.1129–1134.
- Draxler, R. R., Rolph. G.D., 2012. Evaluation of the Transfer Coefficient Matrix (TCM) approach to model the atmospheric radionuclide air concentrations from Fukushima. *Journal of GEOPHYSICAL RESEARCH*, 117 (D05107), 10pp, http://www.agu.org/pubs/crossref/2012/2011JD017205.shtml
- JMA reference to mesoscale analyses and high resolution precipitation analyses

Annex I - Agenda

1. Opening
2. Adoption of Agenda, working arrangements
3. Review of preliminary (11-31 March 2011) ATM runs
4. Evaluation of the sample JMA mesoscale meteorological analysis data files
5. Status of verification data for ATM and meteorological evaluation
6. Presentation and discussion of UNSCEAR requirements
7. Review of the Terms of Reference of the WMO Task Team
8. Revised Work plan and timetable
9. Closing

Annex II - List of Participants

Mr Gerhard **WOTAWA** Zentralanstalt für Meteorologie und Geodynamik (ZAMG) Hohe Warte 38 A-1191 VIENNA **Austria**	Tel: Fax: Email:	+(43 1) 36026 2007 +(43 1) 369 12 33 gerhard.wotawa@zamg.ac.at
Mr Alain **MALO** Canadian Meteorological Centre Meteorological Service of Canada Environment Canada 2121 Trans-Canada Highway Dorval, Québec H9P 1J3 **Canada**	Tel: Fax: Email:	+(1 514) 421 4626 +(1 514) 421 4679 alain.malo@ec.gc.ca
Mr Kazuo **SAITO** Meteorological Research Institute Japan Meteorological Agency (JMA) 1-1, Nagamine, Tsukuba Ibaraki 305-0052 **Japan**	Tel: Fax: Email:	+(81 29) 853 8638 +(81 29) 853 8649 ksaito@mri-jma.go.jp
Mr Matthew **HORT** Met Office UK Fitzroy Road Exeter EX13PB Devon **United Kingdom**	Tel: Fax: Email:	(+44 1392) 886 242 (+44 1392) 885 681 matthew.hort@metoffice.gov.uk
Mr Roland **DRAXLER** Air Resources Laboratory NOAA – Office of Oceanic and Atmospheric Research SSMC3, Room 3350 1315 East-West Highway SILVER SPRING, Maryland (MD) 20910-6233 **United States of America**	Tel: Fax: Email:	+(1 301) 713 0295 ext 117 +(1 301) 713 0119 roland.draxler@noaa.gov
Mr Olivier **ISNARD** (France) UNSCEAR Study Expert Institut de Radioprotection et de Sûreté Nucléaire B.P. 17 – 92262 Fontenay-aux-Roses Cedex, France	Tel: Fax: Email:	+33 (0)1 58 35 73 85 +33 (0)1 46 54 39 89 olivier.isnard@irsn.fr
Mr Florian **GERING** UNSCEAR Study Expert	Tel: Fax:	+49 (0)3018 333 2576 +49 (0)3018 10 333 2576

Bundesamt für Strahlenschutz – SW 2.2 Ingolstädter Landstr. 1 D-85764 Oberschleißheim **Germany**	Email:	fgering@bfs.de
Mr Peter **BEDWELL** (United Kingdom) UNSCEAR Study Expert Health Protection Agency Chilton, Didcot Oxfordshire OX11 0RQ, UK	Tel: Fax: Email:	+44 (0)1235 827437 +44 (0)1235 833891 Peter.Bedwell@hpa.org.uk
Mr Peter **CHEN** WMO Secretariat 7 bis avenue de la Paix Case postale 2300 1211 GENEVE 2 **Switzerland**	Tel: Fax: Email:	+(41 22) 730 8231 +(41 22) 730 8128 pchen@wmo.int

ANNEX III - Terms of Reference

WMO Technical Task Team on Meteorological Analyses – Fukushima Daiichi NPP Accident

Membership and Chairperson

- Roland Draxler, Chairperson (RSMC Washington, USA)
- Matthew Hort (RSMC Exeter, UK)
- Gerhard Wotawa (RSMC Vienna, Austria)
- Kazuo Saito (Meteorological Research Institute, Japan Meteorological Agency, Japan)
- René Servranckx (Chairperson of CBS Coordination Group on Nuclear ERA, RSMC Montreal, Canada)

Terms of work

(a) Determine the relevant meteorological observational data sets and related information required to support the meteorological analyses and identify their archive location and availability;

(b) Determine which of the existing meteorological analyses are of sufficient spatial and temporal detail that can be used to estimate the atmospheric transport, dispersion, and surface deposition of radionuclides that were released from the nuclear accident and identify their archive location and availability;

(c) Identify gaps in the existing meteorological analyses that if addressed would make them more suitable for estimating atmospheric transport, dispersion, and deposition and in coordination with the WMO Secretariat, identify which members will provide updated analyses;

(d) Based upon the observational data and analyses, prepare a report on the temporal and spatial variations in atmospheric conditions during the nuclear accident;

(e) Evaluate the suitability and quality of the observational data and meteorological analyses for computing atmospheric transport, dispersion, and surface deposition by comparing the computational results with radiological measurements;

(f) Provide a number of atmospheric transport, dispersion and deposition (ATM) outputs from several different ATMs using different meteorological analyses;

(g) Liaise and assist where possible with the UN Scientific Committee on the Effects of Atomic Radiation (UNSCEAR), in their study on the levels and effects of exposure due to the Fukushima Daiichi nuclear accident.

(h) Propose possible enhancements to the WMO EER system, including additional products and/or additional modes of operation with the relevant international organizations.

Duration and working arrangements

It is anticipated that the work of the Task Team spans a period of 12 -18 months from December 2011. The Team will work mainly by e-correspondence, and meet face-to-face, as needed. WMO Secretariat will facilitate the work of the team.

(ToR updated, 3 May 2012)

WORLD METEOROLOGICAL ORGANIZATION

THIRD MEETING OF WMO TASK TEAM ON METEOROLOGICAL ANALYSES FOR FUKUSHIMA-DAIICHI NUCLEAR POWER PLANT ACCIDENT

VIENNA, AUSTRIA, 3 – 5 DECEMBER 2012

FINAL REPORT

Dèlia Arnold, Gerhard Wotawa, Matthew Hort, Roland Draxler, Peter Chen, Stefano Galmarini, Kazuo Saito, René Servranckx

EXECUTIVE SUMMARY

The WMO Task Team on Meteorological Analyses for Fukushima Daiichi NPP Accident was formed in late 2011 to develop a series of meteorological analyses in numerical form, using as much observational data and related information as available, that will be suitable for estimating the atmospheric transport, dispersion and deposition of radioactivity released from the Fukushima-Daiichi Nuclear Power Plant in 2011. This is the report of the Task Team's third and final meeting, whose members developed a final record of its work and outputs.

Since the time of the Task Team's second meeting, Mr Draxler engaged the collaboration of the European Commission Joint Research Centre ENSEMBLE project to assist in the evaluation of a set of 18 different "runs" of meteorological and atmospheric dispersion and deposition calculations.

Mr Roland Draxler, the Chairperson of this Task Team, will use the final report of the team to develop suitable condensed text as input to the study on the levels and effects of the radioactivity released from the nuclear accident, being conducted by the United Nations Scientific Committee on the Effects of Atomic Radiation (UNSCEAR).

The report also suggests possible improvements to the present nuclear emergency response arrangements.

1 Opening

1.1 The third meeting of the WMO Technical Task Team (TT) on Meteorological Analyses for Fukushima Daiichi NPP Accident was held at the offices of the Zentralanstalt für Meteorologie und Geodynamik (ZAMG), Vienna, Austria, and opened by the TT's chairperson, Mr Roland Draxler. Mr Michael Straudinger, Director of ZAMG and PR of Austria with WMO, welcomed the participants. He noted the importance of the work of this Task Team and expected that there would be some important suggestions for improving WMO's nuclear emergency response procedures, supporting National Meteorological Services.

Mr Draxler welcomed the participants and expressed appreciation to all the participants for their efforts in this work and for participating at this crucial and final meeting. Mr Peter Chen, on behalf of the WMO Secretariat, added appreciation for the hard work of members over the last year, the outcome of which will meet the requirements expressed by the United Nations Scientific Committee on the Effects of Atomic Radiation (UNSCEAR). Mr Stefano Galmarini of the EC/JRC was invited to participate at this meeting in relation to the EC/ENSEMBLE assessment tools that were used to evaluate the atmospheric transport and dispersion runs carried out by the TT members. The participants expressed their appreciation to ZAMG and Mr Gerhard Wotawa for hosting the meeting and for having provided the local arrangements for the meeting.

Mr Draxler recalled the history of this Task Team's work, including the development of its Terms of Reference at the first meeting (see first meeting report) and agreement by Executive Council at its 64th session (2012), and leading up to this third and final meeting. Mr Draxler also informed the meeting of his participation at, and interactions with the UNSCEAR Expert Groups. In particular, he indicated that UNSCEAR had decided in July 2012 that the dose estimation group would use an ensemble output from the WMO TT as input to their dose calculations. This decision was a change from an earlier understanding that the WMO was only to provide the best meteorological analyses during the period 11 – 31 March 2011, to be applied in the atmospheric transport and dispersion modeling of radionuclides released during the nuclear power plant accident. The meeting noted that UNSCEAR finally established the source term time series in mid-October 2012. It was also noted that UNSCEAR requires a descriptive document on the atmospheric transport and dispersion/deposition results, and meteorological aspects by 14 December 2012.

1.2 Adoption of agenda and working arrangements

Mr Draxler introduced the provisional agenda, which the meeting adopted, and is found in Annex I. Daily working arrangements were decided.

1.3 The list of participants is found in Annex II.

2 Final Report of the Task Team

2.1 The TT members each provided a verbal summary of their respective contributions to this work, and discussed numerous technical issues related to its tasks. Mr Galmarini of EC/JRC provided a briefing on the ENSEMBLE assessment of the 18 ATM modelling results, including the various metrics used in the evaluation. He agreed

to provide suitable text to describe this assessment to be included in the final report of the TT.

2.2 The meeting developed a report of the work of the TT, and agreed to undertake final revisions by the end of January 2013. The version of TT report reached by 21 December 2012 is found in Annex III.

3 AMS Conference session on Fukushima accident

3.1 Mr Draxler recalled that American Meteorological Society (AMS) Committee on Meteorological Aspects of Air Pollution, and the Meteorological Society of Japan (MSJ) will jointly convene a one-day specialty symposium at the AMS 2013 Annual Meeting to review the present status and identify the role of meteorology for the analysis of the transport and dispersion of contaminants from the Fukushima nuclear power plant. A special journal publication is planned.

3.2 Mr Draxler has submitted an abstract of his presentation on the work of this TT. Mr Saito has submitted an abstract of his presentation of the JMA regional ATM for the accident.

3.3 Mr Draxler considered the opinion of TT members regarding the submission of an extended abstract to the planned AMS journal publication. Recalling the deadline for this submission is 10 February 2013, the members were of the general opinion that little time is available to deal with unresolved scientific questions prior to this deadline. Mr Saito indicated that he intends to submit an extended abstract for the journal publication.

3.4 The TT then considered alternative publication opportunities, including the possibility to initiate collaboration with a suitable scientific journal (e.g. Atmospheric Environment) to produce a special issue on meteorological aspects of the Fukushima-Daiichi accident. Such a special issue could include topic areas such as: source term estimation, dispersion and deposition estimation, use of high resolution precipitation analyses, ensemble techniques, etc. Mr Draxler will contact a suitable journal office to explore this possibility, including time-lines, and whether another similar development is already underway. Mr Chen will explore with WMO Secretariat whether such a special publication could be coordinated and developed through WMO. Upon favourable responses, WMO could invite its Members to participate, including all the RSMCs for ERA.

3.5 Mr Wotawa indicated that he plans to make a presentation on the TT's work to the annual meeting of the European Geophysical Union (Vienna, week of 8 April 2013).

4 Cooperation with the Science Council of Japan (SCJ) model evaluation

4.1 Mr Draxler and Mr Hort were contacted by Mr Teruyuki Nakajima, Chairperson of the Working Group for model inter-comparison of the Science Council of Japan (SCJ), who would like to review the modelling capability of the dispersion and deposition of radioactive materials to the land and the ocean as a result of the Fukushima Daiichi Nuclear Power Plant accident. The purpose of this initiative is to compare existing model results in order to access the uncertainty in the results. Mr Draxler provided to

Mr Nakajima the NOAA Web page URL where the TT model results are posted. The SCJ has subsequently contacted WMO informally regarding its interest, or the interest of individual TT members to participate.

4.2 The TT decided not to participate as a group, while Mr Saito indicated that JMA will participate in this model inter-comparison.

5 WMO EER System

5.1 RSMC-ENSEMBLE experiment

5.1.1 Mr Wotawa presented the results of the RSMC ENSEMBLE experiment that was conducted earlier this year, which was based on a fictitious scenario of a NPP accident in USA, on 18 April 2012, 0430 UTC. The results showed a wide range of model results from 9 RSMCs. RSMC Washington is expected to provide its results shortly.

5.1.2 Mr Wotawa agreed to provide the presentation and a summary of the evaluation to Mr Servranckx (Chairperson of the CBS Expert Team on ERA). Mr Servranckx will then communicate this information to the representatives of the RSMCs.

5.1.3 The TT considered the possibility of creating an ENSEMBLE session for the Fukushima-Daiichi ATM results, to open the participation to other RSMCs and possibly other ATM centres. Such a project could support the scientific work of contributors to the possible special journal issue on the meteorological aspects of the Fukushima-Daiichi accident (see agenda item 3).

5.2 Enhancement to the WMO EER system based on TT's experience

5.2.1 The TT discussed the present arrangements, in particular the RSMC-ERA system that serves both WMO Members, the IAEA, and other relevant International Organizations. The Secretariat recalled that under IAEA's Action Plan for Nuclear Safety, established since the Fukushima accident, provides the IAEA/IEC with a broader mandate to assess accident situations, and to predict possible impacts. This would be a more favourable environment to undertake a joint review of IAEA requirements for meteorological products and services for nuclear ERA.

5.2.2 The following suggestions could be pursued by the CBS Expert Team on ERA (chaired by Mr Servranckx), and Secretariat:

- Explore if the formation of an interdisciplinary science forum would be useful to advance the science to support operational ATM programmes (nuclear, non-nuclear):
- Convene with IAEA, a users requirements conference (previous one was in 1993). This is already in the list of actions of the Expert Team on ERA;
- Discuss informally with IAEA about the concept for a new computational framework (operational atmospheric dilution factors, and ensembles) for ATM in ERA, which would provide additional capabilities to IAEA/IEC to apply source information, and to interpret radiological measurements;
- WMO may wish to contact IAEA at the senior management level regarding improved meteorological products and services.

6 Future status of the NOAA hosted web page with TT ATDM results

6.1 Mr Draxler offered to continue hosting the web page, and the TT members gratefully accepted. This web page would be “re-branded” from the current “TT Meteorological Analysis” site, to become a generic site with tools for incorporating ATM results for the Fukushima accident, with the possibility for participating ATM centres to update with improved simulations. In addition Mr Draxler agreed to send the Web php file(s) to participating centres, in sequence, to update each centre’s information and attributions (e.g. logo).

7 Closing

7,1 The meeting closed at 17:15, Wednesday, 5 December 2012

ANNEX I - AGENDA

WMO Task Team on Meteorological Analyis of Fukushima-Daiichi NPP Accident
3 – 5 December 2012, Vienna, Austria

1 Opening and adoption of the agenda

2 Final Report of the Task Team

3 AMS Conference session on Fukushima accident

4 Cooperation with the Science Council of Japan (SCJ) model evaluation

5 WMO EER System

- 5.1 Review and discuss the RSMC-ENSEMBLE experiment
- 5.2 Recommend enhancements to the WMO EER system

6 Future status of the NOAA hosted web page with TT ATDM results

7 Closing

ANNEX II – List of Participants

Mr Gerhard **WOTAWA** Zentralanstalt für Meteorologie und Geodynamik (ZAMG) Hohe Warte 38 A-1191 VIENNA **Austria**	Tel: Fax: Email:	+(43 1) 36026 2007 +(43 1) 369 12 33 gerhard.wotawa@zamg.ac.at
Ms Dèlia **ARNOLD** Zentralanstalt für Meteorologie und Geodynamik (ZAMG) Hohe Warte 38 A-1191 VIENNA **Austria**	Tel: Fax: Email:	+(43 1) 36026 2007 +(43 1) 369 12 33 Deliona.arnold@gmail.com
Mr Christian **MAURER** Zentralanstalt für Meteorologie und Geodynamik (ZAMG) Hohe Warte 38 A-1191 VIENNA **Austria**	Tel: Fax: Email:	+(43 1) 36026 2007 +(43 1) 369 12 33 Christian.maurer@zamg.ac.at
Mr René **SERVRANCKX** Canadian Meteorological Centre Meteorological Service of Canada Environment Canada 2121 Trans-Canada Highway Dorval, Québec H9P 1J3 **Canada**	Tel: Fax: Email:	+(1 514) 421 4704 +(1 514) 421 4679 rene.servranckx@ec.gc.ca
Mr Kazuo **SAITO** Meteorological Research Institute Japan Meteorological Agency (JMA) 1-1, Nagamine, Tsukuba Ibaraki 305-0052 **Japan**	Tel: Fax: Email:	+(81 29) 853 8638 +(81 29) 853 8649 ksaito@mri-jma.go.jp
Mr Matthew **HORT** Met Office UK Fitzroy Road Exeter EX13PB Devon **United Kingdom**	Tel: Fax: Email:	(+44 1392) 886 242 (+44 1392) 885 681 matthew.hort@metoffice.gov.uk
Mr Roland **DRAXLER** Air Resources Laboratory NOAA – Office of Oceanic and Atmospheric Research R/ARL – NCWCP – Rm 4205	Tel: Fax: Email:	+(1 301) 683 1372 +(1 301) 683 1370 roland.draxler@noaa.gov

5830 University Research Court College Park, Maryland 20740 **United States of America**		
Mr Peter **CHEN** **WMO Secretariat** 7 bis avenue de la Paix Case postale 2300 1211 GENEVE 2 **Switzerland**	Tel: Fax: Email:	+(41 22) 730 8231 +(41 22) 730 8128 pchen@wmo.int
Invited Expert: Mr Stefano **GALMARINI** EC Joint Research Centre Via E. Fermi 1, TP 441 21020 Ispra **Italy**	Tel: Fax: Email:	+39 0332 785 382 +39 0332 785 466 stefano.galmarini@jrc.ec.europa.eu

ANNEX III

The World Meteorological Organization's Evaluation of Meteorological Analyses for the Radionuclide Dispersion and Deposition from the Fukushima-Daiichi Nuclear Power Plant Accident

Roland Draxler, Delia Arnold, Matthew Hort, Alain Malo, Stefano Galmarini, Kazuo Saito, Efisio Solazzo, Andrew Jones, Susan Leadbetter, Christian Maurer, Glenn Rolph, Toshiki Shimbori, Gerhard Wotawa, René Servranckx

http://www.wmo.int/pages/prog/www/CBS-Reports/DPFSERA-index.html

気象研究所技術報告一覧表

第１号　バックグラウンド大気汚染の測定法の開発（地球規模大気汚染特別研究班，1978）
Development of Monitoring Techniques for Global Background Air Pollution. (MRI Special Research Group on Global Atmospheric Pollution, 1978)

第２号　主要活火山の地殻変動並びに地熱状態の調査研究（地震火山研究部，1979）
Investigation of Ground Movement and Geothermal State of Main Active Volcanoes in Japan. (Seismology and Volcanology Research Division, 1979)

第３号　筑波研究学園都市に新設された気象観測用鉄塔施設（花房龍男，藤谷徳之助，伴野登，魚津博，1979）
On the Meteorological Tower and Its Observational System at Tsukuba Science City. (T. Hanafusa, T. Fujitani, N. Banno, and H. Uozu, 1979)

第４号　海底地震常時観測システムの開発（地震火山研究部，1980）
Permanent Ocean－Bottom Seismograph Observation System. (Seismology and Volcanology Research Division, 1980)

第５号　本州南方海域水温図－400m（又は 500m）深と 1,000m 深－（1934－1943 年及び 1954－1980 年）（海洋研究部，1981）
Horizontal Distribution of Temperature in 400m (or 500m) and 1,000m Depth in Sea South of Honshu, Japan and Western －North Pacific Ocean from 1934 to 1943 and from 1954 to 1980. (Oceanographical Research Division, 1981)

第６号　成層圏オゾンの破壊につながる大気成分及び紫外日射の観測（高層物理研究部，1982）
Observations of the Atmospheric Constituents Related to the Stratospheric ozon Depletion and the Ultraviolet Radiation. (Upper Atmosphere Physics Research Division, 1982)

第７号　83 型強震計の開発（地震火山研究部，1983）
Strong－Motion Seismograph Model 83 for the Japan Meteorological Agency Network. (Seismology and Volcanology Research Division, 1983)

第８号　大気中における雪片の融解現象に関する研究（物理気象研究部，1984）
The Study of Melting of Snowflakes in the Atmosphere. (Physical Meteorology Research Division, 1984)

第９号　御前崎南方沖における海底水圧観測（地震火山研究部・海洋研究部，1984）
Bottom Pressure Observation South off Omaezaki, Central Honsyu. (Seismology and Volcanology Research Division and Oceanographical Research Division, 1984)

第 10 号　日本付近の低気圧の統計（予報研究部，1984）
Statistics on Cyclones around Japan. (Forecast Research Division, 1984)

第 11 号　局地風と大気汚染質の輸送に関する研究（応用気象研究部, 1984）
Observations and Numerical Experiments on Local Circulation and Medium－Range Transport of Air Pollutions. (Applied Meteorology Research Division, 1984)

第 12 号　火山活動監視手法に関する研究（地震火山研究部，1984）
Investigation on the Techniques for Volcanic Activity Surveillance. (Seismology and Volcanology Research Division, 1984)

第 13 号　気象研究所大気大循環モデルーⅠ（MRI・GCMーⅠ）（予報研究部，1984）
A Description of the MRI Atmospheric General Circulation Model (The MRI・GCMーⅠ). (Forecast Research Division, 1984)

第 14 号　台風の構造の変化と移動に関する研究－台風 7916 の一生－（台風研究部，1985）
A Study on the Changes of the Three - Dimensional Structure and the Movement Speed of the Typhoon through its Life Time. (Typhoon Research Division, 1985)

第 15 号　波浪推算モデル MRI と MRIーⅡの相互比較研究－計算結果図集－（海洋気象研究部，1985）
An Intercomparison Study between the Wave Models MRI and MRIーⅡ －A Compilation of Results－ (Oceanographical Research Division, 1985)

第 16 号　地震予知に関する実験的及び理論的研究（地震火山研究部，1985）
Study on Earthquake Prediction by Geophysical Method. (Seismology and Volcanology Research Division, 1985)

第 17 号　北半球地上月平均気温偏差図（予報研究部，1986）
Maps of Monthly Mean Surface Temperature Anomalies over the Northern Hemisphere for 1891－1981. (Forecast Research Division, 1986)

第 18 号　中層大気の研究（高層物理研究部，気象衛星研究部，予報研究部，地磁気観測所，1986）
Studies of the Middle Atmosphere. (Upper Atmosphere Physics Research Division, Meteorological Satellite Research Division, Forecast Research Division, MRI and the Magnetic Observatory, 1986)

第 19 号　ドップラーレーダによる気象・海象の研究（気象衛星研究部・台風研究部・予報研究部・応用気象研究部・海洋研究部，1986）
Studies on Meteorological and Sea Surface Phenomena by Doppler Radar. (Meteorological Satellite Research Division, Typhoon Research Division, Forecast Research Division, Applied Meteorology Research Division, and Oceanographical Research Division, 1986)

第 20 号　気象研究所対流圏大気大循環モデル（MRI・GCMーⅠ）による 12 年間分の積分（予報研究部，1986）
Mean Statistics of the Tropospheric MRI・GCMーⅠbased on 12－year Integration. (Forecast Research Division, 1986)

第 21 号　宇宙線中間子強度 1983－1986（高層物理研究部，1987）
Multi－Directional Cosmic Ray Meson Intensity 1983－1986. (Upper Atmosphere Physics Research Division, 1987)

第 22 号　静止気象衛星「ひまわり」画像の噴火噴煙データに基づく噴火活動の解析に関する研究（地震火山研究部，1987）
Study on Analysis of Volcanic Eruptions based on Eruption Cloud Image Data obtained by the Geostationary Meteorological satellite (GMS). (Seismology and Volcanology Research Division, 1987)
第 23 号　オホーツク海海洋気候図（篠原吉雄，四竈信行，1988）
Marine Climatological Atlas of the sea of Okhotsk. (Y. Shinohara and N. Shikama, 1988)
第 24 号　海洋大循環モデルを用いた風の応力異常に対する太平洋の応答実験（海洋研究部，1989）
Response Experiment of Pacific Ocean to Anomalous Wind Stress with Ocean General Circulation Model. (Oceanographical Research Division, 1989)
第 25 号　太平洋における海洋諸要素の季節平均分布（海洋研究部，1989）
Seasonal Mean Distribution of Sea Properties in the Pacific. (Oceanographical Research Division, 1989)
第 26 号　地震前兆現象のデータベース（地震火山研究部, 1990）
Database of Earthquake Precursors. (Seismology and Volcanology Research Division, 1990)
第 27 号　沖縄地方における梅雨期の降水システムの特性（台風研究部，1991）
Characteristics of Precipitation Systems During the Baiu Season in the Okinawa Area. (Typhoon Research Division, 1991)
第 28 号　気象研究所・予報研究部で開発された非静水圧モデル（猪川元興・斉藤和雄，1991）
Description of a Nonhydrostatic Model Developed at the Forecast Research Department of the MRI. (M. Ikawa and K. Saito, 1991)
第 29 号　雲の放射過程に関する総合的研究（気候研究部・物理気象研究部・応用気象研究部・気象衛星・観測システム研究部・台風研究部，1992）
A Synthetic Study on Cloud－Radiation Processes. (Climate Research Department, Physical Meteorology Research Department, Applied Meteorology Research Department, Meteorological Satellite and Observation System Research Department, and Typhoon Research Department, 1992)
第 30 号　大気と海洋・地表とのエネルギー交換過程に関する研究（三上正男・遠藤昌宏・新野　宏・山崎孝治，1992）
Studies of Energy Exchange Processes between the Ocean－Ground Surface and Atmosphere. (M. Mikami, M. Endoh, H. Niino, and K. Yamazaki, 1992)
第 31 号　降水日の出現頻度からみた日本の季節推移－30 年間の日降水量資料に基づく統計－（秋山孝子，1993）
Seasonal Transition in Japan, as Revealed by Appearance Frequency of Precipitating-Days. －Statistics of Daily Precipitation Data During 30 Years－(T. Akiyama, 1993)
第 32 号　直下型地震予知に関する観測的研究（地震火山研究部，1994）
Observational Study on the Prediction of Disastrous Intraplate Earthquakes. (Seismology and Volcanology Research Department, 1994)
第 33 号　各種気象観測機器による比較観測（気象衛星・観測システム研究部，1994）
Intercomparisons of Meteorological Observation Instruments. (Meteorological Satellite and Observation System Research Department, 1994)
第 34 号　硫黄酸化物の長距離輸送モデルと東アジア地域への適用（応用気象研究部，1995）
The Long－Range Transport Model of Sulfur Oxides and Its Application to the East Asian Region. (Applied Meteorology Research Department, 1995)
第 35 号　ウインドプロファイラーによる気象の観測法の研究（気象衛星・観測システム研究部，1995）
Studies on Wind Profiler Techniques for the Measurements of Winds. (Meteorological Satellite and Observation System Research Department, 1995)
第 36 号　降水・落下塵中の人工放射性核種の分析法及びその地球化学的研究（地球化学研究部，1996）
Geochemical Studies and Analytical Methods of Anthropogenic Radionuclides in Fallout Samples. (Geochemical Research Department, 1996)
第 37 号　大気と海洋の地球化学的研究（1995 年及び 1996 年）（地球化学研究部，1998）
Geochemical Study of the Atmosphere and Ocean in 1995 and 1996. (Geochemical Research Department, 1998)
第 38 号　鉛直２次元非線形問題（金久博忠，1999）
Vertically 2-dmensional Nonlinear Problem (H. Kanehisa, 1999)
第 39 号　客観的予報技術の研究（予報研究部，2000）
Study on the Objective Forecasting Techniques（Forecast Research Department, 2000）
第 40 号　南関東地域における応力場と地震活動予測に関する研究（地震火山研究部，2000）
Study on Stress Field and Forecast of Seismic Activity in the Kanto Region（Seismology and Volcanology Research Department, 2000）
第 41 号　電量滴定法による海水中の全炭酸濃度の高精度分析および大気中の二酸化炭素と海水中の全炭酸の放射性炭素同位体比の測定（石井雅男・吉川久幸・松枝秀和，2000）
Coulometric Precise Analysis of Total Inorganic Carbon in Seawater and Measurements of Radiocarbon for the Carbon Dioxide in the Atmosphere and for the Total Inorganic Carbon in Seawater（I.Masao, H.Y.Inoue and H.Matsueda, 2000）
第 42 号　気象研究所／数値予報課統一非静力学モデル（斉藤和雄・加藤輝之・永戸久喜・室井ちあし，2001）
Documentation of the Meteorological Research Institute / Numerical Prediction Division Unified Nonhydrostatic Model (Kazuo Saito, Teruyuki Kato, Hisaki Eito and Chiashi Muroi，2001)
第 43 号　大気および海水中のクロロフルオロカーボン類の精密測定と気象研究所クロロフルオロカーボン類標準ガスの確立（時枝隆之・井上(吉川)久幸，2004）
Precise measurements of atmospheric and oceanic chlorofluorocarbons and MRI chlorofluorocarbons calibration scale

(Takayuki Tokieda and Hisayuki Y. Inoue，2004)

第 44 号　PostScript コードを生成する描画ツール"PLOTPS"マニュアル（加藤輝之，2004）
Documentation of "PLOTPS": Outputting Tools for PostScript Code (Teruyuki Kato，2004)

第 45 号　気象庁及び気象研究所における二酸化炭素の長期観測に使用された標準ガスのスケールとその安定性の再評価に関する調査・研究（松枝秀和・須田一人・西岡佐喜子・平野礼朗・澤　庸介・坪井一寛・堤　之智・神谷ひとみ・根本和宏・長井秀樹・吉田雅司・岩野園城・山本　治・森下秀昭・鎌田匡俊・和田　晃，2004）
Re-evaluation for scale and stability of CO_2 standard gases used as long-term observations at the Japan Meteorological Agency and the Meteorological Research Institute (Hidekazu Matsueda, Kazuto Suda, Sakiko Nishioka, Toshirou Hirano, Yousuke, Sawa, Kazuhiro Tuboi, Tsutumi, Hitomi Kamiya, Kazuhiro Nemoto, Hideki Nagai, Masashi Yoshida, Sonoki Iwano, Osamu Yamamoto, Hideaki Morishita, Kamata, Akira Wada，2004)

第 46 号　地震発生過程の詳細なモデリングによる東海地震発生の推定精度向上に関する研究（地震火山研究部，2005）
A Study to Improve Accuracy of Forecasting the Tokai Earthquake by Modeling the Generation Processes (Seismology and Volcanology Research Department, 2005)

第 47 号　気象研究所共用海洋モデル（MRI.COM）解説（海洋研究部，2005）
Meteorological Research Institute Community Ocean Model (MRI.COM) Manual (Oceanographical Research Department, 2005)

第 48 号　日本海降雪雲の降水機構と人工調節の可能性に関する研究（物理気象研究部・予報研究部，2005）
Study of Precipitation Mechanisms in Snow Clouds over the Sea of Japan and Feasibility of Their Modification by Seeding (Physical Meteorology Research Department, Forecast Research Department, 2005)

第 49 号　2004 年日本上陸台風の概要と環境場（台風研究部, 2006）
Summary of Landfalling Typhoons in Japan, 2004 (Typhoon Research Department, 2006)

第 50 号　栄養塩測定用海水組成標準の 2003 年国際共同実験報告（青山道夫，2006）
2003 Intercomparison Exercise for Reference Material for Nutrients in Seawater in a Seawater Matrix (Michio Aoyama, 2006)

第 51 号　大気および海水中の超微量六フッ化硫黄(SF_6)の測定手法の高度化と SF_6 標準ガスの長期安定性の評価（時枝隆之、石井雅男、斉藤 秀、緑川 貴, 2007）
Highly developed precise analysis of atmospheric and oceanic sulfur hexafluoride (SF_6) and evaluation of SF_6 standard gas stability (Takayuki Tokieda, Masao Ishii, Shu Saito and Takashi Midorikawa, 2007)

第 52 号　地球温暖化による東北地方の気候変化に関する研究（仙台管区気象台，環境・応用気象研究部, 2008）
Study of Climate Change over Tohoku District due to Global Warming (Sendai District Meteorological Observatory, Atmospheric Environment and Applied Meteorology Research Department, 2008)

第 53 号　火山活動評価手法の開発研究（地震火山研究部, 2008）
Studies on Evaluation Method of Volcanic Activity (Seismology and Volcanology Research Department, 2008)

第 54 号　日本における活性炭冷却捕集およびガスクロ分離による気体計数システムによる ^{85}Kr の測定システムの構築および 1995 年から 2006 年の測定結果（青山道夫, 藤井憲治, 廣瀬勝己, 五十嵐康人, 磯貝啓介, 新田 済, Hartmut Sartorius, Clemens Schlosser, Wolfgang Weiss, 2008）
Establishment of a cold charcoal trap-gas chromatography-gas counting system for ^{85}Kr measurements in Japan and results from 1995 to 2006 (Michio Aoyama, Kenji Fujii, Katsumi Hirose, Yasuhito Igarashi, Keisuke Isogai, Wataru Nitta, Hartmut Sartorius, Clemens Schlosser, Wolfgang Weiss, 2008)

第 55 号　長期係留による 4 種類の流速計観測結果の比較（中野俊也，石崎 廣，四竈信行, 2008）
Comparison of Data from Four Current Meters Obtained by Long-Term Deep-Sea Moorings (Toshiya Nakano, Hiroshi Ishizaki and Nobuyuki Shikama, 2008)

第 56 号　CMIP3 マルチモデルアンサンブル平均を利用した将来の海面水温・海氷分布の推定（水田 亮, 足立恭将, 行本誠史, 楠 昌司, 2008）
Estimation of the Future Distribution of Sea Surface Temperature and Sea Ice Using the CMIP3 Multi-model Ensemble Mean (Ryo Mizuta, Yukimasa Adachi, Seiji Yukimoto and Shoji Kusunoki, 2008)

第 57 号　閉流路中のフローセルを用いた分光光度法自動分析装置による海水の高精度 pH_T 測定（斉藤 秀, 石井雅男, 緑川 貴, 井上（吉川）久幸, 2008）
Precise Spectrophotometric Measurement of Seawater pH_T with an Automated Apparatus using a Flow Cell in a Closed Circuit（Shu Saito, Masao Ishii, Takashi Midorikawa and Hisayuki Y. Inoue, 2008）

第58号　栄養塩測定用海水組成標準の2006年国際共同実験報告（青山道夫,J. Barwell-Clarke, S. Becker, M. Blum, Braga E.S., S. C. Coverly, E. Czobik, I. Dahllöf, M. Dai, G. O Donnell, C. Engelke, Gwo-Ching Gong, Gi-Hoon Hong, D. J. Hydes, Ming-Ming Jin, 葛西広海, R. Kerouel, 清本容子, M. Knockaert, N. Kress, K. A. Krogslund, 熊谷正光, S. Leterme, Yarong Li, 増田真次, 宮尾 孝, T. Moutin, 村田昌彦, 永井直樹, G. Nausch, A. Nybakk, M. K. Ngirchechol, 小川浩史, J. van Ooijen, 太田秀和, J. Pan, C. Payne, O. Pierre-Duplessix, M. Pujo-Pay, T. Raabe, 齊藤一浩, 佐藤憲一郎, C. Schmidt, M. Schuett, T. M. Shammon, J. Sun, T. Tanhua, L. White, E.M.S. Woodward, P. Worsfold, P. Yeats, 芳村 毅, A. Youénou, Jia-Zhong Zhang, 2008）
2006 Inter-laboratory Comparison Study for Reference Material for Nutrients in Seawater（M. Aoyama, J. Barwell-Clarke, S. Becker, M. Blum, Braga E. S., S. C. Coverly, E. Czobik, I. Dahllöf, M. H. Dai, G. O. Donnell, C. Engelke, G. C. Gong, Gi-Hoon Hong, D. J. Hydes, M. M. Jin, H. Kasai, R. Kerouel, Y. Kiyomono, M. Knockaert, N. Kress, K. A. Krogslund, M. Kumagai, S. Leterme, Yarong Li, S. Masuda, T. Miyao, T. Moutin, A. Murata, N. Nagai, G. Nausch, M. K. Ngirchechol, A. Nybakk, H. Ogawa, J. van Ooijen, H. Ota, J. M. Pan, C. Payne, O. Pierre-Duplessix, M. Pujo-Pay, T. Raabe, K. Saito, K. Sato, C. Schmidt, M. Schuett, T. M. Shammon, J. Sun, T. Tanhua, L. White, E.M.S. Woodward, P. Worsfold, P. Yeats, T.

Yoshimura, A. Youénou, J. Z. Zhang, 2008）

第 59 号　気象研究所共用海洋モデル(MRI.COM)第 3 版解説（辻野博之, 本井達夫, 石川一郎, 平原幹俊, 中野英之, 山中吾郎, 安田珠幾, 石崎廣（気象研究所海洋研究部）, 2010）
Reference manual for the Meteorological Research Institute Community Ocean Model (MRI.COM) Version 3（Hiroyuki Tsujino, Tatsuo Motoi, Ichiro Ishikawa, Mikitoshi Hirabara, Hideyuki Nakano, Goro Yamanaka, Tamaki Yasuda, and Hiroshi Ishizaki (Oceanographic Research Department), 2010）

第 60 号　栄養塩測定用海水組成標準の 2008 年国際共同実験報告（青山道夫, Carol Anstey, Janet Barwell-Clarke, François Baurand, Susan Becker, Marguerite Blum, Stephen C. Coverly, Edward Czobik, Florence D’amico, Ingela Dahllöf, Minhan Dai, Judy Dobson, Magali Duval, Clemens Engelke, Gwo-Ching Gong, Olivier Grosso, 平山篤史, 井上博敬, 石田雄三, David J. Hydes, 葛西広海, Roger Kerouel, Marc Knockaert, Nurit Kress, Katherine A. Krogslund, 熊谷正光, Sophie C. Leterme, Claire Mahaffey, 光田均, Pascal Morin, Thierry Moutin, Dominique Munaron, 村田昌彦, Günther Nausch, 小川浩史, Jan van Ooijen, Jianming Pan, Georges Paradis, Chris Payne, Olivier Pierre-Duplessix, Gary Prove, Patrick Raimbault, Malcolm Rose, 齊藤一浩, 斉藤宏明, 佐藤憲一郎, Cristopher Schmidt, Monika Schütt, Theresa M. Shammon, Solveig Olafsdottir, Jun Sun, Toste Tanhua, Sieglinde Weigelt-Krenz, Linda White, E. Malcolm. S. Woodward, Paul Worsfold, 芳村毅, Agnès Youénou, Jia-Zhong Zhang, 2010）
2008 Inter-laboratory Comparison Study of a Reference Material for Nutrients in Seawater（青山道夫, Carol Anstey, Janet Barwell-Clarke, François Baurand, Susan Becker, Marguerite Blum, Stephen C. Coverly, Edward Czobik, Florence D’amico, Ingela Dahllöf, Minhan Dai, Judy Dobson, Magali Duval, Clemens Engelke, Gwo-Ching Gong, Olivier Grosso, 平山篤史, 井上博敬, 石田雄三, David J. Hydes, 葛西広海, Roger Kerouel, Marc Knockaert, Nurit Kress, Katherine A. Krogslund, 熊谷正光, Sophie C. Leterme, Claire Mahaffey, 光田均, Pascal Morin, Thierry Moutin, Dominique Munaron, 村田昌彦, Günther Nausch, 小川浩史, Jan van Ooijen, Jianming Pan, Georges Paradis, Chris Payne, Olivier Pierre-Duplessix, Gary Prove, Patrick Raimbault, Malcolm Rose, 齊藤一浩, 斉藤宏明, 佐藤憲一郎, Cristopher Schmidt, Monika Schütt, Theresa M. Shammon, Solveig Olafsdottir, Jun Sun, Toste Tanhua, Sieglinde Weigelt-Krenz, Linda White, E. Malcolm. S. Woodward, Paul Worsfold, 芳村毅, Agnès Youénou, Jia-Zhong Zhang, 2010）

第 61 号　強雨をもたらす線状降水帯の形成機構等の解明及び降水強度・移動速度の予測に関する研究（大阪管区気象台・彦根地方気象台・京都地方気象台・奈良地方気象台・和歌山地方気象台・神戸海洋気象台・松江地方気象台・鳥取地方気象台・舞鶴海洋気象台・広島地方気象台・徳島地方気象台・予報研究部, 2010）
Studies on formation process of line-shaped rainfall systems and predictability of rainfall intensity and moving speed（Osaka District Meteorological Observatory, Hikone Local Meteorological Observatory, Kyoto Local Meteorological Observatory, Nara Local Meteorological Observatory, Wakayama Local Meteorological Observatory, Kobe Marine Observatory, Matsue Local Meteorological Observatory, Tottori Local Meteorological Observatory, Maizuru Marine Observatory, Hiroshima Local Meteorological Observatory, Tokushima Local Meteorological Observatory AND Forecast Research Department, 2010）

第 62 号　WWRP 北京オリンピック 2008 予報実証/研究開発プロジェクト（齊藤和雄, 國井勝, 原昌弘, 瀬古弘, 原旅人, 山口宗彦, 三好建正, 黄偉健, 2010）
WWRP Beijing Olympics 2008 Forecast Demonstration/Research and Development Project (B08FDP/RDP)（Kazuo Saito, Masaru Kunii, Masahiro Hara, Hiromu Seko, Tabito Hara, Munehiko Yamaguchi, Takemasa Miyoshi and Wai-kin Wong, 2010）

第 63 号　東海地震の予測精度向上及び東南海・南海地震の発生準備過程の研究（地震火山研究部, 2011）
Improvement in prediction accuracy for the Tokai earthquake and research of the preparation process of the Tonankai and the Nankai earthquakes (Seismology and Volcanology Research Department, 2011)

第 64 号　気象研究所地球システムモデル第 1 版（MRI-ESM1）―モデルの記述―（行本誠史, 吉村裕正, 保坂征宏, 坂見智法, 辻野博之, 平原幹俊, 田中泰宙, 出牛真, 小畑淳, 中野英之, 足立恭将, 新藤永樹, 籔将吉, 尾瀬智昭, 鬼頭昭雄, 2011）
Meteorological Research Institute-Earth System Model Version 1 (MRI-ESM1) — Model Description — (Seiji Yukimoto, Hiromasa Yoshimura, Masahiro Hosaka, Tomonori Sakami, Hiroyuki Tsujino, Mikitoshi Hirabara, Taichu Y. Tanaka, Makoto Deushi, Atsushi Obata, Hideyuki Nakano, Yukimasa Adachi, Eiki Shindo, Shoukichi Yabu, Tomoaki Ose and Akio Kitoh, 2011)

第 65 号　東南アジア地域の気象災害軽減国際共同研究（斉藤和雄, 黒田徹, 林修吾, 瀬古弘, 國井勝, 小司禎教, 上野充, 川畑拓矢, 余田成男, 大塚成徳, Nurjanna Joko Trilaksono, 許智揚, 古関俊也, Le Duc, Kieu Thi Xin, 黄偉健, Krushna Chandra Gouda, 2011）
International Research for Prevention and Mitigation of Meteorological Disasters in Southeast Asia (Kazuo Saito, Tohru Kuroda, Syugo Hayashi, Hiromu Seko, Masaru Kunii, Yoshinori Shoji, Mitsuru Ueno, Takuya Kawabata, Shigeo Yoden, Shigenori Otsuka, Nurjanna Joko Trilaksono, Tieh-Yong Koh, Syunya Koseki, Le Duc, Kieu Thi Xin, Wai-Kin Wong and Krushna Chandra Gouda, 2011)

第 66 号　太平洋における大気－海洋間二酸化炭素フラックス推定手法（杉本裕之, 平石直孝, 石井雅男, 緑川貴, 2012）
A method for estimating the sea-air CO2 flux in the Pacific Ocean (Hiroyuki Sugimoto, Naotaka Hiraishi, Masao Ishii and Takashi Midorikawa, 2012)

第 67 号　太平洋における大気－海洋間二酸化炭素フラックス推定手法（坪井一寛, 松枝秀和, 澤庸介, 丹羽洋介, 中村雅道, 久保池大輔, 岩坪昇平, 齊藤和幸, 花宮義和, 辻健太郎, 大森英裕, 西秀紘, 2012）
Development of a flask sampling and its high-precision measuring system for greenhouse gases observations using a cargo aircraft C-130H (Kazuhiro Tsuboi, Hidekazu Matsueda, Yousuke Sawa, Yosuke Niwa Masamichi Nakamura, Daisuke

Kuboike, Shohei Iwatsubo, Kazuyuki Saito Yoshikazu Hanamiya, Kentaro Tsuji, Hidehiro Ohmori, Hidehiro Nishi, 2012)

第 68 号　国際シンポジウム 電子顕微鏡を用いたエアロゾル研究（五十嵐康人, Weijun Li, Peter.R.Buseck, 岡田菊雄, 張代洲, 足立光司, 藤谷雄二, 嶋寺光, 五藤大輔, 三井千珠, 野島雅, 大島長, 松井仁志, 石元裕史, 松木篤, Pradeep Khatri, 中山智喜, 向井将平, 大石乾詞, 間山憲仁, 坂本哲夫, 直江寛明, 財前祐二, 塩流水洋樹, 田中泰宙, 梶野瑞王, 2013）

International Symposium on Aerosol Studies Explored by Electron Microscopy (Yasuhito Igarashi, Weijun Li, Peter. R. Buseck, Kikuo Okada, Daizhou Zhang, Kouji Adachi, Yuji Fujitani, Hikari Shimadera, Daisuke Goto, Chizu Mitsui, Masashi Nojima, Naga Oshima, Hitoshi Matsui, Hiroshi Ishimoto, Atsushi Matsuki, Pradeep Khatri, Tomoki Nakayama, Shohei Mukai, Kenji Ohishi, Norihito Mayama, Tetsuo Sakamoto, Hiroaki Naoe, Yuji Zaizen, Hiroki Shiozuru, Taichu Y. Tanaka and Mizuo Kajino, 2013)

第 69 号　マグマ活動の定量的把握技術の開発とそれに基づく火山活動度判定の高度化に関する研究（地震火山研究部, 2013）

Development of Quantitative Detection Techniques of Magma Activity and Improvement of Evaluation of Volcanic Activity Level (Seismology and Volcanology Research Department, MRI, 2013)

第 70 号　平成 23 年（2011 年）東北地方太平洋沖地震による津波高の現地調査報告（林豊，前田憲二，対馬弘晃，岡田正實，木村一洋，岩切一宏, 2013）

Reports on Field Surveys of Tsunami Heights from the 2011 off the Pacific Coast of Tohoku Earthquake (Yutaka Hayashi, Kenji Maeda, Hiroaki Tsushima, Masami Okada, Kazuhiro Kimura and Kazuhiro Iwakiri, 2013)

第 71 号　気候研究のための気象研究所アンサンブル予測システムの概要とその応用（藪将吉，水田亮，吉村裕正，黒田友二，向川均, 2014）

Meteorological Research Institute Ensemble Prediction System (MRI-EPS) for climate research - Outline and its applications – (Shoukichi Yabu, Ryo Mizuta, Hiromasa Yoshimura, Yuhji Kuroda, and Hitoshi Mukougawa, 2014)

第 72 号　日本各地域の繰り返し相似地震発生状況に関する研究（地震火山研究部，地震火山部，気象大学校，札幌管区気象台，仙台管区気象台，大阪管区気象台，福岡管区気象台，沖縄気象台, 2014）

Survey of moderate repeating earthquakes in Japan (Seismology and Volcanology Research Department of MRI, Seismology and Volcanology Department, Meteorological College, Sapporo Regional Headquarters, Sendai Regional Headquarters, Osaka Regional Headquarters, Fukuoka Regional Headquarters, and Okinawa Regional Headquarters, 2014)

第 73 号　気象研究所非静力学地域気候モデルによる日本付近の将来気候変化予測について（佐々木秀孝，村田昭彦，川瀬宏明，花房瑞樹，野坂真也，大泉三津夫，水田亮，青栁曉典，志藤文武，石原幸司, 2015）

Projection of Future Climate Change around Japan by using MRI Non-hydrostatic Regional Climate Model (Hidetaka Sasaki, Akihiko Murata, Hiroaki Kawase, Mizuki Hanafusa, Masaya Nosaka, Mitsuo Oh'izumi, Ryou Mizuta, Toshinori Aoyagi, Fumitake Shido, and Koji Ishihara, 2015)

第 74 号　新型自己浮上式海底水圧計の開発（平田賢治，山崎明，対馬弘晃, 2015）

Development of a new pop-up ocean-bottom pressure gauge (Kenji Hirata, Akira Yamazaki, and Hiroaki Tsushima, 2015)

第 75 号　2012年・2013年に日本に接近・上陸した台風の概要と特性（北畠尚子，小山亮，嶋田宇大，櫻木智明，沢田雅洋, 2015）

Summary and Characteristics of Approaching and Landfalling Tropical Cyclones in Japan in 2012 and 2013 (Naoko Kitabatake, Ryo Oyama, Udai Shimada, Tomoaki Sakuragi and Masahiro Sawada, 2015)

気象研究所技術報告は，1978（昭和53）年の初刊以来,気象研究所が必要の都度発行する刊行物であり,気象研究所の研究計画に基づき実施した研究に関する手法、データ、結果等についてのまとめ、または、すでに公表した研究論文類をとりまとめ総合的報告としたものを掲載する。

ONLINE ISSN 2189-8871

気　象　研　究　所　技　術　報　告
第　76　号
平成27年10月　発行

編集兼
発行者　気　象　研　究　所

〒305-0052　茨城県つくば市長峰１－１
TEL(029)853-8535